Understanding magma genesis through analysis of melt inclusions: application of innovative micro-sampling techniques

Rikke Harlou

UNDERSTANDING MAGMA GENESIS THROUGH ANALYSIS OF MELT INCLUSIONS: APPLICATION OF INNOVATIVE MICRO-SAMPLING TECHNIQUES

Ph.D. Thesis by Rikke Harlou

Department of Earth Sciences, Durham University, UK

&

Danish Lithosphere Centre, Copenhagen, DK

March 2007

Declaration

I declare that this thesis, which I submit at Durham University for the degree of Doctor of Philosophy, is my own work. No parts of this thesis have previously been submitted by me or any others for a degree at University of Durham, or any other university. Where scientific material from other publications have been used, it is clearly referenced and acknowledged.

Rikke Harlou

Rikke Harlou

March 2007, Copenhagen, Denmark

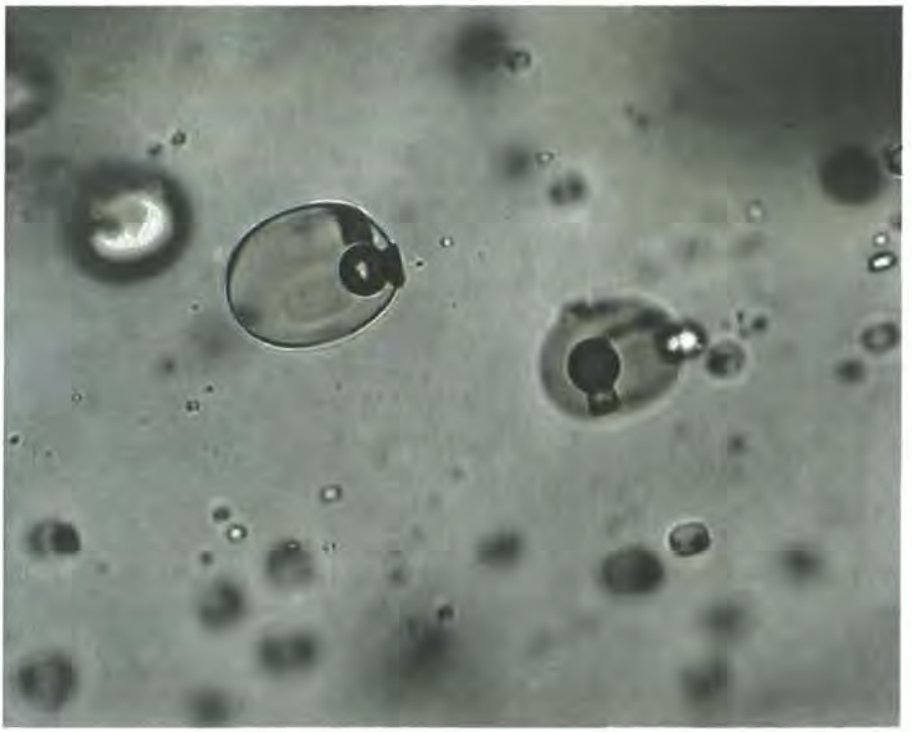

"... evaluation of the relative roles of mantle and crustal processes is difficult unless we can find a way to determine the compositional array of magmas produced in the mantle and at intermediate points in the petrogenesis of a magmatic system. Melts trapped as inclusions in phenocrysts are one means by which such intermediate liquids are preserved. Ideally, each inclusion represents a snapshot of the liquid trapped by the growth of the host crystal, preserving the character of intermediate steps in the formation of a suite of magmas"

(Nielsen et al., 1998).

ABSTRACT

Melt entrapped as inclusions in early-formed phenocrysts provide geochemists with an exceptional opportunity to study sample material from the earliest stages in the formation of a suite of lavas. With a foucus on olivine-hosted melt inclusions, this Ph.D. thesis has explored the potentials for obtaining Sr isotope ratios on individual olivine-hosted melt inclusions, and examined the potentials for Sr isotope studies on melt inclusions to reveal new information on the origin of CFB and OIB.

A novel technique is introduced that facilitate precise and accurate Sr isotope and trace element analysis of individual melt inclusions at sub-nanogram levels - thus applicable to typical melt inclusion suites from OIB and CFB, and in general to '*problems*' where precise and accurate Sr isotope and trace element information is required on sub-nanogram Sr samples. The technique developed combines off-line sampling by micro-milling, micro Sr column chemistry, Sr isotope determination by TIMS, and trace element analysis by ICPMS.

Olivine-hosted melt inclusions from two suites of high $^{3}He/^{4}He$ lavas of the North Atlantic Igneous Province are studied. These reveal that Sr isotope and trace element measurements on individual melt inclusions provide a higher resolution picture of the pre-aggregated melt compositions and the different mantle and crustal components involved in the magma genesis, which otherwise were obscured within the whole-rock data. The Sr isotope and elemental variability recorded by the olivine-hosted melt inclusions contrast the more subtle variations of the host lava suites and raises the question of whether the $^{3}He/^{4}He$ measured in melt inclusions in olivine phenocrysts should be related to the chemistry of melt inclusions rather than the bulk lava chemistry. The study further provides strong evidence that the extreme, high $^{3}He/^{4}He$ signature observed in magmas from the North Atlantic Igneous Province is derived from a depleted component in their source, and hence such He isotopic signature should no longer be regarded as canonical evidence for a primitive, lower mantle source.

TABLE OF CONTENTS

INTRODUCTION

This Ph.D. research project is a result of collaboration between the Danish Lithosphere Centre (Copenhagen, DK) and the Department of Earth Sciences at Durham University (UK) with an enrolment at the Durham University. The thesis is completed in agreement with the requirements for achieving a Ph.D. degree at Durham University. Ph.D. supervisors during the course of this work were professor D.G. Pearson and professor J.P. Davidson from Durham University (Department of Earth Sciences) in addition to assistant professor A.J.R. Kent from the Department of Geosciences, (Oregon State University, USA). Funding was provided by the Danish National Science Foundation (administrated by the Danish Lithosphere Centre) and by the Durham University.

The research presented in this Ph.D. focuses on Sr isotope and elemental information, which may be retrieved from melt inclusions (MIs) entrapped in olivine phenocrysts. The unique nature of MIs, as entrapped droplets of melt compositions present during the growth of the phenocrysts, provides geochemists with an exceptional opportunity to study sample material from the earliest stages in the formation of a suite of magmas. The entrapped MIs are, in theory, physically isolated from the external magmatic system, and so they are unaffected by subsequent modifying processes that may blur the chemistry of the primary characteristics of the bulk lava. Well-preserved MIs may, therefore, preserve valuable information about the geochemical variability among the pre-aggregated melt compositions, and thus indirectly offer insights to the source component(s) involved in the magma genesis. Hence, the goal of this thesis was to gain a detailed understanding of volcanic systems by high spatial resolution studies of MIs hosted by early-formed olivine phenocrysts.

The study of MIs requires substantial sample preparation, which involves hand-picking of olivine, homogenizations experiments, making polished epoxy grain mounts, and microscopic characterization of the individual MIs. The homogenization experiments were carried out using the facilities at the Danish Lithosphere Centre and Oregon State University. Major, trace and selected volatile element compositions of individual MIs and their host olivine were determined using a combination of electron microprobe and laser ablation inductive coupled plasma mass spectrometry (LA-ICPMS). This work was done at the University of Copenhagen and at Oregon State University under the supervision of A.J.R. Kent. Crucial for the remainder of the project

was the development of a technique to allow precise Sr isotope determination of sub-nanogram Sr sample sizes to facilitate Sr isotope determination of individual MIs. This was successfully done at the Arthur Holmes Isotope Geology Laboratory (Department of Earth Sciences, Durham University) under the supervision of D.G. Pearson, G.M. Nowell, C. Ottley, and J.P. Davidson. The technique presented in this Ph.D. thesis combines sampling by micro-milling, micro-chemistry, thermal ionization mass spectrometry (TIMS) and double focusing magnetic sector field ICPMS. This technique provides accurate Sr isotope and trace element compositions of individual olivine-hosted MIs of typical CFB and OIB suites. It allows Sr isotope determination on Sr samples down to 250 pg and 25 pg within an accuracy of between 400 and 175 ppm, respectively. This is more than adequate to resolve the large isotopic variations that are apparent. The analytical work with sub-ng Sr samples also included the development of a protocol for running sub-ng sample on the TIMS and analysis of low trace element concentrations by ICPMS. Essential for this work was maintaining a low and very reproducible total procedural blank (TPB) and the accurate characterization of the Sr isotope and elemental composition of the TPB. This facilitates, that accurate blank corrections can be applied to the collected data.

Olivine-hosted MIs from two locations within the North Atlantic Igneous Province (NAIP) were investigated. One suite came from the ankaramites of Vestfirdir, the NW peninsula of Iceland and represents an OIB setting. The other suite selected for study was a series of picrites from Padloping Island (Baffin Island, Canada). The picrites of Baffin Island represent the western-most, and the earliest magmatism within the NAIP (61 Ma). These lavas erupted through the continental crust during the early stages of continental breakup and are thought to be the surface manifestation of the arrival of the proto-Icelandic mantle plume. The Vestfirdir ankaramites were generated at a much later stage (14 Ma), at which point the Icelandic mantle plume interacted with the mid-Atlantic oceanic ridge. The Vestfirdir ankaramites are believed to relate to the magmatism produced along the Skagi-Snæfellsness rift zone. They are erupted through the older oceanic crust. Retrieving MIs from these two sets of lavas provides the means to study the early chemical variation present among the pre-aggregated melts. Documentation of the chemical variability among these MIs may thus provide information on the different mantle and crustal components involved in the magma genesis. Both sets of samples have the added interest of representing the most unradiogenic He isotope compositions measured in CFB and OIB, respectively.

The present thesis is divided into four main chapters where each chapter represents a scientific paper. *Chapter 1* is a study of the major, trace, and volatile composition of olivine hosted MIs from the Vestfirdir ankaramites. *Chapter 2* describes the technique developed to obtain precise and accurate Sr isotope and trace element analysis of individual MIs at sub-ng levels using

micro-milling, TIMS, and ICPMS. *Chapter 3* and *Chapter 4* are case studies of the Sr isotope variability revealed by olivine hosted MIs from the Vestfirdir ankaramites and the Baffin Island picrites, respectively. Located below is a list of the abbreviations frequently used through out this work.

List of abbreviations used in this Ph.D. thesis

AHIGL	•	Arthur Holmes Isotope Geology Laboratory at the Department of Earth Sciences, Durham University
Ave	•	Average
bc	•	Denotes a blank corrected value
BIP	•	Baffin Island picrites
BM	•	Batch melting
C	•	Common mantle source to MORB suggested by Hanan & Graham (1996)
CFB	•	Continental flood basalts
CM	•	Critical melting
Conc	•	Concentrated
Cpx.	•	Clinopyroxene
DM	•	Depleted mantle
EMA	•	Enriched mantle average used by Ellam & Stuart (2004)
EM	•	Enriched mantle
EMI	•	Enriched mantle endmember I e.g. Weaver (1991) and Hofmann (1997)
EMII	•	Enriched mantle endmember II e.g. Weaver (1991) and Hofmann (1997)
FM	•	Fractional melting
Fo or Fo%	•	Fosterite content in an olivine (see calculation for Mg# below)
FOZO	•	Focus zone, a high $^{3}He/^{4}He$ mantle endmember whose composition is defined by the point of convergence of the global OIB data in Sr-Nd-Pb isotope space e.g. Hart et al. (1992) and Hauri et al. (1994)
GLOSS	•	Global subducting sediment (Plank & Langmuir, 1998)
HREE	•	Heavy rare earth elements (Gd, Tb, Dy, Ho, Er, Tm, Yb, Lu)
HIMU	•	High μ, mantle endmember with high time-integrated U/Pb e.g. Hofmann (1997)
HRDM	•	*He-recharged* depleted mantle component suggested by Stuart et al. (2003) and Ellam & Stuart (2004)
i (subscribed)	•	Subscribed $_i$ means initial, and is used with isotope ratios. An initial Sr isotope ratio (e.g. $^{87}Sr/^{86}Sr_i$) means that the isotope ratio is corrected back to the time of eruption/formation of the rock.
ICPMS	•	Inductively coupled plasma mass spectrometry
ID	•	Identity

ID1 and ID2	•	Depleted components of the Icelandic mantle plum suggested by Thirlwall et al. (2004)
IE1 and IE2	•	Enriched components of the Icelandic mantle plum suggested by Thirlwall et al. (2004)
in prep	•	Publication or work in preparation
in press	•	Publication which is currently in press
K_d	•	Distribution coefficient
LA-MC-ICPMS	•	Laser ablation multi collector inductively coupled plasma mass spectrometry, often just referred to as laser ablation analysis
LILE	•	Large ion lithophile elements (K, Rb, Cs, Sr, Ba, REE, Th, U)
LOD	•	Limit of detection
LOMU	•	Low μ, mantle endmember with low time-integrated U/Pb
LREE	•	Light rare earth elements (La, Ce, Pr, Nd, Pm, Sm)
Ma	•	Millions years
Max	•	Maximum
MC-ICPMS	•	Multi collector inductively coupled plasma mass spectrometry
Mg#	•	Magnesium number:
	•	$Mg\# = 100*(m_{MgO}/M_{MgO})/(m_{MgO}/M_{MgO})+(m_{FeO}/M_{FeO}+m_{Fe2O3}/M_{Fe2O3})$
MI and MIs	•	Melt inclusion and melt inclusions
MICE	•	Moderately incompatible elements
Min	•	Minimum
MORB	•	Mid-oceanic ridge basalt
N	•	Subscripted $_N$ denotes that the trace-trace element ratio is normalized either according to primitive mantle or chondrite values
NAIP	•	North Atlantic Igneous Province
nbc	•	Non-blank corrected
ng	•	Nano-gram (10^{-9} g)
Norm	•	Normalized value according to e.g. a certain value
NSB 987	•	A strontium carbonated standard certified by the National Institute of Standards & Technology - equal to SRM 987. A certificate of analysis can be downloaded from http://www.nist.gov/srm
OIB	•	Oceanic island basalts
Ol.	•	Olivine
pg	•	Picro-gram (10^{-12} g)
PHEM	•	Primitive He mantle - a common mantle component sampled by OIB suggested by Farley et al. (1992)
PIMMS	•	Plasma ionization multi collector mass spectrometry
Plg.	•	Plagioclase
PIP	•	Icelandic plume trend described by Ellam & Stuart (2004)
PM	•	Primitive mantle
PRIM	•	Primordial mantle
Rec	•	Recommended value

REE	•	Rare earth elements (La, Ce, Pr, Nd, Pm, Sm, Eu, Gd, Tb, Dy, Ho, Er, Tm, Yb, Lu)
personal com.	•	Information gained by personal communication
Ref	•	Reference value
REM	•	Radiogenic He-Sr recycled enriched endmember found in the Vestfirdir ankaramites used in *Chapter 3*
SCLM	•	Subcontinental lithospheric mantle
SD	•	Often given as ±2SD, which is used to quote the reproducibility of a number of analyses. Calculated as 2 times the standard deviation on the average value of n analyses.
SE	•	Often given as ±2SE, which is a measure of the internal precision, used to quote the error on an individual analysis.
SIMS	•	Secondary ion mass spectrometry
SpA	•	Super purity acid (not as clean as UpA)
Std.	•	Standard
TIMS	•	Thermal ionization mass spectrometry
TPB	•	Total procedural blank
UpA	•	Ultra purity acid (cleaner than SpA)
µm	•	Micron, a 1/1000 mm
VICE	•	Very incompatible elements

References

Ellam, R. M. & Stuart, F. M. (2004): Coherent He-Nd-Sr isotope trends in high $^{3}He/^{4}He$ basalts: implications for a common reservoir, mantle heterogeneity and convection. Earth and Planetary Science Letters, 228: 511-523.

Farley, K. A., Natland, J. H., & Craig, H. (1992): Binary mixing of enriched and undegassed (primitive?) mantle components (He, Sr, Nd, Pb) in Samoan lavas. Earth and Planetary Science Letters, 111: 183-199.

Hanan, B. B. & Graham, D. W. (1996): Lead and helium isotope evidence from oceanic basalts for a common deep source of mantle plumes. Science, 272: 991-995.

Hauri, E. H., Whitehead, J. A., & Hart, S. R. (1994): Fluid dynamic and geochemical aspects of entrainment in mantle plumes. Journal of Geophysical Research, 99(B12): 24275-24300.

Hofmann, A. W. (1997): Mantle geochemistry: the message from oceanic volcanism. Nature, 385: 219-229.

Plank, T. & Langmuir, C.H. (1998): The chemical composition of subducting sediment and its consequences for the crust and mantle. Chemical Geology, 145: 325-394.

Stuart, F. M., Lass-Evans, S., Fitton, J. G., & Ellam, R. M. (2003): High $^{3}He/^{4}He$ ratios in picritic basalts from Baffin Island and the role of a mixed reservoir in mantle plumes. Nature, 424(3): 57-59.

Thirlwall, M. F., Gee, M. A. M., Taylor, R. N., & Murton, B. J. (2004): Mantle components in Iceland and adjacent ridges investigated using double-spike Pb isotope ratios. Gechimica er Cosmochimica Acta, 68(2): 361-386.

Weaver, B. L. (1991): The origin of ocean island basalt end-member compositions: trace element and isotopic constraints. Earth and Planetary Science Letters, 104: 381-397.

CHAPTER 1

Origin of extreme $^3He/^4He$ signatures in Icelandic lavas: Insights from melt inclusion studies

1.1 Abstract

The variation in He isotopes in many basaltic suites is a puzzle and frequently difficult to link with lithophile chemical and isotope tracers. To link He isotope and lithophile element variations, we characterize major, volatile, and trace element compositions of olivine-hosted melt inclusions (MIs) from three ankaramites from Vestfirdir, the northwest peninsula of Iceland. Olivine separates from two of these lavas have $^3He/^4He$ signatures as high as 42.9 R/R_a, and thus our data provide means to link the He isotope signature with that of the more lithophile elements and isotope systems.

The olivine-hosted MIs reveal substantial major and trace element variations in comparison to the host lava suite e.g. MgO (5.2-10.8 vs. 19.8-25.7 wt.%), K_2O+Na_2O (0.7-4.0 vs. 0.9-1.4), $(La/Y)_N$ (0.8-6.0 vs. 2.0-3.0). Modelling of the major and trace element systematics between MIs and host lavas suggest that they are related by accumulation and fractionation of olivine, clinopyroxene ± plagioclase. The variations in incompatible trace element ratios within the MIs reflect difference in depth and degree of melting. The chemical variations within the MIs further imply that these MIs sample melts derived from at least two distinct mantle sources. It is suggested that one of these mantle sources carries primitive to possible enriched mantle characteristics that may relate to a recycled component. The other mantle source indicated by the MIs relate to a depleted mantle component similar to MORB or ancient depleted mantle.

1.2 Introduction

Helium isotopes are a potentially powerful tool for identifying and tracking different mantle chemical domains. Traditionally, ^3He in mantle derived rocks is believed to represent a primordial volatile component (Farley & Neroda, 1998; Graham, 2002), and high $^3He/^4He$ ratios in oceanic island basalts (OIB) to reflect contributions of ^3He from a relatively undegassed mantle reservoir (e.g. Hart et al., 1992; Hilton et al., 1995; Farley & Neroda, 1998; Hilton et al., 1998; Hilton et al., 1999; Hilton et al., 2000; Graham, 2002). In contrast, melts derived from

mantle sources, such as the mid-ocean ridge basalt (MORB) source, that have been melt depleted and degassed at some time in the past, and/or that might contain a high proportion of He derived from U and Th decay, have correspondingly low $^{3}He/^{4}He$ ratios (Graham, 2002). Likewise, recycled components (e.g. HIMU, EMI, EMII) have radiogenic He signatures due to extensive degassing during emplacement and subsequent processing during subduction and re-melting. This relatively simple model is widely accepted, although alternative interpretations exist. Anderson (1998a & 1998b) suggests that the high $^{3}He/^{4}He$ ratios observed in OIB are due to low ^{4}He or low time integrated U and Th and not excess primordial ^{3}He. It has been further implied that the high $^{3}He/^{4}He$ signature is not an inherited characteristic from an undegassed primordial reservoir, but rather originates within a shallow *He-recharged* refractory mantle reservoir (Anderson, 1998a; Anderson, 1998b; Meibom et al., 2003; Stuart et al., 2003; Ellam & Stuart, 2004). Recent experimental studies show He to be less incompatible than U and Th during mantle melting, which, in contrast to previous assumptions, indicates that it is possible to retain an unradiogenic He signature in depleted mantle residues (Parman et al., 2005). Clearly, further work is needed to better understand the message that He isotopes are delivering.

A complication for understanding the origin of He isotope variations in mantle derived magmatic suites is assessing the relationships between He isotope compositions and those of lithophile or chalcophile chemical and isotope tracers. Although *co-variation* of He isotope compositions with trace element and isotope signatures are observed in some locations (e.g. Graham et al. 1996; Eiler et al., 1998; Stuart et al., 2003; Ellam & Stuart, 2004) there are no clear global systematics (e.g. Graham, 2002; Hofmann, 1997). Furthermore, in contrast to He, there is little evidence from lithophile element abundances and the isotopes of Sr, Nd, and Pb for the survival of primitive mantle (Hofmann et al., 1986; Hofmann, 1997; Graham, 2002). Two primary complications exist for interpreting the variation in He isotope compositions relative to lithophile and chalcophile element and isotope tracers. Firstly, the geochemical behaviour of He (and other noble gases) is markedly different from Sr, Nd, Os, O, REE, and other non-volatile tracers and this may lead to fractionation and/or decoupling between He and lithophile elements during the formation and evolution of mantle derived magmas (e.g Valbracht et al., 1996; Graham, 2002). The second issue is related to sampling. In subaerial and shallow submarine samples, where volatile elements have degassed from the melt, He isotopes are most often measured in separates of phenocryst minerals (generally olivine or clinopyroxene). He and other volatile elements do not derive directly from these minerals, but are entrapped in melt or fluid inclusions, which are released during crushing or melting. In contrast, major and trace element compositions and lithophile and chalcophile isotope systems (Sr, Nd, Pb, Hf, Os), are typically measured on bulk rock powders or in matrix glasses where these are available. This leads to a potential sampling bias, which is often largely ignored, as it is well-established that in a given magmatic system phenocryst phases may have experienced

considerably different magmatic evolution than the melts within which they are eventually erupted (e.g. Davidson et al., 2001; Kent et al., 2002a; Ramos & Reid, 2005; Charlier et al., 2006; Davidson et al., 2007). Thus there is no *a priori* guarantee that the isotope composition of trapped He measured in phenocrysts, and the lithophile and chalcophile tracers measured in bulk rock or glass samples (or even in other phenocryst phases) represent equivalent samples - particularly given the differences in geochemical behaviour of He and lithophile and chalcophile elements - although this is often implicitly assumed to be the case for He isotope studies (e.g. Hilton et al., 1997; Graham et al., 1998; Breddam & Kurz, 2001; Stuart et al., 2003; Macpherson et al., 2005).

In this study we address this question by chemical analysis of silicate MIs within olivine phenocrysts from rocks with well characterized He and radiogenic isotope compositions (Breddam & Kurz, 2001; Hilton et al., 1999; Breddam et al. in prep.). MIs represent samples of the melt compositions present during olivine growth, and thus provide a means to link the bulk composition of the final erupted lava with that present at the time of phenocryst growth and He entrapment. If MI compositions can be shown to be representative of the composition of the lava then this is strong evidence that He isotope compositions measured from olivine separates can also be directly equated with the chemical and isotope compositions of the bulk lava sample. Studies of olivine hosted MIs might also provide a better understanding of the origin of He isotope variations observed among magmatic rocks.

We have measured the volatile (S and Cl), trace, and major element composition of olivine hosted MIs from three Miocene (14 ±0.5 Ma, Berddam et al. in prep) ankaramite lavas from Vestfirdir, NW Iceland. These lavas were selected because olivine separates from these rocks show some of the highest non-cosmogenic $^3He/^4He$ ratios yet measured in terrestrial lavas – up to 42.9 ±0.3 R/R_a[1] (Breddam & Kurz, 2001; Breddam et al., in prep). Further, they have Sr-Nd-Pb isotope compositions that overlap those of the proposed common mantle endmember[2] (C, FOZO, or PHEM, see details in Farley et al., 1992; Hart et al., 1992; Hauri et al., 1994; Hanan & Graham, 1996; Hilton et al., 1999; Starcke et al. 2005). This lead Hilton et al. (1999) to proposed that these lavas characterize the He isotope composition of FOZO, which relies on the assumed equivalence of Sr-Pb-Nd and trace element compositions to He isotope measurements in olivine phenocrysts. Chemical characterization of MIs in olivine from these samples provides a mean to test the relation between phenocrysts, melt, bulk lava, and volatile compositions, and to relate lithophile element signatures to the He isotope composition in these important samples.

---

[1] R/R_a gives the $^3He/^4He$ of the sample relative to the atmospheric $^3He/^4He$ ratio.
[2] Also called the 5th mantle endmember. In the following it is collectively referred to as FOZO.

1.3 Geological framework

The North Atlantic Igneous Province (NAIP) covers a vast area extending from Baffin Island in the west to Norway and Great Britain in the east (Figure 1.1a), This volcanism is thought to be the result continental break up and the arrival of the mantle plume. Today the mantle plume interacts with the mid-oceanic ridge under Iceland giving rise to abundant magmatism compared to both north- and southward away from Iceland along the Mid-Atlantic Ridge. The three ankaramitic lavas of interest for this study are from Vestfirdir, the northwest peninsula of Iceland (Figure 1.1b). At Vestfirdir the flood basalt succession is cut by an unconformity marked by a major laterite-lignite bed. The lower lava pile dips 5° to the northwest and is associated with the extinct (by 14.9 Ma) paleo-rift zone located off-shore to the northwest (Hardarson et al., 1997). Above the unconformity the lavas dip 5° to the southeast, and are erupted from the Skagi-Snæfellsnes paleo-rift zone to which the rifting relocated ~14.9 Ma (Hardarson et al., 1997). The lavas investigated are sampled above the 14.9 Ma unconformity, at 350 m at Selardalur (408772[3]), and 600 m above at Lambadalur (408611) and Burfell (408624), (Figure 1.1c). Hence, they are related to the magmatic activity at Skagi-Snæfellsnes paleo-rift zone and are dated to 14 ±0.5 Ma (Breddam et al. in prep.). The activity at Skagi-Snæfellsnes died out ~7 Ma, at which time the rift had relocated itself to the Western Volcanic Zone (WVZ, ~8 Ma, Figure 1.1b), (Hardarson et al., 1997). The Mid-Atlantic Ridge is today represented by the WVZ and the Northern Volcanic Zone (NVZ), of which the later became active ~ 3 Ma (Hardarson et al., 1997). These two zones are offset along the Mid-Iceland Volcanic Zone (MVZ). In southern Iceland the Eastern Volcanic Zone (EVZ) is currently developing, and with time a ridge jump is expected, which will focus the extension from WVZ to EVZ. These relocations of the rift zone are the result of the general west NW movement of the plate (thus the plate boundary) over a steady plume (Hardarson et al., 1997). The Icelandic plume is today believed to be located below southeast Iceland (Staples et al., 1997; Darbyshire et al., 1998, Darbyshire et al. 2000, Maclennan et al., 2001; Foulger, 2006; Sigmarsson & Steinthórsson, 2007).

The Icelandic volcanism ranges from picritic, tholeiitic to alkali basaltic compositions (e.g. Chauvel & Hémond, 2000; Fitton et al., 2003; Kokfelt et al., 2006; Sigmarsson & Steinthórsson, 2007). The general consensus is that the picrites are derived from a component depleted in incompatible elements combined with radiogenic Nd and unradiognic Sr-Pb isotope composition (Chauvel & Hémond, 2000; Skovgaard et al., 2001; Kokfelt et al., 2006). Alkali basalts are suggested to originate from melting of a component enriched incompatible elements and with unradiogenic Nd, and radiogenic Sr-Pb signatures (Chauvel & Hémond, 2000; Kokfelt

[3] Lava sample 408772 is equal to SEL97 of Hilton et al. (1999).

et al., 2006). In contrast, tholeiitic compositions intermediate between picrites and alkali basalts are suggested to represent mixtures of the two melt types (Chauvel & Hémond, 2000; Kokfelt et al., 2006). He-Sr-Nd-Hf-Os-Pb isotope evidence have been used to argue that at least four different mantle components are sampled by the Icelandic mantle plume - two are enriched and two are depleted (Skovgaard et al., 2001; Thirlwall et al., 2004; Kokfelt et al., 2006). The depleted and enriched refer to VICE/MICE <1 and >1 ratios, respectively (e.g. Nb/Zr, Ba/Y, La/Y etc.). These components are in turn suggested to represent different parts of recycled oceanic lithosphere (e.g. Skovgaard et al., 2001; Thirlwall et al., 2004; Kokfelt et al., 2006). However, it is debatable whether or not the ambient North Atlantic depleted MORB mantle participates in the melt generation on Iceland (e.g. Chauvel & Hémond, 2000; Hanan et al., 2000; Fitton et al., 2003; Thirlwall et al., 2004; Kokfelt et al., 2006).

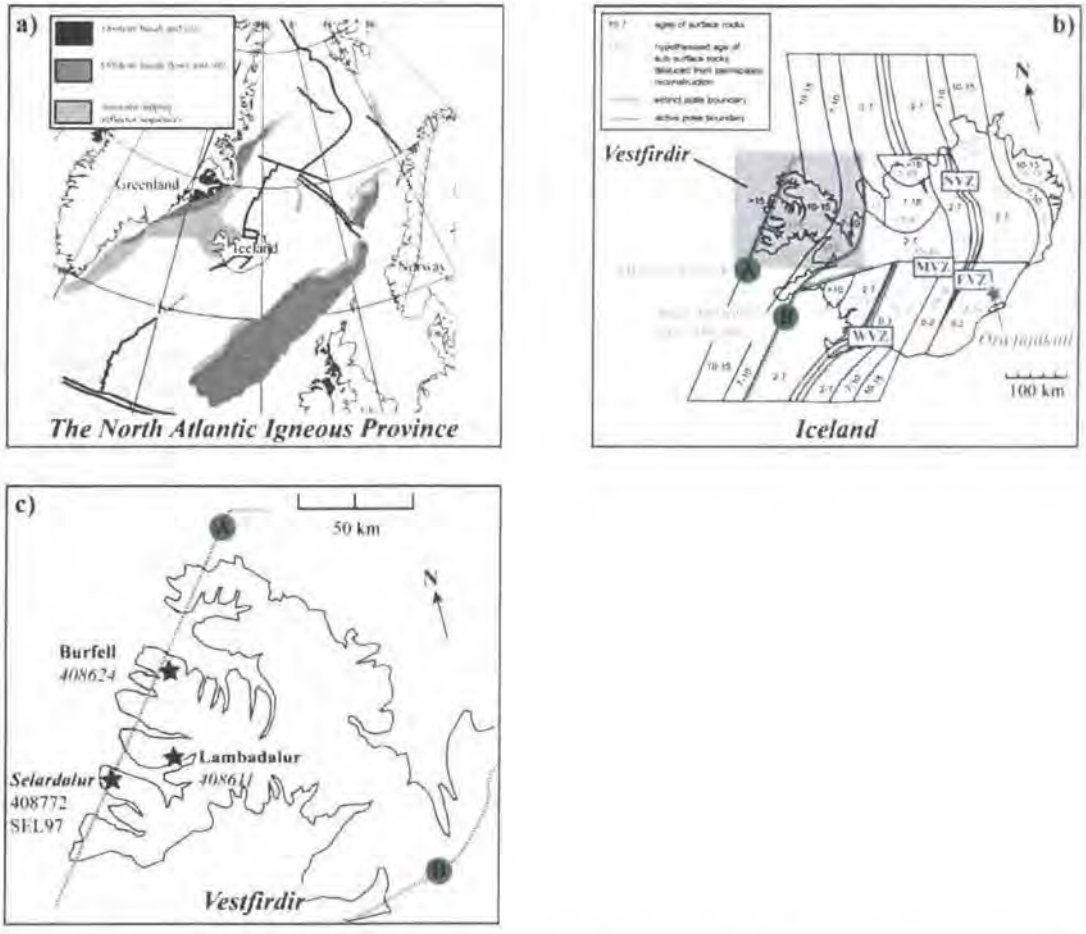

Figure 1.1: a) Map of the North Atlantic Igneous Province (NAIP), notice that the western most volcanic rocks of Baffin Island are not included (after Larsen et al., 1995). b) Map of Iceland showing the present plate boundaries (or rift zones) including the Western, Eastern, Middle and Northern Volcanic Zones (after Foulger & Anderson, 2005). Also shown is the NW paleo-rift zone (A) and Skagi-Snæfellsnes paleo-rift zone (B), which respective became extinct by 14.9 Ma and after 7 Ma (Hardarson et al., 1997). Vestfirdir (NW peninsula of Iceland) is marked by the grey background. The grey star is the location of radiogenic $^{87}Sr/^{86}Sr$ Öræfajökull lavas (Prestvik et al., 2001). c) Vestfirdir sample locations, also included is sample SEL97 (Hilton et al., 1999). The Vestfirdir ankaramites are dated to 14 ±0.5 Ma and are related to the magmatism from Skagi-Snæfellsnes paleo-rift zone (Breddam et al., in prep). Detailed geological map of Iceland is located in Appendix A1.

1.4 Analytical and experimental approach

Olivine grains were handpicked and examined from three ankaramites. Initial observation showed that MIs were relatively abundant in these rocks, but they consisted of mixtures of glass and crystalline phases due to slow post-eruptive cooling and, therefore, they were rehomogenised prior to analysis (Appendix A2). This was done by heating the olivine grains in a carbon crucible in the presence of excess fine powdered graphite in a vertical furnace at the University of Copenhagen. The experiments were carried out over a temperature range of 1200-1280°C at 1 atm in order to determine an approximate crystallization temperature. For the majority of MIs 1280°C appeared to be the lowest temperature at which MIs were completely homogenized. Hereafter, all heating experiments were done at 1280°C for 0.5 hour. Immediately after heating the sample material was quenched in contact with a metal plate in air. Subsequently, the olivine grains were mounted in 25 mm epoxy discs and polished in order to expose the interiors of olivine grains and contained MIs (Appendix A3). Each individual MI was then carefully examined under the microscope, and only primary MIs were selected for the analytical work.

The concentrations of major elements (MgO, SiO_2, FeO_{total}, Al_2O_3, TiO_2, CaO, K_2O, Na_2O, P_2O_5, and MnO), selected trace elements (Ni and Cr), and volatiles (S and Cl) in MIs and host olivine were analyzed by electron microprobe using either the JEOL JXA-8200 Superprobe at the at University of Copenhagen or the Cameca SX-50 at Oregon State University (USA). Analyses using both instruments were made using an accelerating voltage of 15 kV with a 15 nA electron beam defocused to a probe diameter of 5 μm. Standard data collected on three glass standards (BCR-2, BHVO-2, and LO-04-02) during electron microprobe sessions are reported in Table 1.1 and Appendix A5. The analyses of standard glasses show that the recommended concentrations for Na_2O, MgO, Al_2O_3, SiO_2, K_2O, CaO, MnO, and FeO are reproduced within -2.93 to 6.58%, and the concentrations of P_2O_3, TiO_2, and Cr_2O_3 are reproduced within -10.71 to 9.15%. Agreement within -0.42% is obtain for the Cl content of LO-04-02 reported by Kent et al. (1999) and the content measured in this study 0.14 wt.% ±0.01 (2SD, n=140). The average S concentration obtained is 0.11 wt.% ±0.04 (2SD, n=140), this value overlaps the reported value of 0.07 wt.% (n=5) by Kent et al. (1999).

Analysis of trace element (Sc, Ti, Rb, Sr, Y, Zr, Nb, Cs, Ba, La, Ce, Pr, Nd, Sm, Eu, Gd, Dy, Er, Yb, Hf, Ta, Pb, Th, and U) concentrations in selected MIs were performed by laser ablation ICPMS (LA-ICPMS) analysis at Oregon State University. Analyses used a New Wave DUV 193nm ArF Excimer laser and a VG PQ Excell quadrupole ICPMS. Analyses were made under analytical conditions similar to those given in Kent et al. (2004), using a laser spot size of 30 or 50 μm diameter and pulse frequency of 3-4 Hz. Pulse energy was typically 10-12 J/cm^2 and individual analyses represent 40 seconds ablation (Appendix A4). Individual analyses were

corrected for background contributions using intensities measured for 30 seconds prior to each analysis. Concentrations of selected trace elements were calculated using ^{43}Ca as an internal standard and USGS basaltic glass standard BCR-2 as a calibration standard (Table 1.2). Analytical accuracy and precision were assessed by analysis of basalt glass standard BHVO-2 as a secondary standard (Table 1.2). The trace element concentrations of BCR-2 and BHVO-2 are reproduced within respectively -2.72 to 0.50% and -12.47 to 10% of the recommended concentrations (Appendix A6). The larger errors reported for the trace element data collected on BHVO-2 relate to the lower concentrations of most trace elements in BHVO-2 than in BCR-2 (Table 1.2).

Electron microprobe rock standard data			
Std. ID	**BHVO-2**	**BCR-2**	**LO-02-04**
n	148	146	140
Al_2O_3	1.13	1.30	0.57
MnO	0.51	-2.93	6.21
K_2O	-1.25	0.07	-0.93
Cl	-	-	-0.42
Na_2O	6.58	2.87	3.11
SiO_2	1.16	2.17	0.03
FeO	-0.28	-0.84	1.92
CaO	3.52	2.39	5.37
S	-	-	60.08
MgO	1.74	4.38	-0.39
TiO_2	2.43	3.61	9.15
Cr_2O_3	-10.71		4.35
P_2O_3	-3.20	1.97	-10.59

Table 1.1: Summary table of average major, trace, and volatile concentrations collected on basaltic glass standards (BCR-2, BHVO-2, and LO-04-02) during electron microprobe session using the JEOL JXA-8200 Superprobe at the Department of Geography and Geology - Geology Section (University of Copenhagen) or a Cameca SX-50 at Oregon State University. Values are given as Δ%, which is the difference in % between the measured average and the recommended values. The vertical bars mark no data. The full data set is located in Appendix A5. Kent et al. (1999) published reference data for LO-04-02, and reference data for the two USGS standards are given by http:/minerals.cr.usgs.gov/geochem/basaltbcr2.pdf and http:/minerals.cr.usgs.gov/geochem/basaltbhvo2.pdf.

Also presented are trace element compositions obtained by double focusing magnetic sector field ICPMS of individual MIs sampled by micro-milling, and processed through a down scaled version of standard dissolution procedure for silicates. This procedure is described in details in *Chapter 2*, and therefore not further discussed here.

Electron microprobe measured compositions of MIs and their host olivine were used to evaluate the degree of equilibration during homogenization. The calculated K_d value for FeO-MgO exchange between olivine and inclusion ($K_d = olivine_{FeO/MgO}/melt_{FeO/MgO}$) was compared with the accepted value for mantle derived melts at low pressure (0.30 ±0.03, Roeder & Emslie, 1970). MIs, with calculated K_d values different from 0.30 were corrected by incrementally adding or

subtracting equilibrium olivine to/from the melt composition until a K_d of 0.30 was reached. The amount of olivine added or removed by this process will result in dilution or enrichment in the absolute abundance of the incompatible trace elements, but since these were generally less than analytical uncertainties no corrections to trace element abundances were made. This will not significantly alter incompatible element ratios.

LA-ICPMS standard data

Std. ID	BCR-2	BHVO-2	Std. ID	BCR-2	BHVO-2
n	81	23	n	81	23
Element	Δ%	Δ%	Element	Δ%	Δ%
Sc	0.02	-0.67	Nd	-0.91	-5.09
Ti	0.03	0.97	Sm	-0.93	-7.77
Rb	0.11	0.93	Eu	-1.14	-2.13
Sr	0.27	3.52	Gd	-1.22	*-12.47*
Y	0.50	-8.54	Dy	-1.51	*-10.84*
Zr	0.45	-9.41	Er	-1.37	*-10.45*
Nb	0.05	2.29	Yb	-1.53	-6.93
Cs	-0.65	-	Hf	-1.36	-5.52
Ba	-0.29	3.61	Ta	-1.87	-5.26
La	-0.12	-4.12	Pb	-2.72	10.00
Ce	-0.35	3.01	Th	-2.28	-3.29
Pr	-0.60	-0.99	U	-2.25	2.12

Table 1.2: Summary table of the average trace element LA-ICPMS data collected on USGS basaltic glass standards (BCR-2 and BHVO-2). The analysis run on a VG Elemental Excell quadrupole ICPMS equipped with a New Wave DUV 193nm ArF Excimer laser at College of Oceanic and Atmospheric Sciences (Oregon State University). Details on the instrumentation are located in Appendix A4, and the full data set is located in Appendix A6. Δ% is the difference in % between the measured average and recommended values. Recommended values for BCR-2 and BHVO-2 are published by USGS (http:/minerals.cr.usgs.gov/geochem/basaltbcr2.pdf and http:/minerals.cr.usgs.gov/geochem/basaltbhvo2.pdf).

Measured S and Cl contents were also used to screen out MIs that breached and degassed along fractures during rehomogenization (or at low pressure during eruption), as these elements should degas completely from breached MIs during reheating at atmospheric pressure. As noted by Nielsen et al., (1998), the composition of breached MIs may also have been altered by subaerial weathering along fractures. The FeO contents of the Vestfirdir MIs suggest primary S contents of ~1000 ppm (Mathez, 1976), however MIs show a range of S contents from ~0 to 1000 ppm. We interpret this to be the result of low pressure degassing prior to melt trapping, in addition to degassing of breached MIs during homogenization, and this is consistent with the general observation that MIs with low S also have the lowest Cl contents. A limit of 200 ppm S was selected as the lower limit of acceptance, and MIs with S contents lower than this were not used for this study.

1.5 Sample characteristics

1.5.1 Petrology and geochemistry of the Vestfirdir lavas

The lavas selected are highly porphyritic (≥50% phenocrysts) as shown in Figure 1.2a-c. Olivine is the most abundant phenocryst phase (20-30% modal abundance), with clinopyroxene (5-20%) and minor plagioclase (<5%). The olivine phenocrysts show distinctive crystals faces but are often subrounded (euhedral to subhedral). Minor alteration is apparent along rims and fractures. Clinopyroxene and plagioclase show similar textures as the olivine phenocrysts, but often show twinning and zoning which is absent in the olivine phenocrysts. The phenocrysts are set in a medium-grained groundmass mainly consisting of fine plagioclase laths, with smaller micro phenocrysts of clinopyroxene, olivine, and oxides also present.

On a total alkali versus silica plot the Vestfirdir lavas plot in the tholeiitic basalt field (Figure 1.3a). However, we follow Breddam et al. (in prep), who suggest, on basis of the modal proportion of olivine and clinopyroxene and their strong alkaline affinity (see below) that the lavas are referred to as ankaramites. The Vestfirdir ankaramites have broadly similar major element concentrations, although 408611, and 408772 have higher MgO, Ni and Cr combined with lower CaO and SiO_2 compared to 408624 (Figure 1.3, Table 1.3). These systematic differences are likely to be explained by different amounts of accumulation of olivine and clinopyroxene (section 1.5.6). The cumulative origin of these lavas is further supported by their strongly porphyritic nature (Figure 1.2a-c). Sample 408611 differs slightly from 408624 and 408772 by having higher Al_2O_3 and K_2O, but lower TiO_2, even if differences in crystal accumulation are taken into account.

The parental melts are enriched in LREE as the ankaramites have $(La/Y)_N$ of 2.0-3.0 and $(Ce/Sm)_N$ of 1.1-1.4. Primitive mantle normalized trace element abundance patterns show depletions in Rb, Ba, Th, U, and K relative to the neighbouring incompatible elements such as Ta and La (Figure 1.4). The multi trace element patterns of the three lavas are very similar, however 408611 is not as depleted in HREE as 408624 and 408772. The enriched nature of the ankaramites, specifically their higher trace element abundances and ratios, indicate a stronger affinity with the Icelandic alkali basalts than the depleted picrites (Figure 1.4a-b).

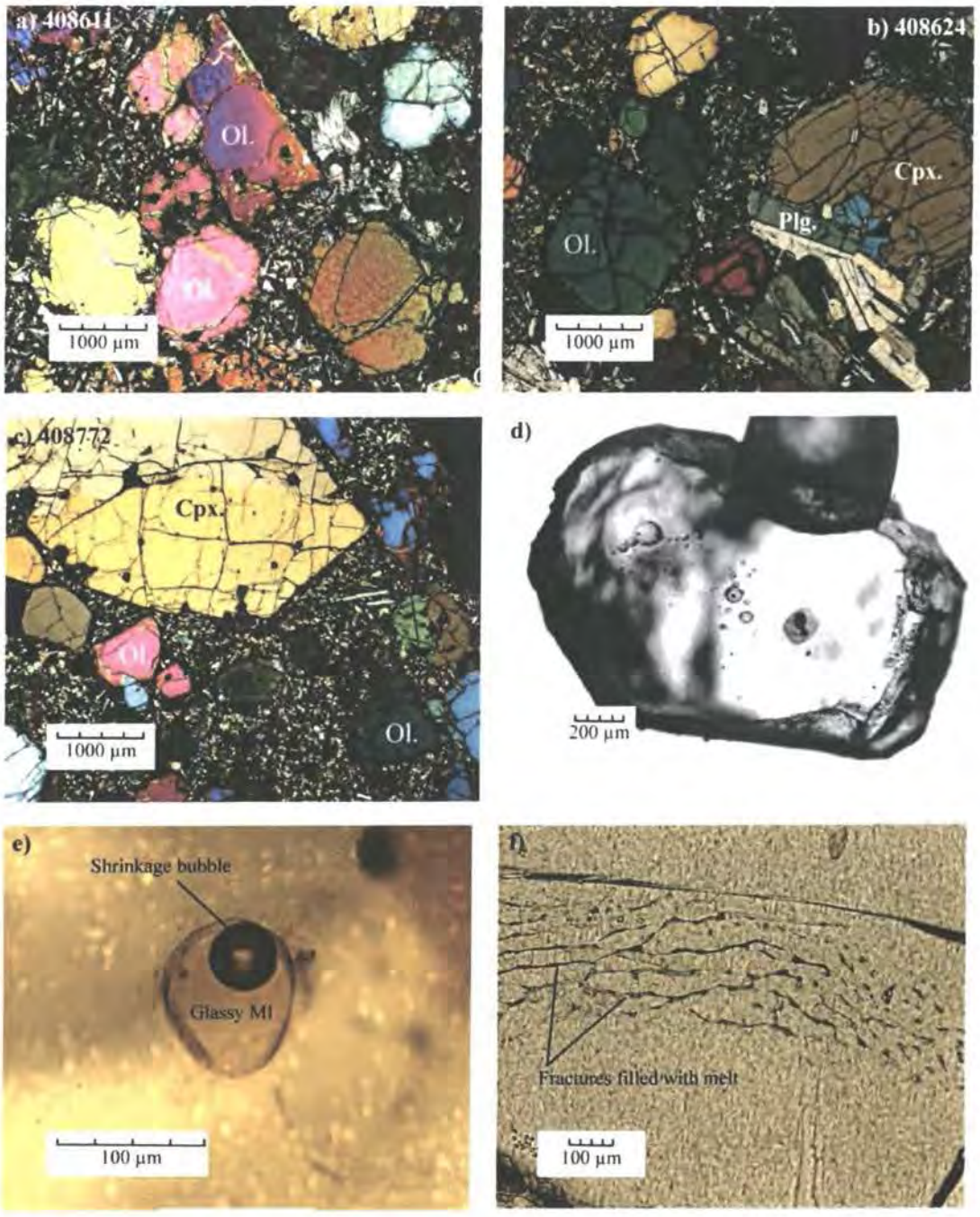

Figure 1.2: a), b), and c) show thin sections of the three Vestfirdir ankaramites of this study in cross-polarized light - 408611, 408624, and 408772, respectively. d) Olivine grain with multiple MIs. e) Example of the most abundant primary MIs - glassy MI with shrinkage bubble. f) Rare olivine grain with fracture filled with secondary melt.

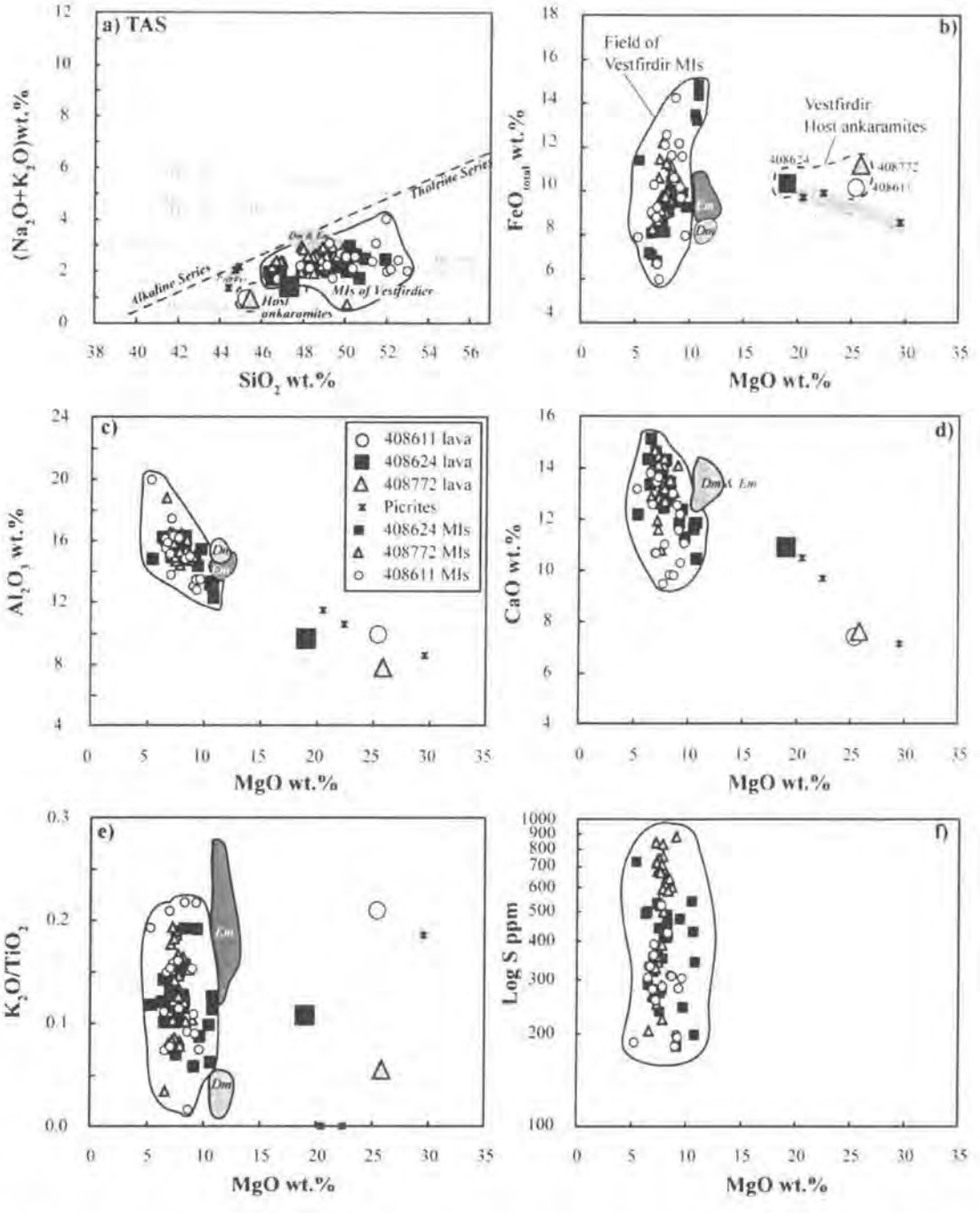

Figure 1.3: Major, trace, and volatile element compositions of olivine-hosted MIs and host ankaramites of Vestfirdir. a) TAS classification diagram shows that both MIs and host lavas plot in the field of basaltic tholeiites. Subdivision into tholeiite and alkaline series are according to MacDonald (1968). b) FeO_{total} vs. MgO, c) Al_2O_3 vs. MgO, d) CaO vs. MgO, and e) K_2O/TiO_2 vs. MgO, f) S versus MgO, notice data below 200 ppm were rejected. g) $(La/Y)_N$ vs. $(Ce/Sm)_N$, h) Nb_N vs. Rb_N. Closed symbols in g) and h) is MI data sampled by the micro-milling technique presented in *Chapter 2* and presented in *Chapter 3*. Enriched (*Em*) and depleted (*Dm*) MI fields and host picrites of the Neovolcanic rift zone of Iceland are included for comparison (Gurenko & Chaussidon, 1995).

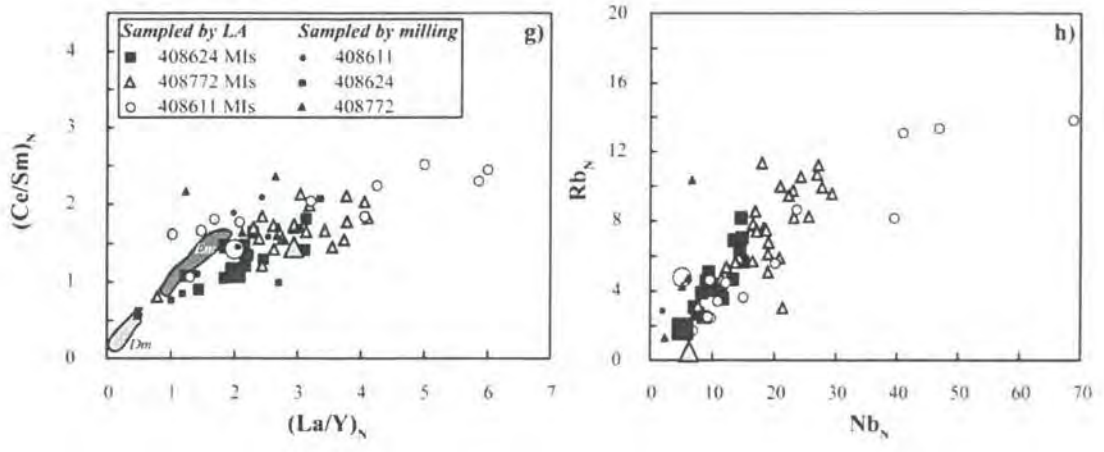

Figure 1.3: Continued

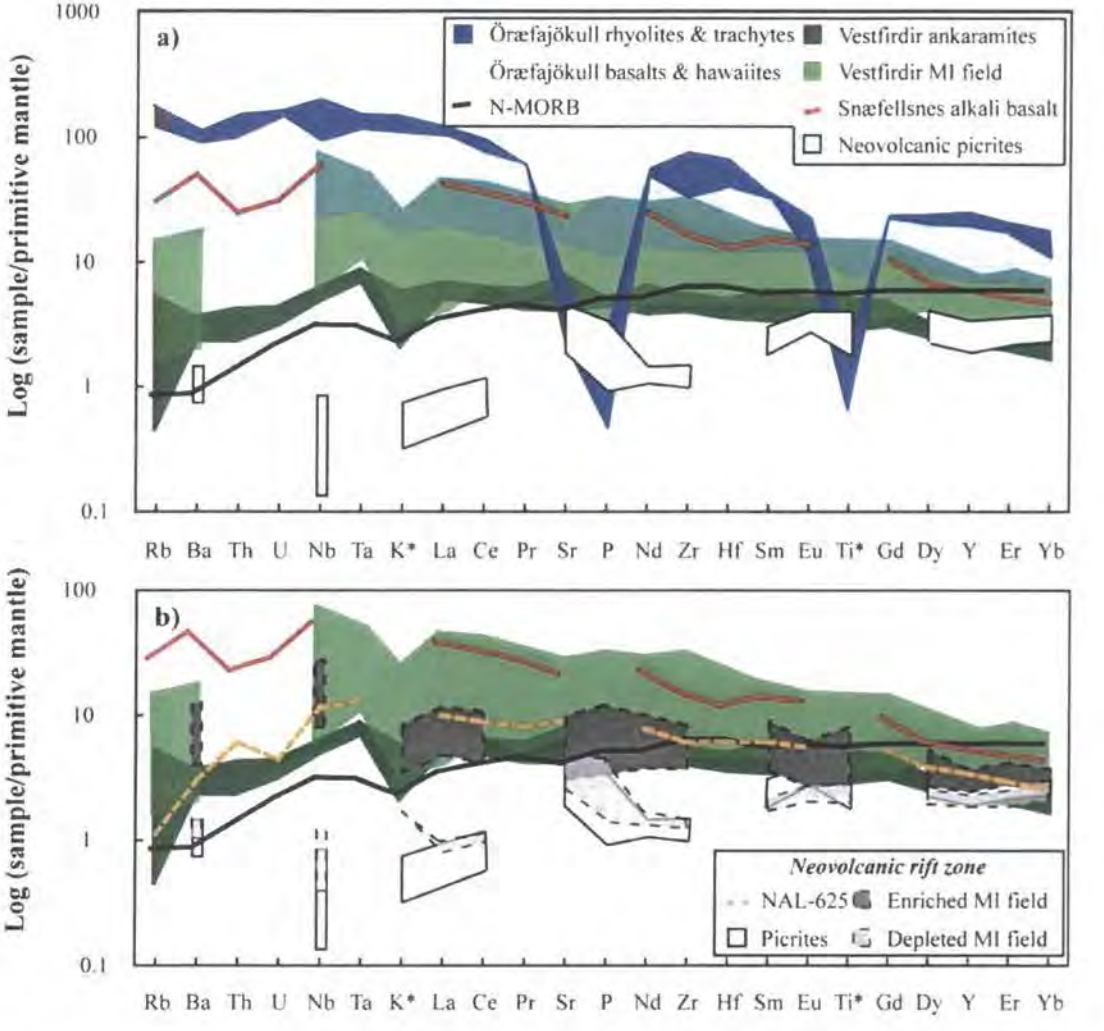

Figure 1.4: See caption on next page.

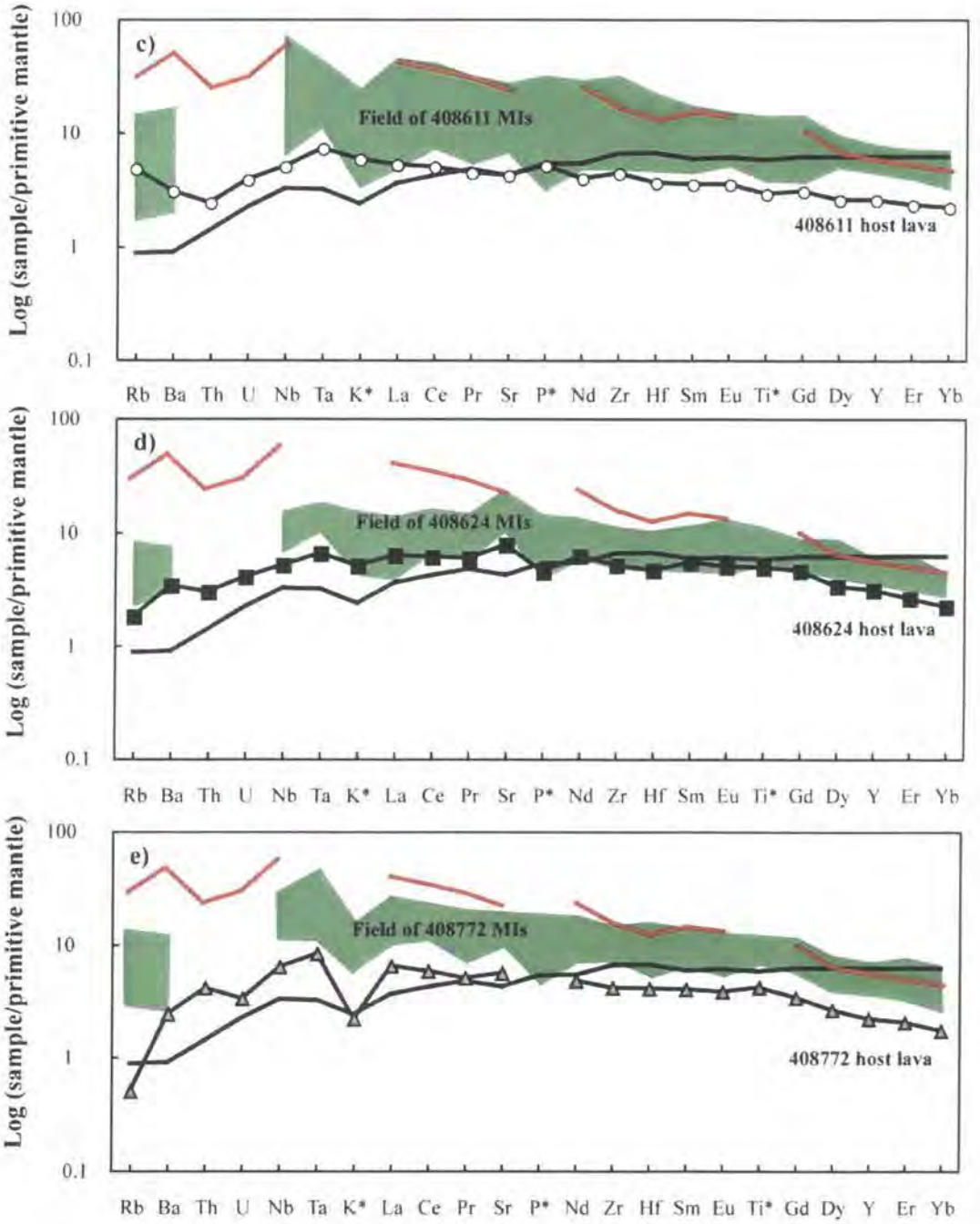

Figure 1.4: Primitive mantle normalized multi element diagrams of MIs and host lavas. All concentrations are analyzed by LA-ICPMS except Ti, K, and P (marked by *), which are obtained by electron microprobe analyses. Normalizing is after (Sun & McDonough, 1989). a) Comparison of the Vestfirdir ankaramites and MIs with a Snæfellsnes alkali basalt (SNS24; Chauvel & Hémond, 2000) and a suite of picrites from and the Neovolcanic Rift Zone of Iceland (Gurenko & Chaussidon, 1995). Also plotted are the younger high $^{87}Sr/^{86}Sr$ lavas of Öræfajökull divide into 'basalts & hawaiites' and 'rhyolite & trachytes' (Prestvik et al., 2001). The reference N-MORB composition is from Sun & McDonough (1989). b) Comparison of the Vestfirdir MI field with the depleted and enriched MI fields revealed in the picrites of Neovolcanic Rift Zone (Gurenko & Chaussidon, 1995). Also plotted is the enriched high $^{3}He/^{4}He$ picrite NAL-625 from Valdalda, which bear strong resemblance to the Vestfirdir ankaramites (Macpherson et al., 2005). In c), d), and e) each of the three ankaramite samples are plotted with their MIs.

Sample ID	408611	408624	408772	SEL97
Rock	*Ankaramite*	*Ankaramite*	*Ankaramite*	*Ankaramite*
Latitude	65.85	66.06	65.7646	-
Longitude	-23.25	-23.30	-24.0419	-
Location	*Lambadalur*	*Burfell*	Selardalur	*Selardalur*
Major elements (wt.%)				
SiO_2	44.94	47.08	45.13	45.94
TiO_2	0.63	1.07	0.90	1.19
Al_2O_3	9.87	9.61	7.70	9.72
MgO	25.17	18.89	25.66	18.74
CaO	7.35	10.85	7.54	10.15
Fe_2O_3	2.07	2.03	2.16	-
FeO	8.23	8.46	9.154	-
Cr_2O_3	0.39	0.27	0.44	0.51
NiO	0.13	0.08	0.13	0.10
MnO	0.17	0.17	0.17	0.15
Na_2O	0.81	1.29	0.87	1.18
K_2O	0.13	0.12	0.05	0.05
P_2O_5	0.11	0.10	0.09	0.06
Total	100	100	100	-
Mg#	84.0	79.4	82.9	77.3
FeO_{total}	10.09	10.29	11.10	11.53
Na_2O+K_2O	0.94	1.40	0.92	1.23
Selected PM normalized trace element ratios				
$(Ce/Sm)_N$	1.43	1.12	1.44	1.36
$(La/Y)_N$	2.00	2.02	2.95	2.18
$(Rb/Sr)_N$	1.14	0.23	0.09	0.48
$(Sr/Nd)_N$	1.06	1.26	1.16	2.12
$(Ti/Zr)_N$	0.63	0.95	0.99	0.82
$(Sm/Nd)_N$	0.89	0.88	0.84	0.88
$(Ba/Zr)_N$	0.70	0.66	0.58	0.71
ΔNb	0.03	-0.02	0.11	0.13

Table 1.3: Major compositions and selected trace element ratios of the three host ankaramites of Vestfirdir (NW Iceland) from Breddam et al. (*in prep.*). The full data set is located in Appendix A7. Also included for comparison is the ankaramite sample analyzed by Hilton et al. (1999) SEL97. Subscribed N denotes that the data is normalized to primitive mantle (PM) using the values from McDonough & Sun (1995).

The He-Sr-Nd-Hf-Os-Pb isotope composition obtained for the three host lavas are presented and discussed in detail in *Chapter 3* (Table 3.1), and therefore only mentioned briefly here. The Vestfirdir ankaramites have intermediate $^{87}Sr/^{86}Sr$ (0.70342-0.70368), high $^{143}Nd/^{144}Nd$ (0.51298-0.51304), and intermediate to slightly elevated Pb isotope ratios ($^{206}Pb/^{204}Pb$: 18.44-18.62, $^{207}Pb/^{204}Pb$: 15.47-15.52, $^{208}Pb/^{204}Pb$: 38.14-38.46) similar to that proposed for FOZO (Figure 1.5). Also, strong resemblance is observed between Sr-Nd-Pb isotope compositions of these ankaramites and the Öræfajökull lavas (Prestvik et al., 2001). Both the $^{176}Hf/^{177}Hf$ and $^{187}Os/^{188}Os$ ratios are relative depleted compared to the overall range for OIB and range from

0.28311 to 0.28316 and 0.12632 to 0.13415 respectively. Two of the ankaramites (408624 and 408772) exhibit extremely high $^{3}He/^{4}He$ (42.9 and 34.8 R/R_a), which are among the most unradiogenic He values yet observed in terrestrial rocks. In contrast, sample 408611 has MORB-like $^{3}He/^{4}He$ (8.2 ±5.1 R/R_a), but also considerably lower He concentrations (and correspondingly less precise analysis). However, in every other aspect (major, trace, and isotope composition) these lavas are extremely similar, therefore the lower $^{3}He/^{4}He$ ratio of sample 408611 is suggested to be the effect of degassing rather than a source feature. Another explanation may be that the MIs in 408611 have a stronger input from a slightly more depleted low $^{3}He/^{4}He$ domain of the source region. Since, the focus of this chapter is on the major and trace elemental variation of the MIs from these lavas, the origin of the isotope variation of the host lavas are discussed in details elsewhere (*Chapter 3*). However, we reflect on the possible link between the geochemistry of the MIs and the He isotope signature of the host lavas.

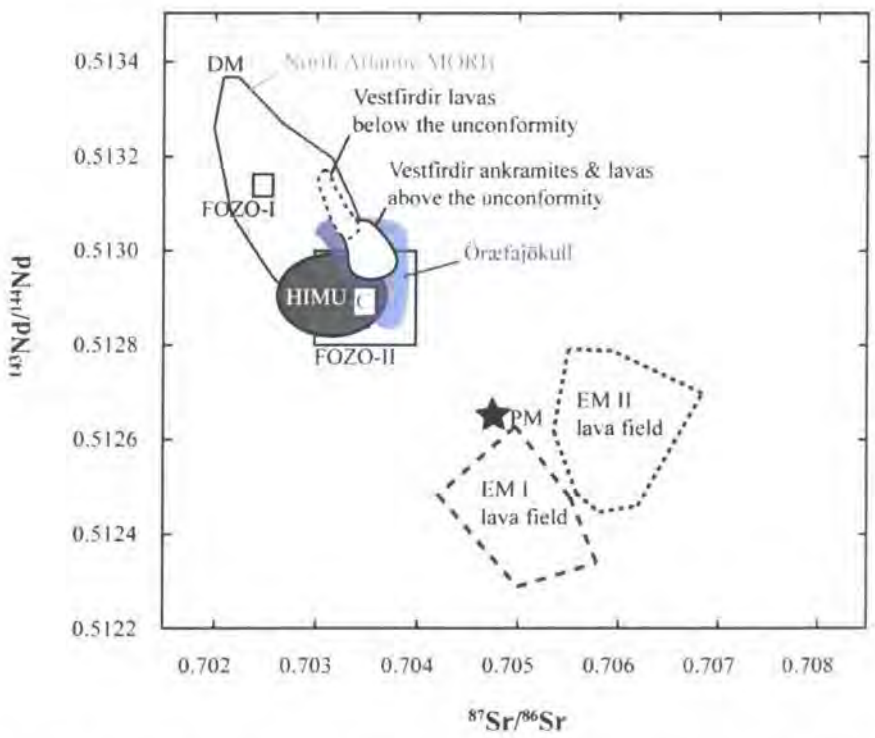

Figure 1.5: Sr-Nd isotope systematic of the Vestfirdir ankaramites (see *Chapter 3*). Lavas from above the unconformity in Vestfirdir plot with the ankaramites, whereas the lavas from below have less radiogenic Sr isotope ratios coupled with radiogenic Nd isotope ratios (Hardarson et al., 1997). Öræfajökull lavas (Prestvik et al., 2001). Lava fields of the North Atlantic MORB (representing melts derived from the depleted mantle DM), HIMU, EMI, and EMII, and primitive mantle (PM) are after Hofmann (1997). Also included are the proposed compositions of the 5th mantle endmember C (Hanan & Graham, 1996), FOZO-I (Hart et al., 1992), or FOZO-II (Hauri et al., 1994).

1.5.2 Geochemistry of phenocryst phases

Olivine: A substantial range is observed in the forsterite contents of the olivine phenocrysts ($Fo_{78.0-90.3}$), (Figure 1.6a-b, Table 1.4a). The olivine hosting MIs from 408611 show the whole range of Fo (79.9-90.3), whereas the majority of olivine in 408624 and 408772 have Fo between 84.4-88.3. The relatively CaO-rich nature of these olivine (0.19-0.36 wt.%) imply that they are phenocrysts of mantle derived magmas rather than olivine from mantle xenoliths (CaO <0.1 wt.% e.g. Hervig et al., 1986), (Figure 1.6b). The olivines have Ni contents between 1100-3300 ppm, and ~15% of the population have Ni contents >2500 ppm, suggesting that they formed in equilibrium with residual mantle (Korenaga & Kelemen, 2000).

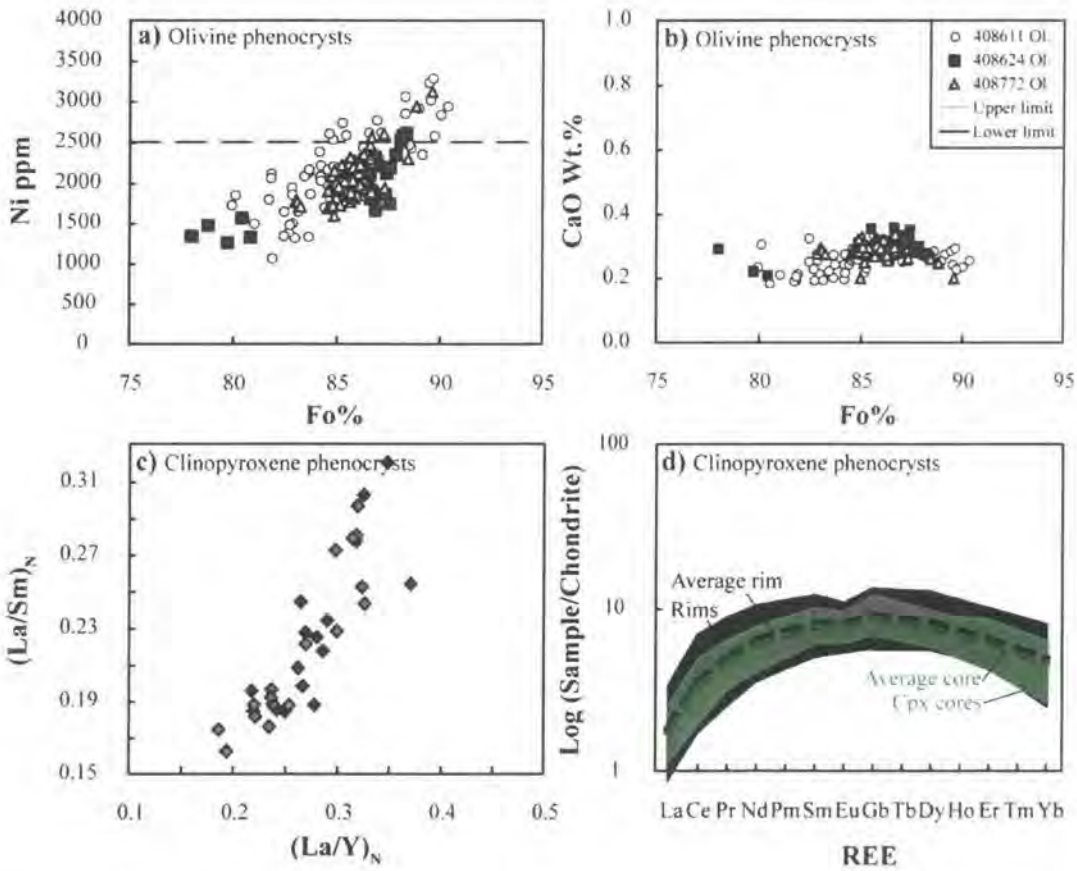

Figure 1.6: Composition of the olivine and clinopyroxene phenocryst of the Vestfirdir ankaramites. a) Fo% vs. Ni, and b) Fo% vs. CaO for olivine, and c) $(La/Y)_N$ vs. $(La/Sm)_N$ and, d) chondrite normalized REE patterns for clinopyroxene. Broken line in a) indicates the lower limit of Ni content in olivine thought to be in equilibrium with residual mantle (Korenaga & Kelemen, 2000). The black field represents the range of rim compositions and green field the range of core compositions. The bold broken line in black and green respectively represents the average rim composition and core composition. Chondrite normalized values are from Sun & McDonough (1989). The full dataset is presented in Appendix A8.

Clinopyroxene: Overall, the clinopyroxenes (diopside) show a coherent field of variation (Table 1.4b). Mg# ranges from 87.8 to 83.4, and as the compositions get more evolved the content of SiO_2, CaO, Al_2O_3, FeO_{total}, TiO_2, Na_2O increase (Table 1.4b, Appendix A8). The clinopyroxene

phenocrysts are depleted in LREE elements compared to MREE and HREE elements (Table 1.4c). $(La/Sm)_N$ varies from 0.16 to 0.32 and $(La/Y)_N$ from 0.19 to 0.37). Limited chemical differences are observed between core and rim compositions (Figure 1.6c-d).

408611 olivine phenocrysts (n=63)

wt%	Al_2O_3	MnO	K_2O	Na_2O	SiO_2	FeO	CaO	SO_3	MgO	NiO	TiO_2	Cr_2O_3	FO%
Ave	0.07	0.21	0.00	0.01	39.10	14.60	0.26	0.00	45.42	0.27	0.02	0.04	84.7
±2SD	0.09	0.10	0.01	0.01	1.69	5.07	0.07	0.01	4.04	0.13	0.02	0.04	5.59
Max	0.22	0.32	0.01	0.03	40.45	19.08	0.33	0.01	49.55	0.42	0.05	0.09	90.3
Min	0.01	0.10	-	-	37.25	9.38	0.19	-	41.87	0.14	-	-	79.9

408624 olivine phenocrysts (n= 33)

wt%	Al_2O_3	MnO	K_2O	Na_2O	SiO_2	FeO	CaO	SO_3	MgO	NiO	TiO_2	Cr_2O_3	FO%
Ave	0.20	0.18	0.00	0.01	39.07	13.70	0.30	0.00	46.16	0.25	0.01	0.05	85.7
±2SD	1.30	0.07	0.01	0.06	1.70	4.75	0.07	0.00	4.55	0.09	0.05	0.05	5.54
Max	3.69	0.31	0.01	0.15	40.39	20.25	0.36	0.01	48.65	0.33	0.14	0.10	88.4
Min	0.02	0.13	-	-	36.47	11.44	0.21	-	40.29	0.16	-	-	78.0

408772 olivine phenocrysts (n=72)

wt%	Al_2O_3	MnO	K_2O	Na_2O	SiO_2	FeO	CaO	SO_3	MgO	NiO	TiO_2	Cr_2O_3	FO%
Ave	0.06	0.19	0.00	0.01	39.41	13.67	0.29	0.00	46.08	0.26	0.01	0.04	85.7
±2SD	0.04	0.07	0.01	0.01	1.49	1.94	0.04	0.01	1.65	0.07	0.02	0.05	2.04
Max	0.11	0.28	0.02	0.02	40.71	16.29	0.34	0.01	48.65	0.40	0.05	0.12	89.6
Min	0.02	0.09	-	-	37.93	10.05	0.20	-	43.89	0.20	-	-	83.0

Table 1.4a: Continued Average (Ave) major element compositions (or oxide wt.%) of olivine phenocryst from the three Vestfirdir ankaramites. Also given are the compositional ranges given by Max (most primitive olivine) and Min (most evolved olivine). The full datasets are located in Appendix A8.

Clinopyroxene phenocrysts (n=19)

wt.%	Al_2O_3	MnO	Na_2O	SiO_2	FeO	CaO	MgO	NiO	TiO_2	Cr_2O_3	Mg#	Ni	CaO/Al_2O_3
Ave	3.85	0.13	0.26	51.62	4.88	20.87	17.05	0.05	0.54	0.74	86.16	287	5.65
±2SD	1.63	0.09	0.09	1.43	0.82	0.67	0.96	0.05	0.23	0.64	2.29	480	2.32
Max	5.32	0.23	0.33	52.70	5.90	21.65	17.96	0.10	0.85	1.24	87.83	794	7.73
Min	2.74	0.05	0.20	50.31	4.40	20.33	16.51	0.01	0.34	0.19	83.42	63	3.87

Table 1.4b: Average (Ave) major element compositions (or oxide wt.%) of clinopyroxene (Cpx.) phenocryst from the three Vestfirdir ankaramites. Also given is the compositional range given by Max (most primitive Cpx.) and Min (most evolved Cpx.). Notice the Ni content is given in ppm. Full data set is located in Appendix A8.

Average clinopyroxene core composition					Average clinopyroxene rim composition				
n=17	$Core_{Ave}$	±2SD	Max	Min	n=17	Rim_{Ave}	±2SD	Max	Min
Trace element concentrations (ppm)					**Trace element concentrations (ppm)**				
Sc	88.80	24.17	113.35	72.90	Sc	88.63	27.60	112.60	73.41
Ti	3089.01	814.05	3908.65	2233.93	Ti	3191.82	1286.15	4871.80	2213.50
Sr	18.40	6.14	23.20	12.99	Sr	18.26	5.57	21.45	13.07
Y	9.46	3.65	12.69	7.23	Y	10.24	6.30	16.81	7.05
Zr	9.95	3.99	13.74	7.27	Zr	10.03	6.35	16.17	6.27
Nb	0.06	0.09	0.17	0.04	Nb	0.04	0.03	0.06	0.02
La	0.40	0.23	0.62	0.27	La	0.42	0.38	0.81	0.21
Ce	1.96	1.21	3.02	1.20	Ce	2.11	1.86	4.28	1.05
Pr	0.44	0.20	0.61	0.30	Pr	0.46	0.33	0.84	0.24
Nd	2.72	1.05	3.64	1.92	Nd	2.91	1.88	4.92	1.68
Sm	1.14	0.32	1.53	0.93	Sm	1.20	0.67	1.87	0.78
Eu	0.44	0.17	0.61	0.35	Eu	0.45	0.20	0.63	0.31
Gd	1.73	0.56	2.47	1.43	Gd	1.81	1.03	2.75	1.16
Dy	1.86	0.68	2.47	1.47	Dy	2.03	1.22	3.26	1.43
Er	0.97	0.44	1.43	0.70	Er	1.04	0.65	1.69	0.74
Yb	0.76	0.36	1.08	0.45	Yb	0.81	0.61	1.38	0.43
Hf	0.45	0.19	0.63	0.34	Hf	0.47	0.31	0.78	0.29

Table 1.4c: Average (Ave) trace element compositions (ppm) of clinopyroxene (Cpx.) phenocryst from the three Vestfirdir ankaramites. Also given are the compositional ranges given by Max (most primitive Cpx.) and Min (most evolved Cpx.). Full datasets are located in Appendix A8.

1.5.3 Morphology and geochemistry of olivine hosted melt inclusions

MIs are abundant in olivine phenocrysts of the Vestfirdir ankaramites. Two types of MIs are observed: The dominant type of MIs are glassy (±shrinkage bubbles) spherical to ovoid in shape and range in size from 20 to 150 μm (Figure 1.2d-e). These MIs occur as isolated inclusions, largely in the cores of phenocrysts, and are interpreted to have been entrapped as olivine phenocrysts grew, and thus are considered primary following the classification of Roedder (1984). The second type of MIs are considerably smaller (<<5 μm) and occur as bands of glassy inclusions without shrinkage bubbles along late healed fractures within olivine grains (Figure 1.2f). These rare inclusion trails were only found in a couple of grains, and are assumed to represent a minor proportion of the total volume of melt trapped within MIs. From this, we suggest that they contribute relatively little to the amount of He released during crushing. In addition, volatile-rich fluid inclusions are not observed in any olivine from these lavas, and therefore we suggest that the larger primary MIs appear to be the dominant host of the volatiles in olivine in these samples.

The MIs typically have higher SiO_2 than their host lavas (46.4-53.0 wt.% vs. 45.0-47.1 wt.%) and total alkalis (0.7-4.0 wt.% vs. 0.9-1.4 wt.%) as well as distinctly lower MgO contents (5.2-10.8 wt.% compared to 18.9-25.7 wt.%), (Table 1.5, Figure 1.3). The MIs from the three lavas

show a range in Mg# from 56.0 to 71.6, which is lower than that observed in the host lavas (77.9-84.0), (Figure 1.6b). The majority of MIs from 408611 have higher FeO_{total} at a given SiO_2 content compared to the MIs of 408624 and 408772, which results in somewhat lower Mg#. Negative correlations are observed for MgO versus SiO_2, Al_2O_3, CaO, Na_2O, and there is a positive trend between MgO and FeO_{total} (Figure 1.3). Similar correlation trends are seen among the host lavas. TiO_2 (0.83-2.92 wt.%) and K_2O (0.03-0.53 wt.%) show a large compositional range, but neither of these components correlates with MgO or SiO_2. The overall, systematic variation of major elements appears governed by the fractionation of olivine in combination with clinopyroxene. In contrast, TiO_2 and K_2O are decoupled from the degree of differentiation. In general, the compositional field of the three populations of MIs overlap each other. However, the MIs of 408611 show greater viability, and often represent the two extremities of the compositional range e.g. see TiO_2, K_2O, FeO_{total}, and Al_2O_3.

The MIs of 408772 and 408624 tend to have slightly higher S concentrations than 408611 (200-876 versus 200-523 ppm, Figure 1.3f), although MIs with lower S occur in all samples and the Cl contents from all three samples overlap and range between 20-290 ppm. As noted above the Vestfirdir MI compositions plot below the concentrations suggested from sulphide saturation. This may be due to shallow degassing of S prior to trapping of some MIs, or may indicate that some melts were undersaturated with respect to S. Neither S nor Cl correlates with MgO or Fo% of the host crystal suggesting that concentration of volatiles is not linked with the degree of differentiation. Cl concentration shows good correlations with TiO_2, K_2O, and REE suggesting that these elements behaved similarly during the melting and differentiation. Furthermore, with the exception of a few MIs, the MI data show little variation in Cl/K_2O and Cl/TiO_2 ratios. The majority of Cl/K_2O ratios are within 2SD error of the average ratios of 0.042 ±0.024, which is comparable to values for the normal mantle, suggesting little widespread assimilation of Cl enriched material occurred, as observed at other ocean islands (Kent et al., 2002b). A small number of inclusions do have elevated Cl/K_2O (>0.1, single one as high as 0.19) and may indicate minor input, via assimilation of hydrothermally altered material (or seawater), which has been suggested elsewhere in Iceland (Eiler et al., 2000). However, these MIs do not show anomalous major or trace element compositions and have thus been included in the remainder of the study (although their removal would not significantly alter our conclusions).

Concentrations of incompatible trace elements are higher in MIs than in their respective host lavas (Figure 1.4), however REE-patterns and PM normalized trace element diagrams from MIs are broadly similar those from their hosts. The REE-patterns are fractionated, with LREE (Ce) at 20 to 115 times chondrite and HREE (Y) at 10 to 20 times chondrite. As with the host lavas, PM normalized trace element diagrams show characteristic depletion of Rb, Ba, U, Th, and K compared to Nb and Ta, La, and Ce. The trace element composition of the MIs of 408624 and

408772 show a relatively narrow range compared to the MIs of 408611 that range towards more enriched compositions. As an example the MIs of 408611 have $(La/Y)_N$ in the range of 1.0 to 6.0 whereas 408624 and 408772 in general have $(La/Y)_N$ <4.1. Furthermore, positive correlation is observed between $(La/Y)_N$ and $(Ce/Sm)_N$ versus K_2O/TiO_2, but also with S and Cl. None of these ratios or elements correlate with indices of differentiation (e.g. MgO or SiO_2). This implies that these variations are linked to the source region(s) and the degree of melting. Good correlations between mobile and immobile elements eg. Nb vs. K_2O, Ba, and Rb suggest limited interaction with altered crust (Figure 1.4h). This also implies a limited mobility of the mobile elements suggesting that crustal fluids do not affect these lavas.

Sample ID	408611 MIs	408611 MIs	408624 MIs	408624 MIs	408772 MIs	408772 MIs
Range	Min	Max	Min	Max	Min	Max
Major elements (oxide wt.%)						
SiO_2	46.78	53.00	46.36	51.95	46.53	50.13
TiO_2	0.83	2.92	1.11	2.29	1.51	2.47
Al_2O_3	12.79	19.98	12.26	16.30	14.39	18.78
MgO	5.23	9.58	5.37	10.77	6.63	9.06
CaO	9.47	13.88	10.45	15.14	10.77	14.67
Fe_2O_3	1.16	3.17	1.33	4.51	1.67	3.36
FeO	4.95	11.40	5.60	11.41	6.64	9.17
Cr_2O_3	0.01	0.33	0.01	0.30	-	1.28
NiO	-	0.03	-	0.30	-	0.06
MnO	0.08	0.24	0.08	0.32	0.10	0.29
Na_2O	1.52	3.58	1.52	2.69	0.64	2.68
K_2O	0.03	0.53	0.09	0.34	0.07	0.36
P_2O_5	-	1.34	-	0.51	-	0.40
FeO_{total}	5.99	14.25	6.80	14.83	8.25	12.19
Na_2O+K_2O	1.70	4.02	1.67	2.96	0.71	2.93
Mg#	56.0	71.6	49.7	68.7	56.5	64.7
Fo% host	81.70	89.60	84.90	88.30	84.80	88.50
Selected PM normalized trace element ratios and ΔNb						
$(Ce/Sm)_N$	1.07	4.01	0.90	1.81	0.81	2.13
$(La/Y)_N$	1.02	6.00	1.11	3.14	0.79	4.12
$(Rb/Sr)_N$	0.00	1.07	0.23	0.54	0.11	1.04
$(Sr/Nd)_N$	0.58	4.89	1.09	2.80	0.59	2.83
$(Ti/Zr)_N$	0.45	0.99	0.86	1.50	0.69	1.15
$(Sm/Nd)_N$	0.41	1.03	0.68	1.23	0.60	0.96
$(Ba/Zr)_N$	0.40	0.90	0.25	0.74	0.32	1.06
ΔNb	-0.27	0.43	-0.31	0.15	-0.08	0.45

Table 1.5: The range of major element composition and selected primitive mantle normalized trace element ratios of olivine-hosted MIs from the Vestfirdir ankaramites. Full data set is located in Appendix A9. The trace element data collected on milled MIs are presented in *Chapter 3*. PM normalization after McDonough & Sun (1995).

1.6 Discussion

1.6.1 Reconstruction of the original melt inclusion compositions

There are complications to overcome when interpreting the major element variations with in MIs, as it is a difficult task to evaluate whether these variations are primary or linked to post entrapment processes due to changes in physical and chemical changes. Reconstructing MI compositions that have undergone chemical exchange with the surrounding magma is a very complex task. Crystallization of the host mineral and other daughter phases within the MI can be experimentally reversed by homogenization experiments possibly combined with recalculations (see details in Danyushevsky et al., 2000). Theoretically, chemical changes can be reversed during the re-equilibration heating experiment (Appendix A2). Nevertheless, over- or under heating may have an effect on the melt compositions. Overheating results in over-contribution of the host olivine to melt, but also may result in degassing. Under heating may fail to melt the daughter crystals and olivine rim grown on the inclusion walls. MgO, FeO, and Ni are particularly affected by over- and under heating, since these elements are strongly compatible in olivine. Based on the assumption that, at the time of entrapment, the MI was in equilibrium with its olivine host, it is possible to recalculate the original melt composition using FeO-MgO exchange between melt and olivine. The choice of K_d value has a pronounced effect on the corrected melt compositions. Specifically for the compositional range in this data set a difference of ±0.03 results in up to approximately 2 wt.% differences in MgO content, whereas the other major oxides are less affected (in general <0.5 wt.%). If the K_d value for this exchange was any higher then more olivine needs to be added to the melt compositions in order to reach equilibrium. Therefore, our recalculated MgO wt.% compositions of the MIs are likely to be a minimum estimate.

An outstanding feature of the Vestfirdir MI data is the large range of FeO_{total} (6-14.8 wt.%) in the uncorrected as well as the corrected MI compositions (Figure 1.3b). It has been shown that MIs hosted in high magnesium olivine phenocrysts commonly have anomalously low FeO contents compared to initial trapped compositions, thus plotting well below the trend of pillow rim glasses and whole rock compositions (Danyushevsky et al., 2000; Danyushevsky et al., 2002a; Danyushevsky et al., 2002b). Such *Fe-loss* is suggested to result from post entrapment re-equilibration between the MIs and their olivine host. Compensation for *Fe-loss* of the MI compositions can be done by correcting back to the FeO_{total} content of the erupted lavas (Danyushevsky et al., 2000). It is possible that some of the variation in FeO_{total} content of the Vestfirdir MIs could be due to *Fe-loss*. The three host lavas plot approximately in the middle of the FeO_{total} field defined by the MI suite. However, the forsterite contents of the host olivine do correlate negatively with the FeO_{total} of the MIs, whereas CaO and SiO_2 show good negative correlations with FeO_{total}. This suggests that the variation in FeO_{total} may reflect true chemical

variations within the source region(s) and/or variation in depth of melting and differentiation processes. In general, lavas from northwest Iceland show a large variation in FeO_{total} (6-15 wt.%, Breddam et al. in prep.) similar to the variation displayed by the Vestfirdir MIs (Figure 1.3b). Therefore, we suggest that overall the major element compositional variations of the three MI populations also reflect some degree of major element heterogeneity in the source region of the Vestfirdir melts combined with variation in the melting systematics. This is in agreement with previous observations by Korenaga & Kelemen (2000) who documented the existence of substantial major element heterogeneity (including FeO_{total} variations) in the mantle sources of the NAIP. Besides, much of the major element systematics can be explained by various degrees of fractionation of olivine and clinopyroxene (section 1.6.3). Consequently, adjustment to a fixed FeO_{total} content by assuming a uniform FeO_{total} content of the parental melts, in this example, potentially blurs the original chemical variations among the entrapped MI compositions.

1.6.2 Contamination en route and alteration processes after emplacement

The ankaramites studied here erupted from the Skagi-Snæfellsnes rift zone, onto older lava flows erupted from the NW Iceland paleo-rift (Figure 1.1), (Hardarson et al., 1997). Thus it is possible that assimilation of older Icelandic crust may have affected their chemistry. Other studies have previously revealed lavas containing a subset of MIs showing more extreme compositions, which are not expressed within the lave suite itself e.g. Kent et al. (2002b), Danyushevsky et al. (2004) and Yaxley et al. (2004). For example, extreme chemical variability of MIs from the Baffin Island picrites suggests a more complicated scenario where contamination by continental crustal lithologies overprinted primary magmatic variations that originated from magma source heterogeneities and variation in magma generation processes (Yaxley et al., 2004, *Chapter 4*). It is suggested that chemical heterogeneities develop along the margins of the magmatic plumbing system due to crystallization (as response to under-cooling) and dissolution processes (see details in Figure 4.14). In these regions partial dissolution of wall rock material plus pre-existing mush-zone phases give rise to more variable (or maybe exotic) melt compositions, which represent all plausible admixtures of the parental melt and melts generated by melting of the wall rock lithologies. Crystals forming in such interaction zones potentially sample melt droplets of variable compositions, whereas MIs entrapped in the central parts of the magma body possible sample less variable melt compositions. In this way, it is possible to generate lavas composed of a mixture of the transporting magma with host crystals entrained from different zones of the same magma plumbing system. This gives rise to extreme variability in MI populations (Danyushevsky et al., 2002b). A common misconception is then that these exotic compositions represent geologically significant melts (Danyushevsky et al., 2004). However anomalous MI compositions often originate from localized small-scale reaction

processes within the magma plumbing system and these processes are only reflected by a few of the MI compositions. They do not reflect the main source effects and processes that control the composition of the lava suite (Danyushevsky et al., 2004). Hence, it is an important task to evaluate chemical variation potentially introduced by contamination *en route* or alterations processes after the emplacement. Once the melt starts to segregate and ascend through the magma conduit-chamber system they are prone to interact with the surrounding lithologies, which may result in modification of the original melt composition. Likewise, near-surface interaction of the lavas with the hydrosphere may result in hydrothermal alteration by meteoric water and seawater. Hydrothermal alteration processes have been documented to introduce characteristic changes to e.g. the concentrations of Cl, LILE, $\delta^{18}O$ values, and Sr isotope compositions (e.g. Staudigel et al., 1995; Eiler et al., 2000; Kent et al., 2002b).

Low temperature (<100°C) hydrothermal activity is characteristic of the Vestfirdir lava sequence, and fluid penetration and circulation takes place to the depth of 1-3 km (Hilton et al., 1998 and references therein). Breddam et al. (in prep.) found sporadic occurrences of brown clay in cavities within the ankaramites, which suggests some hydrothermal alteration by circulation of meteoric water took place after the emplacement. Signs of alteration are also observed on grain margins and along cracks in a few olivine phenocrysts. However, pristine MIs are most likely unaffected by such processes because they are protected by their host mineral from low-temperature chemical interaction with the surroundings. Also, good correlations between fluid-immobile and fluid-mobile elements (e.g. Nb, La, or Ce vs. Rb, Ba, and K_2O) document that the MIs of this data set are unaffected by the hydrothermal alteration processes (Figure 1.3h). In addition, a single $\delta^{18}O$ value published for olivine of sample SEL97 of ~ 5.1‰ (Hilton et al., 1999), which falls within the normal range for melts derived from mantle peridotite of 5.18 ±0.28 (Mattey et al., 1994), suggests no significant alteration by low-temperature fluid processes. Low-temperature fluid-rock interaction (with seawater) would result in higher $\delta^{18}O$ values than typical mantle, whereas lavas affected by higher temperature hydrothermal alteration should have lower than mantle $\delta^{18}O$ values. Negative $\delta^{18}O$ as indicated by hydrothermal fluids at Vestfirdir (Hilton et al., 1998), however the $\delta^{18}O$ value ~ 5.1‰ for SEL97 does not support higher temperature hydrothermal alteration. It is further unlikely that low-temperature alteration by seawater severely affected SEL97 cf. the elevated $\delta^{18}O$ values documented in altered oceanic crust by Staudigel et al. (1995).

Lavas affected by seawater are also expected to acquire high $^{87}Sr/^{86}Sr$, however the effect on Nd isotopes is limited (Staudigel et al., 1995). This is due to relatively high concentration of Sr, but low content of Nd in seawater. The ankaramites shown negative correlation between $^{143}Nd/^{144}Nd$ and $^{87}Sr/^{86}Sr$ (Figure 1.5), and so there is no convincing evidence for interaction of these magmas with seawater or hydrothermally altered crust. In *Chapter 3* it is shown that the

most radiogenic Sr isotope compositions measured on individual MIs are coupled with higher Rb/Sr ratios. Such systematics are inconsistent with seawater alteration as this media has low Rb/Sr but radiogenic $^{87}Sr/^{86}Sr$ ratios. Rare MI compositions show slightly elevated $(Sr/Nd)_N$, and others have slightly elevated Cl/K_2O, otherwise these MIs do not show anomalies that distinguish them from the rest of the Vestfirdir MIs. Seawater and oceanic crust altered by seawater may be enriched in Sr and Cl, and contamination of these components may explain these anomalies. However, in general there is minimal evidence that secondary alteration processes or severe assimilation altered oceanic crustal has affected the geochemistry of the Vestfirdir lavas and their associated MI suite.

1.6.3 The relationship between lavas and melt inclusions

Several studies have documented large compositional variations among MIs within a single lavas from different tectonic environments e.g. Gurenko & Chaussidon (1995), Shimizu (1998), Norman et al. (2002), Kent et al. (2004), Yaxley et al. (2004). This is also true for the three Vestfirdir MI populations (Figure 1.3-1.4). Consequently, it is critical to understand the origin of these chemical variations when evaluating the relationship between the host lavas and their MIs. We have discounted significant effects from crustal contamination or hydrothermal alteration processes (section 1.6.2). Given that the data presented in this paper is collected on homogenous primary MIs, we are confident that the observed compositional variations seen within the data are primary, and thus not the effect of chemical and physical modifications after entrapment. It is further unlikely that the variation is due to the development and trapping of MIs from the localized enriched boundary layer, which may develop immediately around the individual olivine phenocrysts. Preliminary studies have shown that the boundary layer effect is negligible for larger MIs (>20 μm), and only very small inclusions (<5-10 μm) might be affected by boundary layer entrapment (Kuzmin & Sobolev, 2003). Therefore, larger MIs such as those that are the focus of this study, should not be affected by boundary layer effect, and thus we can conclude that the chemical diversities of the Vestfirdir MIs must relate to primary characteristic of the source rock(s), melting, and segregation processes.

We evaluate the relationship between MIs and their host lavas using both the major and trace element compositions of lavas and MIs. At this stage it is important to point out that the Vestifirdir suite is not a simple olivine-melt system, but is more complex due to the involvement of clinopyroxene and ± plagioclase, which makes modelling more complicated. The relationship between the lavas and MI compositions can be tested by modelling accumulation and crystal fractionation processes involving olivine, clinopyroxene, ±plagioclase (Figure 1.7). Modelling of $MgO\text{-}FeO_{total}$ relations suggests that the host lavas 408624 and 408772 may be generated by accumulation of, respectively, 20-45 wt.% olivine and 5-10 wt.% clinopyroxene to their average MI compositions (Figure 1.7a). The average 408611 MI requires

accumulation of equal amounts of olivine and clinopyroxene (40 wt.%) to match its whole rock composition. The effects of accumulation of olivine and clinopyroxene on the average MI trace element compositions that eventually form the host lava compositions are shown in Figure 1.7b through Figure 1.7d. Accumulation of olivine results in a dilution of the REE elements, whereas accumulation of clinopyroxene results in enrichment of the HREE relative to the LREE. Trace element modelling shows similarly that average MIs of 408624 and 408772 respectively require 25 wt.% olivine plus 5 wt.% clinopyroxene and 55 wt.% olivine plus 5 wt.% clinopyroxene to match the host lava compositions. However, the trace element composition of the average MI of 408611 requires addition of 70 wt.% olivine and 25 wt.% clinopyroxene to match with its whole rock composition.

The modelling shows that the higher MgO, moderately elevated FeO and Al_2O_3 plus slightly lower CaO contents of the lavas compared to the '*original melt compositions*' are likely to be caused by the combination of olivine and clinopyroxene accumulation. In contrast, the variations of the MgO, FeO_{total}, Al_2O_3, and CaO within the MIs imply that these melts experienced variable degree of crystal fractionation. The modelling likewise predicts that the lower trace element concentrations of the host lavas relative to the higher concentration of the MIs may be generated by dilution of olivine and clinopyroxene accumulation. Moreover, if each of the host lavas are corrected for olivine and clinopyroxene accumulation they approximate the composition of their respective average MI. The similarities between the shape of the REE and multi trace element diagrams of the MIs and their respective host rocks likewise imply that the melts trapped within olivine phenocrysts are related to their host lavas. This hypothesis gains further support from the high proportion of olivine and clinopyroxene (±plagioclase) phenocryst phases combined with the high MgO contents of the host lavas (Figure 1.2-1.3, section 1.5.1), which imply that the host lavas do not represent discrete liquid compositions, but instead are mixtures of accumulated crystals plus liquid. The overall major element chemistry suggests that the '*original melts*' were of basaltic composition, and that these accumulated a significant amount of olivine and clinopyroxene (±plagioclase) resulting in the present composition of ankaramitic affinity. Neither MIs nor the host lavas are likely to represent pure primary melt compositions, but instead they reflect slightly modified (fractionated) melt compositions. Nevertheless, our models described above imply a strong petrogenetic link between the host lavas and their MIs.

It is important to remember that these estimates of crystal proportions likely represent the combined effects of crystal accumulation (to produce the bulk lava composition) and crystal fractionation (to produce the variable differentiated melts sampled by MIs). Our model is clearly over simplified due to the assumption that the fractionating or accumulating phase composition is equal to the averages composition of each mineral phase. With time, the

fractionating phases are likely to display some compositional changes, which is evidently reflected by the compositional range of the olivine phenocrysts, in particularly of sample 408611 (Figure 1.6a-b). The modelling may be bias towards the melt compositions present at the earliest stages as olivine is the first phase to crystallize. However, there is consistency between the major and trace element systematic predicted by the modelling and the systematic of the Vestfirdir data set.

The modelling of the chemical systematics of major and trace elements of MIs and the host lava suite suggests a strong petrogenetic link as also shown for other MI suites by Kamenetsky et al. (1997), Kent et al. (1999), Kent et al. (2002a), and Norman et al. (2002). It shows that the chemical variations can be explained by variation in melt generation processes and source heterogeneity combined with variation in accumulation and mixing processes. Overall, each lava represents the integration of multiple discrete parcels of melt. These unique melts may be sampled by MIs entrapped by different phenocrysts e.g. olivine, pyroxenes, plagioclase etc. The compositional range documented within each MI population from each phenocryst phase reflects that MIs are entrapped at different locations or at various stages and temperature intervals within the magmatic plumbing system e.g. prior, during, and after melt mixing and accumulation processes takes place. This suggests that the average MI composition found in a suite of phenocrysts from a single lava should represent the composition of the host lava. However, this requires that a large enough number of MIs is analyzed in order to ensure these are representative of the population contained within the different host phenocryst phases within the host lava. This further, means that MIs from a single lava may cover a larger compositional range than is recorded by the whole lava suite. Also, MIs captured in early-formed olivine phenocrysts may be biased towards melt compositions present at the earliest stages.

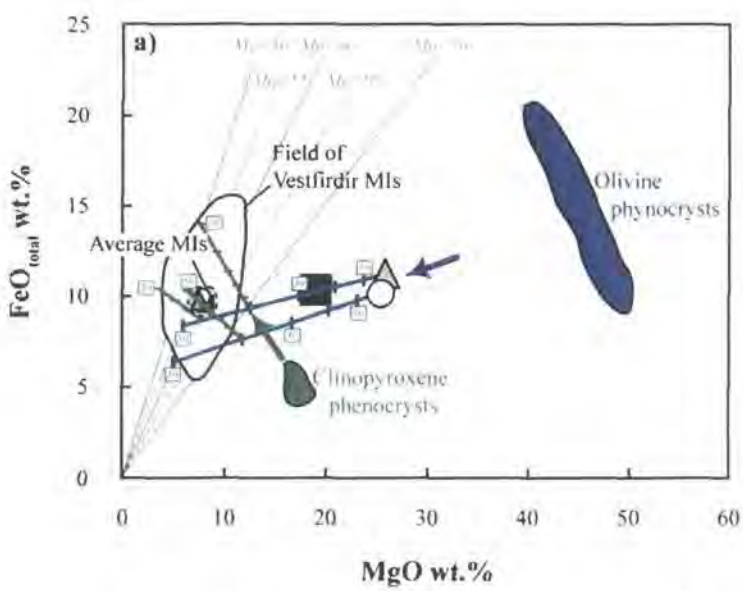

Figure 1.7: See caption on next page.

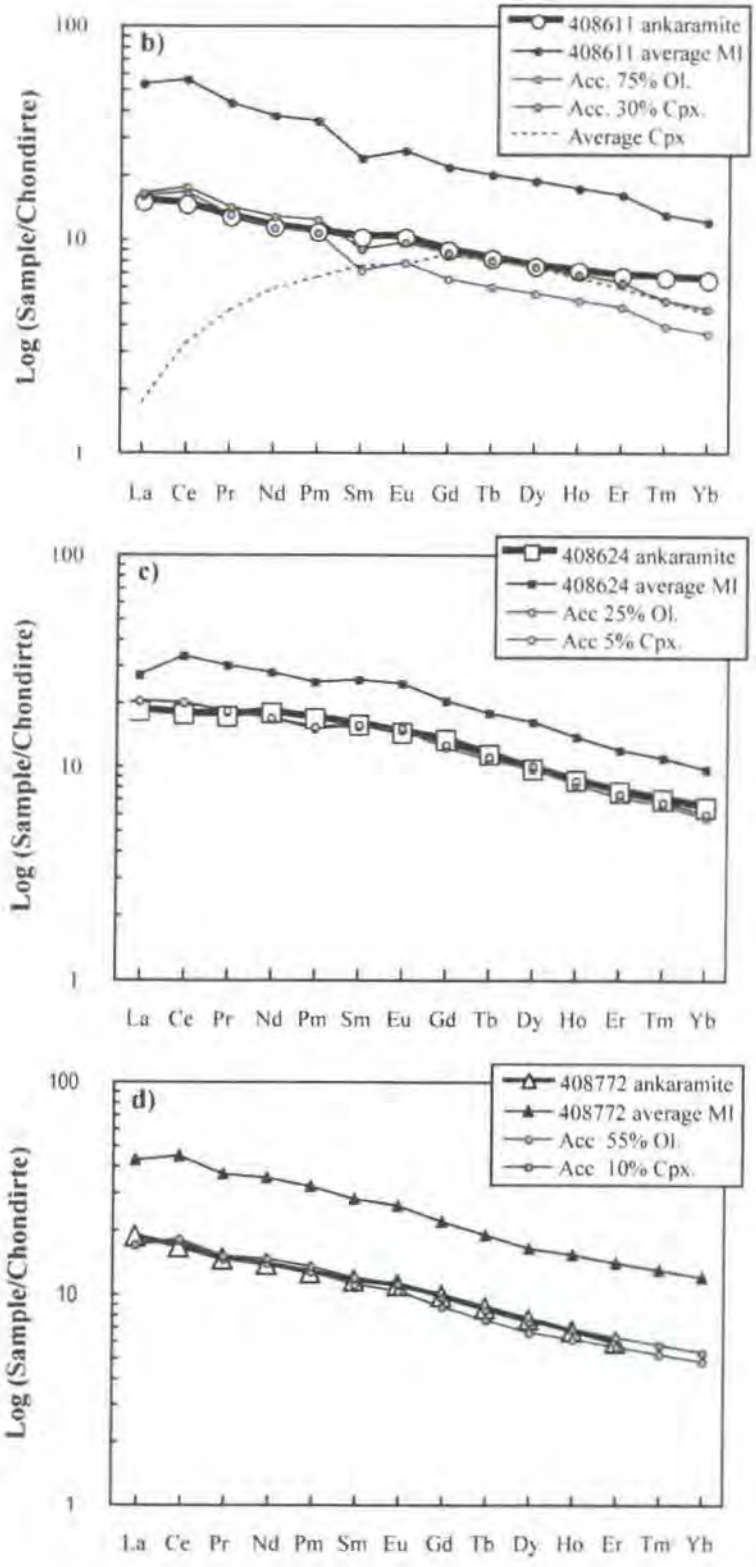

Figure I.7: Relationship between the major and trace element systematic of the ankaramites and their olivine-hosted MIs. a) Corrections for olivine ± clinopyroxene accumulation back to the compositional field of the MIs. Here shown by subtracting the average olivine and clinopyroxene composition (10% increments) from the host lavas in MgO-FeO_{total} space. Similar systematics are true in MgO-CaO space (not shown). b), c) and d) show average chondrite normalized REE-patterns of each of the three MI populations. To obtain the REE-patterns of their respective host lava various amount of olivine and clinopyroxene are added (equal to accumulation) to the melt compositions. All elements are normalized after (Sun & McDonough, 1989).

1.6.4 Chemical variation within the melt inclusion populations

Our models (Figure 1.7) demonstrate that accumulation and fractionation processes can explain the overall chemical difference between the MIs and the bulk lava compositions. However, there are variations in concentrations of components such as K_2O, TiO_2, Cl, and S plus trace element ratios (e.g. $(La/Y)_N$, $(La/Sm)_N$, $(Rb/Sr)_N$, $(Sr/Nd)_N$, $(Ba/Zr)_N$, $(Zr/Ti)_N$ etc.) that cannot be explained by these processes. None of these components or trace element ratios correlates with indices of differentiation (MgO or SiO_2), which suggests a decoupling from the general evolution of the melts. Instead, such chemical variations may relate to source region heterogeneities, contribution from multiple sources and/or physical conditions during the melt generation. To test this we model the variations in the REE spectra and selected trace element ratios generated by aggregated melting at 3 and 7 GPa (equal to respective 90 and 210 km melting depth) of a mantle peridotite (KR4003, Walter, 1998). Two compositional scenarios are investigated, one where the mantle peridotite has a depleted mantle signature and one where the source has trace element characteristics of the primitive mantle (Figure 1.8). Melt compositions generated by batch (*BM*), fractional (*FM*), and critical melting (*CM*) are compared to the characteristics of the Vestfirdir data set in Figure 1.8.

The model of 7 GPa *BM* predicts too high LREE/HREE at low (<5 % for DM, and >12 % for PM) degrees of melting, but as melting increases the REE patterns become less fractionated and the predicted melt compositions partly overlap with the Vestfirdir MI field. Lower pressure (3 GPa) REE spectrums modelled by *BM* (of both sources) are characterized by less fractionated LREE/HREE ratios, more comparable to the REE variation of the Vestfirdir MIs. The *BM* trends in Figure 1.8a show that the Vestfirdir MIs with higher $(La/Y)_N$ at a given $(La/Sm)_N$ may be generated at 7 GPa by either >5 % of a DM or >12 % of a PM, whereas MIs with somewhat lower $(La/Y)_N$ are best modelled by low pressure *BM* (>1 % of a DM or >3 % of a PM). The systematics between $(La/Sm)_N$ and $(Rb/Sr)_N$, $(Ba/Nb)_N$, $(Ba/Y)_N$, $(Ba/Zr)_N$, and $(Zr/Y)_N$ can, to a certain extent, be modelled by mixing of melts derived from a DM representing >0.5 % melting at 3 GPa and >2 % *BM* at 7 GPa. However, *BM* can not reproduce the systematics between $(La/Sm)_N$ vs. $(Sr/Nd)_N$ or $(Ti/Zr)_N$. Furthermore, the absolute concentrations of trace elements predicted by *BM* of a DM are not high enough to cover the full range of the Vestfirdir MIs.

FM modelling at 3 GPa shows that either a depleted mantle or a primitive mantle may reproduce the REE variation in the Vestfirdir MIs (Figure 1.8b). In contrast, melts generated by high pressure (7 GPa) *FM* are too strongly depleted in HREE relative to LREE and are thus inconsistent with the Vestfirdir REE data. However, in general the match between the melt compositions predicted by *FM* at both pressures and the Vestfirdir MI data set is poor (Figure 1. 8b, e, and h). Combining melts derived by *CM* of a depleted mantle at greater depth (7 GPa) with melts drawn from a more enriched source at 3 GPa generates much of the variation

observed among trace element ratios of Vestfirdir MIs (Figure 1.8c, f, and i). A good match of the Vestifirdir MI field in the $(La/Sm)_N$ vs. $(La/Y)_N$, $(Ba/Y)_N$, $(Rb/Sr)_N$, $(Zr/Y)_N$, $(Ba/Zr)_N$, $(Ba/Nb)_N$, $(Nb/Zr)_N$, and $(Ti/Zr)_N$ space is obtained by binary mixing between melts produced by 1.25-10 % CM at 7 GPa of the DM component and melts produced by 1.5-9 % *CM* of a more enriched component at 3 GPa. Like *BM* and *FM*, *CM* predicts a positive correlation between $(La/Sm)_N$ and $(Sr/Nd)_N$, which is at odds with the negative correlation of the MIs. All the modelling variations cannot produce the total elemental variation displayed by the Vestfirdir MIs if only DM and PM endmembers are used. Some of the MI compositions can only be modelled successfully if and endmember more enriched in incompatible elements than PM is involved.

The above modelling shows that it is impossible to reproduce the wide compositional range of the Vestfirdir MIs by variable degree of melting at a constant pressure of a single source component. The compositional diversity of the MIs requires a combination of variable source chemistry and degrees of melting plus variable depth of melting. Variable degrees of *CM* of a two-component source region are preferred over *BM* and *FM*. In order to reproduce the higher concentration of trace elements sampled by the Vestfirdir MIs a reservoir with higher abundances of incompatible trace elements than PM is required in addition to a DM component. The models also show that little difference is predicted in the $(La/Sm)_N$-$(Sr/Nd)_N$ relationship by *BM*, *FM*, and *CM* of either source components at the given pressures. The discrepancy between the $(La/Sm)_N$-$(Sr/Nd)_N$ systematics of the MIs and the predicted melt compositions suggests that it is not caused by variation in melting systematics. $(Sr/Nd)_N$, K_2O, TiO_2, Cl, or S do not correlate with indexes of differentiation. The $(Sr/Nd)_N$ ratios correlate with the trace element ratios examined above (e.g. Rb/Sr, La/Y, Ba/Nb, Ti/Zr etc.), but also with K_2O, TiO_2, Cl, and S. These correlations favour the *CM* models, suggesting that the variability among the MIs are the result of binary mixing between melts derived from two different source components, where the melting process best approximates to critical.

Figure 1.8: Located on the following pages. Batch, fractional, and critical melting models in the space of $(La/Sm)_N$ vs. $(La/Y)_N$ in a), b), and c), $(La/Sm)_N$ vs. $(Ba/Zr)_N$ in d), e), and f), and $(La/Sm)_N$ vs. $(Ti/Zr)_N$ in g), h), and i). The Vestfirdir MI field is shown together with the enriched (*Em*) and depleted (*Dm*) MI fields of the Neovolcanic Zone in Iceland (Gurenko & Chaussidon, 1998). As pyrolite KR4003, a mantle garnet peridotite from Walter (1998) is used. Phase proportions and melt reactions at 3 and 7 GPa are likewise taken from Walter (1998). Two scenarios are modelled for each pressure (or depth), one of a pyrolith with a DM signature (broken lines) and the other pyrolith with a PM signature (full lines). Equations for batch and fractional melting may be found e.g. in Rollinson (1993), and the critical melting equation is from Gurenko & Chaussidon (1998) and references therein. Critical melting is modelled with an α of 1%, which denotes the proportion of melts left in the source region.

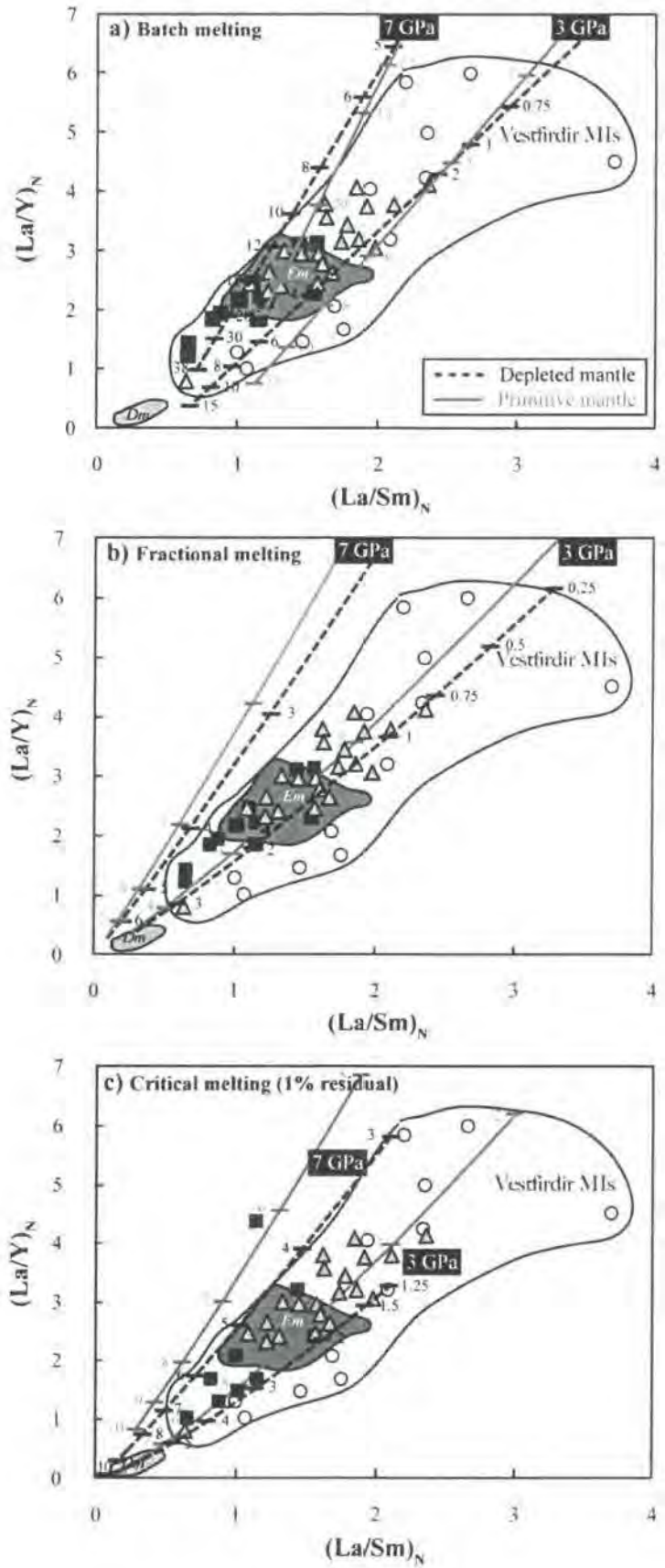

Figure 1.8: Batch, fractional, and critical melting in $(La/Sm)_N$ vs. $(La/Y)_N$ space.

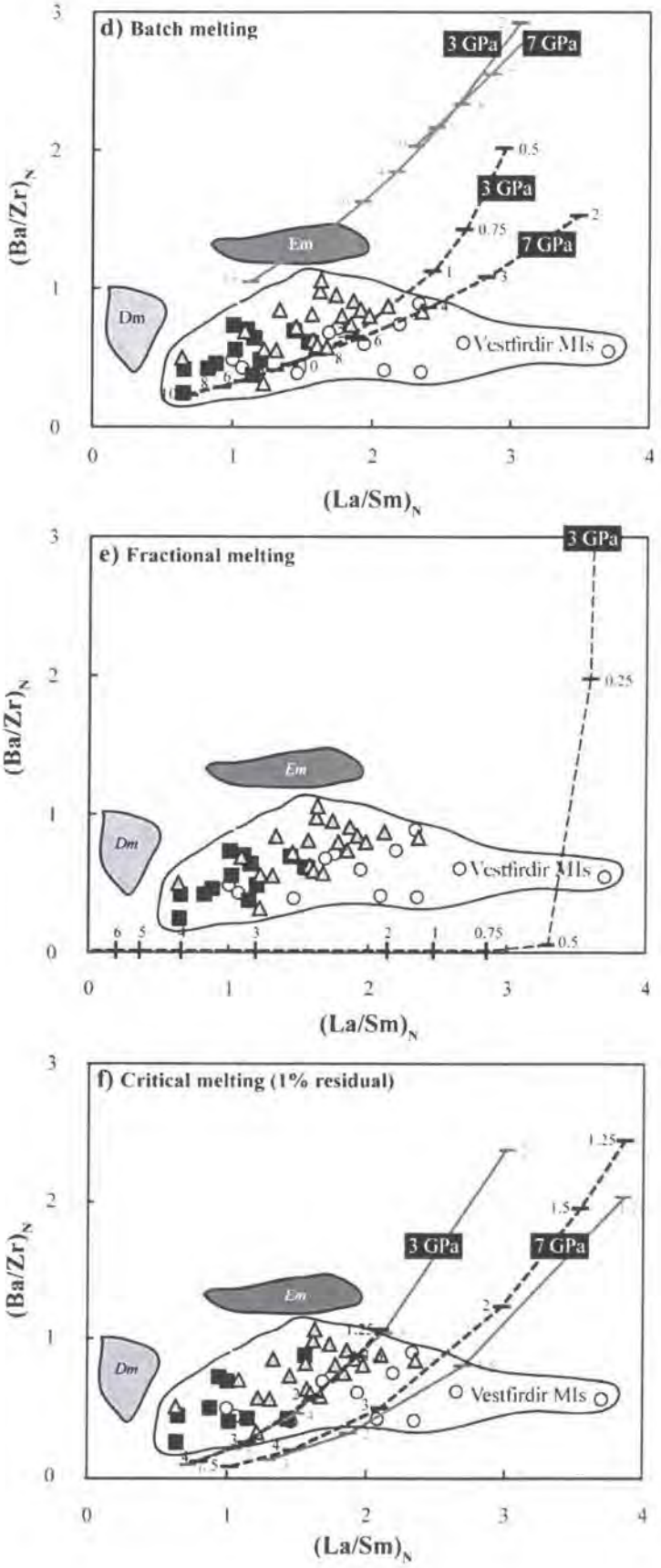

Figure 1.8: Continued. Batch, fractional, and critical melting in $(La/Sm)_N$ vs. $(Ba/Zr)_N$ space.

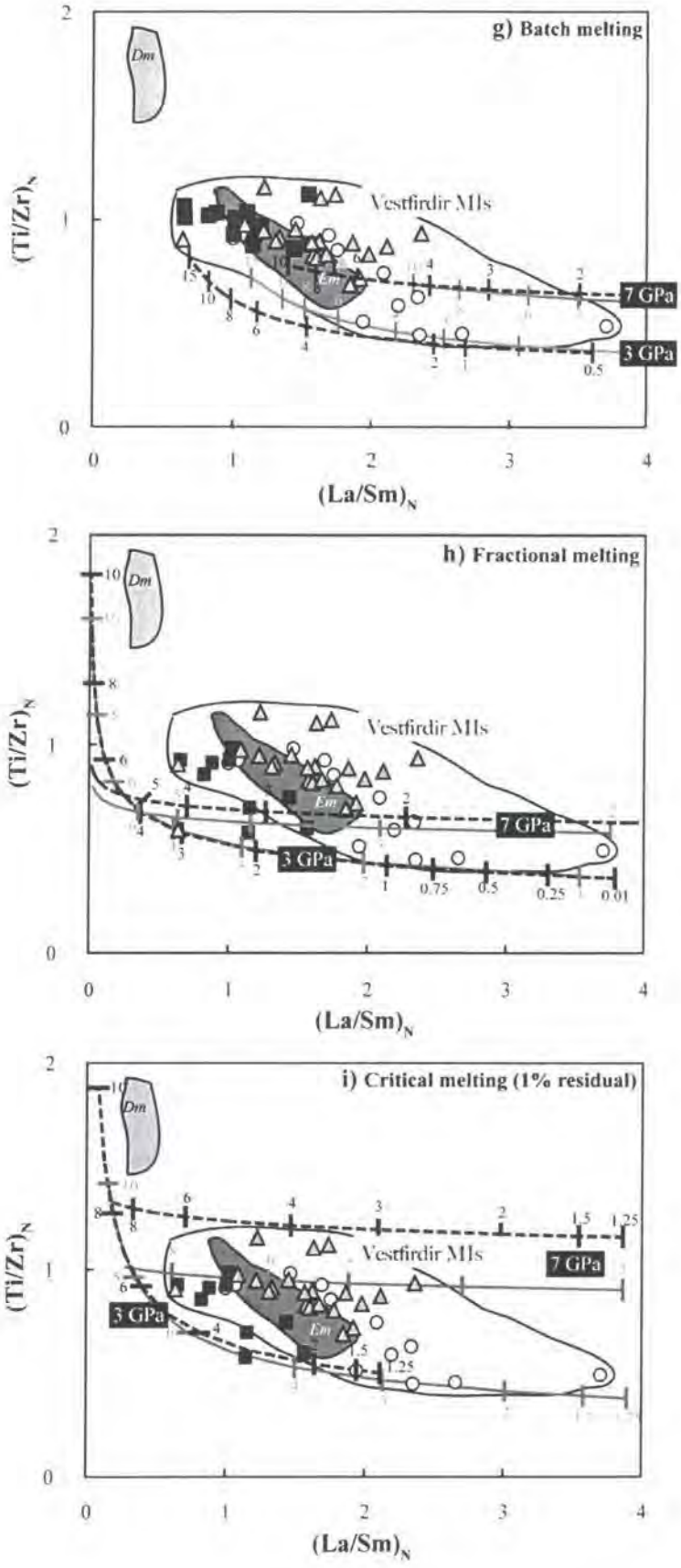

Figure 1.8: Continued. Batch, fractional, and critical melting in $(La/Sm)_N$ vs. $(Ti/Zr)_N$ space.

1.6.5 The source region of the Vestfirdir melts - trace element evidence

MIs found within a single lava, but originating from mixtures of melts derived from multiple source regions, have previous been reported (e.g. Gurenko & Chaussidon, 1995; Shimizu, 1998; Danyushevsky et al., 2002b). Curenko & Chaussidon (1995) showed the existence of both LREE depleted and LREE enriched melt compositions within MIs hosted in primitive olivine in the picrites from Reykjanes and Hengill (Neovolcanic Zone of Iceland) - here the depletion and enrichment is seen relative to the PM. Their modelling suggests that the chemical diversity among the MIs reflects mixing of enriched melts and depleted melt compositions derived from a single mantle column (carrying either PM or DM characteristics) in a proportion of 10-25% to 75-90%. Similarly, Shimizu (1998) documented enriched and depleted MI compositions in olivine phenocrysts from a single basaltic MORB lava from the FAMOUS area (36°49.2'N, 33°15.8'W on the Mid-Atlantic Ridge). This strongly bimodal occurrence of MIs within a single basalt was also ascribed to mixing of melts derived from, respectively an enriched component and a depleted component existing within the same melting column. Importantly, Shimizu (1998) also pointed out the potential influence of chemical modification by AFC processes in the shallow mantle. At Vestfirdir no truly depleted MIs are found that compare with those documented among the MIs from the Icelandic picrites or the sample MORB (Shimizu, 1998), (Figure 1.3-1.4, and 1.9). If the Vestfirdir MIs are compared with the MI populations investigated by Gurenko & Chaussidon (1995) we see that many of the Vestfirdir MIs are even more enriched than the most extreme MORB MIs, having higher LREE abundances (Figure 1.4b). This could have two explanations: I) These MIs contain an even larger contribution of the enriched melt type relative to the depleted melt type. Or II) the source component giving rise to the enriched signature within the Vestfirdir lavas and MIs is more enriched than the PM. The second alternative agrees with the melt modelling performed in section 1.6.4.

Fitton et al. (1997) have used coupled Nb-Zr-Y systematics to examine source features in the Icelandic plume. Others have extensively copied this approach despite concerns being raised over its usefulness (Hofmann, 2006). The ΔNb parameter [ΔNb=1.74+log(Nb/Y)-1.92log(Zr/Y)] for each of the three Vestfirdir MI population spans a wide range, from positive (plume/OIB mantle in this classification) to negative (MORB-like) sources, with a range from (-0.21 to 0.40). Positive ΔNb values dominate, resulting in positive ΔNb values for the host lavas (Figure 1.9, Table 1.3). Hofmann (2006) has suggested that variation in ΔNb is more likely to reflect fractionation of highly incompatible elements from moderately incompatible elements due to varying amounts of garnet and clinopyroxene in the source than fundamental differences in the nature of sources. Clearly, MIs that are sampling early melt fractions are recording this variation in a small melting environment and these variations are being mixed to provide a less

clear signal in the whole rocks. The large variation in ΔNb in only 3 lavas from NW Iceland questions the utility of this parameter in identifying fundamental differences in plume versus MORB type magmas.

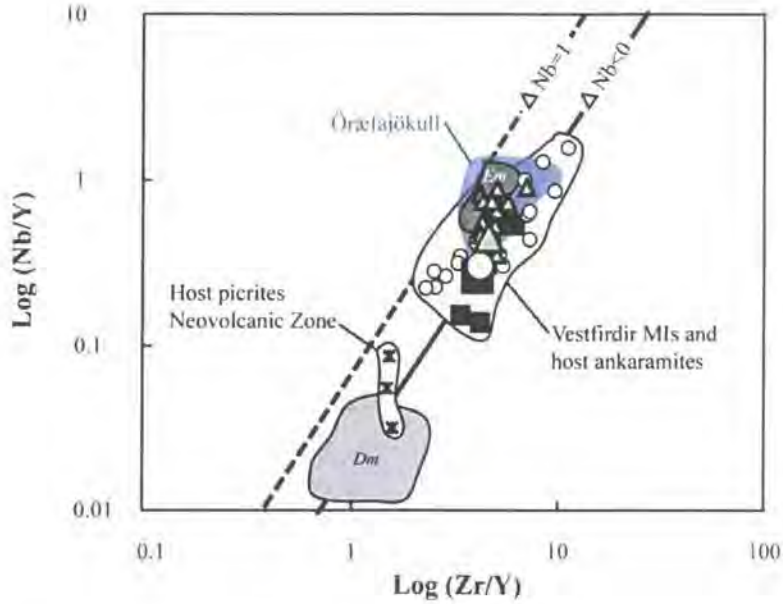

Figure 1.9: ΔNb plot of the Vestfirdir MIs and their host ankaramites. Also included are the enriched and depleted MI fields and host picrites (Gurenko & Chaussidon, 1995) plus the Öræfajökull lava field (Prestvik et al., 2001). For details on the ΔNb terminology and boundaries see Fitton et al. (1997), [ΔNb = 1.74+log(Nb/Y)-1.92log(Zr/Y)].

The Vestfirdir MI dataset shows that the more enriched MIs have higher Rb/Sr, Ba/(Y, Zr), Nb/(La, Ce, Zr), La/(Sm, Y), Zr/Y, and TiO_2, but lower Ba/Nb, Sr/Nd, Sm/Nd, Ti/Zr, and K_2O, than is observed for the more LREE depleted MI compositions. These characteristics are also likely to reflect characteristics found within the respective source components. The strong resemblance of the multi trace element patterns of the Vestfirdir MIs and in particular the most enriched MI compositions of 408611 with the alkali basalt of Snæfellsnes suggest the involvement of a recycled oceanic crustal component as e.g. suggested by Chauvel & Hémond (2000), (Figure 1.4a-b). Partly deviation from such a recycled component is also agreement with the characteristics of the above trace element ratios particular seen among the most enriched MIs. These enriched MIs may also be associated with lower volatile content as they carry lower content of S at a given $(La/Y)_N$ relative to the rest of the Vestfirdir MI spectrum (Table 1.5). A low volatile content is likewise consistent with deviation from a processed recycled component, which brings further support for a enriched recycled component rather then PM origin for the more enriched signature seen within the MIs. Still, the major and trace element systematic of the MIs, as shown by the modelling (section 1.6.4), calls for the participation of melts derived from a DM component in order to explain the more depleted MI compositions of the Vestfirdir MI spectrum.

1.6.6 Source region constraints - isotope evidence

Macpherson et al. (2005) reported high $^{3}He/^{4}He$ signatures and upper mantle like $\delta^{18}O$ values for trace incompatible element depleted glasses and lavas from Central Iceland (Neovolcanic zone), whereas the incompatible trace element enriched lavas from this zone generally display MORB-like $^{3}He/^{4}He$ signatures combined with lower $\delta^{18}O$ values. Macpherson et al. (2005) explain these relationships by a similar mixing model to the one as proposed by Stuart et al. (2003) for the Baffin Island picrites. However, the low $^{3}He/^{4}He$ but incompatible element enriched source component for the Central Icelandic lavas requires higher $^{143}Nd/^{144}Nd$ compared to the Baffin Island enriched source component (Macpherson et al., 2005). Therefore, it is suggested that the enriched endmember obtained its distinctive trace element and low oxygen isotope character through incorporation of recycled hydrothermally altered subducted oceanic crust, whereas the incompatible trace element depleted endmember component is proposed to have gained its high $^{3}He/^{4}He$ signature by secondary He enrichment (Macpherson et al., 2005). Macpherson et al. (2005) propose that the few occurrences of enriched high $^{3}He/^{4}He$ lavas such as Vadalda and Selardalur (408772 and SEL97) further imply that the origin of high $^{3}He/^{4}He$ is independent of the process that controls the evolution of the trace elements, and radiogenic, and stable isotopes ratios of these rocks.

The Vestfirdir data set provide few indications regarding the relationship between the He isotope signature measured on the olivine separates and e.g. the $(La/Y)_N$ and the volatile content (e.g. S, Cl, and He) measured on individual MIs, which may be deduced from Figure 1.10. Sample 408624 and 408772, which are characterized by unradiogenic He signature have MIs that in general show a lower fractionation of HREE from LREE than displayed by many of the 408611 MIs, whereas the more extreme range of $(La/Y)_N$ ratios of 408611 is combined with a low $^{3}He/^{4}He$ signature of 408611. It is also noticed that olivine separates of 408611 have a lower ^{4}He content than the olivine of 408624 and 408772 ($6.68 \cdot 10^{-11}$ vs. $5.12 \cdot 10^{-9}$ and $3.29 \cdot 10^{-10}$ cm^3 STP/g, Table 3.1). These observations may imply that the primary to enriched mantle source component giving raise to the LREE enriched signature carries the radiogenic He signature possibly in combination with a lower volatile content, and that the unradiogenic He signature is linked with the DM source.

The variation in trace element systematics shown by the MI suite from Vestfirdir ankaramites indicate the presence of both main components invoked from the isotope evidence and to this extent the MI study is compatible with models of Icelandic magmatism in general that are based on radiogenic and stable isotopes. To make further progress in linking the MI elemental signatures in detail to the various endmembers invoked from isotope studies it is helpful to examine isotope variability within the MI suite. This is the focus of the *Chapter 3*.

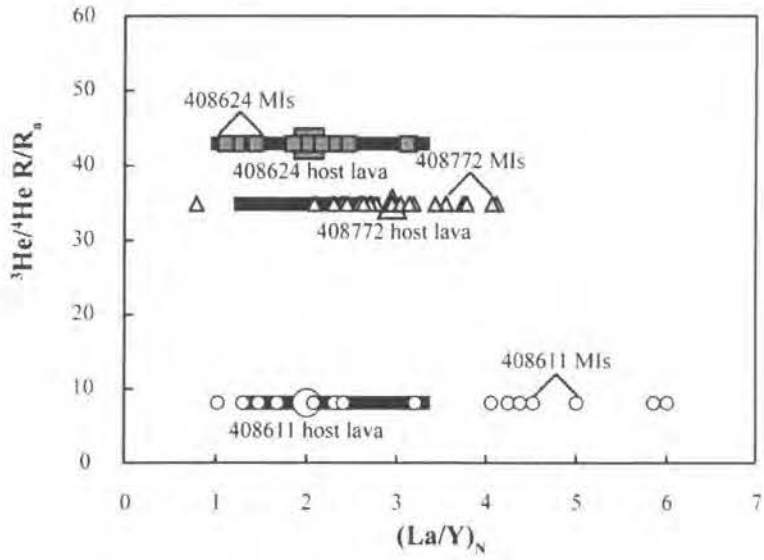

Figure 1.10: The relationship between the $^3He/^4He$ R/R_a signature obtained from olivine separates retrieved from the Vestfirdir ankaramites and the $(La/Y)_N$ ratios measured on single olivine hosted MIs. Larger symbols represent the three host lavas, and the smaller symbols are MIs analyzed by LA-ICPMS. The horizontal black bares represent the range of $(La/Y)_N$ ratios obtained from MIs sampled by micro-milling presented in *Chapter 3*.

1.6.7 Origin of the extreme He isotope signature

MIs preserve the volatiles (including He, S, and Cl), which were present at the time of melt entrapment in the growing olivine phenocrysts. A study of olivine phenocrysts in picritic basalts from the Juan Fernandez Island (Natland, 2003) showed that He occurred in crystal cavities and as bubbles in MIs. Natland (2003) argues that mantle derived volatiles, including He were predominantly incorporated into the Juan Fernandez olivine phenocrysts at shallow level, when a differentiated and degassed magma was mixed with a primitive lava. At this stage it is envisioned that both primary and secondary (melt droplets captured in fractures formed due to secondary contraction) MIs were captured by the olivine phenocrysts. However, the MI compositions from Vestfirdir do not show signs of mixing between such extreme magma endmembers. Therefore, the volatile content, including the extreme $^3He/^4He$ signature, is thought to represent the volatile budget of primitive, relatively undifferentiated melts. Furthermore, the petrography of the olivine phenocrysts of the Vestfirdir strongly implies that the majority of the volatile budget including He is hosted within the large (25-100 μm) primary MIs (Figure 1.2d-e), which dominate the observed inclusion populations. No fluid inclusions were observed in the Vestfirdir olivine populations, and the amount of olivine phenocrysts with very small secondary inclusions along healed fractures is minor (Figure 1.2.f). The secondary MIs are therefore thought to be volumetrically insignificant, - so unless these MIs are exceptionally volatile-rich, they are unlikely to control the volatile budget. In contrast to the Juan Fernandez MIs, the Vestfirdir MIs still hold considerable amounts of S and Cl, which argue against extensive degassing of the melt prior to entrapment. In addition, an estimated

K_d<0.008 for He between olivine and basaltic melt (e.g. Marty & Lussiez, 1993; Hiyagon & Ozima, 1986) strongly suggest that the MIs, not the olivine, are the major host of He.

The high $^3He/^4He$ signature measured on the olivine separates of the Vestfirdir ankaramites is contained within the MIs. The chemical variations within the MIs documented in this chapter shows that these MIs sample melts derived from at least two distinct mantle sources. Chemical evidence suggests that one of these mantle sources carries primitive to possibly enriched mantle characteristics that may relate to a recycled oceanic crustal component. The other source component indicated by the MIs, has a depleted mantle signature, similar to MORB or maybe just ancient depleted mantle. Different workers have recently suggested that both these sources may carry high $^3He/^4He$ ratios (e.g. Stuart et al., 2003; Ellam & Stuart, 2004; Macpherson et al., 2005; Parman et al., 2005; Parman, 2006). Because whole-rock lavas clearly represent the integrated signature of very diverse melts derived from a combination of at least two mantle sources, trying to deduce He isotope and Sr-Nd-Pb isotope relationships is encumbered. To more clearly examine these relationships and try to constrain further whether the extreme unradiogenic He signature originates from the depleted or more primitive components isotope studies of single MIs will be undertaken.

1.7 Conclusions

- The petrography of the olivine phenocrysts of the Vestfirdir implies that the majority of the volatile budget in olivine separates including extreme He signature is hosted within large (25-100 μm) primary olivine-hosted MIs, which dominate the observed inclusion populations. Smaller secondary inclusions along healed fractures are evident in few grains, but appear volumetrically insignificant. Unless these inclusions are exceptionally volatile-rich, they are unlikely to control the volatile budget.

- Each lava and the olivine-hosted MIs contained within it show similar chemical features. The modelling of both the major and trace element systematics suggest that the compositions of MIs in each sample and their host lavas are related by a combination of accumulation and fractionation of olivine, clinopyroxene, and plagioclase. Neither MIs nor lavas appear to represent primary liquids.

- During fractional crystallization of a primitive basaltic melt, the first mineral phase to crystallize is olivine followed by clinopyroxene and later plagioclase. In general, such a fractionation scenario is agreement with petrological constraints of the Vestfirdir lavas. As shown above, olivine and clinopyroxene fractionation systematic can explain the general trend seen within the MIs compositions. Furthermore, the vast abundance of

olivine phenocrysts suggests that olivine was the dominant crystallizing phase, whereas the less abundant clinopyroxene (and plagioclase) phenocrysts played minor roles.

- Variation in trace element ratios within the three MI populations, suggest differences in depth and degree of mantle melting. Furthermore, the trace element modelling requires melt contributions from both incompatible element depleted and enriched source components in the mantle region. This is similar to other models of the melting in OIB and MORB source regions.

- The variety of MIs within a single population of olivine phenocrysts shows that a compositional range is present in close temporal and spatial proximity of the growing olivine crystal. Alternatively, the melt droplets forming the MIs were entrapped in olivine crystals growing in a different part of the same magma chamber system possibly representing different melt batches. These olivine phenocrysts hosting MIs eventually become entrained in an uprising common carrier melt batch.

- Finally, because the He budget of a volcanic rock is dominated by the MI volatile inventory, we suggest that to further constrain the possible origin of high $^{3}He/^{4}He$ signatures in rocks such as the Vestfirdir ankaramites it is necessary to obtain isotope ratios on single MIs to examine the true variation of coupled elemental and isotope systematics in the melts being mixed to form the host lava. *Chapter 3* focuses on this aim.

1.8 References

Anderson, D. L. (1998a): A model to explain the various paradoxes associated with mantle noble gas geochemistry. Proceedings of the National Academy of Sciences, 95: 9087-9092.

Anderson, D. L. (1998b): The helium paradox. Proceedings of the National Academy of Sciences, 95: 4822-4827.

Breddam, K. & Kurz, M. D. (2001): Helium isotope signatures of Icelandic alkaline lavas. EOS, Transactions, American Geophysical Union, 82: F1315.

Breddam, K., Stecher, O., Harlou, R., Peate, D. W., & Kurz, M. D. (in prep): Miocene high-$^{3}He/^{4}He$ ankaramites in NW-Iceland: Trace element constraints on the common component in mantle plumes.

Charlier, B. L.A., Ginibre, C., Morgan, D., Nowell, G. M., Pearson, G. D., Ottley, C. J., & Davidson, J. P (2006): Methods for the microsampling and analysis of strontium isotopes at the crystal scale for petrological and geochronological studies of igneous rocks. Chemical Geology: 114-133.

Chauvel, C. & Hémond, C. (2000): Melting of a complete section of recycled oceanic crust: Trace element and Pb isotopic evidence from Iceland. Geochemistry Geophysics Geosystems, 1.

Danyushevsky, L. V., Della-Pasqua, F. N., & Sokolov, S. (2000): Re-equilibration of melt inclusions traped by manesian olivine phenocrysts from subduction-related magmas: petrological implications. Contributions to Mineralogy and Petrology, 138: 68-83.

Danyushevsky, L. V., Leslie, A. G., Carwford, A. J., & Durance, A. (2004): Melt inclusions in primitive olivine phenocrysts: the role of localized reaction processes in the origin of anomalous compositions. Journal of Petrology, 45(12): 2531-2553.

Danyushevsky, L. V., McNeill, A. W., & Sobolev, A. V. (2002a): Experimental and petrological studies of melt inclusions in phenocrysts from mantle-derived magmas: an overview of techniques, advantages and complications. Chemical Geology, 183: 5-24.

Danyushevsky, L. V., Sokolov, S., & Falloon, T. J. (2002b): Melt inclusions in olivine phenocrysts: using diffusive re-equilibration to determine the cooling history of a crystal, with implication for the origin of olivine-phyric volcanic rocks. Journal of Petrology, 43(9): 1651-1671.

Darbyshire, F. A., Bjarnason, I.T., White, R.S. and Flóvenz, Ó.G. (1998): Crustal structure above the Iceland mantle plume imaged by ICEMELT refraction profile. Geophysical Journal International, 135(3): 1131-1149.

Darbyshire, F. A., White, R. S., & Priestley, K. F. (2000): Structure of the crust and uppermost mantle of Icelenad from a combined seismic and gravity study. Earth and Planetary Science Letters, 181: 409-428.

Davidson, J. P., Morgan, D. J., Charlier, B. L. A., Harlou, R., & Hora, J. M. (2007): Microsampling and isotopic analysis of igneous rocks: Implications for the study of magmatic systems. Annual Review of Earth and Planetary Sciences, 35.

Davidson, J. P., Tepley, F., Palacz, Z., & Meffan-Main, S. (2001): Magma recharge, contamination and residence times revealed by in situ laser ablation isotopic analysis of feldspar in volcanic rocks. Earth and Planetary Science Letters, 184: 427-442.

Eiler, J. M., Farley, K. A., & Stolper, E. M. (1998): Correlated helium and lead isotope variations in Hawaiian lavas. Gechimica er Cosmochimica Acta, 62(11): 1977-1984.

Eiler, J. M., Grônvold, K., & Kitchen, N. (2000): Oxygen isotope evidence for the origin of chemical variations in lavas from Theistareykir volcano in Iceland's northern volcanic zone. Earth and Planetary Science Letters, 184: 269-286.

Ellam, R.M. & Stuart, F. M. (2004): Coherent He-Nd-Sr isotope trends in high $^{3}He/^{4}He$ basalts: implications for a common reservoir, mantle heterogeneity and convection. Earth and Planetary Science Letters, 228: 511-523.

Farley, K. A., Natland, J. H., & Craig, H. (1992b): Binary mixing of enriched and undegassed (primitive?) mantle components (He, Sr, Nd, Pb) in Samoan lavas. Earth and Planetary Science Letters, 111: 183-199.

Farley, K. A. & Neroda, E. (1998): Noble gases in the Earth's Mantle. Annual Review of Earth and Planetary Sciences, 26: 189-218.

Fitton, J. G., Saunders, A. D., Kepton, P. D., & Hardarson, B. S. (2003): Does depleted mantle form an intrinsic part of the Iceland plume? Geochemistry Geophysics Geosystems, 4(3): 1-14.

Fitton, J. G., Saunders, A. D., Norry, M. J., Hardarson, B. S., & Taylor, R. N. (1997): Thermal and chemical structure of the Iceland plum. Earth and Planetary Science Letters, 153: 197-208.

Foulger, G. R. & Anderson, D. (2005): A cool model for the Iceland hotspot. Journal of Volcanology and Geothermal Research, 141, 1-22.

Foulger, G. R. (2006): Older crust underlies Iceland. Geophysical Journal International, 165: 672-676.

Graham, D. W., Castillo, P. R., Lupton, J. E., & Batiza, R. (1996): Correlated He and Sr isotope ratios in South Atlantic near-ridge seamounts and implications for mantle dynamics. Earth and Planetary Science Letters, 144: 491-503.

Graham, D. W., Larsen, L. M., Hanan, B. B., Storey, M., Pedersen, A. K., & Lupton, J. E. (1998): Helium isotope composition of the early Iceland mantle plume inferred from the Tertiary picrites of West Greenland. Earth and Planetary Science Letters, 160: 241-255.

Graham, D. W. (2002): Nobel gas isotope geochemistry of mid-ocean island basalts: Characterization of mantle source reservoirs. Reviews of Mineralogy & Geochemistry, 47, 247-317.

Gurenko, A. A. & Chaussidon, M. (1995): Enriched and depleted primitive melts included in olivine from Icelandic tholeiites: origin by continuous melting of a single mantle column. Geochimica et Cosmochimica Acta, 59(14): 2905-2917.

Gurenko, A. A., Hansteen, T. H., & Schmincke, H. -U. (1998): 22. Melt, crystal, and fluid inclusions in olivine and clinopyroxene phenocrysts from the sumbarine shield stage hyaloclastites of Gran Canaria, Site 953 and 956. Proceedings of the Ocean Drilling Program, Scientific Results, 157. 375-401.

Hanan, B. B., Blichert-Toft, J., Kingsley, R., & Schilling, J.-G. (2000): Depleted Iceland mantle plume geochemical signature: Artifact of multicomponent mixing? Geochemistry Geophysics Geosystems, 1.

Hanan, B. B. & Graham, D. W. (1996): Lead and helium isotope evidence from oceanic basalts for a common deep source of mantle plumes. Science, 272: 991-995.

Hardarson, B. S., Fitton, J. G., Ellam, R. M., & Pringle, M. S. (1997): Rift relocation - a geochemical and geochronological investigation of a palaeo-rift in northwest Iceland. Earth and Planetary Science Letters, 153: 181-196.

Hart, S. R., Hauri, E. H., Oschmann, L. H., & Whitehead, J. A. (1992): Mantle plumes and entrainment: Isotopic evidence. Science, 256: 517-520.

Hauri, E. H., Whitehead, J. A., & Hart, S. R. (1994): Fluid dynamic and geochemical aspects of entrainment in mantle plumes. Journal of Geophysical Research, 99(B12): 24275-24300.

Hervig. R. L., Smith, J. V., & Dawson, J. B. (1986): Lherzolite xenoliths in kimberlites and basalts: petrogenetic and crystallochemical significance of some minor and trace elements in olivine, pyroxenes, garnet and spinel. Transactions of the Royal Society of Edinburgh. Earth Sciences, 77, 181-201.

Hilton, D. R., Barling, J., & Wheller, G. E. (1995): Effect of shallow-level contamination on the helium isotope systematics of ocean-island lavas. Nature, 373: 330-333.

Hilton, D. R., Gronvold, K., Macpherson, C. G., & Castillo, P. R. (1997): Extreme $^{3}He/^{4}He$ ratios in northwest Iceland: constraining the common component in mantle plumes. Earth and Planetary Science Letters, 173: 53-60.

Hilton, D. R., Gronvold, K., Macpherson, C. G., & Castillo, P. R. (1999): Extreme $^{3}He/^{4}He$ ratios in northwest Iceland: constraining the common component in mantle plumes. Earth and Planetary Science Letters, 173: 53-60.

Hilton, D. R., Gronvold, K., Sveinbjornsdottir, A. E., & Hammerschmidt, K. (1998): Helium isotope evidence for off-axis degassing of the Icelandic hotspot. Chemical Geology, 149: 173-187.

Hilton, D. R., Thirlwall, M. F., Taylor, R. N., Murton, B. J., & Nichols, A. (2000): Controls on magmatic degassing along the Fyekajanes Ridge with implications for the helium paradox. Earth and Planetary Science Letters, 183: 43-50.

Hiyagon, H. & Ozima, M. (1986): Partition of noble-gases between olivine and basalt melt. Gechimica er Cosmochimica Acta, 50: 2045-2057.

Hofmann, A. W. (1997): Mantle geochemistry: the message from oceanic volcanism. Nature, 385: 219-229.

Hofmann, A. W., Jochum, K. P., Seufert, M., & White, W. M. (1986): Nb and Pb in oceanic basalts: new constraints on mantle evolution. Earth and Planetary Science Letters, 79: 33-45.

Hofmann, A. W. (2006): Delta Niobium or Delta VICE? Eos Trans. AGU, 87(52), Fall Meet. Suppl., Abstract V34B-08.

Kamenetsky, V. S., Crawford, A. J., Eggins, S. M., & Mühe, R. (1997): Phenocryst and melt inclusion chemistry of near-axis seamounts, Valu Fa Ridge, lau Basin: insight into mantle wedge melting and the addition of subduction components. Earth and Planetary Science Letters, 151: 205-223.

Kent, A. J. R., Baker, J. A., & Wiedenbeck, M. (2002a): Contamination and melt aggregation proceses in continental flood basalts: constraints from melt inclusions in Oligocene basalts from Yemen. Earth and Planetary Science Letters, 202: 577-594.

Kent, A. J. R., Norman, M. D., Hutcheon, I. D., & Stolper, E. M. (1999): Assimilation of seawater-derived components in an oceanic volcano: evidence from glasses and glass inclusions from Loihi seamount, Hawaii. Chemical Geology, 156: 299-319.

Kent, A. J. R., Peate, D. W., Newman, S., Stolper, E. M., & Pearce, J. A. (2002b): Chlorine in submarine glasses from the Lau Basin: seawater contamination and constraints on the composition of slab-derived fluids. Earth and Planetary Science Letters, 202: 361-377.

Kent, A. J. R., Stolper, E. M., Francis, D., Woodhead, J., Frei, R., & Eiler, J. (2004): Mantle heterogeneity during the formation of the North Atlantic Igneous Province: Constrains from trace element and Sr-Nd-Os-O isotope systematics of Baffin Island picrites. Geochemistry Geophysics Geosystems, 5(11): 10.2039/2004GC000743.

Kokfelt, T. F., Hoernle, K., Hauff, F., Fiebig, J., Werner, R., & Garbe-Schönberg, D. (2006): Combined trace element and Pb-Nd-Sr-O isotope evidence for recycled oceanic crust (upper and lower) in the Iceland mantle plume. Journal of Petrology, 47(9): 1705-1749.

Korenaga, J. & Kelemen, P. B., 2000. Major element heterogeneity in the mantle source of the North Atlantic igneous province. Earth and Planetary Science Letters, 184: 251-268.

Kuzmin, D. V. & Sobolev, A. V. (2003): Boundary layer effect on the composition of melt inclusions in olivine. EGS - AGU - EUG Joint Assembly, Abstracts from the meeting held in Nice, France, abstract #5665.

Larsen, H. C., Brooks, C. K., Hopper, J. P., Dahl-Jensen, T., Pedersen, A. K., Nielsen, T. F. D., & field parties 1995 (1995): The Tertiary opening of the North Atlantic: DLC investigations along the east coast of Greenland. Rapport Grønlands Geologiske Undersøgelse, 165: 106-115.

MacDonald, G. A. (1968); Composition and origin of Hawaiian lavas. In: Coats, R. R., Hay, R. L., & Anderson, C. A. (eds.): Studies in volcanology: a memoir in honour of Howel Williams. The Geological Society of America, 116, 477-522.

Maclennan, J., McKenzie, D. M., Gronvöld, K., & Slater, L. (2001): Crustal accretion under northern Iceland. Earth and Planetary Science Letters, 191: 295-310.

Macpherson, C. G., Hilton, D. R., Day, J. M. D., Lowry, D., & Grönvold, K. (2005): High-$^{3}He/^{4}He$, depleted mantle and low-$\delta^{18}O$, recycled oceanic lithosphere in the source of central Icelandd magmatism. Earth and Planetary Science Letters, 233: 411-427.

Marty, B. & Lussiez, P. (1993): Constraints on rare-gass partition-coefficients from analysis of olivine glass from a picritic midocean ridge basalt. Chemical Geology, 106: 1-7.

Mathez, E. A. (1976): Sulfur solubility and magmatic sulfieds in submarine basalt glass. Journal of Geophysical Research, 81(B23): 4269-4276.

Mattey, D., Lowry, D., & Macpherson, C. (1994): Oxygen isotope composition of mantle peridotite. Earth and Planetary Science Letters, 128: 231-241.

McDonough, W. F. & Sun, S. -s. (1995): The composition of the Earth. Chemical Geology, 120: 223-253.

Meibom, A. Anderson, D. L., Sleep, N. H., Frei, R., Chamberlain, C. P., Hren, M. T., & Wooden, J. L. (2003): Are high $^{3}He/^{4}He$ ratios in oceanic basalts an indicator of deep-plume components? Earth and Planetary Science Letters, 208: 197-204.

Natland, J. H. (2003): Capture of Helium and other volatiles during the Growth of olivine phenocrysts in picritic basalts from the Juan Fernandez Islands. Journal of Petrology, 44(3): 421-456.

Nielsen, R. L., Michael, P. J., & Sours-Page, R. (1998): Chemical and physical indicators of compromised melt inclusions. Geochimica et Cosmochimica Acta, 62(5): 831-839.

Norman, M. D., Garcia, M. O., Kamenetsky, V. S., & Nielsen, R. L. (2002): Olivine-hosted melt inclusions in Hawaiian picrites: equilibration melting, and plume source characteristics. Chemical Geology, 183: 143-168.

Parman, S. W., Kurz, M.D., Hart, S. R., & Grove, T. L. (2005): Helium solubility in olvine and implicatios for high $^{3}He/^{4}He$ in ocean island basalts. Nature, 437: 1140-1143.

Parman, S. (2006): The helium isotope evolution of the earth. Geochimica et Cosmochimica Acta, 70(18): 472.

Prestvik, T., Goldberg, S., Karlsson, H., & Grönvold, K. (2001): Anomalous strontium and lead isotope signatures in the off-rift Öræfjökull central volcano in south-east Iceland evidence for enriched endmembers(s) of the Iceland mantle plume? Earth and Planetary Science Letters, 190: 211-220.

Ramos, F. C. & Reid, M. R. (2005): Distinguishing melting of heterogeneous mantle sources from crustal contamination: Insights from Sr isotopes at the phenocryst scale, Pisgah Crater, California. Journal of Petrology.

Roedder, E. (1984): Fluid inclusions. Mineralogical Society of America, Washington, DC: 644 pp.

Roeder, P.L. and Emslie, R.F. (1970): Olivine-liquid equilibrium. Contribution to Mineral and Petrology, 29: 275-289.

Rollinson, H. (1993): Using Geochemical Data: evaluation, presentation, interpretation. Longman Singapore Publisher (Ptr.) Ltd., Singapore. 352.

Shimizu, N. (1998): The geochemistry of olivine-hosted melt inclusions in a FAMOUS basalt ALV519-4-1. Physics of the Earth and Planetary Interiors, 107: 183-201.

Sigmarsson, O. & Steinthórsson, S. (2007): Origin of Icelandic basalts: A review of their petrology and geochemistry. Journal of Geodynamics, 43: 87-100.

Skovgaard, A. C., Storey, M., Baker, J., Blusztajn, J., & Hart, S. R. (2001): Osmium-oxygen isotopic evidence for a recycled and strongly depleted component in the Iceland mantle plume. Earth and Planetary Science Letters, 194: 259-275.

Staples, R. K., White, R. S., Brandsdóttir, B., Menke, W., Maguire, P. K. H., & McBride, J. H. (1997): Färoe-Iceland Ridge Experiment1. Crustal structure of northeastern Iceland. Journal of Geophysical Research, 102(B4): 7849-7866.

Staudigel, H., Davies, G. R., Hart, S. R., Marchant. K. M., & Smidt. B. M. (1995): Large scale isotopic Sr, Nd and O isotopic anatomy of altered oceanic crust: DSDP/ODP sites 417/418. Earth and Planetary Science Letters, 130: 169-185.

Stracke, A., Hofmann, A. W., & Hart, S. R. (2005): FOZO, HIMU, and the rest of the mantle zoo. Geochemistry Geophysics Geosystems, 6(5).

Stuart, F. M., Lass-Evans, S., Fitton, J. G., & Ellam, R. M. (2003): High $^{3}He/^{4}He$ ratios in picritic basalts from Baffin Island and the role of a mixed reservoir in mantle plumes. Nature, 424(3): 57-59.

Sun, S. -s. & McDonough, W. F. (1989): Chemical and isotopic systematics of oceanic basalts: implications for mantle composition and processes. Geological Society Special Publication, No. 42: 313-345.

Taylor, R. N., Thirlwall, M. F., Murton, B. J., Hilton, D. R., & Gee, M. A. M. (1997): Isotopic constraints on the influence of the Icelandic plume. Earth and Planetary Science Letters, 148.

Thirlwall, M. F., Gee, M. A. M., Taylor, R. N., & Murton, B. J. (2004): Mantle components in Iceland and adjacent ridges investigated using double-spike Pb isotope ratios. Gechimica er Cosmochimica Acta, 68(2): 361-386.

Valbracht, P. J., Staudigel, H., Honda, M., McDougall, I., & Davies, G. R. (1996): Isotopic tracing of volcanic source regions from Hawaii: decoupling of gaseous from lithophile magma components. Earth and Planetary Science Letters, 144: 185-198.

Yaxley, G. M., Kamenetsky, V. S., Kamenetsky, M., Norman, M. D., & Francis, D. (2004): Origins of compositional heterogeneity in olivine-hosted melt inclusions from the Baffin Island picrites. Contribution to Mineral and Petrology, 148: 426-442.

Walter, M. J. (1998): Melting of Garnet Peridotite and the Origion of Komatiite and Depleted Lithosphere. Jounal of Petrology, 39(1): 29-60.

CHAPTER 2

Precise and accurate Sr isotope and trace element analysis of melt inclusions at sub-ng levels using micro-milling, TIMS and ICPMS

2.1 Abstract

In this paper, we describe a technique, which allows, for the first time, precise and accurate Sr isotope measurement combined with trace element analysis of individual melt inclusions (MIs), of sample sizes <<1 ng of Sr (Harlou et al., 2005). The technique involves sampling by micro-milling, chemical dissolution, micro Sr column chemistry, TIMS, and ICPMS analyses. For each sample a 10% aliquot of the solution is used for trace element analysis by magnetic sector field ICPMS, while Sr in the remaining 90% is chemically separated and used for $^{87}Sr/^{86}Sr$ determinations by TIMS. During the development of the technique outlined above, we documented in detail the potential sources of blank contributions and their magnitude. The size and the Sr isotope composition of our laboratory total procedural blank (TPB) was established to 4.86 pg ±0.26 pg Sr with an $^{87}Sr/^{86}Sr$ of 0.712932 ±0.000234 (2SE). The total procedural Rb blank was 1.32 ±0.69 pg. This allows accurate blank corrections to be performed. The potential influence of the TPB on the measured $^{87}Sr/^{86}Sr$ isotope composition of sub-ng Sr samples was modelled on the basis of experimental data collected on progressively smaller aliquots of sample solutions, the isotope compositions of which were as distinct as possible from the TPB composition. The TPB was found to have minimal effect (<150 ppm shift) on the $^{87}Sr/^{86}Sr$ isotope ratios of sample material containing down to ~250 pg Sr. Applying a blank correction allows *in-house* standards of this size to be corrected back to within 175 ppm of their accepted values. By applying blank corrections we can confidently measure the Sr isotope composition on sample sizes down to ~25 pg Sr to an accuracy better than 400 ppm. The technique is illustrated by application to a suite of MIs from NW Iceland and their host olivines. It is shown that the effect of a small amount of entrainment of the host olivine during sampling of 50 μm MI has a negligible effect on the measured Sr isotope composition. Furthermore, where MIs are <50 μm it is possible to obtain Sr isotope and trace element data on multiple MIs hosted in a single olivine. This provides similar information to that of the single MI.

2.2 Introduction

Significant advances in understanding the physical mechanism of mantle melting have been made recently, although debate remains concerning the degree and scale of heterogeneity in the source regions of basic magmas. This debate has been further fuelled by pioneering studies of MIs that revealed very large variations (50% of the range in global OIB) in the isotope composition of Pb within MIs from single OIB lavas (Saal et al., 1998). The interpretation of these variations has profound consequences for constraining mantle source region variations and melt aggregation processes during melting. The secondary ion mass spectrometry (SIMS) technique allows both trace element and Pb isotope measurements to be made on the same MI. However, the determination of the Pb isotope compositions of MIs are of relatively low precision (reflecting the low Pb content), and consequently the measurements are limited to ratios involving only ^{206}Pb, ^{207}Pb, and ^{208}Pb (not ^{204}Pb).

With the development of micro sampling techniques and methods for the TIMS analysis of Sr down to the nano-gram level it is now possible to measure Sr isotope compositions routinely at the single crystal and sub-crystal scale with high precision and accuracy (Birck, 1986; Charlier et al., 2006; Davidson et al., 2007). Even with these recent developments in sampling and analysis, obtaining precise and accurate Sr isotope compositions for individual silicate MIs remains a tough challenge, due to their volumetrically limited size (typically <100 μm in diameter) and thus their limited Sr content (<<1 ng total Sr). A recent paper by Jackson & Hart (2006) shows that *in situ* Sr isotope determinations of larger olivine-hosted MIs (50-250 μm) from Samoa containing high concentrations of Sr (400-2500 ppm) can be obtained by laser ablation multi collector inductive coupled plasma mass spectrometer (LA-MC-ICPMS). Their work does not document the size and Sr content of each MI, which makes it difficult to quantify the minimum sample requirements required for Sr isotope analysis using the laser ablation technique. Assuming spherical MIs with a density of 3.00 g/cm^3 and diameter of 250 μm with the range of Sr concentrations quoted by Jackson & Hart (2006) yields total Sr contents of 80 to 500 ng, i.e. several orders of magnitude greater than the amounts of Sr required in the technique described here. While attractive in terms of its speed of application, the LA-MC-ICPMS technique was applicable to less than 50% of the Samoan MIs studied. Given that larger well-preserved MIs that are comparably enriched in Sr as the Samoan MI suite are rare in many lava suites, the laser ablation approach will best suit MIs found in enriched OIB lavas such as EMI and EMII type. The method will not be readily exportable to typical MIs entrapped in olivine phenocrysts of less enriched or depleted OIB, CFB, and MORB.

The objective of this study is to push existing analytical methods further to acquire precise Sr isotope ratios, at the sub-ng level, together with trace element compositions for single MIs. In

this quest there are two main factors to consider, which strongly influence the outcome of our work. Explicitly: I) minimization of the potential total procedural blank (TPB) contribution during chemical processing of the sample material, and II) the performance of the instruments (TIMS and ICPMS).

We introduce a technique that allows the Sr isotope composition of a single MI to be measured in addition to the acquisition of Rb and Sr concentrations combined with other trace elements (Ti, Nb, REE, Y), (Harlou et al., 2005). The method employs micro-milling and micro Sr column chemistry in combination with TIMS (Sr isotope analyses) and double focusing magnetic sector field ICPMS (trace element analyses). We show that the technique can be applied to MIs from typical OIB and CFB suites making it a powerful tool for adding an extra dimension to MI studies already undertaken (e.g. Saal et al., 1998; Shimizu, 1998; Kent et al., 2002; Harlou et al., 2004; Yaxley et al., 2004; Saal et al., 2005) and as such can be extended to any problem where sub-ng Sr isotope analyses are required.

2.3 Specific aims and approach

A method for measuring the Sr isotope composition of MIs must enable analysis of MIs that span the range of concentrations represented by mantle derived basic magmatism. For this reason, we chose to develop our method using a suite of ankaramites from NW Iceland (Vestfirdir) that are relatively low in incompatible element concentrations (≤100 times chondrite), (Breddam & Kurz, 2001; Harlou et al., 2003; Harlou et al., 2004; Breddam et al., in prep.; *Chapter 1*). The MIs within this suite are typical of the wide range shown by OIB volcanic rocks having Sr of 200-600 ppm (Table 2.1). In addition to being able to make relatively precise and accurate Sr isotope analysis, the method needs to be able to obtain Rb and Sr data to make accurate age corrections, and to obtain a reasonably broad suite of trace elements, so that the MIs can be related to other MIs in the suite of rocks of interest where only trace element data may be available. Ideally, the method should allow other determinative methods to be used for further investigation of the MI suite. We outline options for these possibilities below.

Although *in situ* methods for Sr isotope analysis using LA-MC-ICPMS have been developed (Davidson et al., 2001; Ramos et al., 2004; Jackson & Hart, 2006), these approaches are somewhat unsuitable for MI investigations for several reasons. Firstly, many MIs are volumetrically small (often <50 μm) and of relatively low Sr content (Table 2.1). They therefore provide too little material to produce an adequate signal for precise isotope analysis by direct laser ablation. This relates to the overall efficiency of transport of the ablated material to the plasma, and given that only a small proportion of the total sample mass reaches the plasma it is implicitly more difficult to obtain a precise measurements on very small samples. Secondly,

Rb/Sr ratios in all silicate MIs are >0 making accurate isobaric Rb corrections very difficult to perform, especially when compounded with likely problems from Ca-dimer molecular species e.g. Woodhead & Hergt (2000). The Rb corrections are also complicated by the interference of ^{86}Kr on ^{86}Sr. A comparison of $^{84}Sr/^{86}Sr$ and $^{88}Sr/^{86}Sr$ ratios collected during a typical MI analysis by TIMS and LA-MC-ICPMS show the complexity in obtaining accurate Sr isotope (Figure 2.1a). This plot shows that the raw data collected by TIMS conforms to the expected trend for exponential mass fractionation. In contrast, typical LA-MC-ICPMS data that are uncorrected for Kr isobaric interferences plot well away from any expected mass fractionation trend. Moreover, because of difficulties in making accurate Kr corrections, that in part relate to not knowing the true mass fractionation behaviour of Kr relative to Sr, it is extremely difficult to fully correct for Kr interferences such that the interference corrected but non fractionation corrected Sr isotope ratios lie on a viable mass fractionation line (Figure 2.1a). To circumvent these problems Jackson & Hart (2006) correct their $^{84}Sr/^{88}Sr$ to the '*accepted*' value by simply subtracting enough signal to yield the '*accepted*' ratio. A drawback of this approach is that it immediately removes the possibility of using the $^{84}Sr/^{88}Sr$ ratio as a measure of data quality.

Element	Vestfirdir, Lavas	Vestfirdir, MIs	Samoa, MIs	N-MORB	E-MORB	OIB
Rb_{Range}	0.32-3.04	1.11-8.77	26-299	-	-	-
Rb_{Ave}	1.8	4.20	74	0.56	5.04	31
Sr_{Range}	89-185	101-1052*	384-2480	-	-	-
Sr_{Ave}	139	306	795	90	155	660
Nd_{Range}	5.35-8.43	6.53-38.23	-	-	-	-
Nd_{Ave}	6.48	15.87	-	7.30	9.0	38.5
Pb_{Range}	0.25-0.46	0.29-3.72	-	-	-	-
Pb_{Ave}	0.34	1.19	-	0.30	0.30	3.20

Table 2.1: Average concentration and range of Rb, Sr, Nd, and Pb in MORB and OIB. Also, listed are information on olivine-hosted MIs and ankaramite lavas from Vestfirdir in NW Iceland (*Chapter 1*), and for comparison olivine-hosted EMII-type MIs from the Samoan (Jackson & Hart, 2006). Concentrations are given in ppm. * only two MIs have been analyzed with Sr >600 ppm (Appendix A9), if these are excluded the average Sr of the Vestfirdir MIs is 287 ppm. Average N-MORB, E-MORB, and OIB concentrations are from Sun & McDonough (1989), Horizontal bar (-) denotes no data given in literature. Highlighted in grey are the Rb-Sr ranges and averages of MIs from respective Vestfirdir and Samoa MIs. Clearly, the MIs of the Vestfirdir ankaramites MIs are less enriched than the more extreme enriched nature of the Samoa MIs.

A plot of 2 times the internal precision (2SE) versus ^{88}Sr intensity collected on MIs by TIMS in this study and by LA-MC-ICPMS (Jackson & Hart, 2006) shows that a linear relationship exists between the sample size (reflected by the ^{88}Sr intensity) and the internal measurement precision (Figure 2.1b). Jackson & Hart (2006) discarded data collected on MI runs with ^{88}Sr intensities <1 V, in part because of concerns about accurate correction of Kr interferences combined with the complexity of Rb interference corrections. In contrast, the relatively interference free nature of TIMS analyses allow accurate data to be collected on sub-ng Sr samples running at intensities <<1 V (Figure 2.1).

The complications posed by LA-MC-ICPMS analysis on small sample, coupled with the desire to obtain the most accurate and precise data possible, led us to adopt a micro-sampling and chemical pre-concentration procedure. Inherent in this approach is the physical removal, by micro-milling or some other suitable method, of the MI from its host. One potential problem with this approach is the possibility of acquiring some contamination from the host mineral if the MI is small enough to warrant milling at its edges. For this reason, we have chosen to concentrate our efforts on MIs hosted by olivine, a mineral with naturally low Sr. Measurements of olivine free of MIs show that they have very low (sub ppm) levels of Rb (0.003-0.008 ppm) and Sr (0.024-0.129 ppm) such that if a small portion of the host crystal is sampled, it has a negligible effect on the overall Sr budget of the analysis (section 2.5.5). For instance, even if 90% of the milled sample material is olivine and 10% is the MI (200-600 ppm Sr), the contribution of Sr from the olivine is <1% of the total Sr budget. In the case of olivine and quartz, this is not very important, and one could analyse whole grains on the presumption that any Sr recovered is dominated by the MI composition. In any case, for the purpose of petrogenetic tracing it hardly matters whether the Sr is in the MIs or in the surrounding host, since (unlike trace element concentrations) the Sr is sequestered from the melt with no isotope fractionation.

Much of the established elemental analytical work on MIs such as electron micro probing, SIMS, and trace element LA-MC-ICPMS require the MIs to be homogenous (Figure 2.2a). Since in many cases there are strong concentration contrasts among glass and daughter phases it is crucial that heterogeneous MIs (Figure 2.2b) are homogenized experimentally prior to such *in situ* analytical work. One advantage of sampling the MIs by micro-milling is that it does not require the MI to be homogenous prior to sampling, as the total MI is sampled and is homogenized during the dissolution chemistry. Any incorporation of the host olivine during milling dilutes the absolute concentrations of the elements being analyzed, but as stated above, is unlikely too affect the Sr isotope composition.

We choose not to spike our samples with pure ^{84}Sr spike as it is very difficult to estimate the yield of Sr recovered from any given MI, and hence it is easy to seriously over- or under-spike samples. This is due to a combination of varying Sr concentration of the MIs, difficulties in estimating overall sample mass available and varying amounts of surrounding olivine that contribute to the final sample mass. For applications to relatively young volcanic rocks, where the age correction is minimal, the accuracy and reproducibility of the Rb/Sr ratio obtained by ICPMS analysis of sample aliquots is more than adequate. Furthermore, we are able to measure the aliquot taken for ICPMS analysis for a wide variety of other elements of interest, without worrying about variable column yields.

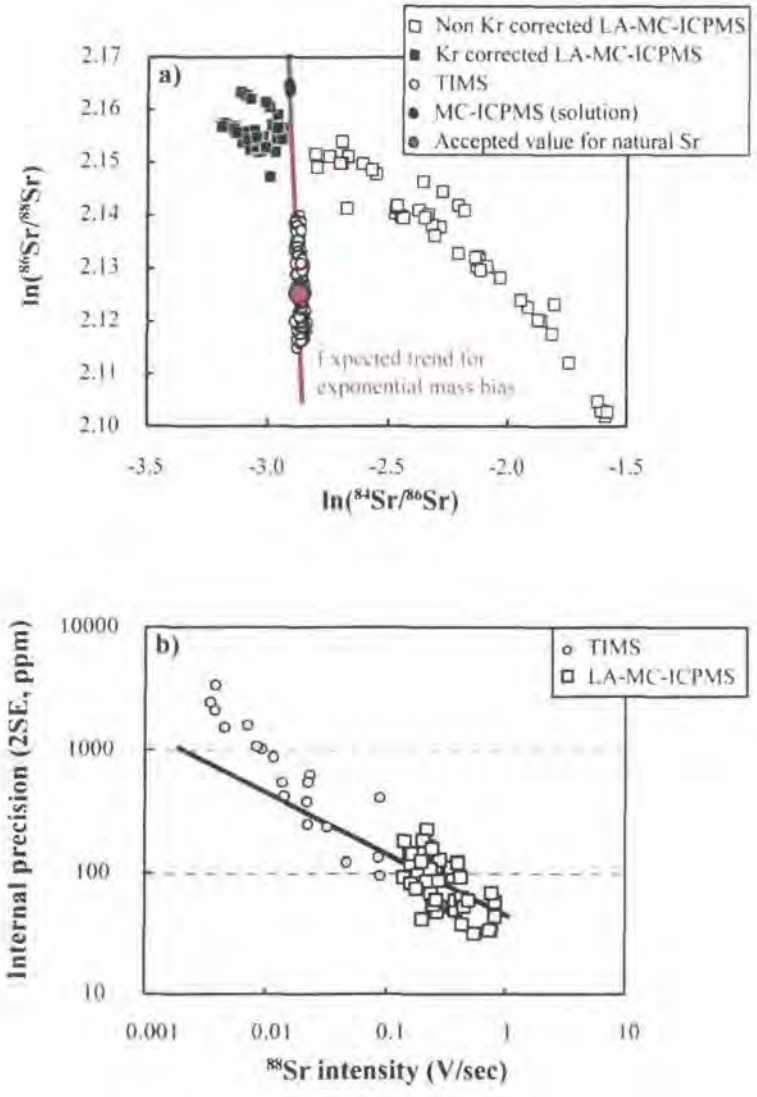

Figure 2.1: a) $\ln(^{84}Sr/^{86}Sr)$ versus $\ln(^{86}Sr/^{88}Sr)$ for a typical TIMS MI analysis compared with non Kr corrected and Kr corrected LA-MC-ICPMS MI analysis. Raw LA-MC-ICPMS data are taken from intensity data reported by Jackson & Hart (2006) and corrected for Kr interferences. Accurate Kr correction should place the *'corrected'* data on a mass fractionation trend. To avoid the problem of needing to know the exact Kr isotope ratio during analysis, Jackson & Hart (2006) correct all data back to the canonical $^{84}Sr/^{86}Sr$ ratio. Also shown is the typical range in mass fractionation obtained for a single solution-mode MC-ICPMS analytical session on the *AHGIL* Neptune, for samples containing >>100 ng Sr that generate ^{88}Sr signals >10 V, sufficient to render Kr based interferences negligible. The *'accepted'* $^{84}Sr/^{86}Sr$ and $^{86}Sr/^{88}Sr$ composition for natural Sr in the NBS 987 standard is likewise included. These values are generated from the relative abundances of naturally occurring Sr isotopes [$\ln(^{84}Sr/^{86}Sr)$ = ln(0.5574/9.8566) = -2.873, and $\ln(^{86}Sr/^{88}Sr)$ = ln(9.8566/82.5845) = -2.126]. The red line passing through both our TIMS data and MC-ICPMS solution-mode analytical session is the expected trend for samples fractionating according to the exponential law. b) The 2SE internal precision (in ppm) versus ^{88}Sr signal for MIs analysed by TIMS in this study and by LA-MC-ICPMS (Jackson & Hart, 2006). ^{88}Sr signal is given as the total integrated ^{88}Sr signal (in V) divided by the length of the analysis in seconds. The black line represents the theoretical precision calculated from counting statistics alone.

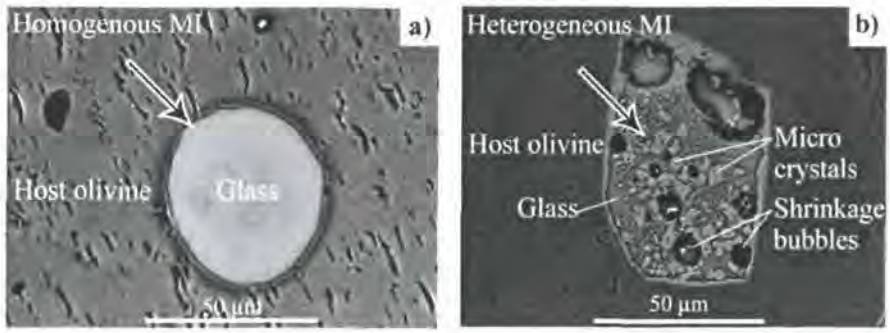

Figure 2.2: MIs example from olivine phenocrysts of the Vestfirdir ankaramites, NW Iceland. a) A spherical homogenous glassy MI, and b) an angular heterogeneous MI consisting of glass, micro crystals, and shrinkage bubbles.

2.4 Experimental

2.4.1 Reagents and equipment

All reagents used for the sample dissolution and column chemistry are ultra purity Teflon distilled acids (UpA) manufactured by Romil Ltd. In the following all acids mentioned are UpA quality, unless otherwise stated. Each batch of new acid is blank checked using the methods described below. Working reagents are produced from these stock acids by diluting with 18.2 mega ohm resistivity water produced from a Milli-Q Element water system (hereafter referred to as MQ H_2O and MQ system).

All the low concentration work (milling, weighing, chemistry, and analysis) was carried out in custom-built class 100 laminar flow work environments. Also, the ultra clean laboratory has a class 100 laminar flow extracted workstation dedicated for low abundance Sr chemistry (<20 ng). For work with samples of <1 ng we established separate reagent bottles plus column leaching facilities, and maintained a separate population of Teflon beakers devoted to ultra-low-level Sr work.

2.4.2 Monitoring of blanks - reagent blanks

When working at sub-ng Sr levels it is crucial to continually monitor both the magnitude of the analytical blank, its variability and its isotope composition, in order to make a meaningful, accurate blank correction. To achieve low and reproducible blank levels it is necessary to obtain a thorough understanding of the potential contributions from all reagents and labware that are involved in the sampling, chemistry and loading procedures. In order to establish this we undertook an extensive testing program that is reported in section 2.5.1.

Items such as tissues for drying were weighed out. Leaching blanks on pipette tips were recorded in terms of the volume of reagent used in the leaching. All tissue plus frit materials were leached in sealed Teflon beakers for 24 hours at 80°C on the hot plate, whereas pipette tips

and centrifuge tubes were leached at room temperature for one week in 2-6M HCl. Following the leaching period, the materials were removed from the Teflon beakers and the leaching reagents were dried down. Storage acids used to keep tweezers and columns were likewise dried down and tested. Also, contamination levels for different coloured centrifugation tubes were monitored. The leaching solutions from plasticware contained significant residual organics that can be difficult to redissolve if dried out at too high temperature or for too long. In such situations, use of Tamapure® hydrogen peroxide aids sample redissolution.

It is important to monitor the cleanness of our reagents and MQ H_2O through time. Therefore, the quality of the MQ H_2O is checked routinely, and each new batch of concentrated acid is tested before use. For all reagent blanks, 30-50 mL of concentrated acids were dried down in dedicated Teflon beakers at 150°C. Aliquots of diluted acids from wash bottles were also blank tested. 200 mL of MQ H_2O was dried down from our storage Teflon bottle, hand operated and foot-operated MQ system respectively.

The residues of the material blanks and reagents including the MQ H_2O are taken up in 250 µL of 3% concentrated (16M) HNO_3 (hereafter labelled 3% HNO_3). In order to test bank contributions from the pre-cleaned beakers 250 µL 3% HNO_3 were pipetted into five 3 mL beakers. To ensure effective redissolution of residues Teflon beakers were heated at 60°C for approximately 30 minutes on the hot plate prior to ICPMS analysis.

2.4.3 Total procedural blanks

All TPB in this study were collected in Teflon beakers from the same population as those used for sample analysis so that potential beaker cross contamination was taken into account. The measurement of the TPB Sr isotope composition is extremely challenging because of the very low analyte levels (<5 pg Sr per TPB, see below). To compensate for this it was necessary to pool multiple TPB to yield sufficient Sr for an adequate signal for analysis (^{88}Sr ~0.1 V). Furthermore, to check the consistency of the composition of our lab TPB this procedure was replicated 3 times during the time interval of this study.

2.4.4 Micro sampling techniques

Sample preparation for MI studies is extremely time consuming, since the process often includes rehomogenization experiments, and the preparation of polished epoxy grain mounts plus detailed microscopic examination (Appendix A2-A3). Micro-milling further increases the preparation time, although homogenization of the MIs prior to sampling is not required. We have used two methods for sampling MIs hosted in olivine phenocrysts. The first approach is to pick whole olivine grains with multiple entrapped MIs. Although relatively rapid this approach has limitations, since it can only be used on extremely fresh host olivine, free of adhering

groundmass glass. Furthermore, this method obviously averages the composition of multiple MIs. While useful data can still be obtained, this '*whole grain*' sampling can mask the full variation in MI isotope compositions. The second approach is to use a micro-mill to selectively extract individual MIs from olivine crystals in grain mounts or thick sections. To access primary, well-preserved individual MIs hosted in altered host olivine phenocrysts the most effective method is to sample by micro-milling, avoiding altered zones.

2.4.4.1 Selection of whole grains and preparation for dissolution

Olivine grains containing single or multiple primary MIs were handpicked under the microscope from coarse crushed sample material. Also, olivine grains free of visible MIs and oxides were picked for the purpose of checking the trace element content and in particular the Sr and Rb content in pure olivine grains (section 2.5.3). It is of extreme importance that grains are carefully selected so that only grains without adhering high Sr groundmass glass are selected for dissolution. Prior to dissolution the olivine crystals are cleaned of any groundmass dust by leaching in an ultrasonic bath for 15 minutes in 2.5 mL of 2M SpA HCl (SpA is super purity quartz distilled acid from Romil Ltd.), followed by three rinses with MQ H_2O. After cleaning the olivine crystals were transferred to 7 mL Teflon beakers for dissolution.

2.4.4.2 Micro-milling and sample preparation

To enable micro-milling, olivine grains containing MIs were mounted in 25 mm epoxy discs. All grain mounts were polished in order to bring the MIs as close to the surface as possible. Each individual MI was carefully examined under the microscope, and only primary, well-preserved unbreached MIs were photographed and mapped out for the micro-milling. The limitations of the binocular microscope mounted on the micro-milling system make it impossible to obtain exact details regarding the morphology of the MIs and their location prior to milling.

For the micro-milling we use the New Wave MicroMill described in detail by Charlier et al. (2006) with small adjustments in the approach. The mill is housed in a custom-built class 100 laminar flow workstation. Prior to milling the grain mounts and drill bits were carefully cleaned in an ultrasonic bath in MQ H_2O and ethanol respectively. A pre-cleaned 4 mm ring of Parafilm was placed around the area to be milled. A droplet of MQ H_2O is then placed in the centre of the Parafilm ring to collect the sample dust during the milling and also to cool the drill bit. The droplet containing the sample is pipetted into a pre-weighed gold weighing boat immediately after milling. The gold weighing boat loaded with the sample material is placed on a hotplate in order to evaporate the MQ H_2O. Once dry the weighing boat plus sample dust is weighed using a Mettler UMT-2 microbalance housed in a class 100 filtered airbox. Finally the weighing boat is transferred to a clean 3 mL Teflon beaker for sample dissolution.

2.4.5 Dissolution of samples

The olivine crystals were dissolved using a standard dissolution procedure for silicates, modified to account for the greatly reduced weight of sample (Appendix B1). The first dissolution step for single olivine grains uses 200 µL 29M HF and 50 µL 16M HNO_3, whereas the multiple grains are dissolved using 750 µL 29M HF and 250 µL 16M HNO_3. Sealed beakers were left on the hotplate over night at 100°C. Samples are then dried down and taken up in 200 or 500 µL respectively of 6M HCl and left overnight at 100°C. After further drying, the samples are taken up in 200 or 500 µL 16M HNO_3, and heated overnight. The dry down residues are taken up in 200 µL 3M HNO_3 and heated at 80°C for an hour. Prior to column chemistry the samples are first centrifuged and next aliquoted.

A down-scaled version of the micro Sr sample dissolution procedure presented in Charlier et al. (2006) was used for the milled sample material (Appendix B1). For the initial dissolution step 100 µL 29M HF and 30 µL 16M HNO_3 were used, followed by dissolution in 100 µL 6M HCl, and next 100 µL 16M HNO_3. The final sample residues are re-dissolved in 200 µL 3M HNO_3 and heated at 80°C for an hour prior to aliquoting and micro Sr column chemistry.

2.4.6 Micro Sr chemistry

2.4.6.1 Aliquots for TIMS and ICPMS

Following dissolution, and prior to column chemistry, a 10% (by volume) aliquot of the 3M HNO_3 is removed from the main sample solution for ICPMS elemental analysis, including Rb and Sr. The remaining solution is assigned to Sr isotope chemistry. We used freshly calibrated pipettes to ensure best possible accuracy during the aliquoting. The aliquoting was double checked by weighing the sample stock solution prior to and after the 10% aliquoting was taken. The 10% aliquots are transferred to pre-cleaned and pre-weighed 3 mL Teflon beakers and taken to dryness. The dried sample residue is then taken up in pre-leached 250 µL of 3% concentrated HNO_3 and transferred to 250 µL test tubes, at which stage they are ready for ICPMS analysis. This minimal sample handling contributes to maintaining excellent TPB (section 2.5.2).

2.4.6.2 Micro Sr column chemistry

The basis of the micro Sr chemistry technique revolves around the use of Sr spec resin by Deniel & Pin (2001) adapted for micro samples by Charlier et al. (2006) and modified as follows for application to MI analysis (Appendix B1).

We use disposable columns made from 1 mL pipette tips fitted with a circular cut piece of pre-cleaned frit (pore size of 30 µm, see Charlier et al., 2006 for further details). Before use, the

columns are leached in dilute (<1M) HCl, first on the hotplate at 60°C for a couple of hours and thereafter left to leach at room temperature for approximately a week or until required. Columns are rinsed thoroughly with MQ H_2O before being placed in the column racks. Using a dropper bottle, two droplets (~60 μL) of pre-cleaned Sr spec resin (details on the resin cleaning protocol given in Charlier et al., 2006) are placed in each column. In order to clean the Sr spec resin further prior to loading the sample, two column volumes (CV) of 6M HCl and 3 CV of MQ H_2O are passed through each column. The resin is pre-conditioned with 2 loads of 100 μL of 3M HNO_3. The sample, dissolved in 3M HNO_3, is now loaded. In order to improve column yields for such small volumes of resin, the eluted sample is collected into the original 3 mL Teflon beaker and reloaded on the column. After sample loading, 0.5 mL of 6M HCl is pipetted into each sample beaker and the beakers are placed on the hotplate (80°C) to leach until required for collection of the Sr fraction. To wash off Rb and Ca we used a total volume of approximately 500 μL of 3M HNO_3 (increments of 50, 100, and 150 μL). The total volume required depends on the column calibration (Appendix B2). The Sr fraction is collected in 300 μL of MQ H_2O into the 3 mL Teflon beakers. The Sr fraction is then dried in preparation for TIMS analysis. Calibrations of this procedure by Deniel & Pin (2001) and Charlier et al. (2006) have shown that it is exceptionally efficient at the removal of Ca, which can inhibit Sr ionization.

2.4.7 Mass spectrometry: TIMS and ICPMS analysis of sub-ng Sr samples

2.4.7.1 Filament loading

All MI Sr samples are loaded onto Re filaments strung on filament holders that are reserved specifically for MI work (Appendix B3). Single Re filaments are outgassed at 3.9 A for 20 minutes before loading. To ensure a small area for the filament load, 2 strips of Parafilm are melted onto the surface, 1 mm apart and the load is placed within this area. A TaF_5 activator is then added (Birck, 1986). The activator is cleaned of Rb following the ammonia precipitation method outlined in Charlier et al. (2006). Approximately 0.5 μL of TaF_5 activator is used for loading both standards (NBS 987) and samples. For standards, a drop of activator is mixed with the required amount of standard on the filament and dried slowly at <1 A. After drying the current is slowly increased to about 2.0 A to burn off the Parafilm. The current is then increased to about 2.2-2.4 A for several seconds causing the filament to glow orange/red. The procedure for loading samples is very similar except that the dried sample residue is picked up in 1.0 μL of 16M HNO_3. All filament holders and associated parts are reserved specifically for sub-ng analytical work.

2.4.7.2 TIMS analysis protocol

TIMS analyses were performed on a ThermoFinnigan Triton at the *AHGIL* (Department of Earth Sciences, Durham University). The *AHGIL* Triton is only used for the isotope analysis of

Os, in negative ion mode, and small Sr samples (<12 ng) in positive ion mode. Each element has its own dedicated source chamber, with associated contact assemblies, ion lens stack and sample magazine. We always clean the positive ion lens stack and sample magazine again prior to a period of sub-ng Sr analytical work. The front protection plate to the ion lens stack is replaced between each magazine of samples and often at the end of the day's analytical session.

Once the magazine is loaded into the Triton the source chamber is pumped down until the pressure reached $<10^{-7}$ mbar before proceeding with analyses. As it is essential to ensure minimal background noise conditions, aided by maintaining the analyzer vacuum below $3x10^{-9}$ Torr, it is recommended that the analyzer gate (line of sight valve) is closed during the initial heating of each filament. Due to the background noise, in particular within the amplifier system, it is crucial to obtaining accurate and precise analyses at the low signal sizes produced. Standard and sample filaments are heated at 50 mA/min until a Rb signal is observed (typically 800-1000 mA) at which point the current is held constant while the Rb is allowed to '*burn off*'. Once the Rb starts to decrease the filament current is increased at the same rate until an ^{88}Sr intensity of ~10 mV is obtained. Using ^{88}Sr in H3 as the control isotope the filament is focussed and a peak centre routine performed. A 30 sec instrument baseline is then performed, with the beam deflected using the x-symmetry lens, prior to the start of an analysis.

Sr is measured using a static multi collection routine and the cup configuration given in Table 2.2. ^{88}Sr is collected in the H3 rather than H2 Faraday because the cup efficiency for H2 changed, for Sr only, by ~50 ppm in 2002 (G.M. Nowell, personal com.). Although H2 was replaced the cup configuration in Table 2.2 has been retained for continuity. For both standards and samples an analysis comprises up to 50 blocks of 10 ratios (section 2.4.7.3) with a 4 second integration time. Amplifier rotation is not used since it provided little improvement in accuracy or precision at low signal sizes.

Cup	Analyte	Interference
L2	^{84}Sr	
L1		^{85}Rb
C (axial)	^{86}Sr	
H1	^{87}Sr	^{87}Rb
H3	^{88}Sr	

Table 2.2: Cup configuration used on for the analysis of Sr on the thermal ionization mass spectrometry (TIMS). The TIMS used is the Thermo-Finnigan Triton at *AHGIL* (Durham University). Species in *italic* is the monitor isotope used for the correction of ^{87}Rb on ^{87}Sr.

2.4.7.3 *Collection and processing of TIMS data*

The maximum ^{88}Sr beam intensity and the longevity of analysis that may be obtained on any given MI is dependant not only on the total amount of Sr on the filament, but on additional factors such as cleanliness of the Sr chemistry and how well it is loaded on the filament. Therefore, despite knowing the approximate amount of Sr loaded on the filament, based on the analysis of the ICPMS trace element aliquot, it is very difficult to predict how any given MI will run. Because of this uncertainty we have adopted a protocol whereby data collection starts very early, when the ^{88}Sr is often too small for high quality $^{87}Sr/^{86}Sr$ data <20 mV, simply as a security measure in case the sample subsequently fails (Figure 2.3). The filament current, and hence ^{88}Sr intensity, is increased during data collection and the $^{86}Sr/^{88}Sr$ ratio continually monitored to assess the degree of fractionation.

Following analysis the data is exported and each sample run is evaluated *offline* in a time resolved sense for the ^{88}Sr and ^{85}Rb intensities and $^{87}Sr/^{86}Sr$ ratio (Figure 2.3). Typically, for a MI analysis the ^{88}Sr grows steadily and may reach several hundred mV before decreasing, becoming increasingly unstable and often ending with a sudden and very short lived spike in ^{88}Sr intensity of >1-2 V (Figure 2.3a). Despite *'burning off'* Rb during the heating stage a small amount (generally less than 0.5 mV) of ^{87}Rb is still sometimes present at the very start of a data collection although this generally decreases to negligible levels within the first 100 ratios. The presence of ^{87}Rb on ^{87}Sr is adequately corrected for as shown by the lack of skew in $^{87}Sr/^{86}Sr$ toward higher values in the first 100 ratios of a typical MI analysis (Figure 2.3b). The spread in $^{87}Sr/^{86}Sr$ is clearly very large early in the analysis (Figure 2.3b), due to the very low ^{88}Sr intensity (<20 mV), but decreases significantly once the ^{88}Sr exceeds 100 mV. Assuming a sample run improves throughout the analysis as in Figure 2.3b, this early data is usually discarded before the remaining ratios are processed further using a standard 2SE rejection criteria. It is important to stress that although the number of early ratios we discard is subjective, the distribution in $^{87}Sr/^{86}Sr$ for this data is Gaussian and hence rejecting it has little effect on the final average Sr isotope composition for the sample. In the case of the example in Figure 2.3b the difference in $^{87}Sr/^{86}Sr$ with and without the first 120 ratios, but including a 2SE rejections, is only 0.175%. The most obvious improvement to the data is the internal precision, which drops from 237 ppm to 94 ppm (2SE) when discarding the first 120 ratios.

2.4.7.4 *ICPMS analysis protocol*

Specific methods were established to analyze the following trace elements Sr, Rb, Ti, Nb, REE, and Y on a ThermoElectron ELEMENT2 double focusing magnetic sector ICPMS at *AHGIL* (Department of Earth Sciences, Durham University) see Appendix B5. The instrument was fitted with a 100 μL/min micromist glass concentric nebuliser operating at an uptake rate of

about 125 µL per minute, together with an ESI stable introduction system quartz dual spray chamber. The Element 2 was tuned using an In standard solution, and prior to analysis the oxide production rate was checked using 1 ppb solutions of Ba, La, Ce, Pr, Nd, Sm, and Gd (Appendix B4). Oxide production was kept below 3% for all elements of interest. Interference on the mass spectrum of Ba, La, Ce, Pr, Nd, Sm, and Gd were monitored and corrected. Details on the running conditions are presented in Table 2.3, and method files are located in Appendix B5.

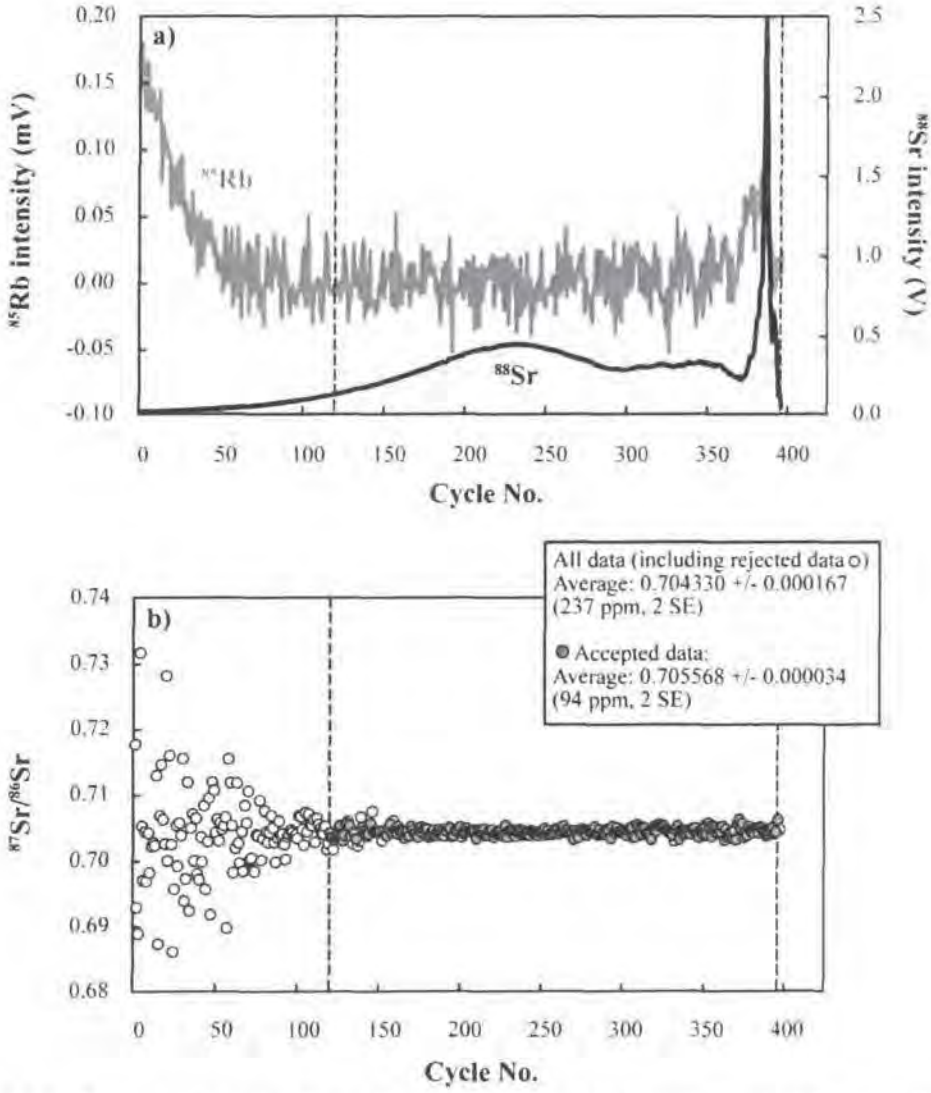

Figure 2.3: a) ^{85}Rb (primary x-axis, mV) and ^{88}Sr (secondary x-axis, V) intensities obtained during a typical TIMS MI Sr analysis at AHIGL (Department of Earth Sciences, Durham University), shown as a function of number of cycles. b) Variation in ^{87}Sr/^{86}Sr measured during the course of the analysis shown above. Early cycles show considerable spread in ^{87}Sr/^{86}Sr ratios primarily as a result of very the small Sr beam size, but show much less variation once ^{88}Sr exceeds ~0.1 V. Data collected prior to cycle 120 (left of the first vertical dashed line in both plots) is manually rejected (white circles) before a standard 2 sigma (SD) rejection is applied to the remaining accepted cycles (filled circles).

Instrument	**Thermo ELEMENT2**: a double focusing magnetic sector field inductive mass plasma mass spectrometer (ICPMS)
Nebuliser and spray chamber	100 μL/min micromist glass concentric nebuliser combined with an ESI stable introduction system quartz dual spray chamber
RF power	1300 watts
Plasma cool gas (Ar) flow rate	16 L/min[1]
Auxillary gas (Ar) flow rate	1 L/min
Nebuliser gas (Ar) flow rate	~0.95 L/min
Resolution	300 (low)
Isotopes measured	^{49}Ti, ^{85}Rb, ^{88}Sr, ^{89}Y, ^{90}Zr, ^{93}Nb, ^{137}Ba, ^{139}La, ^{140}Ce, ^{141}Pr, ^{143}Nd ^{147}Sm, ^{151}Eu, ^{157}Gd, ^{161}Dy, ^{166}Er, ^{172}Yb
Sample time	10-30 msec dependant on isotope
Samples per peak	20
Mass window	60
Runs	4
Passes	3
Total time per sample	52 sec

Table 2.3: The ICPMS running conditions used for determination of low abundance trace element sample material specifically aimed at MI work at *AHIGL* (Department of Earth Sciences, Durham University). Calibration: Matrix matched using international standard materials AGV-1, W-2 and BHVO-1 (Appendix B7). These were supplemented with synthetic solution made from Romil Ltd. 1000 ppm stock solutions to confirm calibration linearity. Sensitivity: optimised to give low oxide generation whilst maintaining high overall sensitivity. Typically oxides CeO/Ce <2.5 % with 1ppb In $>1x10^6$ cps (Appendix B4). Polyatomic oxide generation: on the REE were corrected using simple correction algorithms. Individual 1 ppb Romil Ltd. standard solutions of the interfering elements were analysed at the beginning of an analytical run and the oxide production rate incorporated into the analytical method. This production rate is confirmed during and at the end each session (Appendix B4).

Samples are analyzed against a calibration line derived from standard rock solutions of AGV-1, BHVO-1, and W2 (diluted to match the approximate concentration range of the sample solutions). Once the calibration line is established these standard rock solutions were analyzed as *'unknowns'* to check the consistency of the calibration line. Evaluation of instrumental precision and accuracy is achieved by running synthetic solution containing Rb and Sr (proportion 1:10) respectively covering the range of 0.1 to 20 ppt and 1 to 200 ppt. Details on the quality of the ICPMS data is located in section 2.5.4.

The sample sequence was set up as follows: Samples were analyzed in batches of 10, and between each sample a wash blank (3% HNO_3) was run. The wash blanks were analyzed in order to monitor of the stability and background, but also to monitor the cleanness of the instrument. Bracketing each batch of 10 samples is a selection of rock standard solutions and synthetic Rb-Sr solutions plus a calibration blank, which were used to monitored potential drift of the instrument through the analytical session.

Initial data processing was done using the online software provided by ThermoElectron. Drift correction was done off line using the data collected on standard rock and synthetic Rb-Sr solutions analyzed before and after each batch of samples.

2.5 Results and discussion

2.5.1 Reagent and material blanks

The results of the reagent blank testing are shown in Table 2.4a. The analyses reveal that of the three concentrated stock acids used in the chemistry, the largest Rb-Sr blank contribution comes from HF followed by HNO_3 and HCl. The MQ H_2O (used for dilution of the reagents) has <0.1 pg Sr and <0.04 pg Rb per mL. It was noticed that MQ H_2O tapped and tested right after a filter change generally has a higher level of Rb-Sr-Nd-Hf-Pb. Comparing the acid directly from the stock Teflon bottle, with the acid decanted into wash bottles, and in a smaller Teflon vial (used for pipetting), illustrates the increased level of contamination that results from increased degrees of handling. This is also true for the processing of sample material. Adding more steps potentially introduces new sources of contamination.

The material blank test results are presented in Table 2.4b. In order to limit potential cross contamination from previous sample digestions, dedicated low abundance (<1 ng Sr) Teflon vials were always used. The pre-leaching tests of the 3 different sizes of centrifuge tubes (2 mL, 500 µL, and 250 µL) suggest that the uncoloured 250 µL centrifuge tubes are most suitable for the low concentration work, because they have the lowest Rb and Sr backgrounds. Similar systematics are observed for the colourless and coloured pipette tips. Testing of the different items used in the process of making the disposable micro Sr columns reveals several potential sources of contamination (frit material, frit cutter, pipette tips). This illustrates the importance of pre-cleaning the assembled column by leaching in dilute HCl before use, and that the storage acid should be changed on a regular basis. It is also clear that certain types of tissue, especially Envirotex and Hospitex have very high levels of Sr (17.28 and 68.55 ng/g) and Rb (3.14 and 1.51 ng/g), so their use should be eliminated (Table 2.4b).

The theoretical contribution of Rb and Sr from the each reagent used during the sample processing as percentage of the average TPB is shown in Figure 2.4 (calculations are based on the average concentrations of the stock acids). Depending on the total volume of reagent used in the sample processing, the reagents only account for <15% of Sr, but up to 61% of the Rb content of the average TPB. This suggests that most of the Sr blank contribution is added during the column chemistry, thus originating from the Teflon beaker, centrifuge tube, disposable column, pipette tips, but mostly from the Sr spec resin rather than the reagents (Table 2.4-2.6). In contrast, the Rb content of the TPB seems less affected by such contributions. Analyses of

multiple column blanks gave a similar result to our average TPB (3.98 pg versus 4.86 pg Sr) further suggesting that the resin dominates the Sr blank (Table 2.5). The trace element and Sr isotope signatures of the Sr spec resin was determined by collecting and analyzing the first 600 mL (of a total of 6 L, details on the cleaning procedure is found in Charlier et al., 2006) of cleaning reagent passed through ~10 mL of Sr Spec resin. This initial resin wash yielded ~ 21 ng Sr and 12 pg Rb per mL of resin (Table 2.5). The column chemistry calls for approximately 60 μL resin. 60 μL of uncleaned resin could contain as much as 1.28 ng Sr and 0.7 pg Rb. So if a fraction of this Sr remains after resin cleaning it has a profound influence on the Sr content of the TPB. In contrast, the effect on the Rb content of the TPB is less dramatic.

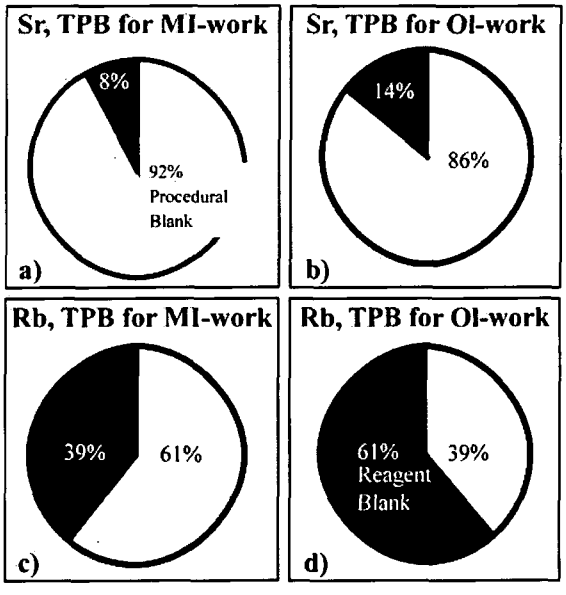

Figure 2.4: Pie charts in a) and b) show the Sr contributions from the reagents and the column procedure itself, while the Rb contributions are shown in c) and d). The procedural blank (TPB) is comprised of contributions from the Teflon beaker, gold weighing boat, frit fitted column, Sr-spec resin, plus pipette tips, and centrifuge tube. The black *'pie portions'* represent the blank contributions accounted for by reagents alone. The white coloured *'pie portions'* represent the percentage of the TPB not related to the reagents. Comparing the Rb-Sr TPB of MI work in a) and c) with the Rb-Sr TPB of the whole olivine grain batch work in b) and d) illustrates that the increased volume of reagents used of the whole grain dissolution increases the overall blank.

Reagent	Storage	Volume (mL)	Concentrations (pg/mL)				
			Rb	Sr	Nd	Hf	Pb
MQ H_2O							
Hand	Stock	200.00	0.07	0.11	-	-	4.20
Hand*	Stock	200.00	0.10	0.17	-	0.01	3.03
Hand	Stock	200.00	0.02	0.03	-	-	2.42
Hand*	Stock	170.00	0.01	0.14	-	0.02	0.24
Foot*	Stock	200.00	0.07	0.13	0.01	0.04	3.57
Foot	Stock	170.00	0.02	0.03	-	0.01	2.18
Foot	Stock	200.00	-	0.07	-	0.01	0.01
Foot*	Stock	200.00	0.11	0.21	0.14	0.02	8.10
UpA HNO_3							
Conc.	Stock	50.00	0.03	0.08	0.01	0.08	0.57
Conc.	Stock	30.00	0.05	0.22	0.01	0.04	5.46
Conc.	Wash	30.00	0.22	0.90	0.13	0.36	8.27
3M	Wash	43.00	0.37	0.31	0.02	0.07	2.96
3M	Beaker	1.00	0.11	0.98	-	0.02	6.77
0.05M	Stock	50.00	0.02	0.06	0.01	0.05	0.83
0.05M	Wash	38.00	0.01	0.13	0.01	0.02	0.20
UpA HCl							
Conc.	Stock	51.50	0.03	0.09	0.01	0.40	0.40
Conc.	Stock	50.00	0.03	0.10	0.02	0.03	1.13
8M	Wash	39.50	0.03	0.09	0.01	0.04	0.40
8M	Beaker	0.39	1.84	9.00	1.46	1.21	53.53
6M	Beaker	0.67	0.64	4.27	0.31	0.42	36.10
2.5M	Stock	49.50	0.05	0.13	0.01	0.02	0.77
2.5M	Wash	30.00	0.04	0.08	0.01	0.05	0.22
UpA HF							
Conc.	Stock	51.00	0.26	0.28	0.10	0.98	1.16
Conc.	Beaker	3.82	0.61	3.24	0.11	14.14	12.58
H_2O_2							
30%	Stock	25.00	0.09	0.83	0.11	0.81	5.23

Table 2.4a: Concentrations (pg/mL) of Rb, Sr, Nd, Hf, and Pb in reagents used during sample preparation and chemical processing. The element concentrations are obtained by double focusing magnetic sector field ICPMS (Thermo ELEMENT2) at *AHIGL* (Department of Earth Sciences, Durham University). Concentrations below the limit of detection are indicated by horizontal bars (-). 'MQ' refer to a Milli-Q Element system from which the H_2O is tapped, and 'hand' and 'foot' denotes it was tapped respectively from the hand operated tap or the foot-operated tap. The star (*) marks that the particular batch of MQ H_2O was tapped right after filter change. The molarity (M) is given for each acid. Conc. means concentrated acid, which is 16M for HNO_3, but 12M for HCL and 29M for HF. UpA is ultra purity Teflon distilled acids from Romil Ltd. Storage denotes which kind of storage unit the reagents are kept in. Following terms indicate: stock is 500 mL Teflon stock bottle, wash is 250 mL Teflon wash bottles, beaker equals 7 mL Teflon beaker.

Material	Leaching reagent	Rb	Sr	Nd	Hf	Pb
Storage acid and rinse of disposable micro columns (pg/mL)						
Storage acid	Old dilute UpA HCl	11.27	74.03	3.10	4.02	860.89
Storage acid	Old dilute UpA HCl	11.36	74.28	3.45	4.66	967.28
Storage acid	New dilute UpA HCl	3.11	10.46	0.60	0.02	162.28
Inside rinse	MQ H_2O	1.67	4.22	0.26	0.29	58.61
Inside rinse	MQ H_2O	1.51	2.86	0.40	1.49	29.33
Outside rinse	MQ H_2O	6.93	14.99	1.78	0.17	159.96
Outside rinse	MQ H_2O	0.56	1.23	0.33	0.07	18.58
Disposable micro column blanks (pg/column)						
Column, thin frit		-	4.09	-	4.46	-
Column, thin frit		-	8.16	-	1.92	-
Column, thin frit		0.37	6.28	-	3.28	-
Column, thin frit		-	6.03	-	-	0.29
Column, thin frit		0.03	6.21	-	-	-
Column, thick frit		0.04	4.72	-	-	-
Column, thick frit		0.01	3.41	-	0.76	-
Column, thick frit		0.16	5.10	-	-	0.67
Column, thick frit		0.03	5.71	-	0.75	-
Column, thick frit		-	3.24	-	-	-
Column, thick frit		-	1.68	-	0.24	-
Ave. Column, thick frit*		0.06	3.98	-	0.38	0.67
3 mL Teflon beaker blanks (from the general stock, pg/beaker)						
3 mL Teflon beaker	3% UpA HNO_3	2.37	8.96	0.87	0.94	28.78
3 mL Teflon beaker	3% UpA HNO_3	2.15	8.56	0.77	0.80	29.29
3 mL Teflon beaker	3% UpA HNO_3	2.83	8.16	0.84	0.84	31.10
3 mL Teflon beaker	3% UpA HNO_3	2.30	8.19	0.85	0.78	27.41
3 mL Teflon beaker	3% UpA HNO_3	2.25	7.44	0.74	0.78	25.91
Colored 2 mL centrifugation tubes (pg/tube)						
Colorless	6M SpA HCl	2.76	13.86	0.62	0.53	20.72
Yellow	6M SpA HCl	6.20	40.08	2.38	0.48	63.30
Orange	6M SpA HCl	4.59	24.22	2.42	0.16	82.89
Red	6M SpA HCl	3.04	45.15	1.54	0.27	61.69
Purple	6M SpA HCl	4.21	30.99	1.54	0.36	453.48
Blue	6M SpA HCl	4.88	23.10	1.45	0.22	55.57
Green	6M SpA HCl	16.90	28.30	1.78	0.34	82.13

Table 2.4b: Materials tested of their content of Rb, Sr, Nd, Hf, and Pb. These materials are used in during sample preparation and chemical processing. The element concentrations are obtained by double focusing magnetic sector field ICPMS (Thermo ELEMENT2) at *AHIGL* (Department of Earth Sciences, Durham University). Concentrations, which are below the limit of detection are indicated by horizontal bars (-). UpA and SpA denote ultra purity Teflon distilled and super purity quartz distilled acid from Romil Ltd.*All MI work presented is processed through micro columns fitted with the thick frit material.

Material	Leaching reagent	Rb	Sr	Nd	Hf	Pb
0.500 mL colourless centrifugation tubes (pg/tube)						
Tube 1	6M SpA HCl	-	4.12	-	4.57	-
Tube 2	6M SpA HCl	-	3.81	-	3.48	-
Tube 3	6M SpA HCl	-	4.77	-	2.41	-
Tube 4	6M SpA HCl	-	3.92	-	2.14	-
Tube 5	6M SpA HCl	0.89	7.03	-	1.85	-
0.250 mL colourless centrifugation tubes (pg/tube)						
Tube 1	6M SpA HCl	1.18	1.78	-	7.59	4.14
Tube 2	6M SpA HCl	0.08	-	-	6.66	-
Tube 3	6M SpA HCl	-	-	-	3.04	-
Tube 4	6M SpA HCl	-	-	-	5.49	-
Tube 5	6M SpA HCl	-	-	0.07	2.49	-
Coloured pipette tips (pg/tube)						
Yellow, 0.250 mL, dirty	2M UpA HCl	0.03	0.26	-	-	0.50
Yellow, 0.250 mL, clean	2M UpA HCl	0.05	0.25	0.01	-	0.44
Colorless, 0.250 mL, dirty	2M UpA HCl	0.02	0.16	0.01	-	0.36
Colorless, 0.250 mL, clean	2M UpA HCl	0.02	0.17	0.01	-	0.28
Blue, 1 mL, dirty	2M UpA HCl	2.30	45.35	1.56	0.12	2.58
Frit material for micro Sr columns (pg/g)						
Frit ring	6M SpA HCl	0.27	1.06	0.13	0.05	49.97
Frit square	6M SpA HCl	0.03	0.15	0.01	0.19	0.66
Frit square	6M SpA HCl	0.16	0.23	0.05	-	1.24
Tissue (ng/g)						
Envirotex	6M SpA HCl	3.14	17.28	0.97	0.19	0.87
Micropure	6M SpA HCl	0.12	11.01	0.45	-	0.60
Hospitex	6M SpA HCl	1.51	68.55	0.20	0.12	4.09
Tools (pg/mL)						
Plastic twizer	2M UpA HCl	0.32	1.77	0.07	0.07	6.77
Plastic twizer	MQ H_2O	8.09	20.46	0.12	0.08	116
Metal frit cutter	MQ H_2O	16.48	25.77	0.10	0.13	628
Tungsten carbide mill bits (including beaker blank, pg/bit)						
Mill bit 1, dirty	MQ H_2O	0.32	8,28	-	-	-
Mill bit 2, clean	MQ H_2O	0.09	4.41	-	-	-
Mill bit 3, clean	MQ H_2O	0.20	6.90	-	-	-
Mill bit 4, clean	MQ H_2O	-	4.61	-	-	-
Mill bit 5, clean	MQ H_2O	0.15	7.60	-	0.13	-

Table 2.4b: Continued.

Batch ID	M14-71	M14-72	Average	0.060 ml
Material	Resin	Resin	Resin	Resin
Sr isotope composition				
$^{87}Sr/^{86}Sr_{Norm}$	0.709937	0.709867	0.709902	
±2SE	0.000051	0.000020	0.000036	
Trace elements (pg/mL)				
Ti	153.21	0.37	*76.79*	4.61
Rb	10.99	12.14	11.57	0.69
Sr	**21.45**	**21.19**	**21.32**	**1.28**
Y	1.11	1.09	1.10	0.07
Zr	199.17	28.61	*11.39*	*0.68*
Nb	3.72	5.08	4.40	0.27
Ba	**10.00**	**8.63**	**9.32**	**0.56**
La	1.20	1.26	1.23	0.07
Ce	1.89	1.82	1.86	0.11
Pr	0.44	0.12	0.28	0.02
Nd	1.39	1.89	1.64	0.1
Sm	-	-	-	-
Eu	-	0.17	*0.17*	0.01
Gd	-	0.14	*0.14*	0.01
Dy	0.57	0.34	0.46	0.03
Er	0.06	-	*0.06*	-
Yb	0.14	0.08	0.11	0.01

Table 2.5: Trace element composition of initial rinse of 10 mL uncleaned Sr spec resin given in pg/mL. Exceptions are concentrations for Sr and Ba (bold numbers), which are given in ng/mL. The first 600 mL cleaning reagent (mixture of MQ H_2O, 6M HCl, 0.05M HNO3, and 0.1M H_2SO_4) were collected, dried down, and prepared for Sr isotope (TIMS) and trace element determination (ICPMS). Two aliquots were analyzed. Concentrations, which are below the limit of detection are indicated by a horizontal bar (-). Listed is the concentration in 60 µL uncleaned resin, which potentially would be contributed to the TPB during micro Sr column chemistry if not cleaned thoroughly. Details on the cleaning procedure of Sr spec resin in Charlier et al. (2006). Concentrations in *italic* denote that only one measurement was obtained or that there is a relative large difference between the two measurements.

2.5.2 Total procedural blanks

2.5.2.1 The Sr isotope and element characteristics of TPB

The most precise and reliable Sr isotope composition of the up-scaled TPB (equal to 60 pooled TPBs) obtained during the course this work is 0.712392 ±0.000234 (2SE), (Table 2.6). The average typical TPB (n=29) has 4.86 ±0.26 pg Sr and 1.32 ±0.69 pg Rb (Table 2.6). The limit of detection (LOD = 3xSD) for the sampling and digestion method was established to be 0.73 pg for Sr and 0.41 pg for Rb. This good level of reproducibility of the TPB allows 50 µm MIs to be analysed, with low Sr contents at levels of uncertainty that are not compromised by irregular blanks. The effect of the TPB on the Sr isotope composition of real samples is assessed in section 2.5.2.2.

Sr isotope and trace elemental characteristics of TPBs associated with MI work							
TPB ID	**TPB_{M14}**	**TPB_{M11}**	**TPB_{14-55}**	**TPB60**	**TPB_{Ave}**	**±2SD**	**LOD**
$^{87}Sr/^{86}Sr$	0.710297	-	0.710642	0.712392	0.711110	0.002247	
±2SE	0.000520	-	0.000900	0.000230			
n	9	12	8	60	29		10
Ti	0.32	0.11	0.16	-	0.20	0.22	0.01
Rb	1.41	0.94	1.62	-	1.32	0.69	0.41
Sr	4.84	4.75	5.00	-	4.86	0.26	0.73
Y	0.10	0.19	0.19	-	0.16	0.10	0.40
Zr	80.59	48.01	80.34	-	69.65	37.47	0.41
Nb	9.62	3.64	3.19	-	5.48	7.17	0.15
Ba	9.71	9.64	9.67	-	9.09	1.97	2.06
La	0.86	0.84	0.39	-	0.73	0.59	0.10
Ce	1.37	1.00	0.28	-	0.98	1.39	0.11
Pr	0.16	0.10	0.06	-	0.11	0.10	0.15
Nd	0.36	0.34	0.37	-	0.36	0.03	0.32
Sm	0.00	0.00	-0.12	-	-0.04	0.14	0.29
Eu	-0.07	0.00	0.01	-	-0.02	0.09	0.09
Gd	-0.60	-0.13	-0.08	-	-0.27	0.57	0.26
Dy	0.02	0.03	0.02	-	0.02	0.02	0.11
Er	-0.01	0.00	-0.03	-	-0.01	0.03	0.05
Yb	0.03	0.02	0.01	-	0.02	0.02	0.07
Rb/Sr	0.292	0.198	0.324	-	0.271	0.130	

Table 2.6: Sr isotope and trace element compositions of 4 pooled total procedural blanks (TPB). The Sr isotope composition of TPB60 was determined in cooperation with V. Martin and L. Font. Each Sr isotopic determination is done on composite TPB samples (combination of either 10, 12, 54, or 60 TPBs pooled together). 'n' denotes the number of pooled TPB. Also, the average TPB composition is listed. Sr isotope compositions have been normalized according to NBS 987 value of 0.710240. Concentrations are given in pg/TPB. The preferred $^{87}Sr/^{86}Sr$ (0.712392) to be used for the blank corrections the ratios collected of TPB60, as this measurement has the best internal precision. LOD denotes the limit of detection defined as 3 times the average standard deviation of the internal precision on 'n' analyte blank analyses. More details are located in Appendix B9.

2.5.2.2 Evaluation of the blank effect

Of most importance for this study is the potential effect of the TPB, and the variations in TPB isotope composition and trace element abundance, on the measured isotope composition of very small samples. Although it is simple to calculate these effects, the best test of the consistency and accuracy of the blank corrections, that also incorporates variable instrumental factors, is to accurately reproduce the Sr isotope composition of '*known*' samples at progressively lower levels of Sr. For these experiments we used a clinopyroxene separate from an eclogite xenolith (UV464), selected for its extremely unradiogenic Sr isotope composition. Also a whole rock powder of one of the Vestfirdir ankaramites lavas (408624) was selected as a proxy for our olivine hosted MIs from the same lava suite (Harlou et al., 2003; Harlou et al., 2004, see also *Chapter 1* and *3*). In the following the two sample materials are referred to as Cpx and Vestfirdir or as *in-house* standards.

To avoid any issues relating to sample isotope heterogeneity a single large dissolution of each sample material was prepared. The Cpx dissolution was made to contain ~300 ng Sr, and the Vestfirdir dissolution ~21 ng Sr. Aliquots were then taken from these dissolutions for analysis, ranging from 20 ng to 25 pg (Figure 2.5, Table 2.7). The largest Sr aliquots from each sample (4 and 20 ng for the Vestfirdir and Cpx respectively) provided precise and accurate $^{87}Sr/^{86}Sr$ '*reference value*' measurements as they are essentially free of any significant blank influence. The smaller aliquots could then be compared to these '*reference values*'. The various aliquots (down to 25 pg), including replicates, were processed through the micro Sr column chemistry in one batch, to avoid any issues of different resin batches having a different blank isotope composition Table 2.7.

The $^{87}Sr/^{86}Sr$ *'reference values'* for Cpx and Vestfirdir were determined by TIMS to be 0.701690 ±0.000012 (2SE) and 0.703490 ±0.000021 (2SE) respectively (Table 2.7). The TIMS measurement of Vestfirdir is in agreement with our MC-ICPMS value of 0.703476 ±0.000014 (2SE) determined on a 400 ppb solution (*Chapter 3*). Table 2.7 also lists the measured $^{87}Sr/^{86}Sr$ ratios for each aliquot size, with the 2SE internal precision, and the average composition for each size where repeats were analysed. The difference (in ppm) between the average $^{87}Sr/^{86}Sr$ obtained for each aliquot size relative to the above *'reference values'* for each sample (ΔRef $^{87}Sr/^{86}Sr$) is illustrated in Figure 2.5.

Batch ID	Sr (ng)	$^{87}Sr/^{86}Sr_{Meas}$	±2SE	$^{87}Sr/^{86}Sr_{Ave}$	±2SD	Δ Ref $^{87}Sr/^{86}Sr_{nbc}$	Δ Ref $^{87}Sr/^{86}Sr_{bc}$
M9-1-21	0.025	0.703394	0.000818				
M9-1-22	0.025	0.703809	0.000480	0.703602	0.000587	2724	206
M9-1-17	0.05	0.703712	0.000656				
M9-1-19	0.05	0.702598	0.000766				
M9-1-14	0.05	0.701997	0.000362	0.702769	0.001740	1538	166
M9-1-1	0.25	0.701825	0.000272				
M9-1-2	0.25	0.701732	0.000103				
M9-1-3	0.25	0.701783	0.000139	0.701780	0.000093	128	-173
M9-1-4	0.5	0.701681	0.000097				
M9-1-6	0.5	0.701706	0.000076	0.701694	0.000035	5	-147
M9-1-7	1.0	0.701734	0.000102				
M9-1-8	1.0	0.701717	0.000100				
M9-1-9	1.0	0.701720	0.000053	0.701724	0.000018	48	-28
M9-1-10	2.0	0.701711	0.000035			30	-8
M9-1-11	4.0	0.701683	0.000024			-10	-29
M9-1-16	20.0	0.701690	0.000012			0	0

Table 2.7a: Sr isotope composition of various sized aliquots of the eclogite clinopyroxene separate (UV464). The $^{87}Sr/^{86}Sr_{meas}$ ratios are the measured $^{87}Sr/^{86}Sr$ ratios, which were determined by TIMS at *AHIGL* (Department of Earth Sciences, Durham University). The $^{87}Sr/^{86}Sr$ of M9-1-16 (marked in grey) is used as the '*reference value*' in Figure 2.5a and 2.6a. ΔRef $^{87}Sr/^{86}Sr_{nbc}$ is the difference (in ppm) between the average or measured non blank corrected ratio of the aliquot (for aliquots <2 ng and ≥2 ng respectively) and that of the 20 ng aliquot. ΔRef $^{87}Sr/^{86}Sr_{bc}$ is the blank corrected difference between each aliquot size and the 20 ng aliquot.

Batch ID	Sr (ng)	$^{87}Sr/^{86}Sr_{Meas}$	±2SE	$^{87}Sr/^{86}Sr_{Ave}$	±2SD	Δ Ref $^{87}Sr/^{86}Sr_{nbc}$	Δ Ref $^{87}Sr/^{86}Sr_{bc}$
M9-2-15	0.025	0.705866	0.000960				
M9-2-16	0.025	0.704877	0.000576				
M9-2-17	0.025	0.704874	0.000668	0.705206	0.001144	2439	358
M9-2-12	0.05	0.704469	0.000470				
M9-2-13	0.05	0.704385	0.000362				
M9-2-14	0.05	0.704818	0.000544	0.704557	0.000459	1517	390
M9-2-1	0.25	0.703630	0.000128				
M9-2-2	0.25	0.703524	0.000137				
M9-2-3	0.25	0.703615	0.000086	0.703590	0.000115	142	-110
M9-2-4	0.5	0.703651	0.000076				
M9-2-5	0.5	0.703570	0.000083				
M9-2-6	0.5	0.703576	0.000133	0.703599	0.000090	155	29
M9-2-7	1	0.703466	0.000134				
M9-2-8	1	0.703530	0.000081				
M9-2-9	1	0.703484	0.000056	0.703493	0.000066	5	-59
M9-2-10	2	0.703542	0.000035			74	42
M9-2-11	4	0.703490	0.000021			0	0

Table 2.7b: Sr isotope composition of various sized aliquots of the ankaramitic lava (408624) from Vestfirdir, NW Iceland. The $^{87}Sr/^{86}Sr_{meas}$ ratios are the measured $^{87}Sr/^{86}Sr$ ratios, which were determined by TIMS at *AHIGL* (Department of Earth Sciences, Durham University). The $^{87}Sr/^{86}Sr$ ratio of M9-2-11 (marked in grey) is used as the '*reference value*' in Figure 2.5b and 2.6b. This '*reference value*' is in agreement with a MC-ICPMS measurement presented in *Chapter 1* of 0.703476 ±0.000014 (2SE) collected on the same whole rock powder. ΔRef $^{87}Sr/^{86}Sr_{nbc}$ is the difference (in ppm) between the average or measured ratio (non blank corrected ratio) of the aliquot (for aliquots <2 ng and ≥2 ng respectively) and that of the 4 ng aliquot. ΔRef $^{87}Sr/^{86}Sr_{bc}$ is the blank corrected difference between each aliquot size and the 4 ng aliquot.

The same data sets, but blank corrected are presented in Figure 2.6. The blank corrected data show that down to ~1 ng Sr the shift in Sr isotope composition due to blank is minimal, certainly less than the typical 2SE internal precision of an analysis, and does not require any correction, provided that the blank remains at its present low level. Between 250 and 500 pg the effect of the blank is also very limited. At the 25 to 50 pg sample sizes a blank correction is clearly necessary (Figure 2.5 and Figure 2.6) and the data suggest we can do this to an accuracy of better than 400 ppm. The additional uncertainty on the blank correction even at such low levels of Sr is still only between ±500 and 200 ppm respectively, based on our current TPB. For typical MIs of 50 to 800 pg analysed as part of the present study the uncertainty associated with the blank correction, based on these aliquoting experiments, is expected to be around ±200 to 75 ppm respectively. This compares very favourably with the estimated ±300 ppm uncertainty in accuracy for interference corrected LA-MC-ICPMS $^{87}Sr/^{86}Sr$ analyses on larger Sr rich MIs where the amount of Sr analysed is on the order of several tens of ng (Jackson & Hart, 2006).

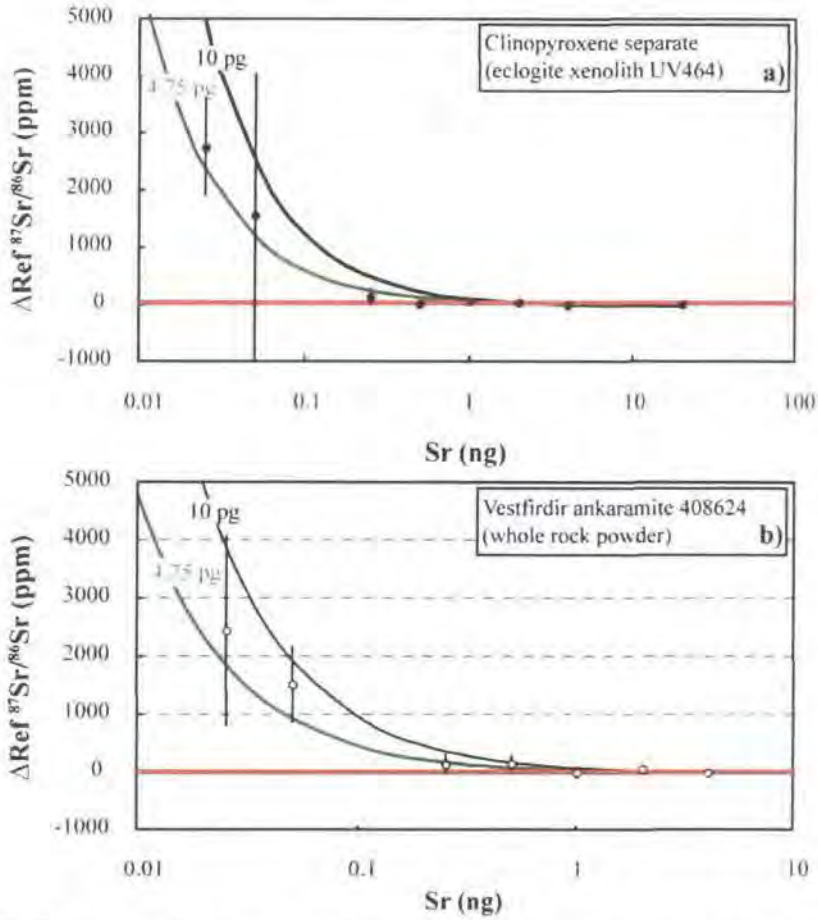

Figure 2.5: $^{87}Sr/^{86}Sr$ (non-blank correction applied) versus aliquot size (ng Sr) for the eclogite clinopyroxene of UV464 (a) and Vestfirdir lava 408624 (b) samples expressed as a ΔRef $^{87}Sr/^{86}Sr$ (aliquot/*'reference value'*) in ppm offset from the *'reference values'* (red line). The two curves illustrate the expected effect of a 4.75 pg (green) and 10 pg (black) Sr TPB with $^{87}Sr/^{86}Sr$ ratio of 0.712932 ±0.000234 (2SE) on decreasing aliquot sizes of the reference isotope composition. The non blank corrected data points show the expected level of displacement away from the *'true'* values, indicating that our measured TPB is a realistic estimate of the TPB pertaining to a typical sample analysis.

2.5.3 Instrumental precision and accuracy for small Sr samples

2.5.3.1 Mass fractionation behavior of Sr at ng to sub-ng levels

Sub-ng sized Sr samples run by TIMS may be expected to display greater mass fractionation than larger loads, since the reservoir of Sr on the filament is smaller and we run MI samples to near exhaustion (Figure 2.3a). While this is true for our study, even compared to 1-10 ng loads run on the same instrument (Charlier et al., 2006), mass fractionation can still be accurately corrected for, so long as the sample adheres to the theoretical mass fractionation law being used (Figure 2.7a-f). This is assessed for each sub-ng sized Sr load of a sample or standard by plotting non-mass bias corrected values of $\ln(^{86}Sr/^{88}Sr)$ versus $\ln(^{84}Sr/^{86}Sr)$, and $\ln(^{87}Sr/^{86}Sr)$. Such plots (Figure 2.7a-f) show that most analytical runs have slopes (fitted with Isoplot) that are within error of that expected for the exponential endmember of the generalized power law (Marechal et al., 1999).

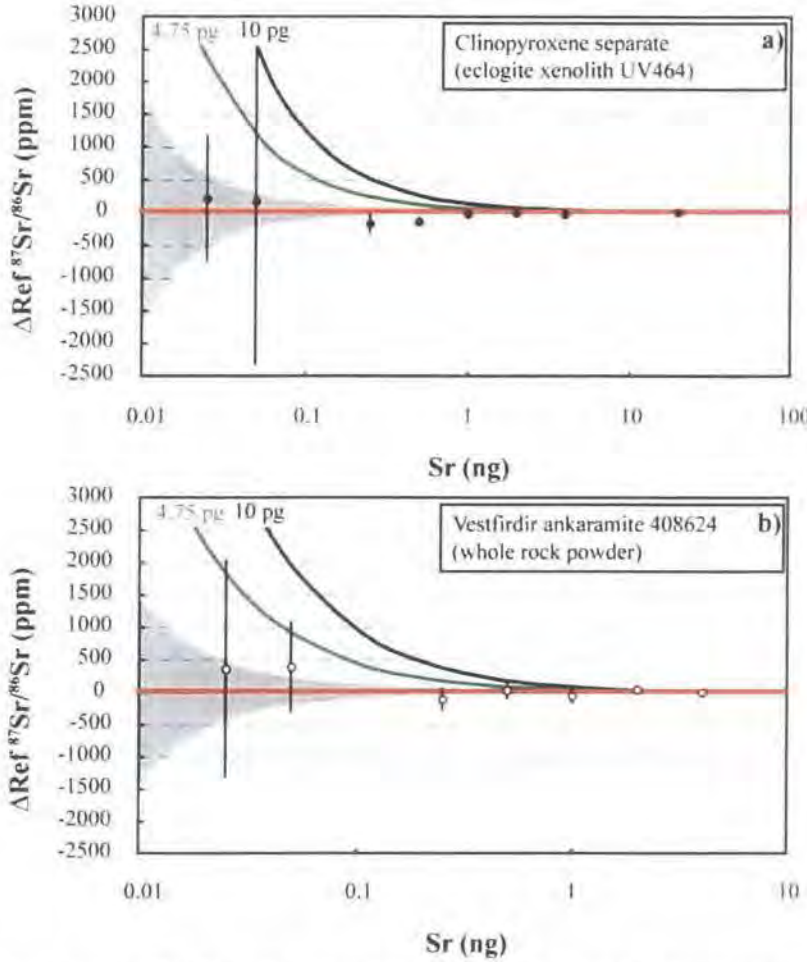

Figure 2.6: Blank corrected $^{87}Sr/^{86}Sr$ versus aliquot size (ng Sr) for the eclogite clinopyroxene (UV464) (a) and Vestfirdir lava (b) aliquots after correction for a 4.75 pg Sr blank with an $^{87}Sr/^{86}Sr$ ratio of 0.712932 (±0.000234). Composition expressed as a ΔRef $^{87}Sr/^{86}Sr$ (ppm) offset from the *'reference values'* (red line). Grey shaded zone represents the expected theoretical increase in uncertainty on the $^{87}Sr/^{86}Sr$ resulting from the blank correction at decreasing Sr aliquot sizes. Uncertainty includes the ±2SD error on the size and composition of the blank and assumes an analyte composition equal to the reference value. The 500 pg Vestfirdir lava aliquot (b) plots outside and above the uncertainty envelope for the 4.75 pg Sr blank correction and may indicate that a slightly larger Sr blank was generated during this analysis.

The $^{84}Sr/^{86}Sr$, $^{87}Sr/^{86}Sr$, and $^{86}Sr/^{88}Sr$ ratios obtained were also plotted against time (cycle No.) to show how mass fractionation typically behaves with time in a run (Figure 2.7g-h) and compares data collected for sub-ng loads of NBS 987 (0.3 and 0.6 ng) to a larger sized load of 6 ng. The '*large*' 6 ng Sr run (Figure 2.7i) shows a systematically decreasing $^{86}Sr/^{88}Sr$ ratio with time, with the value at the end of the run being typically close to or above 0.119. In contrast, the smaller runs show either rapidly fractionating $^{86}Sr/^{88}Sr$ (e.g. Figure 2.7g), extending to values as low as 0.116, or more irregular behaviour (Figure 2.7h) where $^{86}Sr/^{88}Sr$ falls and then rises and falls again, probably due to the mixing of variably fractionated Sr reservoirs on the filament. Despite the less regular mass fractionation behaviour of the smaller, sub-ng sized Sr samples compared with >1 ng loads, in almost all cases, the detailed mass fractionation behaviour

closely approximates one of the generally applied correction models and so even in highly fractionated samples, mass fractionation can be accurately corrected for (Figure 2.7a-f).

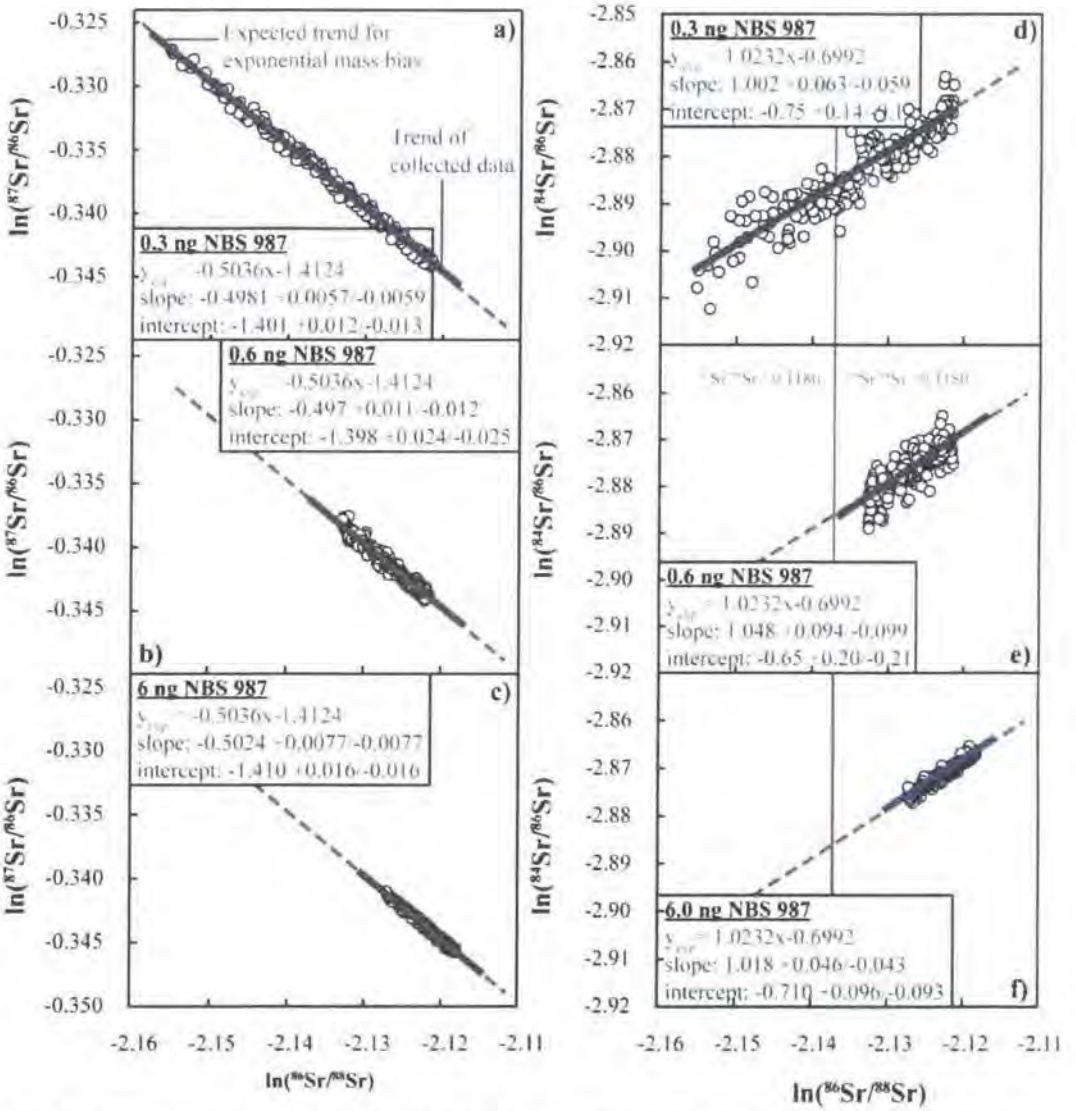

Figure 2.7: Comparison of 0.3, 0.6, and 6 ng NBS 987 standard TIMS analyses run at AGHIL (Department of Earth Sciences, Durham University). a), b) and c) show plots of $\ln(^{86}Sr/^{88}Sr)$ versus $\ln(^{87}Sr/^{86}Sr)$, d), e), and f) are plots of $\ln(^{86}Sr/^{88}Sr)$ versus $\ln(^{84}Sr/^{86}Sr)$. g), h), and i) plots of $^{86}Sr/^{88}Sr$ ratio versus cycle number. Red broken lines (in a through f) show the expected trend for exponential mass bias. The blue lines are the best-fit regressions through the collected data obtained by ISOPLOT. The box compares the slope and intercept of the regression line with that of the theoretical exponential mass fractionation (y_{exp}). Notice that the collected data confirm to the exponential mass fractionation behaviour. The grey lines (in d through i) show the division between data collected above and below $^{86}Sr/^{88}Sr$ ratio equal 0.118.

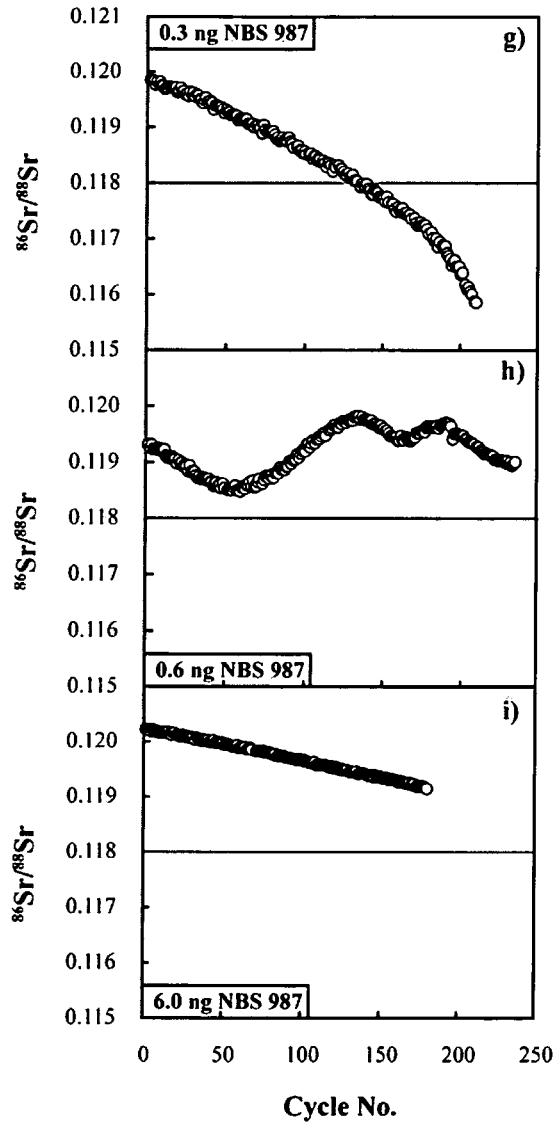

Figure 2.7: continued.

2.5.3.2 Precision, reproducibility and accuracy of Sr isotope ratios for NBS 987 standard solutions

A total of 91 Sr isotope measurements have been made on sub-ng (0.1, 0.3, and 0.6 ng) NBS 987 standard loads during a 9 month period (Figure 2.8). The first 61 standards were analyzed during the course of the Vestfirdir MI work presented in here and *Chapter 3*, and the remaining 30 standards were analyzed in relation with our study of MIs from Baffin Island Picrites (*Chapter 4*). Over the time interval that samples were being analysed sub-ng sized NBS 987 runs gave an average $^{87}Sr/^{86}Sr$ value of 0.710261 ±0.000044 (62 ppm, 2SD), similar to longer-term (9 month) reproducibility and accuracy for sub-ng sized runs of this standard of 0.710261 ±0.000042 (58 ppm, 2SD). The number of analyses, and the average $^{87}Sr/^{86}Sr$ ratio for each of the three standard load sizes are summarized in Table 2.8, and the full NBS 987 data set is located in Appendix B8. The long-term average for sub-ng standards compares very well with

the long terms average for > 1 ng sized NBS 987 runs e.g. Charlier et al. (2006) report 0.710259 ±0.000030 for 6 ng NBS 987 loads (43 ppm, 2SD, n=266). As expected, the reproducibility of the sub-ng sized loads is worse than the larger runs, but, despite a general correlation of decreasing internal precision with decreasing load size (Figure 2.8b), there is no simple relationship between the external precision (reproducibility) and load size, in the range between 0.1 and 0.6 ng. Factors other than simply counting statistics are clearly at play here, but it is not clear what is controlling this variation. Despite the fact that reproducibility does not scale with load size, accuracy, or at least the consistency of the $^{87}Sr/^{86}Sr$ ratio across this range of Sr loads is excellent and indicates that loading blanks are insignificant even at the 100 pg level (Figure 2.8a). In fact, even when the occasional sample runs worse than expected (see run #57, Figure 2.8a), possibly due to a loading error, accuracy is still very good. This generally excellent agreement in the $^{87}Sr/^{86}Sr$ ratio for sample loads over such a large range gives further support to the accuracy of the mass fractionation corrections being made on small, very fractionated Sr runs.

Load size	0.1 ng	0.3 ng	0.6 ng
n	15	46	30
$^{87}Sr/^{86}Sr_{Ave}$	0.710263	0.710261	0.710260
±2SD	0.000030	0.000045	0.000039
±2SD (ppm)	43	63	54

Sub-ng session	Long term	Vestfirdir MI	Baffin Island MI
n	91	61	30
Interval of n	1 through 91	1 through 61	62 through 91
$^{87}Sr/^{86}Sr_{Ave}$	0.710261	0.710261	0.710262
±2SD	0.000042	0.000044	0.000038
±2SD (ppm)	58	62	53

Table 2.8: Presentation of 9 months compilation of TIMS data collected on sub-ng NBS 987 standard Sr loads at *AHIGL* (Department of Earth Sciences, Durham University). This NBS 987 standard data was collected during sessions of MI work respectively presented in *Chapter 3* (Vestfirdir MIs) and *Chapter 4* (Baffin Island MIs). Average $^{87}Sr/^{86}Sr$ and the reproducibilities expressed as 2 standard deviation (2SD) and 2SD ppm of the $^{87}Sr/^{86}Sr$ average value are listed. 'n' denotes number of analysis. Full dataset is located in Appendix B8.

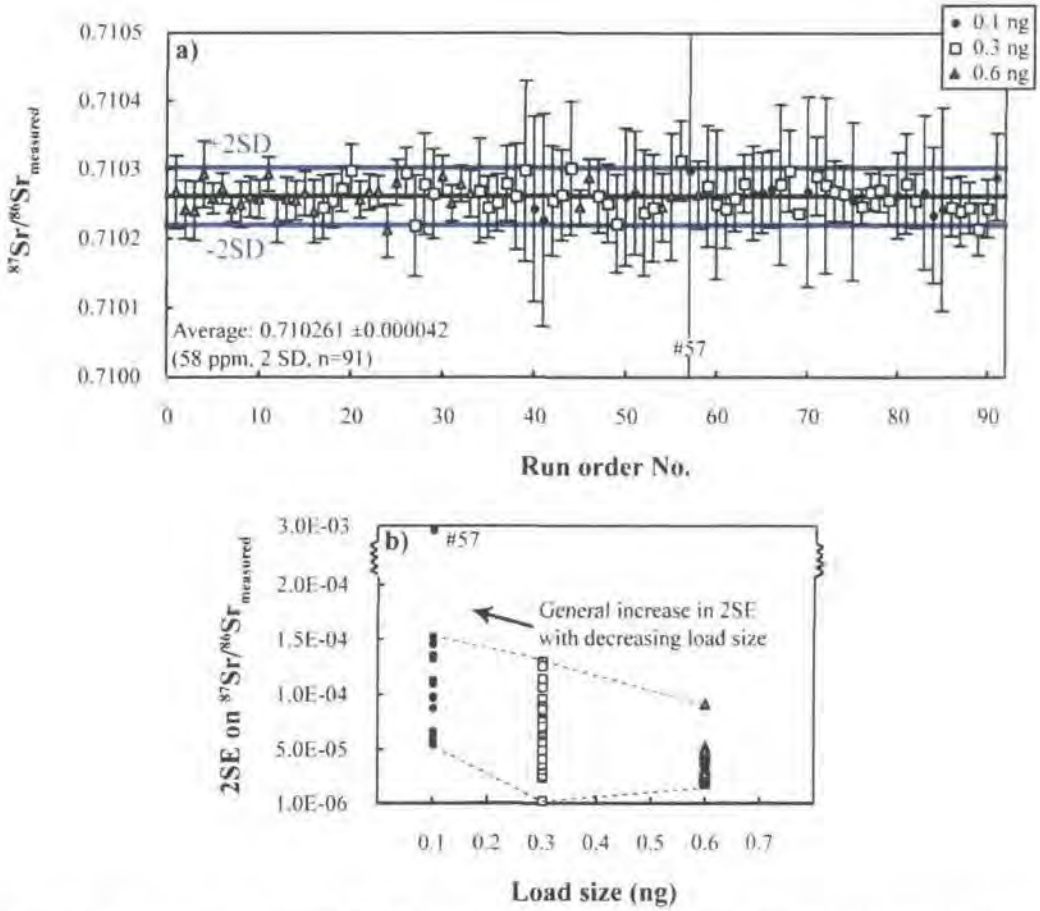

Figure 2.8: a) Variation in measured $^{87}Sr/^{86}Sr$ over a period of 9 months of 91 sub-ng (0.1, 0.3, and 0.6 ng) sized NBS 987 standards analyzed by TIMS at *AHIGL* (Department of Earth Sciences, Durham University), (Appendix B8). The first 61 standards were analyzed as part of the analytical work presented in this paper. An average of 0.710261 ±0.000044 (62 ppm, 2SD) was obtained for the first 61 standards, and an average obtained over the 9 months period of 0.710261 ±0.0000415 (58 ppm, 2SD). As such, this is comparable to the long-term 2 standard deviation external precision of 50 ppm for load sizes down to 3 ng reported by Charlier et al. (2006). Standard #57 shows that even with high internal errors the accuracy is good. The lower and upper green horizontal lines represent respective –2SD and +2SD. b) Relationship between Sr load size versus 2 times the standard error (SE) of the measured internal error on $^{87}Sr/^{86}Sr$ for NBS 987 standard.

2.5.4 Quality of the ICPMS data - precision and accuracy

The capability of the ELEMENT2 to reproduce the recommended Rb/Sr ratios of selected USGS rock standards (AGV-1, BHVO-1, and W2) for concentration ranges equivalent to the aliquots taken for MIs analysis is presented in Table 2.9. Also included is the reproducibility of Rb/Sr ratios for synthetic Rb-Sr element solutions at the 1 to 200 pg concentration levels. The Rb/Sr ratios for AGV-1, BHVO-1, and W2 were generally reproduced within -9.5% and 8.3% of the recommended reference values. The Rb/Sr ratio of the synthetic Rb-Sr solutions containing >5 pg Rb and >50% were reproduce within 2.6 to +3.7%, while the Rb/Sr ratios of the solutions containing 1 pg Rb and 10 pg Sr were not reproduced to the same accuracy (-16.2%).

USGS rock standards								
Std. ID	**Rock conc.**	**n**	**$(Rb/Sr)_{Ave}$**	**$(Rb/Sr)_{Rec}$**	**±2SD**	**Δ%**	**Rb_{Conc}**	**Sr_{Conc}**
AGV-1	25 ppb	9	0.094	0.101	0.011	-6.9	13.4	132.4
AGV-1	50 ppb	7	0.104	0.101	0.009	3.0	26.8	264.8
AGV-1	250 ppb	6	0.099	0.101	0.004	-2.0	134.0	1324.0
AGV-1	500 ppb	5	0.104	0.101	0.005	3.0	268.0	2648.0
BHVO-1	25 ppb	4	0.026	0.024	0.002	8.3	1.92	80.6
BHVO-1	50 ppb	8	0.024	0.024	0.012	0	3.84	161.2
BHVO-1	500 ppb	4	0.024	0.024	0.002	0	38.4	1512.0
W2	25 ppb	2	0.101	0.105	0.002	-3.8	4.1	38.7
W2	50 ppb	9	0.097	0.105	0.011	-7.6	8.1	77.3
W2	250 ppb	2	0.095	0.105	0.018	-9.5	40.7	386.6
W2	500 ppb	4	0.104	0.105	0.005	-1.0	81.4	773.2

Synthetic Rb-Sr solutions								
Std. ID	**Rb:Sr**	**n**	**$(Rb/Sr)_{Ave}$**	**$(Rb/Sr)_{Rec}$**	**±2SD**	**Δ%**	**Rb_{Conc}**	**Sr_{Conc}**
Std 2	**1:10**	9	0.084	0.1	0.019	-16.2	1	10
Std 3	**1:10**	1	0.104	0.1	-	3.7	5	50
Std 5	**1:10**	4	0.103	0.1	0.008	2.6	20	200

Table 2.9: Summary of average ($_{Ave}$) standard rock and synthetic Rb-Sr standard data collected during low concentration session on the ELEMENT 2 at the AHIGL (Department of Earth Sciences, University of Durham). The full dataset is given in Appendix B7. 'n' is the number of replicates. Δ% gives the average difference from the recommended ($_{Rec}$) Rb/Sr ratios values in % for each of the solutions analyzed. The rock and the synthetic Rb-Sr standard solutions were made up in different dilutions covering the range of Rb and Sr concentrations ($_{Conc}$) listed in pg/mL equal to ppt see details in Appendix B7.

2.5.5 Application to melt inclusions - olivine-hosted MIs of the Vestfirdir ankaramites (NW Iceland)

The ultimate goal of this project was to develop a technique, which would allow us to analyze the Sr isotope compositions of individual olivine-hosted MIs of typical MORB, CFB and OIB. The MI sample material chosen to evaluate the technique was from three ankaramite lavas from Vestfirdir, the NW peninsula of Iceland (Figure 1.1). Detailed study of major, trace element, and isotope compositions of these MIs is found in *Chapters 1* and *3* (see also Harlou et al., 2003) and Harlou et al. (2004) in Appendix E1). LA-ICPMS analyses have shown that MIs from this suite of lavas are relatively low in incompatible elements (≤100 times chondrite), with Sr contents generally in the range 200-600 ppm. Only two MIs are documented to have >600 ppm Sr (Appendix A9, Table 2.1). A rough estimate suggests that MIs from these samples in the 50 μm size range contain ≥100 pg Sr, which is within the range that we can accurately analyze with our newly developed technique. Trace element analysis of multiple fresh olivine crystals apparently free of MIs from each of the three ankaramite lavas revealed a Sr content of 0.023 to 0.129 ppm (wt/wt olivine) and 0.0008 to 0.08 ppm Rb (Table 2.10), i.e. very low compared to 200-600 ppm Sr for the Vestfirdir MIs. Therefore, the contribution from the olivine

itself during milling of olivine-hosted MIs is minimal. In theory, given that the MIs are in equilibrium with their host olivine, the Sr isotope composition of the host olivine and its MIs should be identical. This means that in a situation where MIs >50 μm cannot be found and isolated by micro-milling, an alternative is to dissolve whole olivine crystals that contain numerous very small (<50 μm) MIs. This approach can also be used where highly precise Sr isotope data is required that could be obtained, while compromising sampling single MIs, by analysing olivines with multiple large MIs.

To demonstrate the utility of the technique on real samples we present data for some of these MIs in Figure 2.9 and 2.10. It is not our purpose here to interpret the data in the context of their petrogensis as this is done in *Chapters 1* and *3*, and so the description of the data and their possible meaning will be minimal. Firstly, it has been shown in section 2.5.2 that the TPB does not compromise the Sr or trace element data on the low abundance sample material aimed by the method presented in this paper. Furthermore, the coherence between the non blank and blank corrected data set demonstrates that the effect of the blank correction is minimal (Figure 2.5 and 2.6) and the measured Sr isotope variation is dominated by geological factors (Figure 2.9a). Secondly, as shown in Figure 2.9b there is consistency between the trace element data collected on individual MIs sampled by both the micro-milling and analyzed by the technique presented here and the MIs analyzed by laser ablation (*Chapter 1 and 3*). The similarity of the two types of data, exemplified by $(La/Y)_N$ versus $(La/Sm)_N$ indicates, that the precision and accuracy of the two methods must be comparable. The coherence of the two datasets also suggests that the same MI population was sampled during the two studies. Hence, this newly-developed method provides both trace element data and Sr isotope information on individual MIs, which makes it possible to link the collected chemical information to previous MI studies on the same rock collection (e.g. *Chapter 1, 3, and 4.* Yaxley et al., 2004; Harlou et al., 2006). Thirdly, the result of the Vestfirdir MI study demonstrates the existence of substantial variations in the Sr isotope composition within MIs from each of the lavas, which were not seen within the Sr isotopes of the host lava suite (Figure 2.10). Overall, the $^{87}Sr/^{86}Sr$ isotope data collected on milled MIs and whole olivine grains containing MIs overlap (Figure 2.10). However, as the MIs sampled in the whole olivine grains represent an average measurement of multiple MIs, it is possible to sample the overall variation in more detail by sampling and analysing individual MIs, so long as a large number of MIs are analysed. Interestingly, the whole olivine crystals analysed from the Vestfirdir show greater Sr isotope variability than the individual MIs analysed (Figure 2.10). This may indicate that selecting the largest MIs for direct analysis may bias the sampling to the less variable MI compositions. This is a problem that can be overcome by micro analysis, due to the ability to analyse whole olivines containing smaller MIs, but cannot be overcome by the LA-MC-ICPMS approach.

The large Sr isotope variations observed among the MIs and whole olivines containing multiple MIs strongly contrasts with the narrow $^{87}Sr/^{86}Sr$ range of the host lavas, and the overall variation of the Icelandic lavas (Figure 2.10). In fact, these MIs cover up to 77% of the total $^{87}Sr/^{86}Sr$ range observed for the OIB worldwide, whereas the host lavas account for only 5%. As such, the extreme variation observed among $^{87}Sr/^{86}Sr$ in MIs is comparable to the Pb isotope variations within MIs (Saal et al., 1998; Jochum et al., 2004; Kobayashi et al., 2004; Yurimoto et al., 2004; Saal et al., 2005; Jackson & Hart, 2006). The central issue is what causes these variations. The cause of these variations, from a Sr isotope perspective, and their implications for the source regions of mantle derived basalts, will be explored in subsequent chapters.

Sample ID	**408611**	**408624**	**408772**
Mineral	Olivine	Olivine	Olivine
Trace element concentrations (ppm)			
Ti	0.005	0.007	0.003
Rb	0.003	0.008	0.001
Sr	0.024	0.129	0.023
Y	0.060	0.060	0.025
Zr	0.345	0.169	0.158
Nb	0.037	0.028	0.021
Ba	0.002	0.004	0.00
La	0.002	0.004	0.002
Ce	0.005	0.008	0.002
Pr	0.001	0.001	0.001
Nd	0.003	0.006	0.002
Sm	0.001	0.002	0.001
Eu	0.001	0.001	0.001
Gd	0.003	0.003	0.001
Dy	0.007	0.007	0.003
Er	0.008	0.007	0.003
Yb	0.028	0.023	0.011

Table 2.10: The trace element content of olivine phenocrysts free of visible MIs from three ankaramites of Vestfirdir, NW Iceland. Concentrations are determined by double focusing magnetic sector field ICPMS at *AHIGL* (Department of Earth Sciences, Durham University) and are given in ppm. The higher concentration of Rb-Sr in olivine of 408624 may suggest the presents of MIs, which were not detected under the microscope.

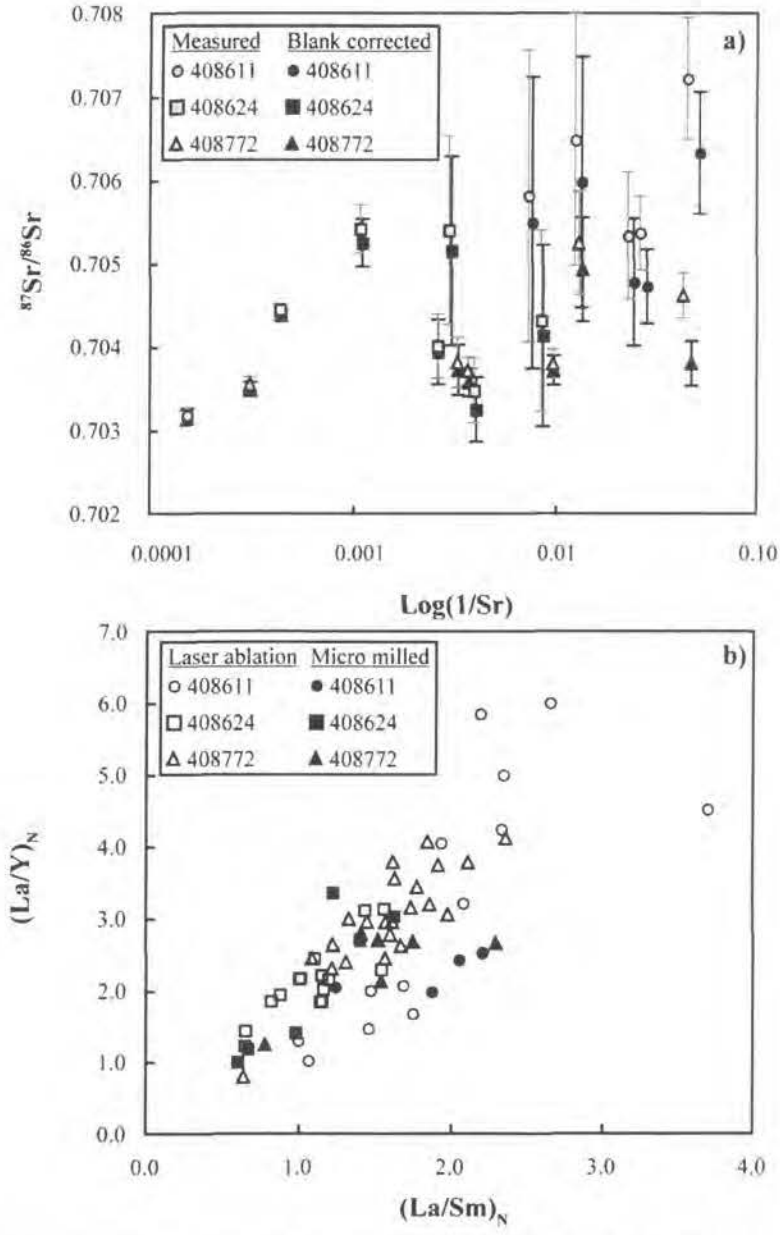

Figure 2.9: Presentation of data collected on individual olivine-hosted MIs from Vestfirdir, NW Iceland (*Chapter 3*). a) Comparison between non blank corrected $^{87}Sr/^{86}Sr$ ratios and blank corrected $^{87}Sr/^{86}Sr$ ratios. Both non-blank and blank corrected ratios have been normalized according to a value for the NBS 987 standard of 0.710240. The limited effect of the blank correction is within the analytical error. b) Comparison between trace element data collected on individual MIs by LA-ICPMS, and data on different MIs from the same rocks sampled by micro-milling and analyzed by the techique describe in this chapter (*Chapter 3*). The two data sets show good coherence, here shown in a plot of $(La/Y)_N$ versus $(La/Sm)_N$. Data normalized to primitive mantle values of (McDonough & Sun, 1995).

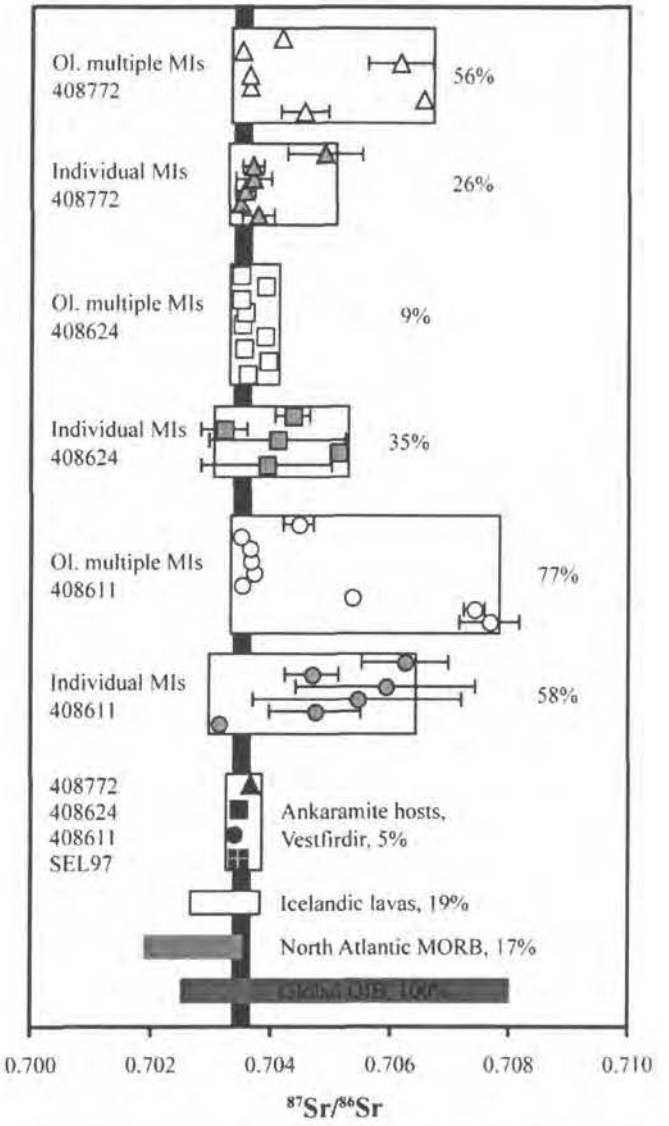

Figure 2.10: Comparison between the $^{87}Sr/^{86}Sr$ isotope ratios collected on individual MIs (grey symbols) and whole olivine grains hosting multiple MIs (open symbols) from each of three ankaramites from Vestfirdir, NW Iceland (*Chapter 3*). Vertical thick black bar represents the $^{87}Sr/^{86}Sr$ isotope composition of their respective host lavas. The $^{87}Sr/^{86}Sr$ isotope range of the MIs is compared to the range of the host lava suite (SEL97 is from Hilton et al., 1999), the general range of lavas from Iceland (Thirlwall et al., 2004) plus the range of the global OIB. The MIs cover up to 77% of the global OIB range, which contrasts with the narrow range shown by the three host lavas (5%) and the general range of Icelandic lavas (19%).

2.6 Conclusion

- An ultra-low blank analytical method has been developed that allows micro-milling of olivine-hosted MIs for combined trace element and Sr isotope measurement.

- The effect of blank contribution to samples as small as 25 pg Sr can be accurately corrected because of the consistency of the total procedural blanks and due to accurate knowledge of the blank isotope composition.

- This study demonstrates that it is possible to obtain very accurate and precise Sr isotope ratio measurements on standards and samples as small as 25 pg. The sub-ng Sr loads, although more fractionated during analysis than larger loads, adhere closely to the exponential case of the generalised power law for mass fractionation and hence satisfactory corrections for mass fractionation can be made.

- The effect of the olivine host on measured elemental and isotope compositions has been shown to be minimal. Because of this, single olivine grains containing multiple, small MIs can be analysed and we can have confidence that the measured ratios should be dominated by the MIs.

- The method permits individual MIs as small as 50 μm, containing as little as 200 ppm Sr, to be analysed for their trace element and Sr isotope composition.

- This sensitivity makes the method presented here much more adaptable to a larger variety of MI suites in depleted rocks than it is possible using LA-MC-ICPMS techniques, and provides the option of studying very small MIs by digestion of whole olivine crystals.

2.7 Reference

Birck, J. L. (1986): Precise K-Rb-Sr isotopic analysis: Application to Rb-Sr chronology. Chemical Geology, 56(56): 73-83.

Breddam, K. & Kurz, M. D. (2001): Helium isotope signatures of Icelandic alkaline lavas. EOS, Transactions, American Geophysical Union, 82: F1315.

Breddam, K., Stecher, O., Harlou, R., Peate, D. W. & Kurz, M. D. (in prep.): Miocene high-$^{3}He/^{4}He$ ankaramites in NW-Iceland: Trace element constraints on the common component in mantle plumes.

Charlier, B. L. A., Ginibre, C., Morgan, D., Nowell, G. M., Pearson, G. D., Ottley, C. J., & Davidson, J. P. (2006): Methods for the microsampling and analysis of strontium isotopes at the crystal scale for petrological and geochronological studies of igneous rocks. Chemical Geology: 114-133.

Davidson, J. P., Morgan, D. J., Charlier, B. L. A., Harlou, R. & Hora, J. M. (2007): Microsampling and isotopic analysis of igneous rocks: Implications for the study of magmatic systems. Annual Review of Earth and Planetary Sciences, 35.

Davidson, J. P., Tepley, F., Palacz, Z., & Meffan-Main, S. (2001): Magma recharge, contamination and residence times revealed by in situ laser ablation isotopic analysis of feldspar in volcanic rocks. Earth and Planetary Science Letters, 184: 427-442.

Deniel, C. & Pin, C. (2001): Single-stage method for the simultaneous isolation of lead and strontium from silicate samples for isotopic measurements. Analytica Chimica Acta, 426: 95-103.

Harlou, R., Kent, A. J. R., Breddam, K., Davidson, J. P., & Pearson, D. G. (2003): Origin of extreme $^{3}He/^{4}He$ signatures in Icelandic lavas: Insights from Inclusion studies. Eos trans. AGU, 87(46), Fall meet., Abstract V32A-1006.

Harlou, R., Kent, A .J. R., Breddam, K., Davidson, J. P., & Pearson, G. (2004): Origin of extreme $^{3}He/^{4}He$ signatures in Icelandic lavas: Insights from melt inclusion studies. Geochimica et Cosmochimica Acta, Supplement 1, 68(11): A597.

Harlou, R., Pearson, D. G., Nowell, G. M., Davidson, J. P., & Kent, A. J. R. (2005): Sr isotope studies of melt inclusions by TIMS. Geochimica et Cosmochimica Acta, Supplement 1, 69(10): A380.

Harlou, R., Pearson, D. G., Davidson, J. P., Kamenetsky, V. S., & Yaxley, G. M. (2006): Source variability and crustal contamination of the Baffin Island picrites – coupled Sr isotope and trace element study of individual melt inclusions. Geochimica et Cosmochimica Acta, Supplement 1, 70(18): A231.

Hilton, D. R., Gronvold, K., Macpherson, C. G., & Castillo, P. R. (1999): Extreme $^{3}He/^{4}He$ ratios in northwest Iceland: constraining the common component in mantle plumes. Earth and Planetary Science Letters, 173: 53-60.

Jackson, M. G. & Hart, S. R. (2006): Strontium isotopes in melt inclusions from Samoa balsatls: Implications fro heterogeneity in the Samoan Plume. Earth and Planetary Science Letters, 245: 260-277.

Jochum, K. P., Stoll, B., Herwig, K., & Hofmann, A. W. (2004): Pb isotopes and trace elements in melt inclusions from Hawaiian basalts using LA-ICPMS and Sr-XRF. Gechimica et Cosmochimica Acta, 68: A564.

Kent, A. J. R., Baker, J. & Wiedenbeck, M. (2002): Contamination and melt aggregation processes in continental flood basalts: constraints from melt inclusions in Oligocene basalts from Yemen. Earth and Planetary Science Letters, 202: 577-594.

Kobayashi, K., Tanaka, R., Moriguti, T., Shimizy, K., & Nakamura, E. (2004): Lithium, boron, and lead isotope systematics of glass inclusions in olivines from Hawaiian lavas: evidence for recycled components in the Hawaiian plume. Chemical Geology, 212: 143-161.

McDonough, W. F. & Sun, S. -s. (1995): The composition of the Earth. Chemical Geology, 120: 223-253.

Marechal, C. N., Télouk, P., & Albaréde, F. (1999): Precise analysis of copper and zinc isotopic compositions by plasma-source mass spectrometry. Chemical Geology, 156: 251-273.

Ramos, F. C., Wolff, J. A., & Tollstrup, D. L. (2004): Measuring $^{87}Sr/^{86}Sr$ variations in minerals and groundmass from basalts using LA-MC-ICPMS. Chemical Geology, 211: 135-158.

Saal, A. E., Hart, S. R., Shimizu, N., Hauri, E. H., & Layne, G. D. (1998): Pb isotopic variability in melt inclusions from oceanic island basalts, Polynesia. Science, 282: 1481-1484.

Saal, A. E., Hart, S. R., Shimizu, N., Hauri, E. H., Layne, G. D., & Eiler, J. M. (2005): Pb isotopic variability in melt inclusions from the EMI-EMII-HIMU mantle end-members and the role of the oceanic lithosphere. Earth and Planetary Science Letters, 240: 605-620.

Shimizu, N. (1998): The geochemistry of olivine-hosted melt inclusions in a FAMOUS basalt ALV519-4-1. Physics of the Earth and Planetary Interiors, 107: 183-201.

Thirlwall, M. F., Gee, M. A. M., Taylor, R. N., & Murton, B. J. (2004): Mantle components in Iceland and adjacent ridges investigated using double-spike Pb isotope ratios. Gechimica er Cosmochimica Acta, 68(2): 361-386.

Woodhead, J. & Hergt, J. M. (2000): Pb-isotope analyses of USGS reference materials. The journal of geostandards and geoanalysis, 24(1): 33-38.

Yaxley, G. M., Kamenetsky, V. S., Kamenetsky, M., Norman, M. D., & Francis, D., (2004): Origins of compositional heterogeneity in olivine-hosted melt inclusions from the Baffin Island picrites. Contribution to Mineral and Petrology, 148: 426-442.

Yurimoto, H., Kogiso, T., Abe, K., Barsczus, H. C., Utsunomiya, A., & Maruyama, S. (2004): Lead isotopic compositions in olivine-hosted melt inclusions from HIMU basalts and possible link to sulfide components. Physics of the Earth and Planetary Interiors, 146: 231-242.

CHAPTER 3

Sr isotope heterogeneity revealed by olivine-hosted melt inclusions in ankaramites from Vestfirdir, NW Iceland

3.1 Abstract

The introduction of a novel method to obtain precise Sr isotope and trace element data on individual olivine-hosted melt inclusions (MIs) brings a new dimension into the study of MIs. In this chapter, we present the first $^{87}Sr/^{86}Sr$ isotope determinations of individual olivine-hosted MIs from three ankaramites from Vestfirdir, NW Iceland. Also presented are Sr isotope measurements obtained on olivine phenocrysts hosting multiple MIs (both single grains and grain aggregates). Substantial variations in the Sr isotope compositions are revealed within MIs from a single lava. The range of $^{87}Sr/^{86}Sr$ in single MIs (0.70315-0.70625) and olivine grains rich in MIs (0.70350-0.70768) is considerably greater than both the host lavas (0.70340-0.70368) and the entire Icelandic lava field (0.7028-0.7038). These MIs have the most radiogenic $^{87}Sr/^{86}Sr$ ratios so far reported from Icelandic magmas, spanning up to 77% of the $^{87}Sr/^{86}Sr$ variation seen within oceanic island basalts globally, whereas the host lavas only cover 5%. This suggests that MIs, in contrast to their host lavas, sample a more detailed record of chemical heterogeneities and processes taking place during the earliest stages of the magmatic system. The Sr isotope and trace element variability among individual MIs together with the Sr-Nd-Hf-Os-Pb systematics of the host lavas clearly imply the involvement of relict crustal and depleted mantle components in the generation of the Vestfirdir ankaramites. The overall geochemical variations documented by MIs and lavas are best explained by mixing between the depleted mantle, recycled hydrothermally altered oceanic lithosphere (pyroxenite component), and minor contributions of subducted sediment. Recycled subducted components are most likely extensively degassed, which implies that the extreme unradiogenic He isotope signature of the ankaramites is linked to the depleted mantle component. It is suggested that a high $^{3}He/^{4}He$ depleted mantle endmember may play an important role in the genesis of lavas throughout the North Atlantic Igneous Province, and this component may likewise be an endmember of many high $^{3}He/^{4}He$ oceanic island basalts.

3.2 Introduction

Numerous studies have shown that valuable geochemical information on the formation and evolution of magmatic rocks can be extracted from MIs entrapped in early-formed crystal phases such as olivine (e.g. Gurenko & Chaussidon, 1995; Saal et al., 1998; Shimizu, 1998; Slater et al., 2001; Gurenko & Chaussidon, 2002; Kent et al., 2002; Jackson & Hart, 2006). MIs represent snapshots of melt compositions present within a magma body at the time of entrapment, and hence these may store important geochemical information which otherwise is hidden within the whole rock compositions. An important feature of a MI is that once it is encapsulated by the growing host phase, it is in principle isolated from major chemical changes to which the carrier melt is subjected e.g. differentiation, mixing, and assimilation processes. Some chemical exchange may take place between the individual MI and its host crystal (Nielsen et al., 1998). If olivine is the host Ni, MgO, and FeO may be strongly affected by post entrapment crystallization. Fortunately, these modifications can be reversed by homogenization experiments (Nielsen et al., 1998; Danyushevsky et al., 2000; Danyushevsky et al., 2002). In contrast to the concentrations, the relative distribution (i.e. trace element ratios) of most other incompatible trace elements (including Sr and Rb) remain unaffected by such post entrapment processes. However, caution should be applied to the selection of MIs and, as in this study, only primary MIs are considered.

Until recently, work on MIs was limited to major and trace element studies. These studies typically revealed that larger compositional variations are preserved among olivine-hosted MIs from a single lava than documented by their respective lava suite (e.g. Gurenko & Chaussidon, 1995; Shimizu, 1998; Gurenko & Chaussidon, 2002; Kent et al., 2002; Norman et al., 2002; Yaxley et al., 2004). Such variations have been suggested to reflect variation in melting conditions of a single source, chemical heterogeneities within the source region, contributions from multiple sources, or crustal contamination processes (see references above). Great advances were made to MI studies, as Pb isotope measurements of individual MIs by SIMS was introduced by Saal et al. (1998). The advantage of radiogenic isotope ratios in contrast to many trace element ratios is that the mass difference between any pair of isotopes is too small to be fractionated during melting or crystallization processes. This means that a magma is expected to have the same isotope characteristics as its source region(s). Hence, isotope ratios provide a means to track contributions from different sources. Since the work of Saal et al. (1998) several Pb isotope studies of individual MIs have revealed that MIs also sample diverse Pb isotope compositions far greater than the isotope diversity of the host lava suite (Saal et al., 1998; Kobayashi et al., 2004; Yurimoto et al., 2004; Saal et al., 2005). With the recent development of novel techniques in geochemistry it is now also possible to determine the Sr isotope compositions of individual olivine-hosted MIs (Harlou et al., 2005; Jackson & Hart, 2006).

To further examine the potential for isotope studies on MIs to reveal new information on the origin of oceanic island basalt (OIB) magmas, this paper focuses on Sr isotope compositions of olivine-hosted MIs. We apply our newly developed technique for precise Sr isotope determinations and trace element ratios of individual MIs (*Chapter 2*, Harlou et al., 2005) to a suite of olivine-hosted MIs from three Miocene (14 ±0.5 Ma, Breddam et al., in prep.) ankaramite lavas from Vestfirdir, the NW peninsula of Iceland. The $^{87}Sr/^{86}Sr$ isotope ratios of individual MIs may provide a higher resolution picture of the pre-aggregated melts and the different components involved in the magma genesis (see also *Chapter 4*). The selected ankaramites have the added interest of possessing some of the highest $^{3}He/^{4}He$ ratios (up to 42.9 R/R_a, Breddam et al., in prep.) measured in OIB volcanism. The general consensus is that the He signatures originate from melt or fluid inclusions within the olivine phenocrysts (Roedder, 1984), hence the Sr isotope and trace element studies of individual MIs may also provide an added dimension to the interpretation of the origin of the He isotope signature.

3.3 Geological setting and sample material

Iceland is thought to be the result of high melt production due to the position of a hot mantle plume beneath the Mid-Atlantic Ridge, creating a region of anomalously thick crust (Figure 3.1a). Geophysical observations of the Icelandic crust suggest that its thickness varies from ~ 40 km above the plume head located beneath the southeast Iceland, to ~20-25 km, at the coastal regions e.g. Staples et al. (1997), Darbyshire et al. (1998), Darbyshire et al. (2000), Maclennan et al. (2001), Foulger (2006). In Vestfirdir the peninsula of NW Iceland (Figure 3.1b) the tholeiitic flood basalt sequence is cut by an unconformity dated to approximately 14.9 Ma (Hardarson et al., 1997). The lower sequence dips 5° to the NW implying that the lavas originate from the NW paleo-rift zone (Figure 3.1), which became extinct by 15 Ma (Hardarson et al., 1997). The lavas above the unconformity dip 5° to the SE, towards the later Skagi-Snæfellsnes rift zone, which was active in the time interval 15 to 7 Ma (Hardarson et al., 1997). The olivine-hosted MIs studied are sampled from three 14 ±0.5 Ma Vestfirdir lavas collected respectively at 350 m at Selardalur (408772), and at 600 m above the unconformity at Burfell (408624) and Lambadalur (408611), (Breddam et al., in prep.). It is suggested that sample 408611 and 408624 may represent part of the same lava flow (Breddam et al., in prep.).

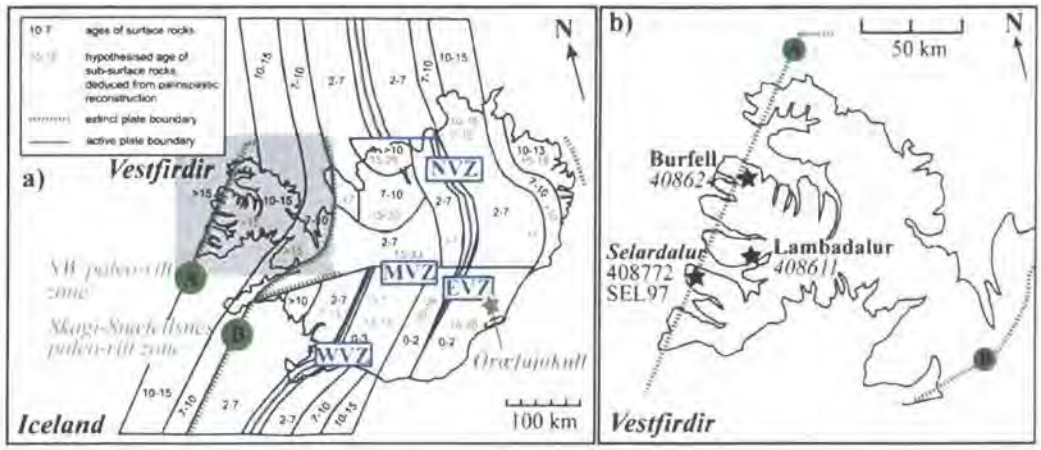

Figure 3.1: a) Map of Iceland showing the present plate boundaries (or rift zones) including the Western, Eastern, Middle and Northern Volcanic Zones (WVZ, EVZ, MVZ and NVZ respectively; after Foulger & Anderson, 2005). Also shown are; the NW paleo-rift zone (A) and Skagi-Snæfellsnes paleo-rift zone (B), which became extinct by 14.9 Ma and after 7 Ma respectively (Hardarson et al., 1997). Vestfirdir is the NW peninsula of Iceland marked by the grey background and enlarged in b). The Vestfirdir ankaramites are dated to 14 Ma ±0.5 and are related to the magmatism from Skagi-Snæfellsnes paleo-rift zone (Breddam et al., in prep). The grey star is the location of radiogenic $^{87}Sr/^{86}Sr$ Öræfajökull lavas (Prestvik et al., 2001). b) Sample locations in Vestfirdir. Sample 408772 is equivalent to SEL97 from Hilton et al. (1999). Detailed geological map of Iceland is located in Appendix A1.

The lavas are strongly porphyritic containing up to 50% phenocrysts (Figure 1.2a-c). The dominant phenocryst phase is olivine (20-30% modal abundance). Clinopyroxene (5-20 %) and minor amounts of plagioclase (<5%) are also present. The groundmass is medium grained, consisting mainly of fine plagioclase laths in addition to clinopyroxene, olivine and opaque phases. Chemically these lavas classify as olivine tholeiitic basalts (Figure 1.3a). However, on the basis of modal proportion of olivine and clinopyroxene, and the alkaline affinities of these rocks they are referred to as ankaramites (*Chapter 1*). Relative to the Icelandic picrites, these lavas have very strong alkaline affinities such as high MgO (18.9-25.7 wt.%) combined with lower SiO_2 (44.9-47.1 wt.%), Al_2O_3 (7.7-9.9 wt.%), and CaO (7.4-10.9 wt.%), and high TiO_2 (0.60-1.19 wt.%), and K_2O (0.05-0.13 wt.%), (Table 3.1). The multi element and rare earth element patterns of these ankaramites bear strong resemblance to the Icelandic alkali basalts, and are thus more enriched than the Icelandic picrites (Figure 1.4a-b). The ankaramites are characterized by mild enrichment in LREE [$(Ce/Sm)_N$ of 1.1-1.4; $(La/Y)_N$ of 2.0-3.0)], and relative depletions are observed for Rb, Ba, Th, U, and K compared to Ta, and La (Table 3.1). In respect to the over all Sr-Nd-Pb isotope signature of Icelandic lavas, these ankaramites have relatively radiogenic $^{87}Sr/^{86}Sr_i$ ratios (0.703399-0.703675) for their $^{143}Nd/^{144}Nd_i$ ratios (0.512946-0.513023), plus intermediate $^{206}Pb/^{204}Pb$ (18.44-18.62) and slightly elevated $^{207}Pb/^{204}Pb$ (15.47-15.52) and $^{208}Pb/^{204}Pb$ (38.14-38.46) isotope compositions (Table 3.1). The ankaramites have somewhat enriched $^{176}Hf/^{177}Hf$ (0.283112-0.283132) compared to the Hf isotope range of mid-oceanic ridge basalts (MORB), but depleted relative to the worldwide Hf isotope range of OIB (Nowell et al., 1998). Also, their Os isotope ratios range from depleted MORB-like to slightly more enriched $^{187}Os/^{188}Os$ ratios (0.12632-0.13415), but overall the Os

isotopes are depleted when compared to the overall range of OIB e.g. Hauri (2002b). Extremely unradiogenic $^{3}He/^{4}He$ ratios are documented in 408624 and 408772 (42.87 ±0.33 and 34.79 ±1.64 R/R_a), whereas 408611 has MORB-like $^{3}He/^{4}He$ composition (8.15 ±5.08 R/R_a), (Breddam et al., in prep.; Table 3.1). However, it is suggested that the more radiogenic He isotope composition of 408611, which is accompanied with low ^{4}He concentration, is the result of degassing. That all three ankaramites initially had unradiogenic He isotope signatures is further supported by the strong similarity between their major, trace element, and Sr-Nd-Pd-Hf-Os isotope compositions (Breddam et al. in prep; Table 3.1).

Sample ID	**408611**	**408624**	**408772**	**SEL97**
Rock	*Ankaramite*	*Ankaramite*	*Ankaramite*	*Ankaramite*
Latitude	65.85	66.06	65.7646	-
Longitude	-23.25	-23.30	-24.0419	-
Fjord	*Dyrafjordur*	*Sugandafjordu*	*Arnarfjordur*	*Arnarfjordur*
Location	*Lambadalur*	*Burfell*	Selardalur	*Selardalur*
Isotope ratios				
$^{3}He/^{4}He$	8.15	42.87	34.79	37.7
±2SE	5.08	0.33	1.64	2.00
^{4}He (cm^3 STP/g)	$6.68x10^{-11}$	$5.02x10^{-9}$	$3.29x10^{-10}$	$8.90x10^{-10}$
$^{87}Sr/^{86}Sr$	0.703419	0.703476	0.703677	0.703465
$^{87}Sr/^{86}Sr_i$	0.703399	0.703472	0.703675	0.703457
±2SE	0.000008	0.000008	0.000012	0.000010
$^{87}Rb/^{86}Sr_i$	0.0993	0.0202	0.0078	0.0042
$^{143}Nd/^{144}Nd$	0.513039	0.513023	0.512977	0.512969
$^{143}Nd/^{144}Nd_i$	0.513023	0.051307	0.512946	0.512953
±2SE	0.000003	0.000005	0.000004	0.000009
$^{176}Hf/^{177}Hf$	0.283160	0.283132	0.283112	-
±2SE	2.80E-06	3.20E-06	2.50E-06	-
$^{187}Os/^{188}Os$	0.12632	0.13254	0.13415	-
±2SE	0.00060	0.00004	0.00005	-
Os (ppb)	3.024	0.527	0.810	-
$^{206}Pb/^{204}Pb$	18.44	18.48	18.62	18.65
$^{207}Pb/^{204}Pb$	15.47	15.47	15.52	15.47
$^{207}Pb/^{204}Pb$	38.14	38.17	38.46	38.45

Table 3.1: Sr-Nd-Pb-Hf-Os isotope, major (oxide), and trace element compositions of three ankaramite lavas from Vestfirdir (NW Iceland). Sr-Nd-Hf isotopes compositions are determination by MC-ICPMS, Os isotopes by TIMS, and the trace element concentrations by ICPMS at the *AHIGL* (Department of Earth Sciences, Durham University). He and Pb isotopes and major element compositions are from Breddam et al. (in prep.). Also included, is data on SEL97 from Hilton et al. (1999), which is sampled at the same location as sample 408772 of this study. Subscribed i denotes an initial isotope ratio, which is the 14 Ma eruption age of the Vestfirdir ankaramites.

Sample ID	408611	408624	408772	SEL97
Major elements (wt.%)				
SiO_2	44.94	47.08	45.13	45.94
TiO_2	0.63	1.07	0.90	1.19
Al_2O_3	9.87	9.61	7.70	9.72
MgO	25.17	18.89	25.66	18.74
CaO	7.35	10.85	7.54	10.15
Fe_2O_3	2.07	2.03	2.16	-
FeO	8.23	8.46	9.154	-
Cr_2O_3	0.39	0.27	0.44	0.51
NiO	0.13	0.08	0.13	0.10
MnO	0.17	0.17	0.17	0.15
Na_2O	0.81	1.29	0.87	1.18
K_2O	0.13	0.12	0.05	0.05
P_2O_5	0.11	0.10	0.09	0.06
Mg#	84.0	79.4	82.9	77.3
FeO_{total}	10.09	10.29	11.10	11.53
Na_2O+K_2O	0.94	1.40	0.92	1.23
Trace element concentrations (ppm)				
Cr	1287	902	1496	1728
Ni	998	593	982	759
Rb	3.044	1.155	0.318	2.7
Sr	88.65	165.34	118.00	185
Cs	0.009	-	0.014	-
Ba	21.5	24.0	17.0	33
Th	0.206	0.256	0.351	-
U	0.081	0.086	0.070	-
Pb	0.247	0.455	0.323	-
Nb	3.60	3.70	4.52	10
Ta	0.30	0.27	0.34	-
Zr	49.0	58.1	46.6	75
Hf	1.12	1.45	1.27	-
Y	11.7	14.3	10.0	12
La	3.55	4.37	4.47	3.95
Ce	8.89	10.88	10.31	8.8
Pr	1.22	1.65	1.40	-
Nd	5.35	8.43	6.51	5.61
Sm	1.56	2.43	1.78	1.62
Eu	0.59	0.85	0.65	0.84
Gd	1.83	2.77	2.03	1.94
Tb	0.32	0.44	0.33	-
Dy	1.90	2.49	1.94	1.82
Ho	0.42	0.51	0.38	-
Er	1.12	1.28	0.99	-
Tm	0.16	0.18	0.14	-
Yb	1.09	1.11	0.85	0.84
Lu	0.17	0.17	0.12	0.12

Table 3.1: Continued

3.4 Method

Olivine phenocrysts hosting primary, spherical glassy MIs in the size range from 50 to 150 μm were handpicked and cleaned of adhering glass matrix. Random olivine grain were selected for two different sampling approaches; I) *'individual'* sampling of MIs by micro-milling using the New Wave MicroMill at *AHIGL* (Department of Earth Sciences, Durham University), and II) *'batch'* sampling by separating Sr from single olivine or aggregates (1, 5, 10, or 15 crystals). The olivine grains from which MIs were to be sampled individually, were mounted in 25 mm epoxy discs (Appendix A3). Each grain mount was polished in order to bring the MIs as near to the polished surface as possible. The milled MI material and whole grain aggregates were processed using a downscaled version of the micro Sr dissolution procedure using a combination of concentrated HF and HNO_3 (see details in *Chapter 2*, Appendix B1, Harlou et al., 2005, Charlier et al., 2006). The total volume of the whole grain solutions was put through micro Sr column chemistry to chemically separate out the Sr. Before processing the milled sample solutions through the micro Sr column chemistry, 10% aliquots were taken for trace element analysis (Ti, Rb, Sr, Y, Zr, La, Ce, Nd, Sm, Gd, Dy, Er) by double focusing magnetic sector field ICPMS at the *AHIGL* (Department of Earth Sciences, Durham University). During the analytical session Rb/Sr ratios of 10 ppt and 100 ppt rock standard solutions (AGV-1, BHVO-1, and W2) were reproduce within –7.1 to 2.77% of the recommended ratios (Table 3.2, Appendix C1). The limit of detection (LOD), calculated as 3 times the standard deviation (n=20) on the internal error of the Rb and Sr measurements of an analyte blank, was established to 0.17 pg/mL and 0.28 pg/mL (Appendix C2). The remaining 90% aliquot of each milled sample solution was then processed through micro-Sr column chemistry. The Sr isotope was determined by TIMS (Thermo-Finnigan Triton) at the *AHIGL* (Department of Earth Sciences, Durham University). During the TIMS session 61 sub-ng NBS 987 standards were analyzed for which an average $^{87}Sr/^{86}Sr$ of 0.710261 ±0.000044 (61 ppm, 2SD) was obtained (Table 3.3, Appendix C3). The total procedural blank (TPB) had Rb and Sr contents of 0.94 ±0.15 and 4.75 ±0.59 pg (2SE) respectively, and its $^{87}Sr/^{86}Sr$ ratio is determined as 0.712932±0.000234 (2SE), (Table 3.4). All Sr isotope data reported on micro-milled MIs is blank- and back-corrected to an eruption age of 14 Ma. As trace element data was not collected on the whole grain dissolutions, blank- and age-correction are not applied to the $^{87}Sr/^{86}Sr$ ratios collected. Given the larger Sr content of these bulk grain samples as multiple MIs are sampled together, the Sr contribution of the TPB should have a more limited effect and may therefore be disregarded. The largest age correction applied to the MIs (MI11-21) was 0.0104%, and a similar age-correction to all MIs would not change the bulk data as it is within the 2SE analytical errors. Further details on the sampling and analytical technique plus evaluation of the TPB are discussed in *Chapter 2* (section 2.5.2.2).

Std. ID	W-2 (250 ppb)		W-2 (25 ppb)		BHVO-1 (25 ppb)		AGV-1 (250 ppb)		AGV-1 (25 ppb)	
n		2		2		4		6		9
	Rec_{conc}	Δ%	Rec_{conc}	Δ%	Rec_{conc}	Δ%	Rec_{conc}	Δ%	Rec_{conc}	Δ%
Trace elements composition (pg/mL)										
Ti	2.20	*-16.36*	0.22	*-14.70*	0.54	*-11.10*	2.12	*-10.07*	0.21	-2.78
Rb	40.72	-2.03	4.07	*-10.43*	1.92	-7.08	134.00	-2.51	13.40	1.77
Sr	386.62	3.11	38.66	-3.62	80.60	-6.42	1324.00	-5.10	132.40	-0.71
Y	42.72	6.58	4.27	*17.42*	5.52	4.58	42.00	-5.98	4.20	-0.07
Zr	185.74	-4.29	18.57	*14.28*	35.80	-0.01	450.00	-6.49	45.00	2.18
Nb	15.52	-3.15	1.55	1.08	3.90	-4.28	28.80	-5.49	2.88	0.96
Ba	334.16	*15.75*	33.42	*87.85*	27.80	*90.90*	2442.00	-4.42	244.20	4.30
La	21.22	3.52	2.12	*23.89*	3.16	8.30	76.00	-4.03	7.60	3.18
Ce	46.06	2.31	4.61	*18.06*	7.80	1.15	132.00	-4.54	13.20	3.51
Pr	5.88	5.20	0.59	*14.34*	1.14	-3.25	13.00	-3.82	1.30	1.80
Nd	26.44	*14.48*	2.64	*23.25*	5.04	*10.92*	68.00	-4.13	6.80	4.33
Sm	6.72	7.43	0.67	*26.02*	1.24	3.94	11.80	0.48	1.18	0.18
Eu	2.24	*12.92*	0.22	-6.32	0.41	6.35	3.32	-2.00	0.33	-0.09
Gd	7.26	*25.71*	0.73	11.91	1.28	*10.35*	10.40	-4.27	1.04	-4.76
Dy	7.42	*20.42*	0.74	9.68	1.04	*17.52*	7.60	-1.02	0.76	1.09
Er	4.46	1.90	0.45	*11.96*	0.48	-9.47	3.22	*-24.73*	0.32	*-39.30*
Yb	4.06	*22.54*	0.41	*19.62*	0.40	*-56.69*	3.34	-2.66	0.33	3.58
Rb/Sr	0.11	-4.99	0.105	-7.09	0.024	-0.49	0.101	2.77	0.21	2.50

Table 3.2: Trace element data collected on USGS rock standard solutions (AGV-1, BHVO-1. W2) during low abundance Vestfirdir MI analytical session on the double focusing magnetic sector field ICPMS (Finnigan ELEMEN2) at *AHIGL* (Department of Earth Sceinces, Durham University). Marked in grey are the concentrations of each element in the dilutions of each of the standard rock solutions, these concentrations are based on USGS reference value available from http://minerals.cr.usgs.gov./geo_chem_stand/. Details on the ICPMS analytical protocol is located in section 2.4.7.4 and Appendix B4-B5. The full dataset is located in Appendix C1.

Whole rock dissolutions were prepared applying a standard dissolution procedure for silicates using a mixture of concentrated HF and HNO_3. In the first step of dissolving the whole rock powder is taken up in a mixture of concentrated HF and HNO_3 in the proportion 3:1. After 24 hours on the hotplate the dissolution is dried down and following taken up in 1 mL concentrated HNO_3 and left on the hotplate to digest another 24 hours. Subsequent to the final dry down, the residue is taken up into solution in 1 mL 3M HNO_3. A 150 µL aliquot of the each 3M HNO_3 sample solution was put through the Sr spec column chemistry (see details in *Chapter 2*, section 2.4.4, and Appendix B1). The rest of the sample solutions were prepared for Nd-Hf column chemistry, thus dried down and taken up in 1 mL 1N HCl. The Hf-Nd column procedure used is found in Nowell et al. (1998). Sr-Nd-Hf isotope compositions were measured using the MC-ICPMS (Thermo-Finnigan Neptune) at *AHIGL* (Department of Earth Sciences, Durham University). During the three different isotope MC-ICPMS sessions standard data was collected on respectively NBS 987, J&M, and JCM475. An average $^{87}Sr/^{86}Sr$ average of 0.710251 ±0.000012 (16.9 ppm, 2SD, n=10) was obtained for NBS 987, an $^{143}Nd/^{144}Nd$ average of 0.511103 ±0.000006 (11.5 ppm, 2SD, n=10) for J&M, and an $^{176}Hf/^{177}Hf$ average of 0.282144 ±0.000008 (29.2 ppm, 2SD, n=4) for JMC475 (Table 3.5).

Whole rock Re-Os chemical procedures for whole rock digested in Carius tubes, Os extractions, and isotope determination were done following Pearson & Woodland (2000). The Os isotope ratios were analyzed by negative TIMS (Thermo-Finnigan Triton) at *AHIGL* (Department of Earth Sciences, Durham University). Over the period of this study, 273 of the University of Maryland College Park Johnson Matthey Os standard were analyzed, for load sizes varying from 0.017 to 3.5 ng, which gave a $^{187}Os/^{188}Os$ value of 0.11382 ±0.00024 (2SD), (D.G. Pearson, personal com.).

n	Load size (pg)	$^{87}Sr/^{86}Sr_{Ave}$	±2SD	±2SD (ppm)
5	0.1	0.710259	0.000054	76
26	0.3	0.710264	0.000048	68
30	0.6	0.710260	0.000038	54
61	Total	0.710261	0.000044	61

Table 3.3: TIMS NBS 987 standard data collected on sub-ng (0.1, 0.3, and 0.6 ng) load sizes on the *AHIGL* TIMS (Department of Earth Sciences, Durham University). 'n' denotes number of analyzes. See also Figure 2.8, Appendix C1 and B8.

Sr isotope and trace element composition of the TPB		
	TPB60	
$^{87}Sr/^{86}Sr$	0.712392	
±2SE	±0.000234	
Trace elements	**TPB_{M11}**	**±2SE**
Ti	659.34	0.01
Rb	0.94	0.15
Sr	4.75	0.59
Y	0.19	0.08
Zr	48.01	5.23
Nb	3.64	0.09
Ba	9.64	0.33
La	0.84	0.09
Ce	1.00	0.16
Pr	0.10	0.05
Nd	0.34	0.03
Sm	-	0.05
Eu	-	0.02
Gd	-	0.05
Dy	0.03	0.07
Er	-	0.03
Yb	0.02	0.07

Table 3.4: Trace element composition of TPB_{M11} and the Sr isotope composition of TPB60 are used for blank corrections of the Vestfirdir MIs. See section 2.5.2 for details on characterization of the TPB and its effect.

Standard ID: NBS 987		Standard ID: J&M		Standard ID: JMC475	
$^{87}Sr/^{86}Sr$	±2SE	$^{143}Nd/^{144}Nd$	±2SE	$^{176}Hf/^{177}Hf$	±2SE
0.710250	0.000012	0.511100	0.0000070	0.282146	0.0000076
0.710249	0.000012	0.511096	0.0000064	0.282143	0.0000070
0.710249	0.000012	0.511098	0.0000060	0.282138	0.0000084
0.710259	0.000012	0.511113	0.0000048	0.282149	0.0000100
0.710254	0.000012	0.511111	0.0000038		
0.710254	0.000012	0.511092	0.0000072		
0.710254	0.000014	0.511098	0.0000074		
0.710249	0.000012	0.511106	0.0000046		
0.710247	0.000010	0.511106	0.0000062		
0.710242	0.000012	0.511107	0.0000052		
n	10	**n**	10	**n**	4
Average	0.710251	**Average**	0.511103	**Average**	0.282144
±2SD	0.000012	**±2SD**	0.000006	**±2SD**	0.000008
±2SD (ppm)	16.9	**±2SD (ppm)**	11.5	**±2SD (ppm)**	29.2
$^{87}Sr/^{86}Sr_{Rec}$	0.710240	$^{143}Nd/^{144}Nd_{Rec}$	0.51110	$^{176}Hf/^{177}Hf_{Rec}$	0.282160
$Correction_{factor}$	0.999845	$Correction_{factor}$	1.000014	$Correction_{factor}$	1.000057

Table 3.5: Standard data collected on rock standards (NBS 987, J&M, and JMC475) collected by MC-ICPMS during Sr-Nd-Hf whole rock session at *AHIGL* (Department of Earth Sciences, Durham University).

3.5 Results

Detailed description of major and trace element systematic of MIs from the Vestfirdir ankaramites are presented in *Chapter 1*. The ICPMS trace element ratios of the milled MIs agree with the compositional range reported in *Chapter 1* of MIs analyzed by LA-ICPMS (Figure 3.2). The similar compositional coverage suggests that the same MI populations were sampled during both sessions, and it shows that the data quality of the newly developed analytical method is comparable. Thus, our findings and conclusion relate directly to the MIs studied from the same samples in *Chapter 1*, Harlou et al., (2003), Harlou et al. (2004). The trace element compositions of the MIs range from slightly depleted to more enriched relative to primitive mantle (PM) having $(La/Y)_N$ of 0.8-6.0 and $(Ce/Sm)_N$ of 0.8-4.0. Positive correlations are observed between PM normalized LREE/HREE, LREE/MREE, and Rb/Sr ratios, and negative correlations are observed among LREE/HREE vs. Ti/Zr and Sr/Nd (Figure 3.2). A few MIs, sampled by both micro-milling and LA-ICPMS, are displaced above the main trend in $(La/Y)_N$ vs. $(Sr/Nd)_N$ plot.

Batch ID	M11-1	M11-2	M11-3	M11-5	M11-20	M11-21	M11-6	M11-7	M11-8
Sample ID	408611	408611	408611	408611	408611	408611	408624	408624	408624
Isotope characteristics									
$^{87}Sr/^{86}Sr_{Meas}$	0.703206	0.705356	0.705829	0.706508	0.705390	0.707240	0.705438	0.704468	0.705420
$^{87}Sr/^{86}Sr_{Norm}$	0.703185	0.705335	0.705808	0.706487	0.705369	0.707219	0.705417	0.704447	0.705399
$^{87}Sr/^{86}Sr_{Blank}$	0.703155	0.704776	0.705487	0.705976	0.704722	0.706327	0.705249	0.704372	0.705153
$^{87}Sr/^{86}Sr_i$	0.703147	0.704747	0.705459	0.705934	0.704693	0.706254	0.705205	0.704365	0.705122
±2SE	0.000095	0.000764	0.001750	0.001510	0.000446	0.000730	0.000290	0.0000676	0.001140
$^{87}Rb/^{86}Sr_i$	0.0388	0.1474	0.1404	0.2114	0.1486	0.3678	0.2246	0.0347	0.1574
Relative abundance of trace elements (ppm)									
Ti	73247.62	4484.28	7307.47	8179.97	3938.35	3036.42	124727.11	359469.55	37638.27
Rb	88.10	2.09	6.35	5.44	1.82	2.46	70.13	27.39	17.82
Sr	6571.30	41.07	130.80	74.40	35.34	19.36	903.21	2283.77	327.62
Y	294.93	6.98	8.73	12.85	3.34	6.19	134.03	554.62	31.49
Zr	938.81	18.30	161.12	93.58	195.35	38.79	1115.27	2628.69	348.71
Nb	16.15	0.14	-	-	1.33	-	34.80	82.68	41.96
Ba	17.89	34.94	203.44	73.40	29.17	31.01	864.31	1276.67	1413.18
La	60.89	2.16	4.42	4.72	0.74	1.86	54.77	83.92	14.40
Ce	132.25	6.54	14.50	12.40	3.05	4.84	99.61	276.58	38.67
Pr	18.46	0.86	1.09	1.29	0.17	0.46	13.74	48.88	4.27
Nd	75.31	3.90	5.90	5.45	1.45	1.69	60.98	294.33	14.41
Sm	699.44	1.12	3.21	1.49	0.67	0.64	25.19	90.26	5.72
Eu	14.10	0.31	0.51	0.38	0.12	0.19	4.04	33.59	1.44
Gd	27.56	1.37	1.41	1.50	0.62	0.74	18.41	120.96	6.14
Dy	37.77	1.12	1.37	1.88	0.59	0.85	20.37	110.61	5.47
Er	31.28	0.53	0.68	1.15	0.34	0.53	11.20	36.91	2.44
Yb	74.66	1.06	1.15	1.83	0.36	1.08	19.67	43.22	3.26
1/Sr	0.00	0.02	0.01	0.01	0.03	0.05	0.00	0.00	0.00
Selected PM normalized trace element ratios									
$(La/Sm)_N$	-	1.24	-	2.06	-	1.88	1.40	0.60	1.63
$(La/Y)_N$	1.37	2.05	3.35	2.43	1.48	1.99	2.71	1.00	3.03
$(Ce/Sm)_N$	-	1.45	-	2.09	-	1.89	0.99	0.77	1.69
$(Rb/Sr)_N$	0.45	1.69	1.61	2.43	1.71	4.22	2.58	0.40	1.81
$(Sr/Nd)_N$	5.60	0.68	1.42	0.88	1.56	0.73	0.95	0.50	1.46
$(Ti/Zr)_N$	0.67	-	0.39	0.75	-	0.67	0.96	1.18	0.93
$(Zr/Y)_N$	1.29	1.07	7.50	2.96	-	2.54	3.38	1.93	4.50
$(Sm/Nd)_N$	-	0.88	-	0.83	-	1.15	1.26	0.94	1.21
$(Ba/Y)_N$	-	3.26	15.17	3.72	5.69	3.26	4.20	1.50	29.21

Table 3.6: Sr isotope ratios (TIMS), trace element concentrations (ICPMS), and selected primitive mantle normalized trace element ratios (of olivine-hosted MIs from the Vestfirdir ankaramites (NW Iceland). Both TIMS and ICPMS analyses were carried out at *AHIGL* (Department of Earth Sciences, Durham University). Primitive mantle values used for normalization are after McDonough & Sun (1995). See trace element content of each MI normalized 100 μm-sized MI in Appendix C4.

Batch ID	M11-9	M11-15	M11-16	M11-10	M11-11	M11-12	M11-13	M11-14	M11-17
Sample ID	408624	408624	408624	408772	408772	408772	408772	408772	408772
Isotope characteristics									
$^{87}Sr/^{86}Sr_{Meas}$	0.704333	0.704032	0.703497	0.704637	0.703576	0.703733	0.703834	0.703818	0.705264
$^{87}Sr/^{86}Sr_{Norm}$	0.704312	0.704011	0.703476	0.704616	0.703555	0.703712	0.703813	0.703797	0.705243
$^{87}Sr/^{86}Sr_{Blank}$	0.704132	0.703940	0.703250	0.703800	0.703496	0.703574	0.703722	0.703717	0.704928
$^{87}Sr/^{86}Sr_i$	0.704113	0.703936	0.703227	0.703778	0.703485	0.703568	0.703710	0.703700	0.704901
±2SE	0.001090	0.000386	0.000388	0.000270	0.000087	0.000167	0.000300	0.000176	0.000624
$^{87}Rb/^{86}Sr_i$	0.0949	0.0218	0.1178	0.1101	0.0570	0.0290	0.0622	0.0845	0.1323
Relative abundance of trace elements (ppm)									
Ti	7056.71	7884.37	10864.60	1832.69	150003.54	11449.12	16345.74	4781.83	3213.53
Rb	3.80	2.88	10.06	0.81	63.21	2.69	6.54	2.98	3.37
Sr	115.73	382.09	246.87	21.30	3208.97	268.43	303.95	102.08	73.67
Y	11.35	9.70	4.84	2.10	212.53	15.61	25.52	8.35	4.31
Zr	47.84	31.83	90.34	11.13	1135.31	189.23	168.76	45.80	15.10
Nb	2.06	-	-	1.71	6.58	3.68	4.76	4.37	-
Ba	213.64	33.67	93.32	19.20	369.95	37.05	46.78	31.78	41.48
La	2.41	1.73	2.45	0.39	86.76	5.02	10.76	3.38	1.73
Ce	7.00	5.67	10.72	2.79	248.85	13.70	29.97	7.90	4.57
Pr	0.95	0.69	0.75	0.13	28.15	1.74	3.53	1.13	0.35
Nd	4.59	4.04	4.13	0.80	125.09	7.22	17.33	4.77	1.69
Sm	1.59	1.67	1.30	0.32	36.73	2.10	4.91	1.24	0.49
Eu	0.51	0.52	0.39	0.06	12.25	0.64	1.46	0.43	0.11
Gd	1.93	1.89	1.11	0.40	41.76	2.35	5.25	1.36	0.54
Dy	2.10	1.70	1.11	0.46	36.31	2.70	4.24	1.27	0.52
Er	0.82	1.11	0.51	0.17	20.63	1.66	2.55	0.82	0.56
Yb	1.10	1.45	0.57	0.28	27.60	2.17	3.30	1.15	0.95
1/Sr	0.01	0.00	0.00	0.05	0.00	0.00	0.00	0.01	0.01
Selected PM normalized trace element ratios									
$(La/Sm)_N$	0.98	0.67	1.22	0.78	1.53	1.54	1.42	1.76	2.30
$(La/Y)_N$	1.41	1.18	3.35	1.24	2.70	2.13	2.79	2.68	2.66
$(Ce/Sm)_N$	1.10	0.85	2.07	2.16	1.69	1.63	1.53	1.59	2.35
$(Rb/Sr)_N$	1.09	0.25	1.35	1.26	0.65	0.33	0.72	0.97	1.52
$(Sr/Nd)_N$	1.62	6.07	3.84	1.71	1.65	2.39	1.13	1.37	2.80
$(Ti/Zr)_N$	1.27	-	1.04	1.42	1.14	0.52	0.83	0.90	-
$(Zr/Y)_N$	1.71	1.33	7.58	2.15	2.17	4.92	2.69	2.23	1.42
$(Sm/Nd)_N$	1.06	1.26	0.96	1.24	0.90	0.89	0.86	0.80	0.88
$(Ba/Y)_N$	12.25	2.26	12.55	5.96	1.13	1.55	1.19	2.48	6.26

Table 3.6: Continued

Batch ID	n	MIs	mg	$^{87}Sr/^{86}Sr_{meas}$	$^{87}Sr/^{86}Sr_{norm}$	±2SE
MIs of 408611						
M2-1	5	multiple	3.25	0.707701	0.707679	0.000508
M2-2	10	multiple	5.44	0.707440	0.707418	0.000176
M2-3	5	multiple	8.25	0.705378	0.705356	0.000088
M2-4	10	multiple	27.00	0.703538	0.703516	0.000033
M2-5	15	multiple	25.06	0.703742	0.703720	0.000032
M2-6	1	multiple	3.37	0.703684	0.703662	0.000003
M2-7	1	multiple	2.15	0.703669	0.703647	0.000137
M2-8	1	multiple	1.08	0.703519	0.703497	0.000063
M2-9	1	multiple	2.41	0.704489	0.704467	0.000254
MIs of 408624						
M2-10	5	multiple	7.21	0.703918	0.703896	0.000054
M2-11	10	multiple	15.00	0.703969	0.703947	0.000028
M2-12	5	multiple	23.98	0.703628	0.703606	0.000016
M2-13	10	multiple	43.49	0.703565	0.703543	0.000009
M2-15	1	multiple	6.95	0.703536	0.703514	0.000014
M2-16	1	multiple	6.89	0.703586	0.703564	0.000023
M2-17	1	multiple	4.92	0.703510	0.703488	0.000018
M2-17	1	multiple	4.92	0.703513	0.703491	0.000011
M2-18	1	multiple	2.02	0.703920	0.703898	0.000012
MIs of 408772						
M2-19	4	multiple	11.26	0.704579	0.704557	0.000400
M2-20	10	multiple	9.86	0.706582	0.706560	0.000045
M2-21	5	multiple	22.84	0.703674	0.703652	0.000014
M2-24	1	multiple	7.34	0.703666	0.703644	0.000013
M2-25	1	multiple	1.36	0.706185	0.706163	0.000550
M2-26	1	multiple	3.93	0.703538	0.703516	0.000002
M2-27	1	multiple	3.34	0.704209	0.704187	0.000017

Table 3.7: Sr isotope analyses (TIMS) of bulk olivine samples, consisting of single or aggregates of olivine phenocrysts rich in MIs. $^{87}Sr/^{86}Sr$ listed are the measured and normalized values accordingly to NBS 987 of 0.710240. Trace element data were not collected, therefore these ratios are not blank or age corrected. 'n' gives number of olivine phenocryst in each sample, 'multiple' means that multiple MIs were pooled, hence the reported Sr isotope ratios represent averages.

Both individually sampled and pooled MIs document significant trace element and Sr isotope variability MIs (0.70315-0.70625 vs. 0.70349-0.70768, Table 3.6-3.7, Figure 3.3-3.4). $^{87}Sr/^{86}Sr$ measurements obtained from single MIs and pooled MIs are in reasonable agreement (Figure 3.4a). However, in detail the most extreme Sr isotope compositions may be lost by the bulk approach, as these represent an average $^{87}Sr/^{86}Sr$ composition of multiple MIs. For example, a larger Sr isotope diversity is observed among the milled MIs compared with the isotope information extracted from the pooled MIs of sample 408624, yet this is not the case for the MIs of sample 408611 and 408772 (Figure 3.4a). Nevertheless, it is expected that the likelihood of

sampling the extreme ends of the Sr isotope range is greater when the individual MIs are samples.

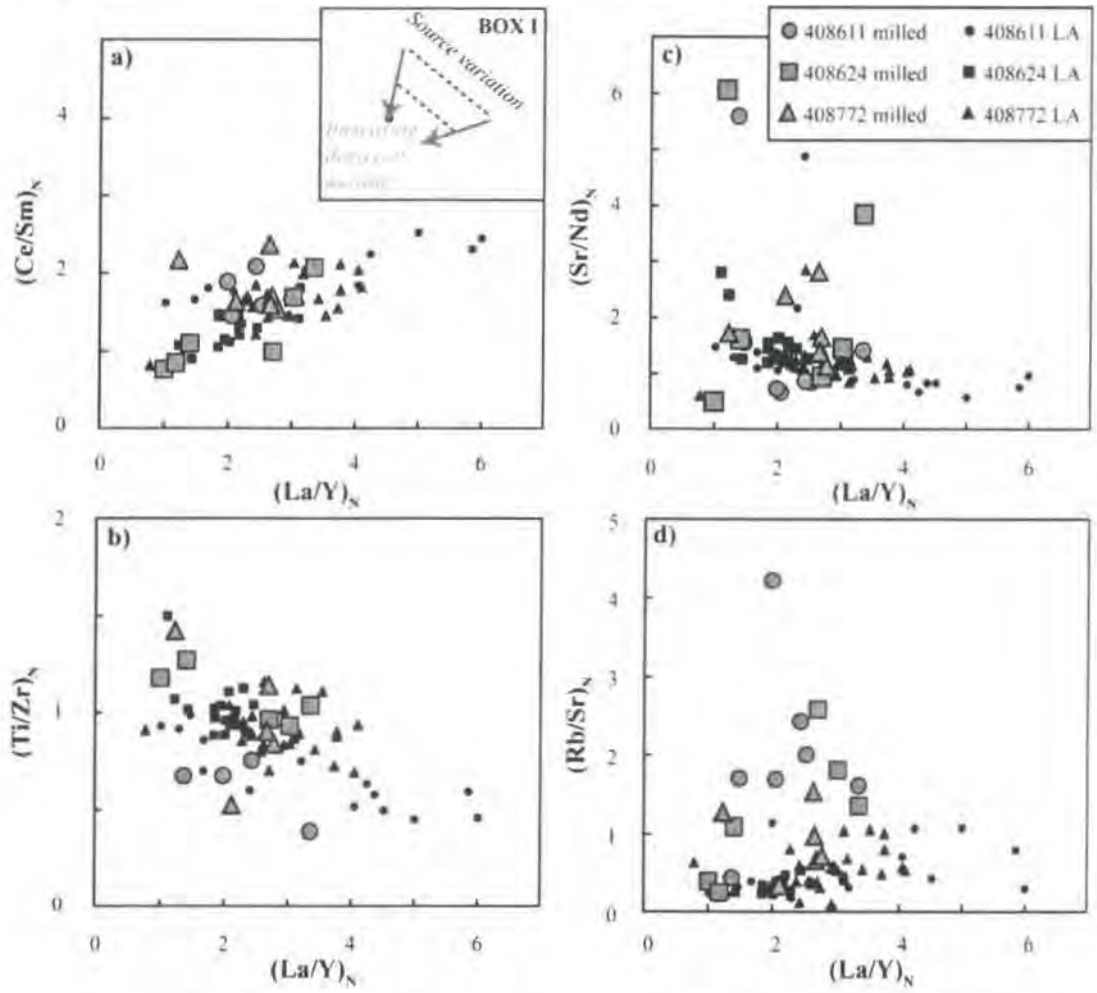

Figure 3.2: Primitive mantle (PM) normalized trace element ratios of individual olivine-hosted melt inclusions (MIs) of the Vestfirdir ankaramites sampled by micro-milling (grey symbols) compared to MIs sampled and analyzed by LA-ICPMS (black symbols). a) $(La/Y)_N$ vs. $(Ce/Sm)_N$. b) $(La/Y)_N$ vs. $(Ti/Zr)_N$. c) $(La/Y)_N$ vs. $(Sr/Nd)_N$. d) $(La/Y)_N$ vs. $(Rb/Sr)_N$. Subscripted $_N$ denotes all trace element ratios are normalized to PM using values from McDonough & Sun (1995). BOX 1 in a) illustrates schematically how the scatter in the data may be explained by variable degree of melting and source chemistry.

The overall $^{87}Sr/^{86}Sr$ diversity sampled by the MIs (0.70315-0.7077) is extreme when compared to the range observed for the host lavas (0.70340-0.70368), but also extreme when compared to the overall range of Sr isotope compositions recorded in Icelandic lavas (0.70285-0.70380, compiled from Kokfelt et al., 2006, Thirlwall, et al., 2004, Prestvik et al., 1999), (Table 3.1 and 3.6-3.7, Figure 3.4a). Hence, the radiogenic Sr ratios of the Vestfirdir MIs represent the most extreme radiogenic Sr isotope compositions found on Iceland. From a global perspective, these MIs document a considerable variation as they cover 77 % of the total Sr isotope range measured on OIB. In contrast, the host ankaramite suite only covers 5 %, and the overall Sr isotope range previous documented by Icelandic lavas covers <20 % of the global OIB range. Sr

isotope data reported from OIB lavas such as Iceland or Hawaii define ranges, which have Gaussian distribution (Figure 3.4b). In contrast, the smaller dataset for Vestfirdir MIs is not Gaussian, and appear to contain MIs from at least two different components.

If the Sr isotope compositions are plotted against selected trace element ratios, two trends among the MIs are revealed (Figure 3.3). '*Trend I*' is described by MIs with relatively unradiogenic and more homogenous $^{87}Sr/^{86}Sr$ ($\leq$0.704) over the range of $(La/Y)_N$, $(Sr/Nd)_N$, and $(Ti/Zr)_N$. In contrast, '*Trend II*' is steep, and is described by MIs displaying a positive correlation between $^{87}Sr/^{86}Sr$ and $(La/Y)_N$, or $(Rb/Sr)_N$, but an inverse correlation with $(Sr/Nd)_N$ and $(Ti/Zr)_N$. Overall, the MIs display a positive relationship between $^{87}Sr/^{86}Sr$ and Rb/Sr, however *Trend II* MIs extend to much higher $^{87}Sr/^{86}Sr$ ($\geq$0.704) and $(Rb/Sr)_N$ values than MIs of *Trend I* MIs. This grouping of MIs cannot be ascertained from the trace element ratios alone (Figure 3.2, *Chapter 1*).

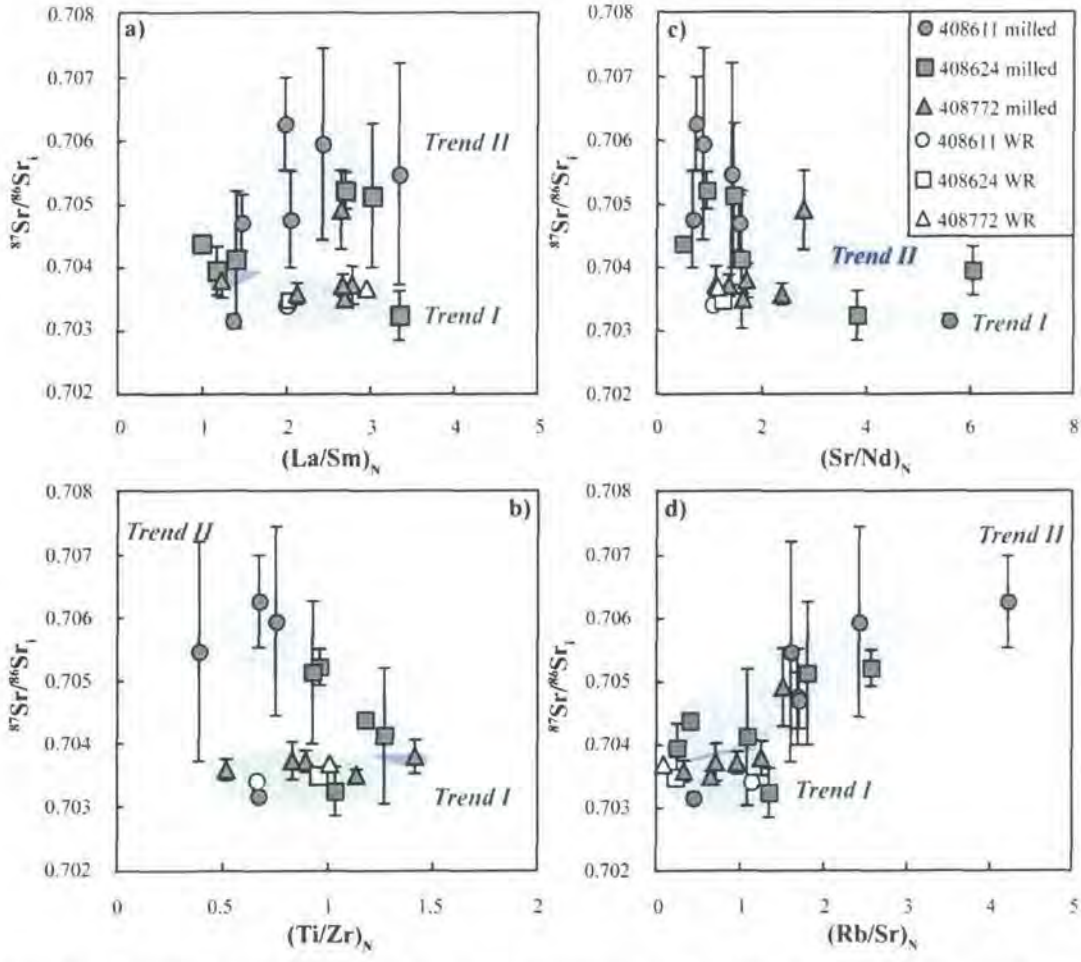

Figure 3.3: Initial Sr isotope composition (blank and age corrected back to 14 Ma, also) versus trace element ratios obtained on olivine-hosted MIs from the ankaramites of Vestfirdir. a) $^{87}Sr/^{86}Sr$ vs. $(La/Y)_N$, b) $^{87}Sr/^{86}Sr$ vs. $(Ti/Zr)_N$, c) $^{87}Sr/^{86}Sr$ vs. $(Sr/Nd)_N$, and d) $^{87}Sr/^{86}Sr$ vs. $(Rb/Sr)_N$. Error bars show the 2SE error on each the individual $^{87}Sr/^{86}Sr$ analysis. Blue and green shading represent respective *Trend I* and *Trend II* MIs.

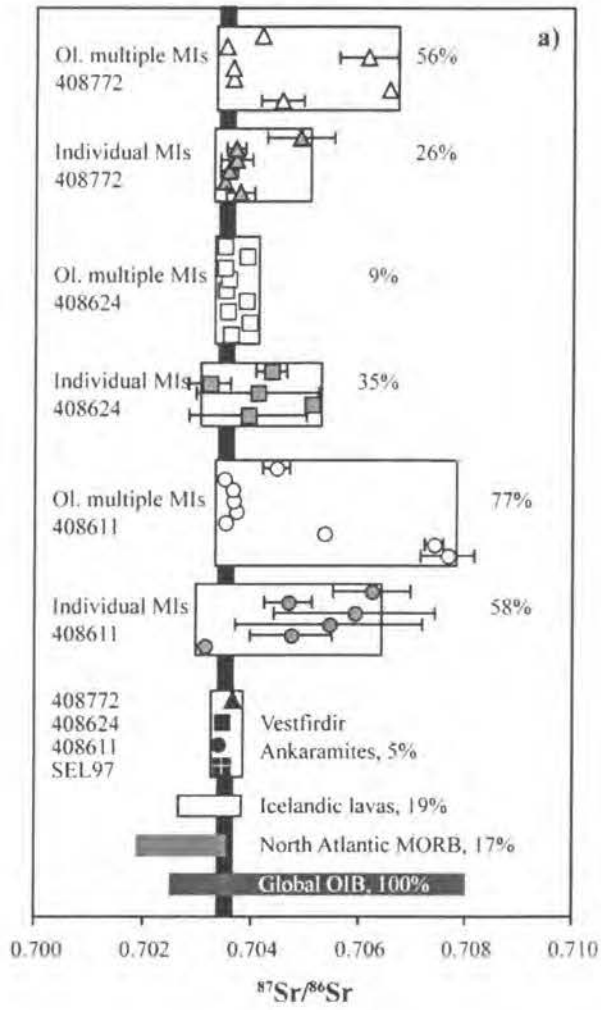

Figure 3.4: a) Comparison of the $^{87}Sr/^{86}Sr$ isotope range revealed by individual MIs (grey symbols) and bulk olivine analysis (open symbols) for each of three lavas with the host ankaramite suite (including SEL97, Hilton et al. 1999). The variation in Sr isotope range revealed by the MIs is compared to the Sr isotope range of the host ankaramite the overall range seen in Icelandic lavas (Thirlwall et al., 2004; Kokfelt et al., 2006), and the global OIB (Hofmann, 1997). Black vertical bar show the range of the host ankaramites. The percentages indicate how much an overlap there is with the Global OIB. b) Curves comparing the total $^{87}Sr/^{86}Sr$ distribution of lavas from Iceland (red line, data compilation from http://earthref.org), Hawaii (black broken line, data compilation from http://earthref.org), with the MIs populations from Vestfirdir. Blue curve is the distribution detected for the individual MIs, whereas the green curve is the *'total'* of data colleted on individual MIs and grain aggregates (multiplied by 10). Blue curve sample numbers refer to the left Y-axis, whereas the others refer the Y-axis on the right. The curves clearly illustrate the greater variability documented by the MIs of Vestfirdir compared to the narrow single-peaked data (Gaussian distributions) reported for the OIB data from both Hawaii and Iceland. The non-Gaussian distribution of the MI data suggests the involvement of multiple sources.

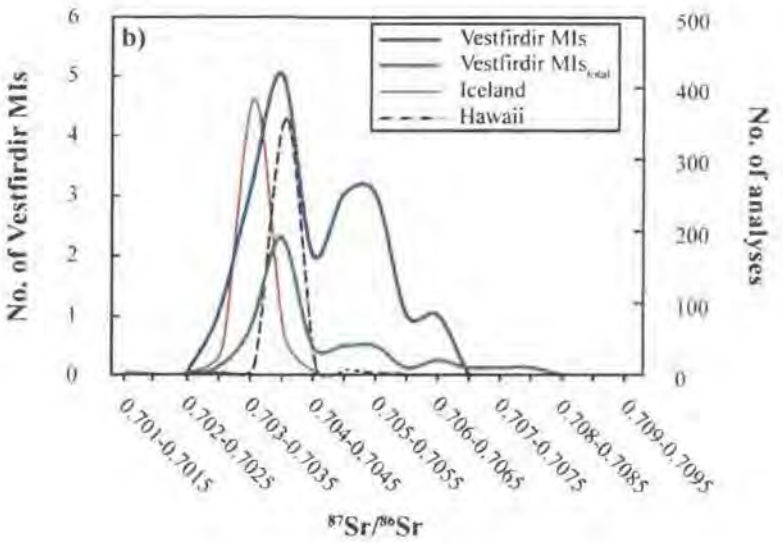

Figure 3.4: Continued

3.6 Discussion

A previous study by Hilton et al. (1999) proposed that the extreme unradiogenic He combined with somewhat radiogenic Sr-Nd-Pb composition of the Seladalur ankaramite (SEL97) is derived from the 5th mantle component common to many mantle plumes - namely FOZO e.g. Hart et al. (1992) and Hauri et al. (1994). FOZO is defined as the *Focus Zone*, a high $^{3}He/^{4}He$ mantle end-member whose composition is defined by the point of convergence of the global OIB data in Sr-Nd-Pb isotope space (Hart et al., 1992). However, olivine-hosted MIs from this sample plus other Vestfirdir ankaramites show that the individual MIs record substantial Sr isotope variability amongst the pre-aggregated melts (Figure 3.3-3.4). The MIs have both less unradiogenic and significantly more radiogenic $^{87}Sr/^{86}Sr$ ratios than the host lava suite. Such Sr isotope variability cannot be derived from a single source component, but requires multiple source components with distinct Sr isotope signatures. At least two components are required, one with an unradiogenic $^{87}Sr/^{86}Sr$ ($\leq$0.703) and one with radiogenic $^{87}Sr/^{86}Sr$ ($\geq$0.708). The MIs with the lowest $^{87}Sr/^{86}Sr$ ratios indicate the involvement of a relative depleted mantle (DM) component. The absence of continental crust on Iceland precludes that these melts acquired their radiogenic Sr due to contamination by continental crust *en route* to eruption e.g. as documented for Baffin Island picrites (*Chapter 4*, Yaxley et al., 2004; Harlou et al., 2006). Yet, chemical and Sr isotope variation may be introduced by interaction with older, possibly hydrothermally altered oceanic crust during ascent. Below, we explore the possible origin of the Sr isotope diversity recorded by the Vestfirdir MIs. In terms of evaluating whether the Sr isotope diversity is related to interaction with the underlying oceanic crust, or if the diversity reflects heterogeneities present within the convecting mantle sampled by the Icelandic mantle plume.

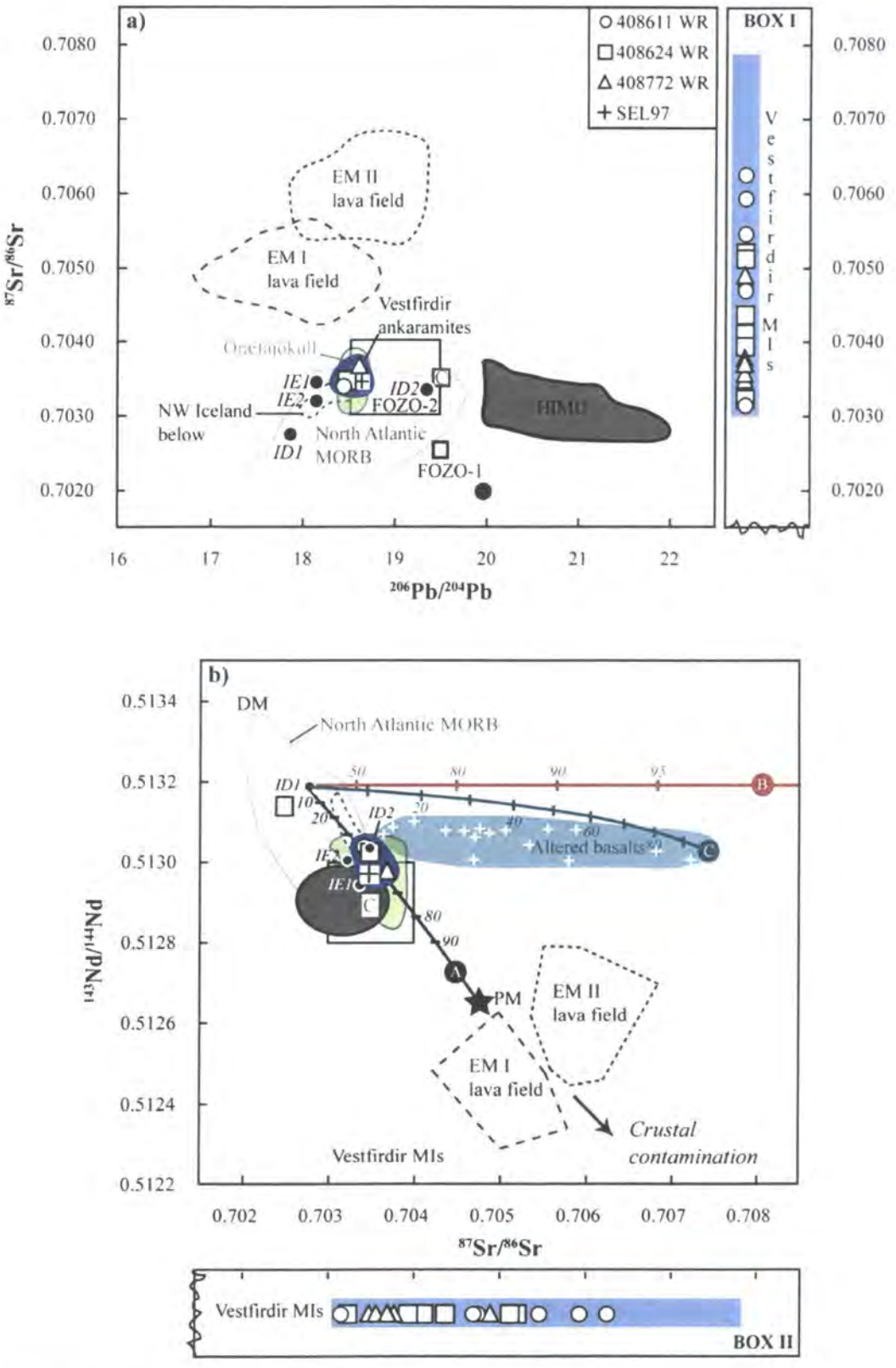

Figure 3.5: See caption on the next page.

Figure 3.5: a) $^{206}Pb/^{204}Pb$ vs. $^{87}Sr/^{86}Sr$, and b) $^{87}Sr/^{86}Sr$ vs. $^{143}Nd/^{144}Nd$ diagrams showing the variation of Vestfirdir ankaramites (Table 3.1, Hilton et al., 1999) in relation to the compositions of other mantle-derived basalts and defined mantle reservoirs. Plotted on the $^{87}Sr/^{86}Sr$ axis are the individual Sr isotope compositions of each MI with no reference to their Nd and Pb isotope composition, along with the range of the Sr isotope ratios obtained on olivine aggregates (blue bar). PM and the lava fields of HIMU, EMI, and EMII are by Hofmann (1997), the composition of FOZO-1 (Hart et al., 1992), FOZO-2 (Hauri et al., 1994), and C (Hanan & Graham, 1996). The two depleted (ID1, ID2) and two enriched (IE1, IE2) endmember compositions of the Icelandic mantle plume suggested by Thirlwall et al. (2004) are included for comparison. Also included are the fields of lavas from below the 15 Ma unconformity in NW Iceland (Hardarson et al., 1997), the Öræfajökull lavas (Prestvik et al., 2001). An example of lavas altered by seawater is included in b) (Staudigel et al., 1995). Three mixing lines are shown in b). Mixing line A is generated between the depleted mantle represented by ID1 (Thirlwall et al., 2004) and the PM. Mixing line B represents mixing between ID1 and seawater. Parameters used for seawater are: $^{87}Sr/^{86}Sr$ ~0.70906 (Elderfield & Schultz, 1996), Sr ~ 5.1 ppm (Drever, 1997), $^{143}Nd/^{144}Nd$ ~ 0.5124 (Stille et al., 1996), and Nd ~ 120 ppb (Drever, 1997). Mixing line C is generated between ID1 and the most extensively altered basalt composition (417/418 vcl top) from Staudigel et al. (1995). Tick marks and adjacent numbers indicated increment in % of each of the three components ID1 is mixed with. Notice that pure mixing of melts derived from DM and PM cannot generate the more radiogenic Sr isotope compositions found among the MIs. Neither does the whole-rock data conform to mixing line B or C, which suggest that these ankaramites are not affected by hydrothermal alteration or assimilation of older altered Icelandic crust. Hence, a radiogenic Sr component involved in the genesis of the Vestfirdir ankaramites must reside in the mantle.

3.6.1 Interaction with altered oceanic crust

The Vestfirdir ankaramites erupted through and onto sub-aerially erupted flood basalts formed in relations to the NW paleo-rift zone (Figure 3.1, e.g. Hardarson et al., 1997; Hilton et al., 1999; Foulger, 2006) and thus the chemistry of lavas may be affected by assimilation of the older Icelandic crust. The Sr isotope composition of the lavas immediate below the unconformity (~14.9 Ma) at Vestfirdir show considerable overlap with the Sr isotope range of the lavas above (Hardarson et al., 1997), and none of these lavas carry as extreme radiogenic $^{87}Sr/^{86}Sr$ as those sampled by some of the MIs. Hence, assimilation of the older lava sequence cannot by itself provide a source of radiogenic Sr. In fact, no basalt on Iceland with $^{87}Sr/^{86}Sr$ as high as the Vestfirdir MIs has been documented, and therefore direct assimilation of known Icelandic basalt during ascent can be precluded. Neither can the radiogenic Sr reservoir be generated by *in situ* Rb decay. As the oldest crust below Iceland might as old as 37 Ma (Foulger, 2006), an initial $^{87}Rb/^{86}Sr$ of >5.8 is required to change from an $^{87}Sr/^{86}Sr$ ratio of 0.703 to for example 0.706. Such Rb/Sr values are very unlikely for basaltic lavas, and inconsistent with the measured $^{87}Sr/^{86}Sr$ and Rb/Sr ratios of the older lavas below the unconformity (Hardarson et al., 1997).

Low $\delta^{18}O$ values in some Icelandic lavas document that parts of the crust are affected by hydrothermal alteration via meteoric water (e.g. Condomines et al., 1983; Gautason & Muehlenbachs, 1998; Eiler et al., 2000a; Macpherson et al., 2005). If the Vestfirdir melts had interacted with hydrothermally altered crust, they should have $\delta^{18}O$ values lower than typical mantle values (e.g. Condomines et al., 1983; Eiler et al., 2000b; Prestvik et al., 2001;

Macpherson et al., 2005). Only a single $\delta^{18}O$ value has been reported for a Vestfirdir ankaramite, which is a $\delta^{18}O$ of ~ 5.1 for SEL97 (Macpherson et al., 2005). This value falls at the lower end of the range expected for mantle peridotite derived melts (5.18 ±0.28 ‰, Mattey et al., 1994), but is within error of the mean and indicates no significant interaction with low $\delta^{18}O$ hydrothermally altered crust for this sample. Besides, meteoric water is not by itself a source of Sr or Rb, and therefore the $^{87}Sr/^{86}Sr$ signature of these lavas should remain unaffected even if exposed to alteration by this media.

However, we cannot preclude the assimilation of unexposed high $^{87}Sr/^{86}Sr$ basalt that may have experienced extensive low-temperature alteration by seawater during the early sub-aqueous evolution of Iceland. As circulation of seawater [$^{87}Sr/^{86}Sr$ ~ 0.70916 (Elderfield & Schultz, 1996; and references therein), Sr ~ 8.1 ppm (Drever, 1997)] through the oceanic crust can have a significant effect on the Sr budget of some rocks and may result in radiogenic Sr isotope signature plus elevated $\delta^{18}O$ e.g. Staudigel et al. (1995) and Elderfield & Schultz (1996). In contrast, the effect on the Nd isotope composition is minimal due to the low Nd concentration of seawater [$^{143}Nd/^{144}Nd$ ~ 0.5124, Stille et al., (1996); 120 ppb Nd, Drever, (1997)]. A simple binary mixing model predicts a mixing relationship of 60% to 40% between altered oceanic crust (417/418 vcl top, Staudigel et al. 1995) and DM (*ID1*, Thirlwall et al., 2004) to regenerate the most radiogenic $^{87}Sr/^{86}Sr$ of the MIs (Figure 3.5b). Whereas, a rock-water ratio of approximately 7/93 is required to generated the $^{87}Sr/^{86}Sr$ of 0.706 by direct seawater alteration (Figure 3.5b). The model furthermore predicts that interaction with altered crust or pure seawater should be reflected in relatively constant $^{143}Nd/^{144}Nd$ values over the range of $^{87}Sr/^{86}Sr$ ratios, similar to what is observed for altered oceanic crust (Staudigel et al., 1995). The model also indicates that elevated $^{87}Sr/^{86}Sr$ ratios should be accompanied by low Rb/Sr ratios, which is unlike the relationship between the $^{87}Sr/^{86}Sr$ and Rb/Sr ratios of *Trend II* (Figure 3.3d). The normal mantle-like $\delta^{18}O$ of SEL97, the negative correlation between Sr-Nd isotope compositions and the good correlation between mobile and immobile elements e.g. Nb vs. K_2O, Ba, and Rb (Figure 1.3h) are inconsistent with extensive assimilation of altered crust or interaction with seawater.

Little geochemical evidence is found that suggests that the host ankaramites and MIs are affected by direct hydrothermal alteration or by assimilation of older, hydrothermally altered Icelandic crust. It seems unlikely, if such processes generated the Sr isotope variability observed among the Vestfirdir MIs without also affecting the whole rock isotope signature. This strongly indicates that the source of the radiogenic Sr explicitly recorded by the MIs does not reside within the Icelandic crust, but instead must be located within the convecting mantle sampled by the Icelandic mantle plume.

3.6.2 Variability generated within a chemically diverse mantle

The geochemical diversity among OIB and MORB lavas have led to the recognition of the existence of several chemical distinct components within the mantle e.g. the depleted MORB mantle, PM, HIMU, EMI, EMII, FOZO (Zindler & Hart, 1986; Weaver, 1991; Hart et al., 1992; Hofmann, 1997). In relation to the overall mantle array in the space of Sr-Nd-Hf-Os-Pb isotope chemistry, the Vestfirdir ankaramites represent relatively depleted compositions (Figure 3.5-3.7, Table 3.1). However, if the Sr-Nd-Pb isotope composition of the Vestfirdir ankaramites is compared with the Sr-Nd-Pb isotope range previously reported from Iceland, the Vestfirdir ankaramites have relatively enriched Sr-Nd, intermediate $^{206}Pb/^{204}Pb$, but slightly elevated $^{207}Pb/^{204}Pb$ and $^{208}Pb/^{204}Pb$ isotope compositions (Figure 3.5). And if the Sr isotope range of the Vestfirdir MIs is included, the $^{87}Sr/^{86}Sr$ range is extend substantially beyond the overall range documented for any Icelandic lava and beyond any estimate for PM (Figure 3.5b). Such Sr isotope variability can not be generated by binary mixing of melts purely derived from DM and PM (Figure 3.5b), neither can the variation in trace element as documented in *Chapter 1*. The most extreme, radiogenic $^{87}Sr/^{86}Sr$ MI values imply that a component with more radiogenic Sr than PM is involved i.e. a recycled component. The lower $^{87}Sr/^{86}Sr$ values of the MIs document the existence of a DM component within the mantle region sampled by the Icelandic mantle plume (Figure 3.5). Works by Thirlwall et al. (2004) and Kokfelt et al. (2006) have suggested that the Sr-Nd-Pd isotope spectrum of Icelandic lavas is generated by melts or melt mixtures derived from four mantle components of which two are depleted and two are enriched (Figure 3.7). However, none of these components possesses the radiogenic $^{87}Sr/^{86}Sr$ signature documented by the lavas and MIs of Vestfirdir (Figure 3.5 and 3.7). This implies the existence of an additional mantle component with $^{87}Sr/^{86}Sr \geq 0.70768$ present in the mantle region sampled by the Icelandic plume, or that the Sr signature of one of the enriched mantle (EM) components predicted by Thirlwall et al. (2004) and Kokfelt et al. (2006) is underestimated.

Entrainment of recycled subducted oceanic crust component(s) into the Icelandic plume has been proposed as an explanation to some of the Sr-Nd-Pb-Hf-Os isotope variations seen among the Icelandic lavas e.g. (Chauvel & Hémond, 2000; Hanan et al., 2000; Prestvik et al., 2001; Skovgaard et al., 2001; Kokfelt et al., 2006; Thirlwall et al., 2004). The estimated age of such recycled oceanic lithosphere is Archaean to Late Archaean (3-2.6 Ga), (Chauvel & Hémond, 2000; Skovgaard et al., 2001; Thirlwall, 1995). Others have suggested, the existence of a relict component derived from Paleozoic hydrothermally altered oceanic lithosphere (Iapetus) subducted during the formation of the Laurasian super-continent (Foulger et al., 2005), or fragments of continental lithosphere left beneath Iceland after the breakup of Greenland and Europe (Foulger & Anderson, 2005; Foulger, 2006; Paquette et al., 2006). In these scenarios, the Icelandic alkali basalts are thought to be derived from melting of the basaltic portion of the

recycled oceanic crust having relatively unradiogenic $^{143}Nd/^{144}Nd$, radiogenic $^{87}Sr/^{86}Sr$ and $^{206}Pb/^{204}Pb$ (Chauvel & Hémond, 2000). The Icelandic picrites may result from melting of the gabbroic part (rich in plagioclase and clinopyroxene) resulting in elevated $^{143}Nd/^{144}Nd$ combined with low $^{87}Sr/^{86}Sr$ and $^{206}Pb/^{204}Pb$ (Chauvel & Hémond, 2000). Both rock types also require melt contributions from the harzburgitic portion of the recycled lithosphere. However, models where the melt is derived purely from recycled oceanic lithosphere (e.g. Chauvel & Hémond, 2000; Kokfelt et al., 2006) are not consistent with the high $^{3}He/^{4}He$ ratios of the Vestfirdir ankaramites, since a recycled component is extensively degassed, and therefore such reservoir is expected to have a low $^{3}He/^{4}He$ signature (section 3.6.3-3.6.4).

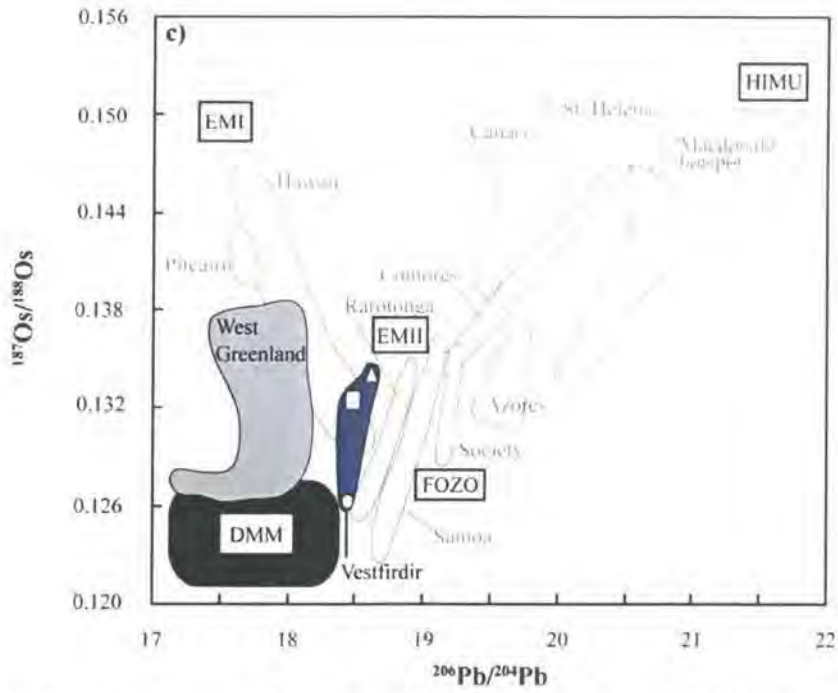

Figure 3.6: The relationship between $^{206}Pb/^{204}Pb$ and $^{187}Os/^{188}Os$ displayed by the global OIB after Hauri (2002b). The plot also the location of the different mantle endmembers; DM, FOZO, HIMU, EMI, and EMII. Superimposed is the Vestfirdir data (Table 3.1), and the West Greenland picrites represending data compiled from Lightfoot et al. (1997), Schaefer et al. (2000), and D. G. Pearson (unpublished data).

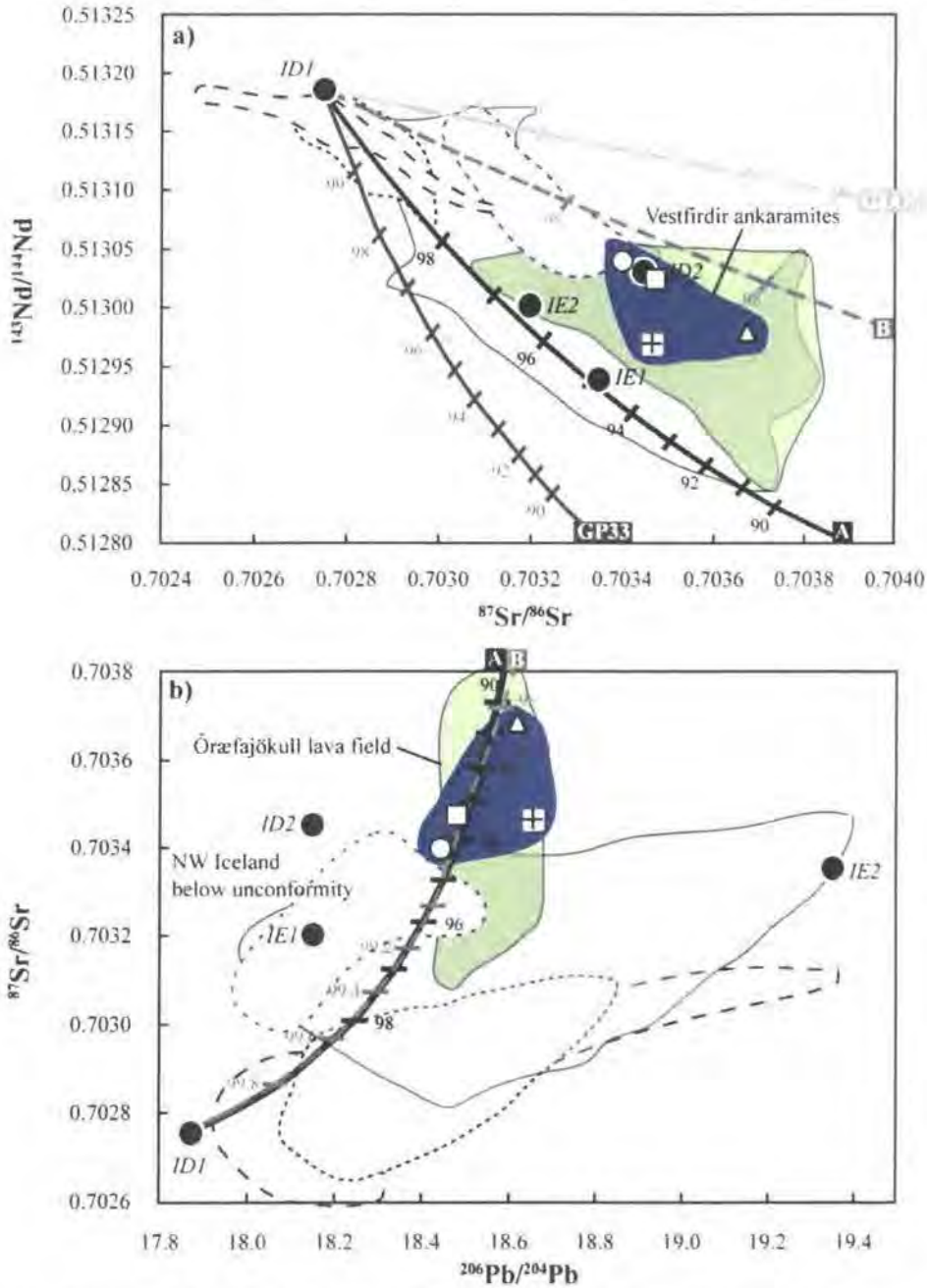

Figure 3.7: Variation of $^{87}Sr/^{86}Sr$, $^{143}Nd/^{144}Nd$ and $^{206}Pb/^{204}Pb$ for the Vestfirdir ankaramites (Table 3.1, Hilton et al., 1999) compared to the overall range of Icelandic lava fields after Kokfelt et al. (2006) and the four Icelandic plume components (*ID1, ID2, IE1, IE2*) suggested by Thirlwall et al. (2004). Also included are the Öræfajökull lavas (Prestvik et al., 2001) that bear strong resemblance to the Vestfirdir ankaramites. The Vestfirdir ankaramites and their MIs are explained as the result of mixing among melts derived from the depleted mantle (DM equal to ID1 by Thirlwall et al. 2004), a recycled hydrothermally altered oceanic crustal which contains a pyroxenite component (represented by GP33; Pearson et al. 1991) and a sediment components (GLOSS; Plank & Langmuir, 1998). 'A' and 'B' represent mixtures of GP33 and GLOSS respectively containing 98.5% GP33 and 1.5% GLOSS, and 90 % GP33 and 10 % GLOSS. Four mixing lines between DM and GP33, GLOSS, A, and B are shown. Numbers adjacent to tick marks on the mixing lines indicate percentage of the DM component relative to GP33, GLOSS, A or B. Best match for the Vestfirdir data is obtained by mixing between the DM and 'B'. 'B' is hereafter referred to as REM (recycled enriched mantle).

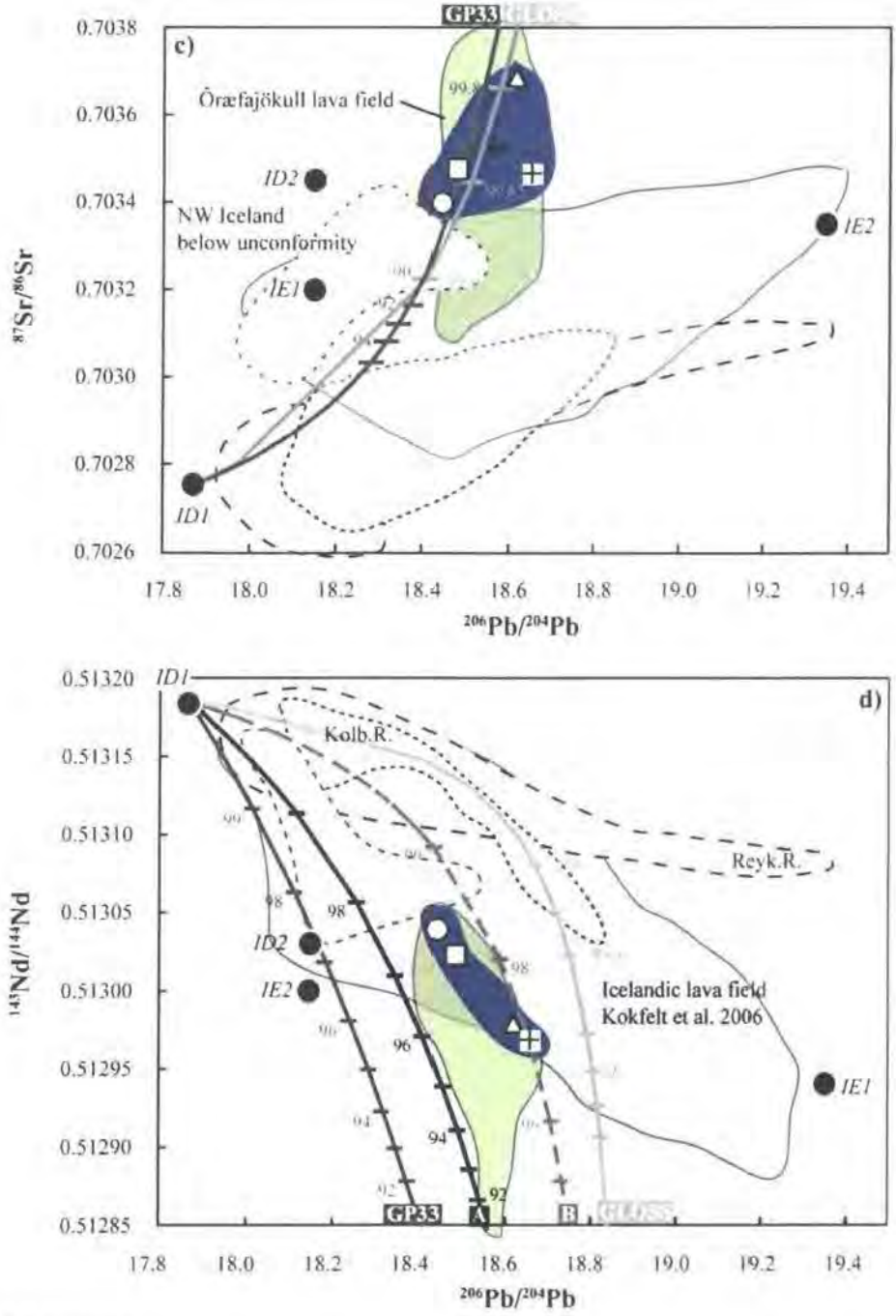

Figure 3.7: Continued

3.6.2.1 The radiogenic Sr signature - an enriched, recycled mantle source component

The very radiogenic $^{87}Sr/^{86}Sr$ and high Rb/Sr ratios of the MIs of *Trend II* strongly imply that the Icelandic mantle plume contains a more extreme radiogenic $^{87}Sr/^{86}Sr$ component than previous studies have suggested e.g. Kokfelt et al. (2006), Thirlwall et al. (2006). Also, the range from DM-like Os whole-rock isotope composition towards more elevated $^{187}Os/^{188}Os$ ratios (Figure 3.6, Table 3.1), and the systematics of the Hf isotope support the involvement of a

recycled component in genesis of the host ankaramites (Table 3.1). The intermediate $^{206}Pb/^{204}Pb$ and slightly elevated $^{207}Pb/^{204}Pb$ and $^{208}Pb/^{204}Pb$ ratios of the ankaramites suggests a recycled LOMU rather than a HIMU component (Figure 3.5-3.6). The intermediate $^{206}Pb/^{204}Pb$ values further point towards EMII-like rather than EMI-like source characteristics, which also gains support from the Sr and Os isotope systematics of the Vestfirdir ankaramites. The overall isotope systematic of the host ankaramites, displaying increasing Sr-Os isotope ratios with decreasing Nd-Hf, suggest an increase of input of the enriched component through 408611 to 408624 and 408772 (Figure 3.5-3.6, Table 3.1).

The isotope variability and trace element composition of EMI and EMII lavas are best modelled by mixing between variable proportions of subducted oceanic lithosphere and lower or upper continental crust e.g. (Stracke et al., 2004; Willbold & Stracke, 2006). Therefore, we choose to model the enriched, radiogenic Sr component using a pyroxenite (GP33; Pearson et al., 1993) as a proxy of recycled hydrothermally altered oceanic lithosphere, while the radiogenic sediment input is modelled by adding minor amounts of sediment using GLOSS (Plank & Langmuir, 1998). The depleted Icelandic plume component '*ID1*' (Thirlwall et al., 2004) is chosen as representative of the depleted, low $^{87}Sr/^{86}Sr$ mantle endmember of the Icelandic lava array. Two composite enriched mantle endmembers are generated by mixing variable amounts of subducted pyroxenite with GLOSS (Figure 3.7). 'A' is a mixture made by of 90% GP33 and 10% GLOSS, while 'B' contains 98.5% pyroxenite and 1.5% GLOSS. Compositions may be generated by mixing melts derived from the DM and component 'B' in the proportion 97-99% to 1 to 3% provide the best match for the Sr-Nd-Pb systematic of the Vestfirdir ankaramites. 'B' will in the following be referred to as recycled enriched mantle component (REM), a recycled oceanic lithosphere component holding a crustal signature similar to GLOSS. The model further predicts that the $^{87}Sr/^{86}Sr$ variability among the MIs require larger inputs (1 to 15%) from the radiogenic Sr component REM. This mixing scenario is in agreement with modelling of trace element systematics of the MIs and lavas of Vestfirdir presented in *Chapter 1*. This shows that the compositional range of the Vestfirdir MIs documents variable mixing proportions between melts derived from a REM and the DM. In comparison to the host lavas and the MIs of *Trend I*, the more radiogenic $^{87}Sr/^{86}Sr$ ratios of the MIs of *Trend II* record lager contributions of melt derived from the high $^{87}Sr/^{86}Sr$ REM component.

3.6.2.2 The unradiogenic Sr signature – a depleted mantle source component

The Sr-Nd isotope characteristics of the ankaramites place them at the edge of the North Atlantic MORB field (Figure 3.5), which, in agreement with many previous studies, suggests a strong involvement of a depleted component in the genesis of the Icelandic lavas (e.g. Fitton et al., 1997; Hanan et al., 2000; Fitton et al., 2003; Thirlwall et al., 2004; Macpherson et al., 2005; Kokfelt et al., 2006; Thirlwall et al., 2006). The modelling above likewise predicts that a DM

signature dominates the whole rock composition of the Vestfirdir ankaramites. A dominant derivation from a DM component is in agreement with the systematic Sr-Nd-Hf-Os isotope variation displayed among the ankaramites (Figure 3.5-3.7, Table 3.1). In particular, the unradiogenic Sr-Os combined with radiogenic Nd-Hf of sample 408611 implies a strong link to a DM (Table 3.1). The somewhat more radiogenic Sr-Os-Pb, but more unradiogenic Nd-Hf isotope ratios of 408624 and 408772 agree with an increased input from the high $^{87}Sr/^{86}Sr$ REM component to these rocks relative to 408611 and the low $^{87}Sr/^{86}Sr$ MIs of *Trend I.* It is further noticeable from the Os isotope ratios that the high $^{3}He/^{4}He$ lavas fields of localities within the NAIP extend from the DM field towards more enriched compositions (Figure 3.6). These lava fields do not trend from or towards the FOZO composition, which argue further against a derivation from FOZO as proposed by Hilton et al. (1999). Neither does the Sr-Nd-Hf-Pb systematic of these rocks support the involvement of a HIMU source. The involvement of the DM gains further support from MIs and lavas with PM normalized ratios of (Rb, Th, U, Nb)/La <1, Rb/Sr <1, Ce/(La, Pb) >1, and Sr/Nd >1 (exceptions are higher Rb/La and Rb/Sr >1 for 408611), (*Chapter 1*). These ratios suggest that the source rock in the past experienced melt extraction, which gave rise to a source rock depleted in the most incompatible trace elements (Rb through Nb, and Pb) relative to PM. These depletions are consistent with the depleted isotope systematic of the ankaramites, and thus the existence of low $^{87}Sr/^{86}Sr$, DM component within the source region tapped by the Vestfirdir ankaramites.

3.6.3 Implications for the He systematics of the Vestifirdir ankaramites

The incompatible nature of volatiles in magma systems means that the best way to study early magmatic volatiles, before they become subjected to major degassing and atmosphere interaction, is to analyse their compositions in melt and gas inclusions trapped in early formed phenocryst phases such as olivine (Hauri, 2002a; Saal et al., 2002). The Vestfirdir ankaramites have been shown to contain some of the highest $^{3}He/^{4}He$ measured from mantle-derived lavas (Breddam et al. in prep., Table 3.1). This He is predominantly contained within MIs, and so the Sr isotope and trace element data presented here have direct bearing on the origin and evolution of this controversial high $^{3}He/^{4}He$. Thus, it seems more meaningful to relate the $^{3}He/^{4}He$ in olivine directly with the Sr isotope measured in the MIs, than to the whole rock lithophile isotope ratios.

The origin of the very high $^{3}He/^{4}He$ signature carried by the Vestfirdir ankaramites is rather enigmatic, since high $^{3}He/^{4}He$ signatures as measured on olivine separates from these rocks traditionally would be ascribed to contributions from primordial mantle (e.g. Graham, 2002 and references therein). As shown above, the Vestfirdir MIs and ankaramite suite are dominated by a DM component, with minor REM input (1-15%), and so the He isotope signature is likely to be derived from one of these components rather than an additional primordial mantle

component. The melt portions derived from ancient recycled oceanic and crustal components are unlikely to hold an unradiogenic He signature, because recycled reservoirs are extensively processed during initial magmatic emplacement, and subsequent subduction and remelting. Neither is the Icelandic crust itself a reservoir of unradiogenic He (Condomines et al., 1983; Macpherson et al., 2005), and therefore it is also implausible that the Vestfirdir melts obtained elevated $^{3}He/^{4}He$ ratios through assimilation processes during ascent. Instead, the unradiogenic He signature is most obviously linked to the DM component revealed by the depleted Sr-Nd-Hf-Os signatures (Figure 3.5-3.6), which dominates the overall isotope characteristics of the MIs and host lavas.

This suggestion contradicts the general assumption that high $^{3}He/^{4}He$ ratios are indicative of a primordial undegassed mantle component e.g. Graham (2002). However, a linkage between DM signatures have recently been suggested for another high $^{3}He/^{4}He$ locality within NAIP - namely for the Baffin Island picrites (Stuart et al., 2003; Ellam & Stuart, 2004; Harlou et al., 2006; *Chapter 4*). An association of the high $^{3}He/^{4}He$ with a depleted reservoir gains support from a new study by Parman et al. (2005), whose solubility experiments document He to be more compatible than U+Th during mantle melting. This observation has been used to show how high $^{3}He/^{4}He$ can be directly related to DM via mantle melting through time (Parman et al., 2005; Parman, 2006). Hence, the $^{3}He/^{4}He$ ratio of a given reservoir is very much a product of its original He concentration, $(U+Th)/^{3}He$, the time, and its melt extraction history (e.g. Meibom et al., 2003; Parman et al., 2005; Parman, 2006).

The high $^{3}He/^{4}He$ recorded in the Vestfirdir ankaramites is a characteristic of the NAIP as a whole (e.g. Graham et al., 1998; Hilton et al., 1999; Peate et al., 2003; Stuart et al., 2003; Macpherson et al., 2005; Tachibana et al., 2006; Breddam et al., in prep.). In general, little systematic correlation is documented between He isotopes and whole rock lithophile isotope signatures e.g. Graham (2002). Nevertheless, Stuart et al. (2003) and Ellam & Stuart (2004) found good correlation between He and Sr-Nd isotope ratios and trace element ratios (e.g. La/Sm) in lavas from various locations within the North Atlantic Igneous Province (NAIP, Figure 1.1), the so-called proto-Icelandic plume trend (PIP, Figure 3.8a-b). It has further been proposed that the PIP trend has implication for the global continental flood basalt (CFB) and OIB data. The preferred model by Ellam & Stuart (2004) suggests the PIP correlation in He-Nd-Sr space results from mixing between a hybrid *He-recharged* DM (HRDM) and an EM average endmember (Figure 3.8a-b). The model proposes that the HRDM endmember represents a global DM endmember, which has gained a high $^{3}He/^{4}He$ by incorporating a limited amount of He-rich primordial mantle (in general <10% PM), before it mixes with the low $^{3}He/^{4}He$ EM component. It is striking that hardly any lavas with unradiogenic He and more PM like Sr-Nd signatures exist, which would have suggested more variable contributions from a primordial

mantle reservoir to the global OIB family (Figure 3.8a-b). Their model implies that the HRDM is a uniform high $^{3}He/^{4}He$ endmember resulting of a fixed mixing relationship between DM and primordial mantle components (Ellam & Stuart 2004). The size of contribution of primordial mantle required to generate the HRDM component is sensitive to the chosen Sr/Nd value of the two endmembers. If the HRDM component is modelled using the Sr/Nd ratios respective of the DM and PM of Sun & McDonough (1989), a larger proportion of primordial mantle is required than proposed by Ellam & Stuart (2004). This has a further implication for the size of volume of primordial, high $^{3}He/^{4}He$ material within the Earths mantle. Crucial to this HRDM model is also that the DM component gains low U+Th/He without introduction of changes to its overall element and isotope chemistry, hence a mechanism that fractionates He from U+Th and other lithophile tracers is required (Stuart et al., 2003). This is possible with the *'standard model'* that presumes that He behaves more incompatibly than U and Th during mantle melting events e.g. Kurz (1993). However, this assumption conflicts with the newest study by Parman et al. (2005), which suggest the opposite.

Figure 3.8: He-Sr (a, c, and e) and He-Nd (b, d, and f) isotope relationships in the Vestfirdir ankaramites. Also included are the BIP field (Stuart et al., 2003), and various OIB fields reproduced after Graham et al. (1998). Reproduced in a) and b) are the binary mixing model, by which Ellam & Stuart (2004) explain the correlations between He and Sr-Nd isotopes observed among lavas of the NAIP, the so called Proto-Iceland Plume (PIP) trends. The high $^{3}He/^{4}He$ depleted component of the PIP-trends termed HRDM (He recharged depleted mantle) is suggested to be a hybrid component resulting from a uniform mixing relationship between the low $^{3}He/^{4}He$ DM and the high $^{3}He/^{4}He$ primordial mantle (PRIM). The other endmember of the PIP-trends is speculated to be a low $^{3}He/^{4}He$ enriched mantle average (EMA). Using the data presented in this study a new model is proposed, which provides an alternative explanation to the observed correlation between He and Sr-Nd isotope ratios for the Vestfirdir ankaramites and the Baffin Island picrites. This model may be applicable to Global OIB data. In this model a $DM_{high3He/4He}$ endmember is used, that has gained its high $^{3}He/^{4}He$ through mantle melting, as He is more compatible than U+Th during mantle melting (see details in Parman et al., 2005). The low $^{3}He/^{4}He$ enriched mantle endmember represents subducted, recycled oceanic lithosphere (REM). EM component is not uniform worldwide, as diverse material has been subducted through time. Therefore, its $^{87}Sr/^{86}Sr$ and $^{143}Nd/^{144}Nd$ composition varies from province to province (e.g. REM_a to REM_b) reflecting variable age and chemistry of the subducting *'package'*. Two different pyroxenites are used as proxies of the recycled oceanic lithosphere respectively REM_a (GP101) and REM_b (GP33) both from Pearson et al. (1993). Plots in c) and d) show that the binary mixing between REM_a and $DM_{high3He/4He}$, while e) and f) mixing between REM_b and $DM_{high3He/4He}$. The compositions of the respective endmembers and the data information used to generate the range of mixing lines are presented in Appendix C5. Full lines are mixing trends between the respective endmembers as labelled in colour. Round circles labelling the mixing trends (A through F) represent each different K-values given by either $k=([He]_x/[Nd]_x)/([He]_y/[Nd]_y)$ or $k=([He]_x/[Sr]_x)/([He]_y/[Sr]_y)$, these values are accounted for in detail in Appendix C5. Broken lines connect points of equal proportions of X and Y on the different mixing trends shown for each 10% increment. This modelling shows that the Vestfirdir ankaramites can be reproduced by mixing between the high $^{3}He/^{4}He$ DM and a low $^{3}He/^{4}He$ REM component. The REM required at Vestfirdir may not be as extreme as the one required by the OIB of Samoa or Heard.

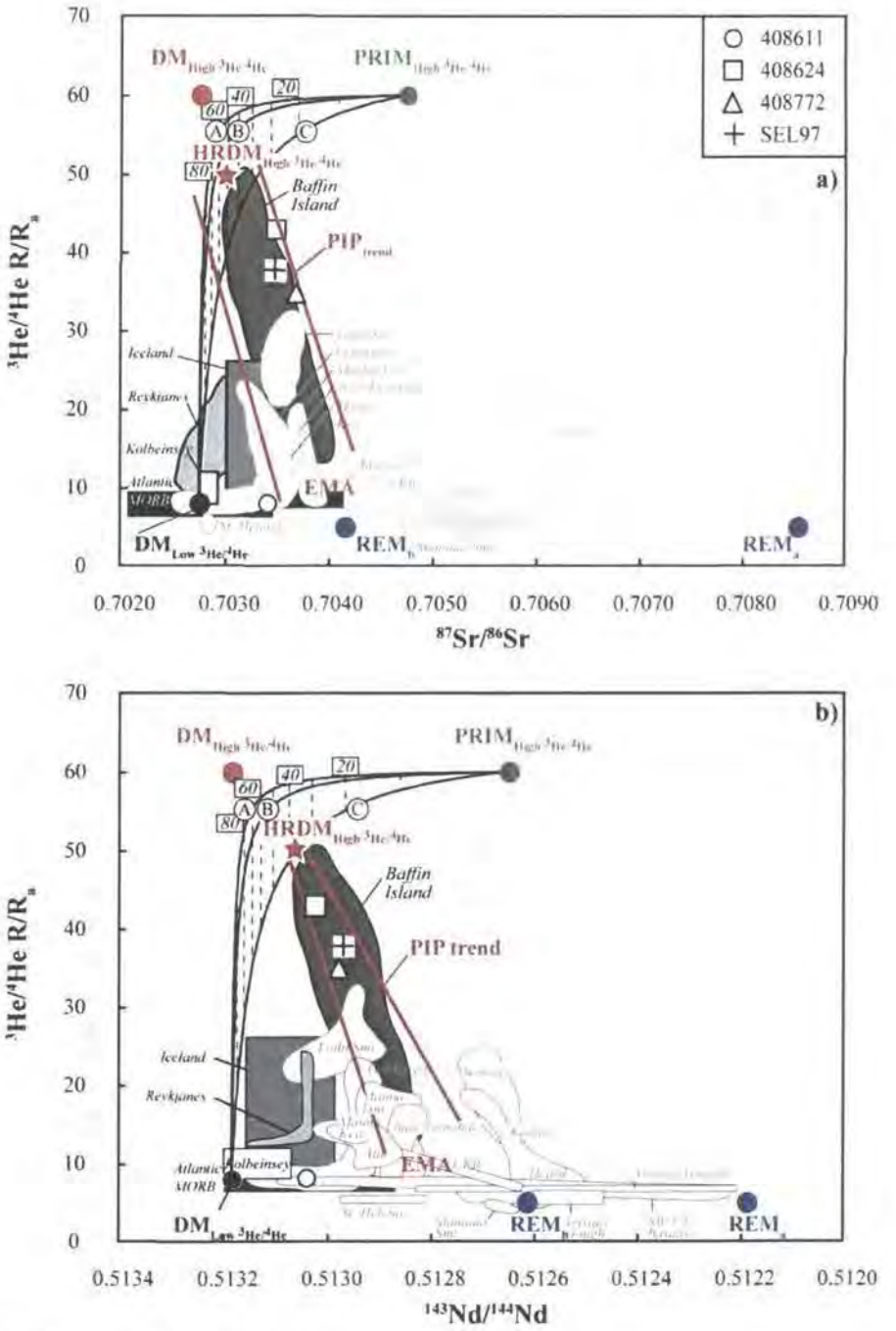

Figure 3.8: See figure caption on previous page.

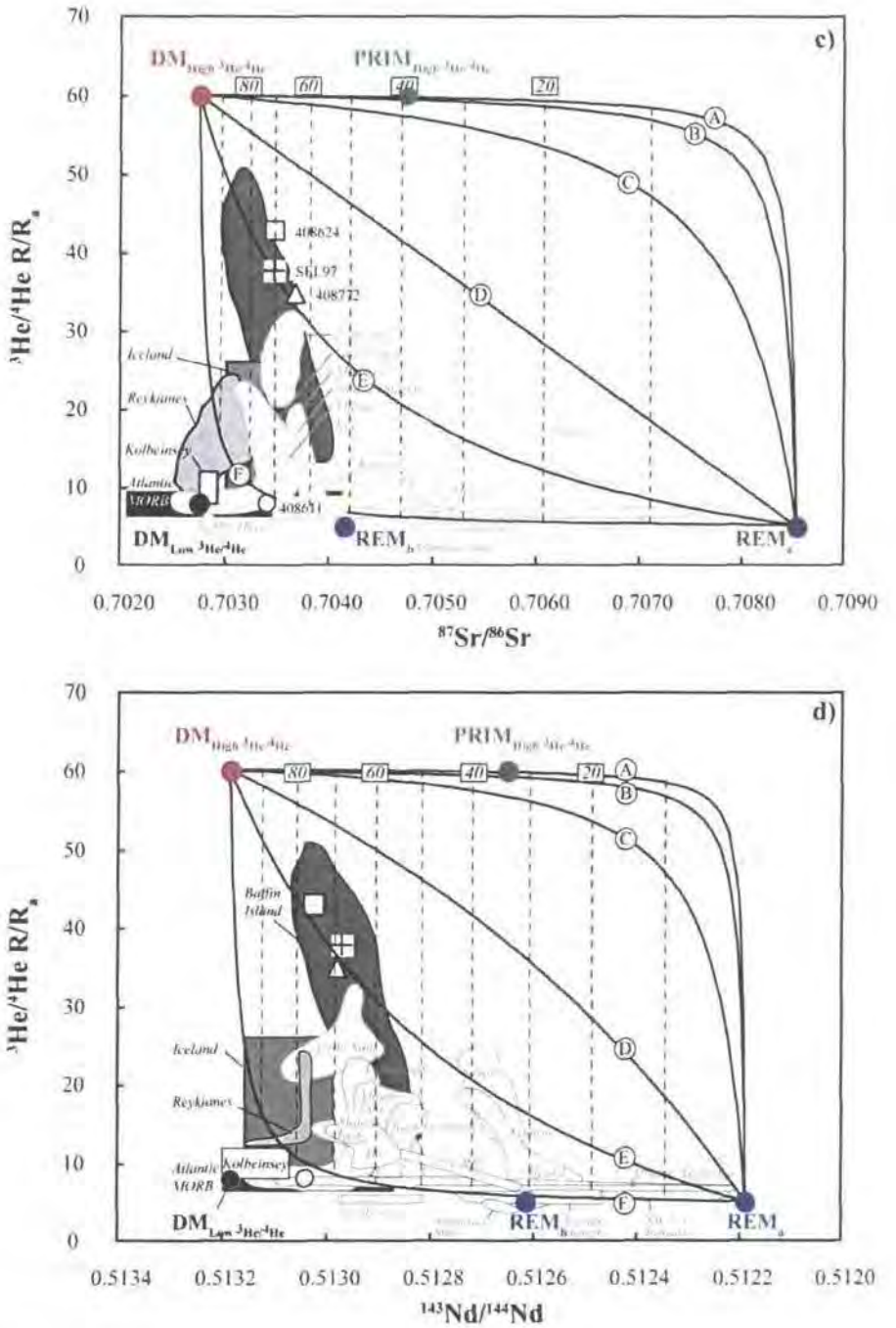

Figure 3.8: Continued

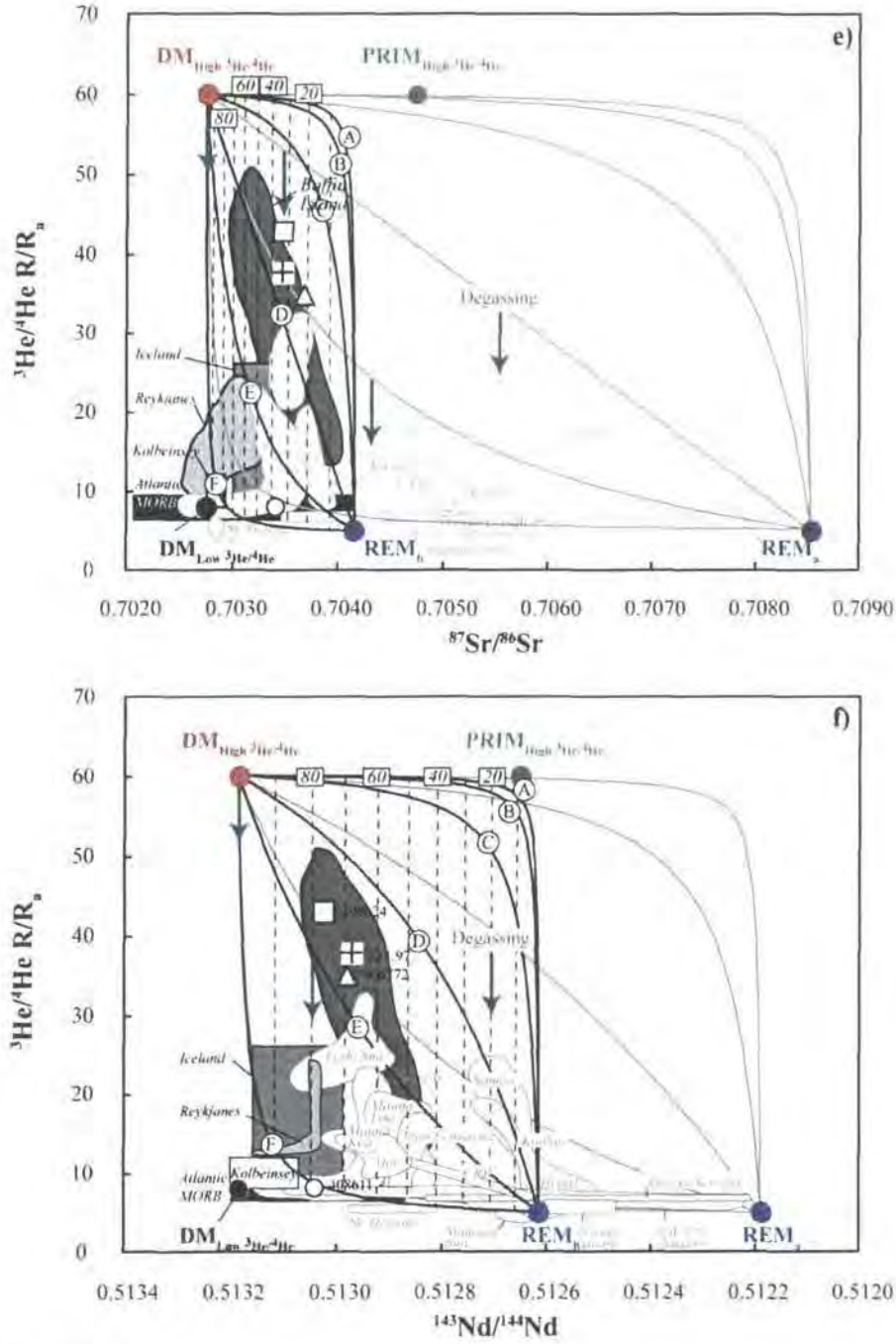

Figure 3.8: Continued

Here we propose an alternative model, which shows that the relationship between He and Sr-Nd isotope composition can be modelled by two-component binary mixing between a high $^{3}He/^{4}He$ DM component and the low $^{3}He/^{4}He$ enriched, recycled mantle component (Figure 3.8c-f). The DM component is suggested to have obtained its high $^{3}He/^{4}He$ and it depleted Sr-Nd-Hf-Os signature through previous melt extraction events in accordance with the scenario proposed by Parman et al. (2005). The composition of the recycled endmember most likely varies in composition from one province to the other, as diverse crustal material has been subducted through time. Therefore, we suggest that the enriched low $^{3}He/^{4}He$ mantle endmember globally has variable compositions depending on both its respective pre-recycled composition, and its age (Figure 3.8c-f). The high $^{3}He/^{4}He$ lavas of the NAIP may require an input of less extreme low $^{3}He/^{4}He$ mantle component (Figure 3.8e-f), whereas the more enriched OIB (Heard and Samoa) require large inputs (>60%) of a more extreme enriched mantle component (Figure 3.8c-d). Our model provides a more straightforward origin for a high $^{3}He/^{4}He$, DM endmember component. It also provides a better account of the lower gas contents of OIB compared with MORB (the *'helium paradox'* of Anderson (1998); e.g. Farley & Neroda, 1998; Ozima, 1994), as it provides depleted reservoirs with high $^{3}He/^{4}He$ ratios combined with low He concentrations (Parman et al., 2005). Hence, the high $^{3}He/^{4}He$ signature of the Vestfirdir ankaramites may be explained by significant contribution from this ^{3}He-rich DM component, and the trend towards more radiogenic He compositions suggests increasing involvement of a radiogenic He-Sr REM component. Larger contribution of REM material is required by the radiogenic Sr isotope ratios and higher Rb/Sr sampled by the MIs of *Trend II*, whereas the MIs of *Trend I* are dominated by the high $^{3}He/^{4}He$ DM (cf. section 3.6.2, Figure 3.3d). Degassing, or mixing between unradiogenic and radiogenic He DM components may equally explain the lower $^{3}He/^{4}He$ ratios of 408611. However, the existence of radiogenic MIs of *Trend II* among the MIs of 408611 witnesses that this lava also samples the REM melts. Samples displaced horizontally from the trend towards higher $^{87}Sr/^{86}Sr$ and lower $^{143}Nd/^{144}Nd$ are merely the result of larger contributions from degassed EM reservoirs or crustal contamination; an example of this is CS/7 from Baffin Island (Stuart et al., 2003). Hence, deviation from the overall correlation in He vs. lithophile isotope and trace element ratios may easily be disrupted by degassing, mixing, and contamination processes. This may also provide an explanation to the often observed decoupling between $^{3}He/^{4}He$ and lithophile isotope and trace element ratios in whole rock studies.

The strong linkage of an extreme high $^{3}He/^{4}He$ signature to a DM component as observed for the Baffin Island picrites (Stuart et al., 2003, Ellam & Stuart, 2004, Harlou et al., 2006; *Chapter 4*) and now also for the Vestfirdir ankaramites, may suggest that this high $^{3}He/^{4}He$ DM component has been sampled by the Icelandic mantle plume throughout the history of NAIP, and it may be a widespread phenomenon within this region - if not globally. Our model

presented in Figure 3.8, applies to many of the high $^{3}He/^{4}He$ OIB provinces. Still, this scenario does not obviate the existence of undegassed primordial mantle, and that some high $^{3}He/^{4}He$ lavas may inherit their unradiogenic He signature via contributions from such mantle reservoirs.

3.7 Conclusions

- Olivine-hosted MIs from the Vestfirdir ankaramites reveal a substantial Sr isotope range, which is beyond that documented by the host lava suite (0.70315-0.70768 versus 0.70344-0.70368). In fact these MIs carry the most radiogenic $^{87}Sr/^{86}Sr$ ratios ever registered on Iceland. In comparison with global OIB the MIs cover 77% of the total Sr isotope range, while the host lavas cover only 5%.

- Little evidence was found in support of hydrothermal alteration or assimilation of hydrothermally altered older Icelandic crust. Therefore, it is unlikely that such processes generated the Sr isotope variability among these MIs, or had an effect on the Sr-Nd isotope systematics of the whole rock compositions. Neither is the age difference between the underlying lava sequence and the Vestfirdir ankaramites enough for the older lavas to generate high $^{87}Sr/^{86}Sr$ (~0.70768) by radioactive decay of ^{87}Rb to ^{87}Sr. Hence, the radiogenic Sr signature is source related, and must be linked, to component(s) residing in the mantle region sampled by the Icelandic mantle plume.

- The model presented requires that two components take part in the genesis of the Vestfirdir ankaramites; a depleted mantle (DM) with an unradiogenic He-Sr signature, and a recycled oceanic lithospheric mantle component with a radiogenic He-Sr signature possibly holding both a pyroxenitic and a sediment component (REM). The MIs of *Trend I* are dominantly derived from the unradiogenic He-Sr DM, while MIs of *Trend II* require up to a 15% input from the radiogenic He-Sr REM component. The more subtle variation of the host ankaramites suggests that the overall input from the radiogenic He-Sr REM component is <3%. This model also, provides a relatively straightforward explanation for the high $^{3}He/^{4}He$, DM endmember of many of the global high $^{3}He/^{4}He$ lavas. It implicates a high $^{3}He/^{4}He$ DM reservoir with a low He concentration, which also provides an explanation of the lower gas contents of many OIB relative to MORB.

- The link of the extreme high $^{3}He/^{4}He$ to a DM component contrasts with previous assumptions of unradiogenic He implying a contribution from primordial mantle component, but is in accordance with the experimental results by Parman et al. (2005). The linkage between a DM source and the unradiogenic He signature is documented at Baffin Island picrites (Stuart et al., 2003; Harlou et al., 2006; *Chapter 4*), in Central

Icelandic lavas (Macpherson et al., 2005), and now also in this study for the Vestfirdir ankaramites. Hence, a unradiogenic He DM component may be a widespread phenomenon in the NAIP.

- This study also shows that Sr isotope and trace element measurements of single MIs provide a higher resolution picture of the pre-aggregated melt compositions and the source components involved in the genesis of the Vestfirdir ankaramites, which otherwise are obscured within the whole rock data. It is further suggests that He isotope data collected on olivine separates should be related to isotope data collected on MIs hosted by olivine and ***not*** whole rock data.

3.8 References

Anderson, D. L. (1998): The helium paradox. Proceedings of the National Academy of Sciences, 95: 4822-4827.

Breddam, K., Stecher, O., Harlou, R., Peate, D. W., & Kurz, M. D. (in prep.): Miocene high-$^{3}He/^{4}He$ ankaramites in NW-Iceland: Trace element constraints on the common component in mantle plumes.

Charlier, B. L. A., Ginibre, C., Morgan, D., Nowell, G. M., Pearson, G. D., Ottley, C. J., & Davidson, J. P. (2006): Methods for the microsampling and analysis of strontium isotopes at the crystal scale for petrological and geochronological studies of igneous rocks. Chemical Geology: 114-133.

Chauvel, C. & Hémond, C. (2000): Melting of a complete section of recycled oceanic crust: Trace element and Pb isotopic evidence from Iceland. Geochemistry Geophysics Geosystems, 1: 10.1029/1999GC000002.

Condomines, M., Grönvold, K., Hooker, P. J., Muehlenbachs, K., O'Nions, R. K., Óskarsson, N., & Oxburgh, E. R. (1983): Helium, oxygen, strontium and neodymium isotopic relationships in Icelandic volcanics. Earth and Planetary Science Letters, 66: 125-136.

Danyushevsky, L. V., Della-Pasqua, F. N., & Sokolov, S. (2000): Re-equilibration of melt inclusions traped by manesian olivine phenocrysts from subduction-related magmas: petrological implications. Contributions to Mineralogy and Petrology, 138: 68-83.

Danyushevsky, L. V., McNeill, A. W., & Sobolev, A. V. (2002): Experimental and petrological studies of melt inclusions in phenocrysts from mantle-derived magmas: an overview of techniques, advantages and complications. Chemical Geology, 183: 5-24.

Darbyshire, F. A., Bjarnason, I. T., White, R. S., & Flóvenz, Ó. G. (1998): Crustal structure above the Iceland mantle plume imaged by ICEMELT refraction profile. Geophysical Journal International, 135(3): 1131-1149.

Darbyshire, F. A., White, R. S., & Priestley, K. F. (2000): Structure of the crust and uppermost mantle of Icelenad from a combined seismic and gravity study. Earth and Planetary Science Letters, 181: 409-428.

Drever, J.I. (1997): The Geochemistry of Natural Waters: Surface and Groundwater Environments (3rd Edition). 436pp.

Eiler, J.M., Grönvold, K., & Kitchen, N. (2000a): Oxygen isotope evidence for the origin of chemical variations in lavas from Theistareykir volcano in Iceland's northern volcanic zone. Earth and Planetary Science Letters, 184: 269-286.

Eiler, J. M., Schiano, P., Kitchen, N., & Stolper, E. M. (2000b): Oxygen-isotope evidence for recycled crust in the sources of mid-ocean-ridge basalts. Nature, 403: 530-534.

Elderfield, H. & Schultz, A. (1996): Mid-ocean ridge hyderothermal fluxes and the chemical composition of the ocean. Annual Review of Earth and Planetary Sciences, 24: 191-224.

Ellam, R. M. & Stuart, F. M. (2004): Coherent He-Nd-Sr isotope trends in high $^{3}He/^{4}He$ basalts: implications for a common reservoir, mantle heterogeneity and convection. Earth and Planetary Science Letters, 228: 511-523.

Farley, K. A. & Neroda, E. (1998): Noble gases in the Earth's Mantle. Annual Review of Earth and Planetary Sciences, 26: 189-218.

Fitton, J. G., Saunders, A. D., Kepton, P. D., & Hardarson, B. S. (2003): Does depleted mantle form an intrinsic part of the Iceland plume? Geochemistry Geophysics Geosystems, 4(3): 1-14.

Fitton, J. G., Saunders, A. D., Norry, M. J., Hardarson, B. S., & Taylor, R. N. (1997): Thermal and chemical structure of the Iceland plum. Earth and Planetary Science Letters, 153: 197-208.

Foulger, G. R. (2006): Older crust underlies Iceland. Geophysical Journal International, 165: 672-676.

Foulger, G. R. & Anderson, D. L. (2005): A cool model for the Iceland hotspot. Journal of Volcanology and Geothermal Research, 141: 1-22.

Foulger, G. R., Natland, J. H. & Anderson, D. L. (2005): A source for Icelandic magmas in remalted Iapetus crust. Journal of Volcanology and Geothermal Research, 141: 23-44.

Gautason, B. & Muehlenbachs, K. (1998): Oxygen isotopic fluexes associated with high-temperature processes in the rift zones of Iceland. Chemical Geology, 145: 275-286.

Graham, D. W. (2002): Nobel gas isotope geochemistry of mid-ocean island basalts: Characterization of mantle source reservoirs. Reviews of Mineralogy & Geochemistry, 47.

Graham, D. W., Larsen, L. M., Hanan, B. B., Storey, M., Pedersen, A. K., & Lupton, J. E. (1998): Helium isotope composition of the early Iceland mantle plume inferred from the Tertiary picrites of West Greenland. Earth and Planetary Science Letters, 160: 241-255.

Gurenko, A. A. & Chaussidon, M. (1995): Enriched and depleted primitive melts included in olivine from Icelandic tholeiites: origin by continuous melting of a single mantle column. Geochimica et Cosmochimica Acta, 59(14): 2905-2917.

Gurenko, A. A. & Chaussidon, M. (2002): Oxygen isotope variations in primitive tholeiites of Iceland: evidence from a SIMS study of glass inclusions, olivine phenocrysts and pillow rim glasses. Earth and Planetary Science Letters, 205: 63-79.

Hanan, B. B., Blichert-Toft, J., Kingsley, R., & Schilling, J. -G. (2000): Depleted Iceland mantle plume geochemical signature: Artifact of multicomponent mixing? Geochemistry Geophysics Geosystems, 1.

Hanan, B. B. & Graham, D. W. (1996): Lead and helium isotope evidence from oceanic basalts for a common deep source of mantle plumes. Science, 272: 991-995.

Hardarson, B. S., Fittion, J. G., Ellam, R. M., & Pringle, M. S. (1997): Rift relocation - a geochemical and geochronological investigation of a palaeo-rift in northwest Iceland. Earth and Planetary Science Letters, 153: 181-196.

Harlou, R., Kent, A. J. R., Breddam, K., Davidson, J. P., & Pearson, D. G. (2003): Origin of extreme $^{3}He/^{4}He$ signatures in Icelandic lavas: Insights from Inclusion studies, Eos Trans. AGU, 84(46), Fall Meet. Suppl., Abstract V32A-1006.

Harlou, R., Kent, A.J.R., Breddam, K., Davidson, J. P., & Pearson, G. (2004): Origin of extreme $^{3}He/^{4}He$ signatures in Icelandic lavas: Insights from melt inclusion studies. Geochimica et Cosmochimica Acta, Supplement 1, 68(11): A579.

Harlou, R., Pearson, D. G., Nowell, G. M., Davidson, J. P., & Kent, A.J.R. (2005): Sr isotope studies of melt inclusions by TIMS. Geochimica et Cosmochimica Acta, Supplement 1, 69(10): A380.

Hart, S. R., Hauri, E. H., Oschmann, L. H., & Whitehead, J. A. (1992): Mantle plumes and entrainment: Isotopic evidence. Science, 256: 517-520.

Hauri, E. H. (2002a): SIMS analysis of volatiles in silicate glasses, 2: isotopes and abundances in Hawaiian melt inclusions. Chemical Geology, 2002: 115-141.

Hauri, E. H. (2002b): Osmium isotopes and mantle convection. Philosophical transactions of the Royal Society, Mathematical, Physical and Engineering Sciences, 360(150): 2371-2382.

Hauri, E. H., Whitehead, J. A., & Hart, S. R. (1994): Fluid dynamic and geochemical aspects of entrainment in mantle plumes. Journal of Geophysical Research, 99(B12): 24275-24300.

Hilton, D. R., Gronvold, K., Macpherson, C. G., & Castillo, P. R. (1999): Extreme $^{3}He/^{4}He$ ratios in northwest Iceland: constraining the common component in mantle plumes. Earth and Planetary Science Letters, 173: 53-60.

Hofmann, A.W. (1997): Mantle geochemistry: the message from oceanic volcanism. Nature, 385: 219-229.

Jackson, M. G. & Hart, S. R. (2006): Strontium isotopes in melt inclusions from Samoa basalts: Implications fro heterogeneity in the Samoan Plume. Earth and Planetary Science Letters, 245: 260-277.

Kent, A .J. R., Baker, J. A., & Wiedenbeck, M. (2002): Contamination and melt aggregation proceses in continental flood basalts: constraints from melt inclusions in Oligocene basalts from Yemen. Earth and Planetary Science Letters, 202: 577-594.

Kobayashi, K., Tanaka, R., Moriguti, T., Shimizy, K., & Nakamura, E. (2004): Lithium, boron, and lead isotope systematics of glass inclusions in olivines from Hawaiian lavas: evidence for recycled components in the Hawaiian plume. Chemical Geology, 212: 143-161.

Kokfelt, T. F., Hoernle, K., Hauff, F., Fiebig, J., Werner, R., & Garbe-Schönberg, D. (2006): Combined trace element and Pb-Nd-Sr-O isotope evidence for recycled oceanic crust (upper and lower) in the Iceland mantle plume. Journal of Petrology, 47(9): 1705-1749.

Kurz, M. D. (1993): mantle heterogeneity beneath oceanic islands - some inferences from istoopes. Philosophical transactions of the Royal Society London, A342: 91-103.

Lightfoot, P. C., Hawkesworth, C. J., Olshefsky, K., Green, T., Doherty, W., & Keays, R. R. (1997): Geochemistry of Tertiary tholeiites and picrites from Qeqertarssuaq (Disko

Island) and nuussuaq, West Greenland with implications for the mineral potential of comagmatic intrusions. Contribution to Mineral and Petrology, 128: 139-163.

Maclennan, J., McKenzie, D. M., Gronvöld, K., & Slater, L. (2001): Crustal accretion under northern Iceland. Earth and Planetary Science Letters, 191: 295-310.

Macpherson, C. G., Hilton, D. R., Day, J. M. D., Lowry, D., & Grönvold, K. (2005): High-$^{3}He/^{4}He$, depleted mantle and low $\delta^{18}O$, recycled oceanic lithosphere in the source of central Iceland magmatism. Earth and Planetary Science Letters, 233: 411-427.

Mattey, D., Lowry, D., & Macpherson, C. (1994): Oxygen isotope composition of mantle peridotite. Earth and Planetary Science Letters, 128: 231-241.

McDonough, W. F. & Sun, S. -s. (1995): The composition of the Earth. Chemical Geology, 120: 223-253.

Meibom, A., Anderson, D. L., Sleep, N. H., Frei, R., Chamberlain, C. P., Hren, M. T., & Wooden, J. L. (2003): Are high $^{3}He/^{4}He$ ratios in oceanic basalts an indicator of deep-plume components? Earth and Planetary Science Letters, 208: 197-204.

Nielsen, R. L., Michael, P. J., & Sours-Page, R. (1998): Chemical and physical indicators of compromised melt inclusions. Geochimica et Cosmochimica Acta, 62(5): 831-839.

Norman, M. D., Garcia, M. O., Kamenetsky, V. S., & Nielsen, R. L. (2002): Olivine-hosted melt inclusions in Hawaiian picrites: equilibration melting, and plume source characteristics. Chemical Geology, 183: 143-168.

Nowell, G. M., Kempton, P. D., Noble, S. R., Fitton, J. G., Saunders, A. D., Mahoney, J. J., & Taylor, R. N. (1998): High precision Hf isotope measurements of MORB and OIB by thermal ionisation mass spectrometry: insights into the depleted mantle. Chemical Geology, 149: 211-233.

Ozima, M. (1994): Noble gas state in the mantle. Reviews of Geophysics, 32(4): 405-426.

Paquette, J., Sigmarsson, O., & Tiepolo, M. (2006): Continental basement under Iceland revealed by old zircons. EOS, Transactions, American Geophysical Union, 87(52): V33A-0642.

Parman, S. (2006): The helium isotope evolution of the earth. Geochimica et Cosmochimica Acta, 70(18): 472.

Parman, S. W., Kurz, M. D., Hart, S. R., & Grove, T. L. (2005): Helium solubility in olvine and implications for high $^{3}He/^{4}He$ in ocean island basalts. Nature, 437: 1140-1143.

Pearson, D. G., Davies, G. R. & Nixon, P. H. (1993): Geochemical constraints on the petrogenesis of diamond facies pyroxenites from the Beni Bousera Peridotite Massif, North Morocco. Journal of Petrology, 34(1): 125-172.

Pearson, D. G. & Woodland, S. J. (2000): Solvent extraction/anion exchange separation and determination of PGEs (Os, Ir, Pt, Pd, Ru) and Re-Os isotopes in geological samples by isotope dilution ICP-MS. Chemical Geology, 165: 87-107.

Peate, D. W., Baker, J. A., Blichert-Toft, J., Hilton, D. R., Storey, M., Kent, A. J. R., Brooks, C. K., Hansen, H., Pedersen, A. K., & Duncan, R. A. (2003): The Prinsen af Wales Bjerge Formation lavas, East Greenland. The transition from tholeiitic to alkalic magmatism during Palaeogene continental break-up. Journal of Petrology, 44: 279-304.

Plank, T. & Langmuir, C. H. (1998): The chemical composition of subducting sediment and its consequences for the crust and mantle. Chemical Geology, 145: 325-394.

Prestvik, T., Goldberg, S., Karlsson, H., & Grönvold, K. (2001): Anomalous strontium and lead isotope signatures in the off-rift Öræfjökull central volcano in south-east Iceland evidence for enriched endmembers(s) of the Iceland mantle plume? Earth and Planetary Science Letters, 190: 211-220.

Prestvik, T., Torske, T., Sundvoll, B., & Karlsson, H. (1999): Petrology of early Tertiary nephelinites of mid-Norway. Additional evidence for an enriched endmember of the ancestral Icelandic plume. Lithos, 46: 317-330.

Roedder, E. (1984): Fluid inclusions. Mineralogical Society of America, Washington, DC: 644pp.

Saal, A. E., Hart, S. R., Shimizu, N., Hauri, E. H., & Layne, G. D. (1998): Pb isotopic variability in melt inclusions from oceanic island basalts, Polynesia. Science, 282: 1481-1484.

Saal, A. E., Hart, S. R., Shimizu, N., Hauri, E. H., Layne, G. D., & Eiler, J. M. (2005): Pb isotopic variability in melt inclusions from the EMI-EMII-HIMU mantle end-members and the role of the oceanic lithosphere. Earth and Planetary Science Letters, 240: 605-620.

Saal, A. E., Hauri, E. H., Langmuir, C. H., & Perfit, M. R. (2002): Vapour undersaturation in primitive mid-ocean-ridge basalt and the volatile content of Earth's upper mantle. Nature, 419: 451-455.

Schaefer, B. F., Parkinson, I. J., & Hawkesworth, C. J. (2000): Deep mantle plume osmium isotope signature from West Greenland Tertiary picrites. Earth and Planetary Science Letters, 175: 105-118.

Shimizu, N. (1998):. The geochemistry of olivine-hosted melt inclusions in a FAMOUS basalt ALV519-4-1. Physics of the Earth and Planetary Interiors, 107: 183-201.

Skovgaard, A. C., Storey, M., Baker, J., Blusztajn, J. and Hart, S. R. (2001): Osmium-oxygen isotopic evidence for a recycled and strongly depleted component in the iceland mantle plume. Earth and Planetary Science Letters, 194: 259-275.

Slater, L., McKenzie, D., Gronvold, K., & Shimizu, N. (2001): Melt generation and movement beneath Theistareykir, NE Iceland. Journal of Petrology, 42: 321-354.

Staples, R. K., White, R. S., Brandsdóttir, B., Menke, W., Maguire, P. K. H., & McBride, J. H. (1997): Färoe-Iceland Ridge Experiment 1. Crustal structure of northeastern Iceland. Journal of Geophysical Research, 102(B4): 7849-7866.

Staudigel, H., Davies, G. R., Hart, S. R., Marchant. K. M., & Smidt, B. M. (1995): Large scale isotopic Sr, Nd and O isotopic anatomy of altered oceanic crust: DSDP/ODP sites 417/418. Earth and Planetary Science Letters, 130: 169-185.

Stille, P., Steinmann, M., & Riggs, S. R. (1996): Nd isotope evidence for the evolution of the paleocurrents in the Atlantic and Tethys Oceans during the past 180 Ma. Earth and Planetary Science Letters, 144(1): 9-19.

Stracke, A., Willbold, M., & Hemond, C. (2004): The origin of EM1 signatures in basalts from Tristan da Cunha and Gough. EOS, Transactions, American Geophysical Union, Fall. Meet. suppl. Abstract, 85(47).

Stuart, F. M., Lass-Evans, S., Fitton, J. G., & Ellam, R.M. (2003): High $^{3}He/^{4}He$ ratios in picritic basalts from Baffin Island and the role of a mixed reservoir in mantle plumes. Nature, 424(3): 57-59.

Sun, S. -s. & McDonough, W. F. (1989): Chemical and isotopic systematics of oceanic basalts: implications for mantle composition and processes. Geological Society Special Publication, No. 42: 313-345.

Tachibana, Y., Kaneoka, I., Gaffney, A., & Upton, B. (2006): Ocean-island basalt-like source of kimberlite magmas from West Greeland revealed by high $^{3}He/^{4}He$ ratios. Geology, 34(4): 273-276.

Thirlwall, M. F. (1995): Generation of the Pb isotopic characteristics of the Iceland plume. Jounal of Geological Society, 152(6): 991-996.

Thirlwall, M. F. Gee, M. A. M., Lowry, D., Mattey, D. P., Murton, B. J., & Taylor, R. N. (2006): Low $\delta^{18}O$ in the Icelandic mantle and its orgins: Evidence from Reykjanes Ridge and Icelandic lavas. Geochimica et Cosmochimica Acta, 70: 993-1019.

Thirlwall, M. F., Gee, M. A. M., Taylor, R. N., & Murton, B. J. (2004): Mantle components in Iceland and adjacent ridges investigated using double-spike Pb isotope ratios. Gechimica er Cosmochimica Acta, 68(2): 361-386.

Weaver, B.L. (1991): The origin of ocean island basalt end-member compositions: trace element and isotopic constraints. Earth and Planetary Science Letters, 104: 381-397.

Willbold, M. & Stracke, A. (2006): Trace element composition of mantle end-members: Implications for recycling of oceanic and upper and lower continental crust. Geochemistry Geophysics Geosystems, 7(4).

Workman, R. K., Hart, S. R., Jackson, M., Regelous, M., Farley, K. A., Blusztajn, J., Kurz, M., & Staudigel, H. (2004): Recycled metasomatized lithosphere as the origin of the enriched mantle II (EM2) end-members: Evidence for the Samoan volcanic Chain. Geochemistry Geophysics Geosystems, 5(4), Q04008, doi:10.1029/2003GC000623.

Yaxley, G. M., Kamenetsky, V. S., Kamenetsky, M., Norman, M. D., & Francis, D. (2004): Origins of compositional heterogeneity in olivine-hosted melt inclusions from the Baffin Island picrites. Contribution to Mineral and Petrology, 148: 426-442.

Yurimoto, H., Kogiso, T., Abe, K., Barsczus, H. C., Utsunomiya, A., & Maruyama, S. (2004): Lead isotopic compositions in olivine-hosted melt inclusions from HIMU basalts and possible link to sulfide components. Physics of the Earth and Planetary Interiors, 146: 231-242.

Zindler, A. & Hart, S. (1986): Chemical Geodynamics. Annual Review of Earth and Planetary Sciences, 14: 493-571.

CHAPTER 4

Source variability plus crustal contamination in the Baffin Island picrites - A coupled Sr isotope and trace element study of melt inclusions

4.1 Abstract

The Sr isotope compositions of individual olivine-hosted melt inclusions from 5 picritic lavas from Baffin Island reveal large Sr isotope variability ($^{87}Sr/^{86}Sr_i$: 0.70306-0.70906). This strongly contrasts with the narrow range shown by their host lavas ($^{87}Sr/^{86}Sr_i$: 0.70308-0.70366). The range in melt inclusion $^{87}Sr/^{86}Sr_i$ exceeds the Sr isotope diversity of North Atlantic MORB and is comparable to the global OIB range. Previous whole rock studies of the Baffin Island picrites suggest that the chemical variations observed within the lavas reflect mixing between melts derived from a variety of mantle reservoirs ranging from a high ^3He primordial endmember, through primitive enriched material to a depleted MORB source mantle, possibly represented by a single heterogeneous mantle source. However, the heterogeneous major and trace element composition of olivine-hosted melt inclusions from this location (Yaxley et al., 2004), combined with the newly-revealed Sr isotope variation within the melt inclusions indicates a significant role for crustal contamination in the genesis of the Baffin Island picrites. Despite this, trace element systematics appear to also require mantle source variation. The least radiogenic Sr isotope composition of the melt inclusions confirms a depleted isotope signature in primitive Baffin Island picritic melts that accompanies the highest $^3He/^4He$ ratios (~50 R/R_a) found so far in global magmatism.

4.2 Introduction

The voluminous picritic lava flows occurring in the Southeast of Baffin Island (Canada, Northwest Territories) are among the most primitive post-Achaean magmas erupted on Earth and so are thought to have escaped major melt modifying processes en route to the surface (Clarke, 1970; Francis, 1985; Robillard et al., 1992; Stuart et al., 2003; Kent et al., 2004). Recent whole rock geochemical studies reveal that the Baffin Island picrites (BIP) have the most extreme $^3He/^4He$ ratios (~50 R/R_a) so far recorded in samples from the Earth's mantle (Stuart et al., 2003). Furthermore, there is remarkable coherence between radiogenic isotopes

(Sr, Nd), La/Sm, and $^{3}He/^{4}He$ that infer varying contributions from mantle reservoirs ranging from a high ^{3}He primordial endmember, through '*primitive enriched*' material to depleted MORB source mantle (Stuart et al., 2003; Ellam & Stuart, 2004). Clearly, better constrains on the potential source contributions to these rocks is crucial in order to understand their petrogenesis and in a broader dimension, the origin of the high $^{3}He/^{4}He$ signatures. Early formed olivine-hosted melt inclusions (MIs) may sample relatively undiluted melt fractions from these components before substantial melt aggregation and full mixing occurred. Isotope studies, using Sr isotope and trace element measurements of single MIs (Harlou et al., 2005; Harlou et al. 2006, *Chapter 2 and 3*), may thus provide a higher resolution picture of these source contributions and should also track the potential contribution of crustal contamination to the geochemistry of these rocks. Crustal contamination is common in flood basalts erupted in continental areas and especially in the North Atlantic Igneous Province (e.g. Brooks & Nielsen, 1982; Thompson et al., 1984; Pedersen, 1985; Holm et al., 1993; Lightfoot et al., 1997; Kerr et al., 1999; Stuart et al., 2000). Removing the veil of crustal inputs is critical to deciphering source variations.

In this contribution we apply a newly-developed method to obtain precise Sr isotope ratios of individual MIs at sub-ng levels (Harlou et al., 2005; *Chapter 2*). We focus our attention on the compositional variability displayed by olivine-hosted MIs from a set of picrites from Padloping Island (SE Baffin Island). The primitive nature of the MgO-rich BIP occurring here suggests that these lavas represent probes of primary, high pressure (2.5-3 GPa) deep mantle derived melts (Clarke, 1970; Francis, 1985). Previous studies of lavas from this area have arrived at varying conclusions over the importance of crustal and mantle inputs to the magmas (Clarke, 1970; Francis, 1985; Robillard et al., 1992; Stuart et al., 2003; Ellam & Stuart, 2004; Kent et al., 2004; Yaxley et al., 2004).

Robillard et al. (1992) found the BIP sequence to be derived from a mix between two chemically distinct lava types with varying LREE/HREE fractionation; the slightly '*enriched*' or '*E-type*', typically characterized by $(La/Sm)_N$ of 1.1-1.2 and the '*normal*' or '*N-type*', characterized by having $(La/Sm)_N$ of 0.6-0.7 (Table 4.1). Similarly, Kent et al. (2004) suggested that the BIP represent mixtures of melts from two distinct sources existing in close proximity of each other - a depleted source (similar to the North Atlantic depleted upper mantle) and an enriched source that was not fully constrained, but suggested to be recycled altered oceanic lithosphere. Kent et al. (2004) found limited chemical evidence for the role of crustal contamination, and concluded that only minor contributions from crust and subcontinental lithospheric mantle (SCLM) were possibly involved in the generation of these melts. Stuart et al. (2003) and Ellam & Stuart (2004) both recognized an important role for both enriched and depleted mantle (EM and DM) in the source of BIP, but their DM component was required to be

'*He-recharged*' to account for the fact that the most depleted rocks in terms of lithophile radiogenic isotope systematics have the highest $^{3}He/^{4}He$ values. Only a single high $^{3}He/^{4}He$ lava (CS/7) was found to be affected by crustal contamination, otherwise both papers conclude that the role of crustal contamination in the BIP was minor. Sample CS/7 was thought to retain its high $^{3}He/^{4}He$ signature because the contamination process took place after the crystallization of olivine (Ellam & Stuart, 2004). In contrast, a major and trace element study of olivine-hosted MIs by Yaxley et al. (2004) concluded that the heterogeneous nature of the BIP MIs reflect crustal contamination of these melts by granitic liquids, melting of gabbroic cumulates, and the generation of quartz undersaturated K-rich liquids in the crust. These different studies, focusing on varying approaches, illustrate the complexity of chemical signatures in the BIP and highlight the need for a more detailed study that can accurately constrain the role of crust in generating the geochemical signatures shown by the host rocks. This is important if we are to properly correlate mantle source signatures shown by lithophile elements with the information being supplied by He isotope studies.

Lava type	N-type	E-type
Trace element characteristics		
$(La/Sm)_N$	<0.7	>1.1
K_2O/TiO_2	<0.05	>0.05
REE pattern	Slightly depleted	Mildly enriched
Isotope characteristics		
$\delta^{18}O$	5.15-5.22‰	4.84-5.16‰
$^{3}He/^{4}He$ R/R_a	50	<8
$^{87}Sr/^{86}Sr_i$	<0.7032	0.7032-0.7039
$^{143}Nd/^{144}Nd_i$	>0.51299	<0.51296
$^{187}Os/^{188}Os_i$	0.1220-0.1247	0.1261-0.1303

Table 4.1: Summary of chemical characteristics of the *N-type* and *E-type* melts found within the Baffin Island picrites (BIP). The information is compiled from Francis (1985), Robillard et al. (1992), Stuart et al. (2003), Kent et al. (2004), Yaxley et al. (2004), and this study. Slightly depleted and mildly enriched REE patterns are relative to the primitive mantle (PM). Subscribed i refers to initial, meaning the eruption age of the BIP, which is 61 Ma. R/R_a indicates that the $^{3}He/^{4}He$ ratio of the rock (R) is normalized to the atmospheric $^{3}He/^{4}He$ ratios (R_a) of $1.39x10^{-6}$.

4.3 Geological setting

The volcanic rocks of Baffin Island comprise the western-most expression of a magmatic province that includes basaltic and picritic lavas from the West and East coasts of Greenland and as far East as the inner Hebrides of Britain (Figure 4.1). This province is known collectively as the North Atlantic Igneous Province (NAIP) e.g. White & McKenzie (1989), White & McKenzie (1995), Saunders et al., (1997). At Baffin Island the lavas erupted through Achaean

continental crust during the initial stages of volcanism within NAIP - approximately 60 Ma ago during the opening of the Davis Strait resulting from the separation of Greenland from Baffin Island (White & McKenzie, 1989). This volcanism is believed to be a manifestation of the arrival and early melting of the proto-Icelandic hotspot (White & McKenzie, 1995). Today, the lavas are found as costal outcrops between Cape Searle and Cape Dyer along the eastern coast of Baffin Island (Figure 4.1b), and the source area is thought to be located offshore northeast of the present line of outcrops (Clarke & Upton, 1971). The volcanic rocks rest directly on an eroded Achaean basement or conformably on middle Paleoproterozoic terrestrial sediments (Clarke & Upton, 1971). The lower parts of the lava succession erupted subaqueously and make up approximately 150 m of pillow breccias and pillow lavas (Clarke & Upton, 1971; Jackson, 1998). In contrast, the upper part of the sequence erupted subaerially, and consists of 300 m of thin lava flows with oxidized vesicular flow tops (Clarke & Upton, 1971; Robillard et al., 1992; Jackson, 1998). The BIP correlate with the earliest erupted lavas of the Anaanaa Member in West Greenland (Pedersen et al., 2002), but in contrast to the lavas on the western coast of Greenland, which comprises picrites through plagioclase basalt, the Baffin Island lavas are mostly picritic in composition (Clarke, 1970).

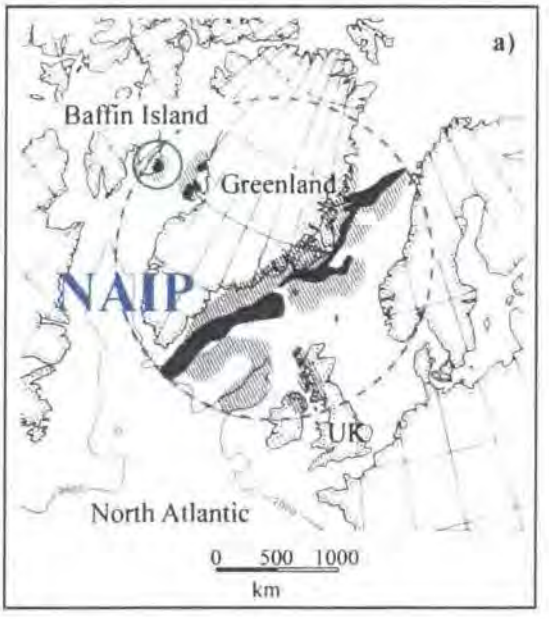

Figure 4.1: a) The extent of the North Atlantic Igneous Province (NAIP) is encircled by the blue broken line. Baffin Island makes up the western-most volcanic expression (blue circle). The map is a reconstruction back to magnetic anomaly 23 after White & McKenzie (1989). Extrusive volcanic activity is shown in black and the hatch areas show the earlier activity in the region. b) Detailed map of SE Baffin Island after Clarke & Upton (1971) showing the outcrops of picrites from Cape Searle to Cape Dyer. Samples of this study are from Padloping Island (blue box). Further details are available from the geology map of Okoa-Padloping Island area by Jackson (1998).

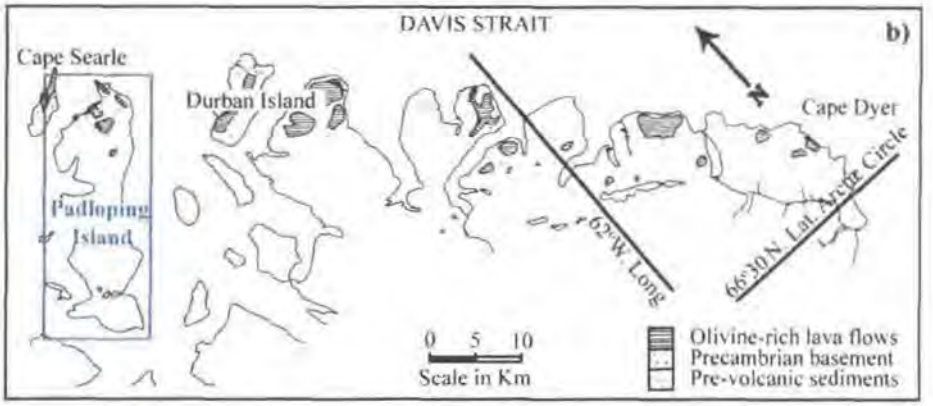

Figure 4.1: Continued

4.3.1 Petrology of the Baffin Island picrites

The BIP are strongly porphyric with 15-33 volume % mm-sized olivine phenocrysts (Francis, 1985; Robillard et al., 1992; Kent et al., 2004; Yaxley et al., 2004). The groundmass is microcrystalline or glassy and contains microlites of olivine, plagioclase, clinopyroxene, and opaque minerals (Francis, 1985; Robillard et al., 1992; Kent et al., 2004; Yaxley et al., 2004).

4.3.2 Baffin Island basement lithologies

The Baffin Island basement is dominated by Middle Paleoproterozoic lithologies, which covers metasediments, granitoids, granidiorite, charnockites, and amphibolites, but also Archean gneisses and granite intrusions occur. For further details on the basement geology of Baffin Island the reader is referred to Jackson (1998).

4.4 Sample description

Olivine-hosted MIs for this study have been obtained from the same suite of BIP samples from Padloping Island that Yaxley et al. (2004) investigated, and a detailed description of sample petrography can be found therein. Samples investigated are Pd6, Pd12, Pd23, Pd26, and Pd66. In addition, sample Pd3 was added to the whole-rock collection. The samples represent chilled margins collected from individual lava flows. These are strongly olivine porphyritic and thus rich in mm-sized olivine crystals. Micro-phenocrysts of plagioclase are also present. The groundmass is usually microcrystalline or glassy. Overall, these lavas are chemically and petrographically similar to the ones previously studied (Clarke, 1970; Clarke & Upton, 1971; Francis, 1985; Robillard et al., 1992; Stuart et al., 2003; Ellam & Stuart, 2004; Kent et al., 2004), therefore our findings and conclusions should relate directly to these studies.

Olivine phenocrysts containing spherical to ellipsoid glassy (clear) or microcrystalline (yellow to brown) primary silicate MIs were handpicked for trace element and Sr isotope determinations. MIs range in size up to 200 μm. Most abundant are pristine MIs <75 μm,

whereas the larger intact MIs are rare. Olivine grains were mounted in epoxy and polished until their MIs were near to the surface (Appendix A2). Each MI was then carefully examined under the microscope, and only pristine MIs were selected for study.

A selection of crustal lithologies that represent the basement on Baffin Island and vary from Archean to Middle Paleoproterozoic in age were chosen for tracing potential crustal contaminants that may have interacted with the BIP during ascent. Samples were selected for trace elemental and Sr isotope analysis from the following map units[1]: *PCgl* (Middle Paleoproterozoic, granitoids), *Aph* (Achaean, quartzofledspathic gneisses), *Pcc* (Middle Paleoproerozoic, charnockites), *PHma* (Middle Paleoproerozoic, metasediment), and *PHb* (Middle Paleoproerozoic, amphibolite). Further details of the individual lithologies can be found in Jackson (1998).

4.5 Experimental approach

4.5.1 Melt inclusions (micro-milling, chemistry, TIMS, ICPMS, electron microprobe)

The host olivine phenocrysts were analysed for major and selected trace elements (Ni and Cr) using the JEOL JXA-8200 Superprobe at the Department of Geography and Geology - Geology Section (University of Copenhagen). Each olivine was probed near the mill pit from where the MI was sampled, but also the centre and the rim of the grain were analysed. During the electron microprobe session data was collected on BCR-2, BHVO-2, and LO-04-02 USGS glass standards, which is presented in Appendix A5. The standard glasses analyses show that the recommended concentrations for Na_2O, MgO, Al_2O_3, SiO_2, K_2O, CaO, MnO, and FeO were reproduced within -2.93 to 6.58%, and the concentrations of TiO_2, Cr_2O_3, and NiO were reproduced within -10.71 to 9.15% (Table 1.1).

The sampling of the MIs was done using the New Wave MicroMill at *AHIGL* (Department of Earth Sciences, University of Durham). The technique is presented in Harlou et al. (2005) and described in detail in *Chapter 2*. Single MIs $\geq$50 μm were sampled and processed individually, whereas zones having multiple MIs <<50 μm were sampled and processed as an aggregate. Sampling of the MIs by micro-milling means that the whole MI plus minor contributions of the host olivine are sampled together. The measured concentrations are therefore not absolute, as they are based on approximate inclusion sizes and estimates of the proportion of MI to entrained olivine of each individual milled sample. However, the trace elements of interest (including Sr and Rb) are strongly incompatible in olivine (e.g. see the GERM partition coefficient database for olivine on http://earthref.org), thus incorporation of olivine with the MI has a negligible

[1] Map units are written in *italic* and refer to the geology map of Okoa Bay – Padlopin Island area by Jackson (1998).

effect on the trace element ratios (Section 2.5.5). The sample chemistry was adapted for sub-ng samples using the basic method presented by (Charlier et al., 2006), and details specifically aimed at sub-ng Sr sample sizes can found in *Chapter 2* (Appendix B1). A 10% aliquot was taken of each sample dissolution for trace element determination by double focusing magnetic sector field ICPMS at the *AHIGL* (Department of Earth Sciences, Durham University). The remaining 90% was put through a Sr spec column for chemical separation of Sr followed by determination by TIMS at *AHIGL*. During the course of the BIP work 30 sub-ng sized (100-300 pg) NBS 987 standards were analyzed, and an average $^{87}Sr/^{86}Sr$ of 0.710262 ±0.000038 (2SD) was obtained (Table 4.2, Appendix D1). This is comparable to the long-term precision and accuracy reported in *Chapter 2* on sub-ng (100, 300, and 600 pg) NBS 987 standards of 0.710261 ±0.000042 (2SD, n=91). All reported Sr isotope compositions of the MIs are normalized to 0.710240. Typical *in-run* errors for samples depend on sample size and vary from 5-200 ppm (2SE), (Appendix D1). Given the excellent external precision obtained on sub-ng NBS 987 standards it is clear that the mass spectrometry uncertainty on Sr isotope ratios for MIs is dominated by counting statistics as a function of analyte size (*Chapter 2*).

NBS 987 load (ng)	n	$^{87}Sr/^{86}Sr_{Ave}$	±2SD	±2SD (ppm)
0.1	10	0.710263	0.000030	42.9
0.3	20	0.710261	0.000041	58.1
Total	30	0.710262	0.000038	52.8

Table 4.2: Average Sr isotope composition and the reproducibility (±2SD) of 30 sub-ng NBS 987 standards analyzed by TIMS (Thermo-Electron Triton) at the *AHIGL* (Department of Earth Sciences, Durham University). Full data set is located in Appendix D1 (see also Appendix B8, and Figure 2.8). 'n' gives the number of analyses.

Trace element data collected on rock standard solutions (AGV-1, BHVO-1, and W2) and synthetic Rb-Sr solutions during the ICPMS session are reported in Table 4.3 and Appendix D2. On average, the recommended Rb/Sr ratios of the AGV-1, BHVO-1, and W2 solutions were reproduced within 2.72%, 2.07%, and -5.86%, respectively, and the Rb/Sr ratios synthetic Rb-Sr solutions were reproduced within -8.97% (see details in Appendix D2). The limited of detection (LOD) for Rb and Sr were established to 0.41 and 0.73 pg/mL. The LODs for all the analyzed trace element are listed in Table 4.4.

For this batch of MIs the total procedural blank (TPB) had 4.84 ±0.33 pg Sr and 1.41 ±0.14 pg Rb (n = 9, Table 4.4, Appendix D3). The Sr isotope composition of the TPB was constrained by processing 60 separate dissolutions and column passes, which were pooled into one analyte. This approach provided a TPB with sufficient Sr (>200 pg) to facilitate a precise Sr isotope determination. This value gave Sr isotope composition of 0.712932 ±0.000234 (Table 4.4). The characterisation of the TPB made it possible to apply accurate blank corrections to both Sr isotope and trace element data. In general, the Sr content of the samples analyzed ranges from 20 pg to 1250 pg. In the worst case a ~20% correction on the Sr content was applied. A

correction of -0.001935 (~0.3%) to the $^{87}Sr/^{86}Sr$ ratio is applied to our smallest Sr sample (M14-20, 17.49 pg Sr) and to the largest Sr sample (M14-37, 1242.86 pg Sr) -0.000036 (~0.005%) is applied. Using the Rb/Sr ratio obtained by ICPMS, the $^{87}Sr/^{86}Sr$ was corrected back to the eruption age of 61 Ma (Storey et al., 1998). All $^{87}Sr/^{86}Sr$ ratios and trace element MI data reported in the following text and figures are blank corrected, and the Sr isotope data is also age corrected according to an eruption age of 61 Ma. A detailed evaluation of the TPB effect on the measured isotope composition of sub-ng samples is given in *Chapter 2* (section 2.5.2), where it is also demonstrated that the blank correction is, <200 ppm and <400 ppm for analyte levels down to 250 pg and 25 pg Sr, respectively.

Std. ID	AGV-1	BHVO-1	W2	Rb-Sr
n	12	12	13	11
Offset from reference values (%)				
Ti	0.56	1.57	-4.94	-
Rb	2.41	-2.40	-4.40	-5,36
Sr	-0.30	-4.15	1.58	3,63
Y	-7.74	-2.62	3.36	-
Zr	4.26	-3.26	-2.42	-
Nb	*15.82*	7.76	3.55	-
Ba	0.29	-6.74	2.63	-
La	1.34	-3.26	-0.93	-
Ce	3.27	-4.31	-2.12	-
Pr	*21.50*	*-10.96*	-8.71	-
Nd	-5.03	0.47	-1.07	-
Sm	-6.12	-2.59	-2.91	-
Eu	-5.04	-0.79	-3.58	-
Gd	*-13.47*	-8.10	-4.83	-
Dy	*-10.45*	1.89	2.82	-
Er	4.85	-4.36	-6.47	-
Yb	-6.45	-2.64	0.92	-
Rb/Sr	2.72	2.07	-5.86	-8,97

Table 4.3: Summary table of the standard rock and synthetic Rb-Sr solutions analyzed by double focusing magnetic sector field ICPMS (Thermo ELEMENT2) during low concentration BIP MI session at *AHIGL* (Department of Earth Sciences, Durham University). Listed are the average offsets from the USGS recommended concentrations. These averages are weighted according to the number (n) of analysis of each solution run at different concentration levels. See full data set in Appendix D2. Grey numbers in italic marks concentrations for that were not reproduced within ±10% of the recommended value.

Whole-rock powders of lavas and crustal rocks were put through a standard dissolution procedure for silicates using a mixture of concentrated HF and HNO_3 (Ottley et al., 2003). Re and Rh internal spikes were added to the sample solutions giving a final solution of 20 ppb. The trace element analyses were run on a Perkin Elmer Sciex Elan 6000 ICPMS at *AHIGL* (Department of Earth Sciences, Durham University). Calibration lines were established using the following USGS rock standards: BHVO-1, AGV-1, BE-N, SRM 688, and BIR-1 (Table

4.5). An '*in house*' rock standard (GP13, Ottley et al., 2003) was used to check the precision and accuracy of the calibration line (Table 4.5). Four TPB were repeatedly analyzed in order to check the consistency of the chemical procedure, the background of the machine through out the session, and to facilitate blank correction (Table 4.5). The limit of detection (LOD) for Sr and Rb was established to <0.02 ppm, and <0.01 ppm respectively. The average TPB contains ~0.01 ppm Sr, whereas the content of Rb is below the LOD.

Description	TPB_{M14}	$\pm 2SD_{M14}$	$Reagent_{Blank}$	LOD
n	9	9	10	10
Element				
Ti	0.32	0.01	0.00	0.01
Rb	1.41	0.14	0.13	0.41
Sr	4.84	0.33	0.42	0.73
Y	0.10	0.11	*-0.10*	0.40
Zr	80.59	1.59	0.04	0.41
Nb	9.62	0.25	*-0.04*	0.15
Ba	9.71	0.76	0.86	2.06
La	0.86	0.06	0.03	0.10
Ce	1.37	0.08	0.05	0.11
Pr	0.16	0.07	0.00	0.15
Nd	0.36	0.16	*-0.14*	0.32
Sm	*0.00*	0.13	*-0.08*	0.29
Eu	*-0.07*	0.03	*-0.03*	0.09
Gd	*-0.60*	0.09	*-0.19*	0.26
Dy	0.02	0.05	*-0.02*	0.11
Er	*-0.01*	0.02	*-0.02*	0.05
Yb	0.03	0.04	*-0.01*	0.07

Table 4.4: The element composition of the total procedural blank (TPB_{M14}). Here determined as an average of 9 individual total procedural blanks (TPB) processed with Baffin Island MIs. All trace element concentrations are obtained by double focusing magnetic sector field ICPMS (Thermo ELEMENT2) at *AHIGL* (Department of Earth Sciences, Durham University). Concentrations are given in pg/mL, which for the TPB_{M14} equals pg/sample. The reproducibility of the TPB is given by $\pm 2SD_{M14}$. The $Reagent_{Blank}$ is the average composition of 10 analysis of 3% UpA HNO_3, which is the reagent the samples are taken up in for ICPMS analysis. The limit of detection (LOD) is given by 3 times the SD error on the average SE error of the 10 $Reagent_{Blank}$ analyses. Concentrations in *grey italic* are close to or below the LOD. Negative numbers indicate concentrations that are below LOD. TPB_{M14} is the composition used for the blank correction of the trace element content of the BIP MIs, and the Sr isotope compositions were corrected using TPB60. The TPB60 is determined to have an $^{87}Sr/^{86}Sr$ ratio of 0.712932 ±0.000234 (2SE), (see details in *Chapter 2*). The background data set for this table is located in Appendix D3.

Std. ID	AGV-1	BE-N	BHVO-1	BIR-1	GP13	SRM688	W2	TPB	±2SD
n	3	3	3	3	7	3	3	13	
Offset from reference values (%)								**Concentration (ppm)**	
Sc	-4.08	1.20	-3.61	-3.65	5.99	-5.06	0.18	*-0.08*	0.51
Ti	-1.32	-0.57	0.37	0.00	5.70	-0.94	-3.18	0.00	0.00
V	-1.63	-0.97	-0.49	3.65	4.78	3.15	1.11	*-0.05*	0.13
Cr	*-25.53*	0.14	1.93	3.89	4.84	-2.59	-8.57	0.23	0.30
Mn	*-10.94*	1.75	3.24	4.09	*-11.34*	0.90	1.18	0.00	0.00
Co	3.48	1.30	0.50	5.81	0.51	0.34	-0.10	0.01	0.01
Ni	*20.95*	8.80	*11.01*	*18.21*	-1.99	12.72	*-16.47*	0.25	0.16
Cu	-3.34	-0.22	0.77	-4.33	6.45	-8.32	-1.42	*-0.20*	0.84
Zn	-3.70	3.06	4.41	-4.45	0.00	*-14.58*	-4.53	0.05	0.18
Ga	1.59	4.95	-0.94	-5.90	6.92	-7.55	-1.91	0.01	0.01
Rb	0.34	1.96	-4.14	*-24.07*	-1.58	0.24	-4.03	0.00	0.01
Sr	2.42	5.62	-7.83	-2.13	-4.52	-4.10	-2.99	0.01	0.01
Y	-3.81	3.01	-0.83	2.83	2.21	*23.57*	5.11	0.00	0.00
Zr	2.42	2.90	-3.69	*-33.01*	5.86	-9.54	-5.85	0.00	0.01
Nb	3.16	*18.18*	-1.84	*-67.50*	*-13.57*	-6.75	-3.02	0.00	0.00
Cs	-0.20	-5.44	*827.27*	*-97.67*	*15.00*	*-84.38*	3.56	0.00	0.01
Ba	0.71	1.01	-2.89	*-11.51*	0.00	*-14.34*	4.37	0.04	0.08
La	0.49	-1.33	-2.43	*-29.38*	2.73	-4.00	0.12	0.00	0.00
Ce	2.03	-4.03	-4.79	*-24.82*	-2.22	*-11.11*	-1.22	0.00	0.00
Pr	*35.01*	5.99	-1.98	*-22.60*	0.44	*-25.23*	6.73	0.00	0.00
Nd	-1.08	-0.62	3.40	1.94	2.78	-8.69	4.59	0.00	0.00
Sm	0.19	3.25	1.73	5.21	0.94	-2.43	0.86	0.00	0.00
Eu	-0.93	3.01	2.01	-1.76	-0.32	-2.28	-0.40	0.00	0.00
Gd	-5.97	*11.17*	1.11	5.47	2.87	-1.75	7.07	0.00	0.00
Tb	-5.21	0.96	1.61	-5.98	-0.88	3.17	4.44	0.00	0.00
Dy	-6.19	0.01	2.06	7.79	-2.31	-0.90	3.54	0.00	0.00
Ho	-5.68	4.13	-1.26	*15.20*	0.15	-9.81	7.84	0.00	0.00
Er	8.77	-2.66	-0.31	-9.10	-0.25	-3.07	-4.16	0.00	0.00
Tm	*-17.97*	*-12.03*	3.18	-4.81	3.85	12.07	-3.38	0.00	0.00
Yb	-0.12	2.61	-0.88	-1.90	-0.63	1.24	1.34	0.00	0.00
Lu	-3.75	9.38	3.45	5.58	2.59	-2.14	-0.15	0.00	0.00
Hf	1.46	5.94	1.51	-0.39	2.12	-4.34	-4.59	0.00	0.00
Ta	-0.65	*10.99*	1.87	*-30.65*	*-46.83*	-5.32	*-10.09*	0.00	0.00

Table 4.5: The trace element concentrations of the USGS and NIST rock standards (GP13, W2, BHVO-1, AGV-1, Be-N, SRM688, BIR-1) analyzed during ICPMS (Perkin Elmer Sciex Elan 6000) whole rock session at *AHIGL* (Department of Earth Sciences, Durham University) are reproduced within the percents (%) of the recommended values. The reference values for each rock standard listed in Appendix D4. Values in grey italic mark concentrations, which were not reproduced within ±10% of the reference values. Also listed is the average composition of 4 TPB, and its 2SD reproducibility. The full dataset is located in Appendix D4.

Std. ID	n	$^{87}Sr/^{86}Sr$	±2SD	±2SD (ppm)
NBS 987	13	0.710258	0.000011	15
BHVO-1	6	0.710491	0.000014	20

Table 4.6: $^{87}Sr/^{86}Sr$ isotope composition of NBS 987 and BHVO-1 collected by MC-ICPMS (Thermo-Electron Neptune) during whole-rock Sr isotope session at the *AHIGL* (Department of Earth Sciences Durham University). The full data set is located in Appendix D5.

Whole rock dissolutions for isotope determinations were prepared using a downscaled version of the above silicate dissolution procedure appropriately for 100 mg sample sizes. The initial step of dissolving whole rock powder includes 1 mL concentrated HNO_3 plus 3 mL concentrated HF. After 24 hours on the hotplate the dissolution is dried down to a moist gel, and this residue is then taken up in 1 mL concentrated HNO_3 and left on the hotplate for 24 hours. After a final dry down the sample is taken up in 1 mL 3M Teflon distilled HNO_3 and hereafter the sample is ready for the Sr spec column chemistry. Whole rock Sr isotope determinations were done using the Neptune MC-ICPMS at *AHIGL*. To monitor accuracy and the reproducibility of the mass spectrometry we repeatedly analyzed a NBS 987 solution. An average for NBS 987 of 0.710258 ±0.000010 (14.1 ppm, 2SD, n=13) was obtained throughout the session (Table 4.6). This compares to the long-term reproducibility of $^{87}Sr/^{86}Sr$ for this standard of 0.710267 ±0.000025 (35 ppm, 2SD, n=216) on the *AHIGL* Neptune (Nowell et al., 2003). Accuracy and reproducibility of the sample dissolution, column chemistry plus mass spectrometry were addressed by repeated analysis of the rock standard BHVO-1. An average $^{87}Sr/^{86}Sr$ BHVO-1 of 0.703491 ±0.000018 (26.2 ppm, 2SD, n=6) was obtained for 6 standards during the course of this study (Table 4.6). This value is within error of the value of 0.703475 ±0.000017 (n=8) obtained via TIMS analyses by Weis et al. (2005). The whole-rock Sr isotope data is likewise normalized to NBS 987 of 0.710240. The Sr isotope data presented in the following is and age corrected back to an age of 61 Ma. 61 Ma, which is the eruption age of the BIP, thus also the age where crustal contamination may have taken place.

4.6 Results

4.6.1 Geochemistry of the host lavas - Baffin Island picrites

Detailed description of the major and trace element systematics of the BIP studied here are given by Yaxley et al. (2004). The 6 lavas have similar major element composition, with Mg# of 69.4 to 78.0, combined with a narrow range of FeO_{total} (10.6-10.8, Table 4.7). The lavas have MgO content that range from 14.0 to 21.4 wt.%, and are thus within the normal range documented by previous studies of the BIP (Clarke & Upton, 1971; Francis, 1985; Robillard et al., 1992). Variation in MgO appears to be easily explained by variation in the amount of fractionation or accumulated of olivine e.g. Robillard et al. (1992).

More distinct compositional variation among the lavas is observed in their trace element and isotope compositions (Table 4.1). Based on K/Ti, and $(La/Sm)_N$ ratios Robillard et al. (1992) suggested a division of the lavas into *E-type* and *N-type,* where *N-type* lavas have K/Ti <0.05 and $(La/Sm)_N$ <0.7, and the *E-type* has K/Ti >0.5 and $(La/Sm)_N$ >1.1 (Table 4.1). This grouping is clearly seen in the multi element diagrams (Figure 4.2a). The *N-type* lavas are depleted in the most incompatible elements (Rb through Nd). *E-type* melts are less depleted than the *N-type* and

typically more enriched than primitive mantle (PM) between Rb and Nd, displaying REE patterns that are enriched in LREE over HREE. Recent works have shown that the *N-type* and *E-type* compositions are characterised by distinctive He-Sr-Nd-Os isotope characteristics (Table 4.1). *N-type* has $^{3}He/^{4}He$ ~50 R/R_a, low $^{87}Sr/^{86}Sr_i$ (<0.7032) and $^{187}Os/^{188}Os$ (0.1220-0.1247) combined with high $^{143}Nd/^{144}Nd_i$ (>0.51299), and *E-type* has $^{3}He/^{4}He$ <43.9 R/R_a, higher $^{87}Sr/^{86}Sr_i$ (0.7032-0.7039) and $^{187}Os/^{188}Os_i$ (0.1261-0.1303), but $^{143}Nd/^{144}Nd_i$ <0.51296 (values compiled from Robillard et al., 1992; Stuart et al., 2003; Kent et al., 2004). Kent et al. (2004) also observed subtle variations in the $\delta^{18}O$ range for the *N-type* and *E-type* (5.15-5.55‰ versus 4.84-5.22‰).

Sample ID	Pd3	Pd6	Pd12	Pd23	Pd26	Pd66
Rock	*Picrite*	*Picrite*	*Picrite*	*Picrite*	*Picrite*	*Picrite*
Type	*E-type*	*N-type*	*N-type*	*E-type*	*E-type*	*E-type*
$^{87}Sr/^{86}Sr$ isotope ratios						
$^{87}Sr/^{86}Sr_{Meas}$	0.703287	0.703129	0.703097	0.703309	0.703300	0.703689
$^{87}Sr/^{86}Sr_{Norm}$	0.703269	0.703111	0.703079	0.703291	0.703282	0.703671
$^{87}Sr/^{86}Sr_i$	0.703266	0.703104	0.703075	0.703286	0.703278	0.703662
±2SE	0.000012	0.000012	0.000015	0.000013	0.000012	0.000013
Major element compositions as oxides (wt.%) from Yaxley et al. (2004)						
SiO_2	45.95	45.46	45.87	46.38	47.13	-
TiO_2	0.90	0.77	0.82	1.06	1.03	-
Al_2O_3	12.04	10.83	11.40	13.55	13.35	-
MgO	18.16	21.36	19.83	14.02	14.56	-
FeO_{total}	10.68	10.59	10.64	10.83	10.78	-
MnO	0.18	0.17	0.17	0.18	0.18	-
CaO	10.32	9.12	9.83	11.55	11.34	-
Na_2O	1.16	1.01	1.09	1.42	1.41	-
K_2O	0.02	0.02	0.02	0.03	0.04	-
P_2O_5	0.07	0.06	0.06	0.09	0.09	-
LOI	0.53	0.82	0.24	0.43	0.31	-
Total	100.01	100.21	99.97	99.54	100.22	-
Mg#	74.9	78.0	76.6	69.4	70.3	-
Selected PM normalized trace element ratios						
$(La/Sm)_N$	0.95	0.57	0.58	0.97	0.94	1.09
$(La/Y)_N$	1.23	0.66	0.69	1.14	1.25	1.20
$(La/Yb)_N$	1.28	0.66	0.70	1.27	1.30	1.31
$(Rb/Sr)_N$	0.04	0.10	0.05	0.06	0.05	0.12
$(Sr/Nd)_N$	1.01	1.03	1.08	0.92	1.00	1.09
$(Ba/Y)_N$	0.54	0.34	0.27	0.53	0.71	1.08
$(Zr/Y)_N$	1.24	1.07	1.14	1.12	1.23	1.07

Table 4.7: $^{87}Sr/^{86}Sr$ isotope, major element compositions, and selected trace element ratios of the Baffin Island Picrites. Sr isotope ratios and trace element analyses were done at *AHIGL* by MC-ICPMS and ICPMS, respectively. Full trace element data set is located in Appendix D6. Subscribed i is the initial eruption age of 61 Ma of the BIP. PM normalization after McDonough & Sun (1995).

In accordance with the classification by Robillard et al. (1992), samples Pd6 and Pd12 are *N-type*, while Pd3, Pd23, Pd26, and Pd66 are *E-type*. The major and trace element plus Sr isotope characteristics of these lavas are comparable with the lavas previously studied from Baffin Island (Francis, 1985; Robillard et al., 1992; Stuart et al., 2003; Kent et al., 2004), (Figure 4.2-4.4). The initial (61 Ma) Sr isotope compositions range from 0.70308 to 0.70366. In comparison with previous studies, these *N-type* lavas extend to more depleted $^{87}Sr/^{86}Sr_i$ compositions (0.70308), and the *E-type* reaches more radiogenic $^{87}Sr/^{86}Sr_i$ ratios (0.70327 to 0.70367), (Figure 4.4). The lavas show slight positive correlations between $^{87}Sr/^{86}Sr_i$ and $(La/Sm)_N$ and $(Ba/Y)_N$ (Figure 4.4a and c).

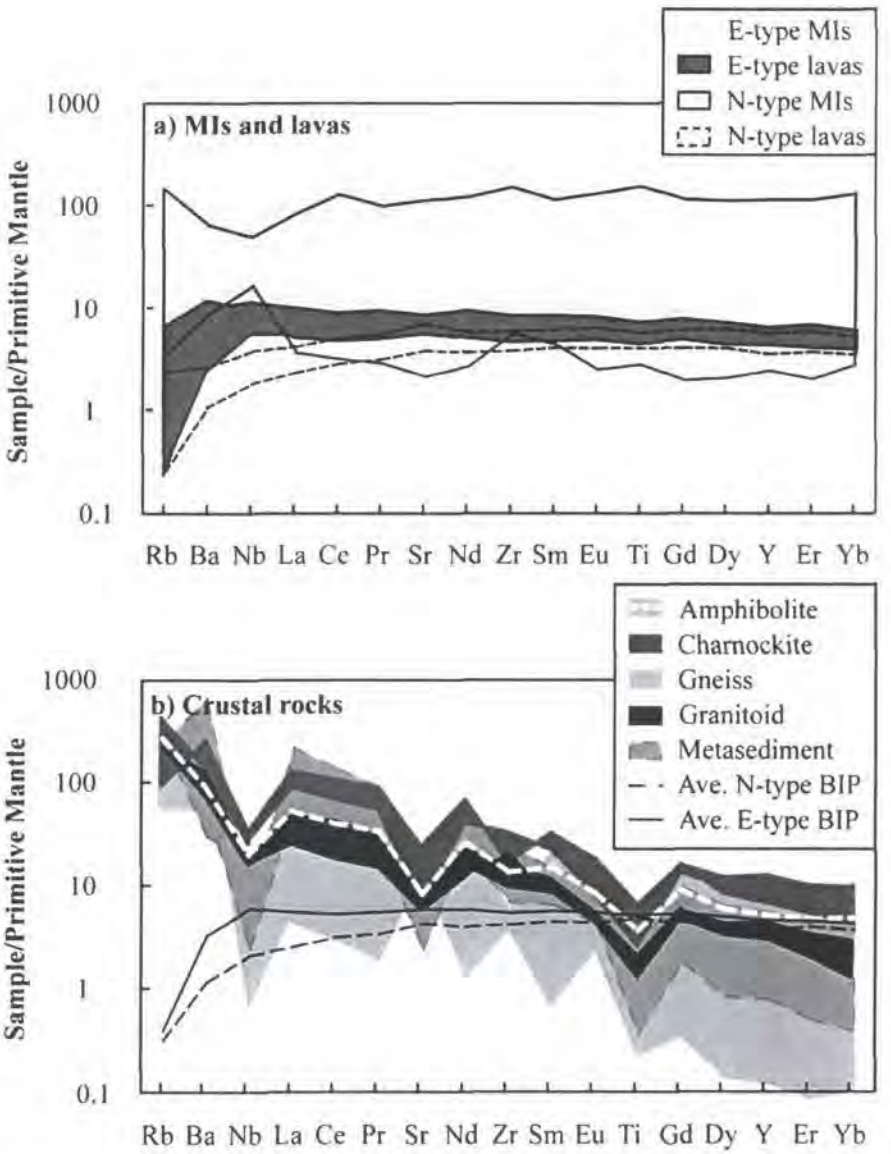

Figure 4.2: Multi element diagrams showing a) MIs and host BIP lavas divided into *N-type* and *E-type* melt compositions according to classification by Robillard et al. (1992), and b) the crustal rocks from Baffin Island basement. Concentrations are normalized to primitive mantle (PM) after McDonough & Sun (1995). In the following figures PM normalized trace element ratios are denoted with a subscripted $_N$.

4.6.2 Trace element and Sr isotope compositions of selected crustal rocks from Baffin Island

The trace element and Sr isotope compositions of the crustal rocks representing the Baffin Island basement are presented in Table 4.8, Appendix D7, and Figure 4.2-4.4. The gneisses show two different styles of multi element enrichment patterns (Figure 4.2b). Sample JD70-214-1 has the highest concentration of trace elements, with fractionated HREE relative to LREE [$(La/Yb)_N$ of 7.7)], and moderate incompatible to strong depletion of Rb, Nb, Sr, Zr, and Eu. In contrast, sample JD70-C280 and JD70-E418 have lower contents of trace elements and both have strongly fractionated REE [$(La/Y)_N$ of 34.7-51.2] and deep troughs for Rb, Nb, La, Ce, Pr, Nd, and Sm, but a positive anomaly for Eu. These two gneisses also have distinct extreme $(Sr/Nd)_N$, $(Ba/Nb)_N$, and $(Ba/Y)_N$ (respectively >10, >1000, and >1800) compared with the other Baffin Island crustal rocks (Figure 4.3-4.4). The $^{87}Sr/^{86}Sr_{61Ma}$ isotope composition of the gneisses spans from 0.7277 to 0.7594, where JD70-214-1 is the least radiogenic of the three (Table 4.8).

The granitoids represent a very homogenous group in regards to trace element and Sr isotope compositions (Table 4.8). They show depletion of HREE relative to LREE [$(La/Y)_N$ of 8.5-32.4] and the multi element patterns are steep with deep troughs for Nb, Sr, and Ti (Figure 4.2b). The $^{87}Sr/^{86}Sr_{61Ma}$ isotope composition of the ganitoids range from 0.7684-0.7923 (Figure 4.4).

The multi element enrichment pattern of charnockites show strong depletion of HREE compared to LREE [$(La/Y)_N$ of 9.3-28.9] and deep troughs for Nb, Sr, Eu, and Ti (Figure 4.2b, Table 4.8). Sample JD70-E256 additionally shows depletions for Rb and Zr. Sample JD70-E256 is further distinguished by a relatively unradiogenic $^{87}Sr/^{86}Sr_i$ composition (0.7178) and low $(Rb/Sr)_N \sim 4$, whereas the two other samples have $^{87}Sr/^{86}Sr_{61Ma}$ of 0.8372- 0.8509, and $(Rb/Sr)_N \sim 60$ (Figure 4.4).

The amphibolite (JD70-D239-2) shows fractionation of HREE from LREE resulting in a depleted multi element pattern (Figure 4.2b, Table 4.8). $(La/Y)_N$ is slightly enriched (11.0), and Nb, Sr, Zr, Eu, and Ti are depleted relative to PM. The amphibolite has the least radiogenic $^{87}Sr/^{86}Sr_{61Ma}$ (0.7755) and the least enriched trace element signature of all the crustal rocks analyzed (Figure 4.3 and 4.4).

The REE of the highly anatectic metasediments (JD70-304-1, JD70-312-1, JD70-E294-1) are more strongly fractionated than the slightly anatectic metasediments (JD70-258-1, JD70-294-2, JD70-303-2), $(La/Yb)_N$ of 36-369 vs. 7-16, (Figure 4.2b, Table 4.8). As a group they show variable degrees of depletion in Rb, Nb, Sr, and Ti. In addition the slightly anatectic

metasediments have positive Eu anomalies, whereas the highly anatectic *metasediments* have negative anomalies. A single sample (JD70-258-1) stands out by having significantly higher LREE/HREE, $(Ba/Nb)_N$ and $(Ba/Y)_N$ ratios (Figure 4.3-4.4). The $^{87}Sr/^{86}Sr_{61Ma}$ ratios range from 0.7293 to extremely radiogenic values of 0.9753 (Table 4.8). Amongst these rocks are the most radiogenic Sr and most enriched crustal compositions (Figure 4.2-4.4).

Sample ID	**JD70-250**	**JD70-272-1**	**JD70-E256**	**JD70-214-1**	**JDC70-280**	**JDC70-E418**
Rock	*Charnockite*	*Charnockite*	*Charnockite*	*Gneisses*	*Gneisses*	*Gneisses*
Map unit	*Pcc*	*Pcc*	*Pcc*	*Agn*	*Agn*	*Agn*
Sr isotope ratios						
$^{87}Sr/^{86}Sr_{Meas}$	0.841779	0.855917	0.715122	0.728072	0.748264	0.760999
$^{87}Sr/^{86}Sr_{Norm}$	0.841761	0.855899	0.715104	0.728054	0.748246	0.760981
$^{87}Sr/^{86}Sr_{61Ma}$	0.837234	0.850885	0.714808	0.727759	0.747099	0.759419
±2SE	0.000011	0.000016	0.000017	0.000011	0.000010	0.000011
Selected PM normalized trace element ratios						
$(La/Sm)_N$	4.03	3.55	3.96	2.73	7.43	6.68
$(La/Y)_N$	9.17	7.23	18.73	5.35	42.76	28.40
$(La/Yb)_N$	11.81	9.34	28.86	7.72	51.52	34.69
$(Rb/Sr)_N$	59.11	65.37	3.91	3.89	15.11	20.56
$(Sr/Nd)_N$	0.17	0.14	0.36	0.44	12.23	10.90
$(Ba/Y)_N$	15.92	11.47	37.13	4.97	1879.73	1854.57
$(Zr/Y)_N$	3.32	2.35	2.50	0.52	46.05	24.34

Sample ID	**JD70-197-2**	**JD70-318-2**	**JDC70-304**	**JD70-D239-2**
Rock	*Granitoid*	*Granitoid*	*Granitoid*	*Mafic*
Map unit	*Pcgl*	*Pcgl*	*Pcgl*	*PHB*
Sr isotope ratios				
$^{87}Sr/^{86}Sr_{Meas}$	0.774056	0.771383	0.794484	0.777997
$^{87}Sr/^{86}Sr_{Norm}$	0.774038	0.771365	0.794466	0.777979
$^{87}Sr/^{86}Sr_{61Ma}$	0.771999	0.768413	0.792265	0.775491
±2SE	0.000011	0.000010	0.000013	0.000011
Selected PM normalized trace element ratios				
$(La/Sm)_N$	4.74	3.18	4.27	3.51
$(La/Y)_N$	13.59	5.74	12.72	10.18
$(La/Yb)_N$	32.38	8.50	19.32	10.96
$(Rb/Sr)_N$	26.80	38.80	28.86	32.69
$(Sr/Nd)_N$	0.53	0.48	0.34	0.31
$(Ba/Y)_N$	24.58	29.68	22.71	17.64
$(Zr/Y)_N$	3.19	4.62	4.20	2.62

Table 4.8: Sr isotope composition and selected primitive mantle normalized trace element ratios of selected basement lithologies of Baffin Island. Sr isotope ratios and trace element analyses were at *AHIGL* by MC-ICPMS and ICPMS, respectively. Full trace element data set is located in Appendix D7. The subscribed i indicate that the $^{87}Sr/^{86}Sr$ are corrected to an age of 61 Ma. 61 Ma is the eruption age of the BIP, and therefore also the period during which crustal contamination may have taken place. PM normalization after McDonough & Sun (1995).

Sample ID	JD70-258-1	JD70-294-2	JD70-303-2	JD70-304-1	JD70-E236-1	JD70-E294-1
Rock type	*Metasediment*	*Metasediment*	*Metasediment*	*Metasediment*	*Metasediment*	*Metasediment*
Map unit	*PHmb*	*PHmb*	*PHmb*	*Phma*	*Phma*	*Phma*
Sr isotope ratios						
$^{87}Sr/^{86}Sr_{Meas}$	0.730154	0.901624	0.743830	0.820062	0.800911	0.978878
$^{87}Sr/^{86}Sr_{Norm}$	0.730136	0.901606	0.743812	0.820044	0.800893	0.978860
$^{87}Sr/^{86}Sr_{61Ma}$	0.729321	0.896482	0.742944	0.815901	0.797571	0.969410
±2SE	0.000016	0.000015	0.000010	0.000013	0.000013	0.000012
Selected PM normalized trace element ratios						
$(La/Sm)_N$	15.65	9.43	4.67	3.61	3.26	4.41
$(La/Y)_N$	266.57	78.34	21.35	7.28	8.86	12.89
$(La/Yb)_N$	368.61	157.94	35.88	6.76	14.58	15.53
$(Rb/Sr)_N$	10.76	66.52	11.44	54.20	43.55	121.77
$(Sr/Nd)_N$	0.42	0.21	0.93	0.22	0.26	0.10
$(Ba/Y)_N$	801.24	68.63	99.34	13.15	5.44	21.76
$(Zr/Y)_N$	30.44	8.73	5.60	3.07	3.31	3.29

Table 4.8: Continued

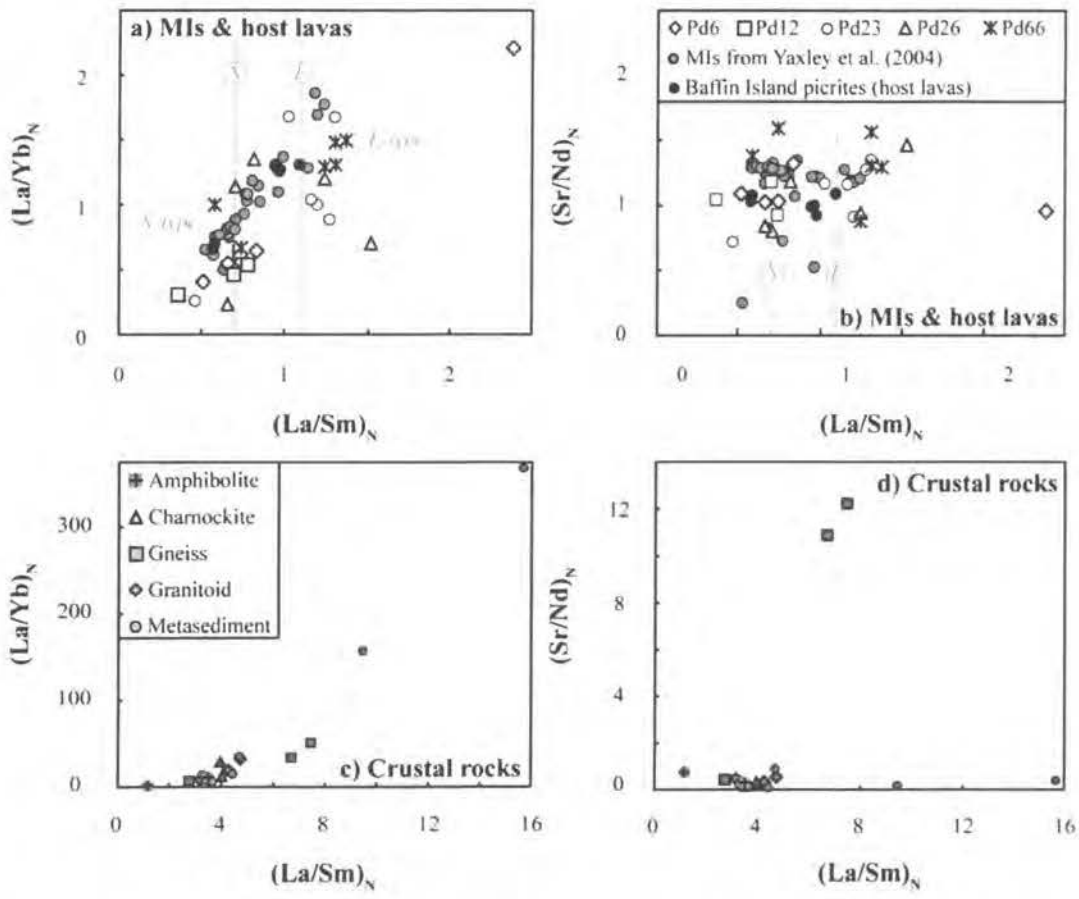

Figure 4.3: PM normalized trace element ratios plots of Baffin Island MIs, host lavas, and selected crustal rocks. a) and b) show the range of $(La/Sm)_N$ vs. $(La/Y)_N$ and $(Sr/Nd)_N$ for MIs and host lavas. Grey lines mark the limits of *N-type* and *E-type* melts compositions cf. Robillard et al. (1992). For comparison MIs (grey circles) from Yaxley et al. (2004) and BIP lavas from Kent et al. (2004) are included. Plots c) and d) show the range of $(La/Sm)_N$ vs. $(La/Y)_N$ and $(Sr/Nd)_N$ of the crustal rocks.

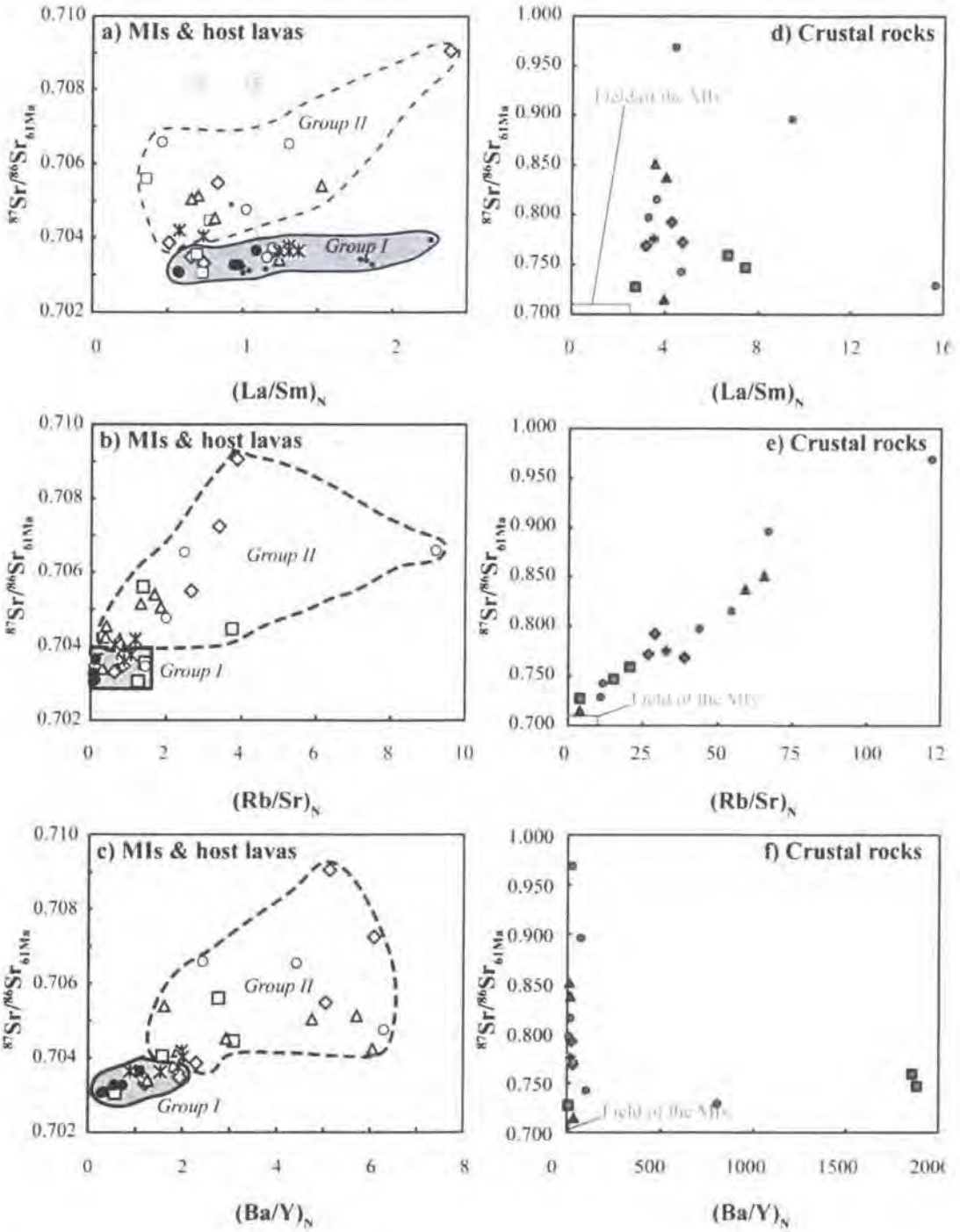

Figure 4.4: $^{87}Sr/^{86}Sr_{61Ma}$ vs. selected PM-normalized trace element ratios. a), b), and c) show $(La/Sm)_N$, $(Rb/Sr)_N$, and $(Ba/Y)_N$ vs. $^{87}Sr/^{86}Sr_{61Ma}$ for host lavas and MIs. *Group-I* includes MIs with slightly increasing $^{87}Sr/^{86}Sr_{61Ma}$ over the range of the respective trace element ratios and *Group-II* describes MIs with more radiogenic $^{87}Sr/^{86}Sr_{61Ma}$ ratios combined with variable to elevated trace element ratios (section 4.6.4). Plots d), e), and f) show $(La/Sm)_N$, $(Rb/Sr)_N$, and $(Ba/Y)_N$ vs. $^{87}Sr/^{86}Sr_{61Ma}$ for the crustal rocks of Baffin Island. The field, in which the MIs plot is shown for comparison in d), e), and f). Legend is as in Figure 4.3. The grey lines in a) mark the division between N- and E-type lavas defined by Robillard et al. 1992 (Section 4.6.1).

4.6.3 Geochemistry of the olivine phenocrysts

The forsterite (Fo) content of the olivine phenocrysts hosting the silicate MIs sampled in this work range from 89.0 down to 84.3 with an average of 87.0 ±2.8 (2SD), (Figure 4.5, Table 4.9). NiO and CaO contents are similar to those found by Yaxley et al. (2004). The range in olivine Fo contents is within that documented by Yaxley et al. (2004) for this suite of rocks and within the range for BIP in general (Francis, 1985; Kent et al., 2004). Previous studies have found rare olivine crystals with Fo contents >90 (Kent et al., 2004; Yaxley et al., 2004). Despite the fact that no olivines with Fo >90 have been recorded during this study, we believe that our olivine phenocrysts are representative of those found throughout the BIP, and so the results should be generally applicable.

Olivine	$Ave_{Ol\text{-}Pd6}$	±2SD	$Ave_{Ol\text{-}Pd12}$	±2SD	$Ave_{Ol\text{-}Pd23}$	±2SD	$Ave_{Ol\text{-}Pd66}$	±2SD	$Ave_{Ol\text{-}Pd66}$	±2SD
n	15		30		21		18		12	
Major element compositions (oxides wt.%)										
Al_2O_3	0.06	0.13	0.10	0.21	0.07	0.13	0.07	0.14	0.08	0.17
MnO	0.18	0.35	0.18	0.35	0.19	0.37	0.19	0.38	0.23	0.45
TiO_2	0.00	0.01	0.00	0.01	0.01	0.01	0.01	0.02	0.01	0.02
Cr_2O_3	0.08	0.17	0.10	0.20	0.07	0.13	0.07	0.14	0.06	0.13
MgO	47.57	95.13	47.45	94.91	46.75	93.50	46.51	93.02	44.87	89.74
SiO_2	40.31	80.62	40.29	80.58	40.01	80.01	40.29	80.59	39.89	79.78
FeO	11.13	22.26	11.18	22.37	12.28	24.57	12.22	24.45	14.30	28.59
CaO	0.31	0.62	0.30	0.61	0.31	0.62	0.31	0.62	0.34	0.67
NiO	0.36	0.71	0.37	0.75	0.32	0.64	0.31	0.63	0.22	0.45
Na_2O	0.00	0.01	0.01	0.01	0.01	0.01	0.01	0.01	0.00	0.01
K_2O	0.00	0.00	0.00	0.00	0.00	0.00	0.00	0.01	0.00	0.01
Total	100.00		100.00		100.00		100.00		100.00	
Fosterite content (Fo) in %										
Fo	88.2		88.1		87.0		87.0		84.6	
Fo_{range}	88.2-88.3		87.6-89.0		86.0-87.4		86.3-87.4		84.3-85.0	

Table 4.9: Average major element composition of olivine phenocrysts from each of the BIP, which contained the MIs that were sampled by micro-milling. Fo range give the range of Fo observed within olivine phenocrysts from each sample. Concentrations determinations by electron microprobe were carried out at the Department of Geography and Geology – Geology Section (University of Copenhagen). Full data set is located in Appendix D8.

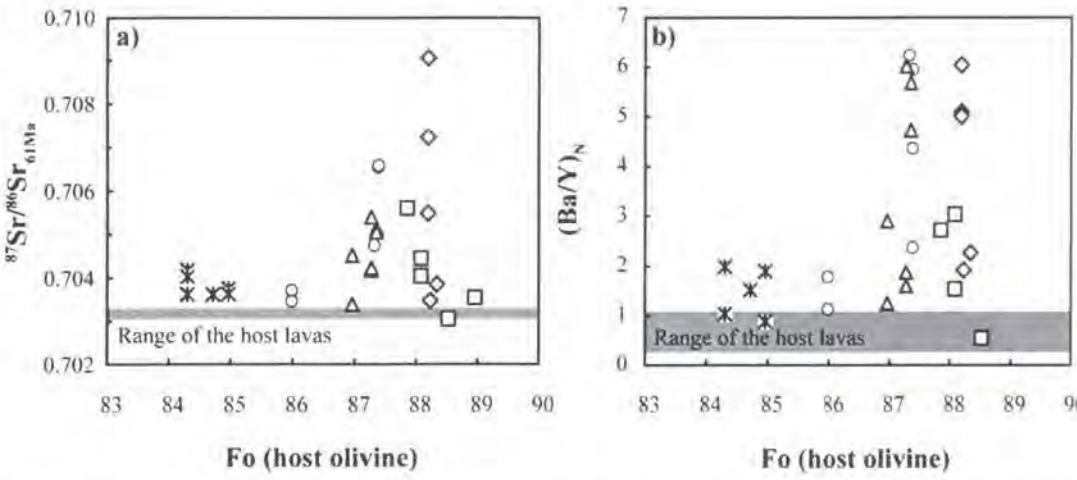

Figure 4.5: Forsterite (Fo) range of olivine phenocrysts of the BIP hosting the sampled MIs vs. a) $^{87}Sr/^{86}Sr$ of entrapped MIs, and b) $(Ba/Y)_N$ of entrapped MIs. For comparison the $^{87}Sr/^{86}Sr$ range of the BIP is shown as a horizontal field in grey. Legend is as in Figure 4.3. Full olivine data set is located in Appendix D8.

4.6.4 Geochemistry of the olivine-hosted melt inclusions

The trace element and Sr isotope data of the MIs analyzed here (Table 4.10) complements the trace element dataset for olivine-hosted MIs from Padloping Island presented by Yaxley et al. (2004). No correction for post entrapment modification by reaction with the host olivine is required for our dataset, because we have chosen to study elements that are highly incompatible in olivine and so there is no effect on trace element ratios or Sr isotope compositions. This is confirmed by analyses of MI free host olivine phenocrysts from this and other locations that reveal background levels of all the elements of interest (section 2.5.5).

The *N-type* and *E-type* classification used for whole rocks is also applicable to their MIs, but in keeping with other studies that have compared variations in whole rocks and MIs, more variation is seen within the MI populations e.g. Gurenko & Chaussidon, 1995; Shimizu, 1998; Kent et al., 1999; Kent et al., 2002a; Norman et al., 2002; Yaxley et al., 2004. There is a greater range in LREE/MREE and LREE/HREE fractionation in the BIP MIs compared with their host lavas suite [$(La/Sm)_N$: 0.36-2.38, $(La/Yb)_N$: 0.31-2.21 vs. $(La/Sm)_N$: 0.66-1.31, $(La/Yb)_N$: 0.57-1.09, Figure 4.3]. In general, MIs from this study have notably higher values for many trace element ratios e.g. $(Rb/Ba)_N$, $(Rb/Sr)_N$, $(Sr/Nd)_N$, $(Ba/La)_N$, $(Ba/Ce)_N$, $(La/Nb)_N$, $(Zr/Y)_N$ compared to the host lavas (e.g. Figure 4.2-4.4). Overall, the trace element characteristics of this MI data set are similar to the larger MI suite investigated by Yaxley et al. (2004) suggesting sampling from the same suite (Figure 4.3). Hence, our conclusions should be applicable to their BIP MI dataset as a whole.

MI ID_{M14}	M14-1	M14-12	M14-13	M14-14	M14-2	M14-3	M14-4	M14-5
Host Rock ID	Pd6	Pd6	Pd6	Pd6	Pd6	Pd6	Pd12	Pd12
Size (μm)	100x50	100x80	100x80	75	80	125	75	125x150
n	1	1	1	1	1	1	1	1
Type	N (I)	E (II)	N (II)	E (II)	N (II)	N(I)	N (II)	N (I)
Sr isotope composition								
$^{87}Sr/^{86}Sr_{Norm}$	0.703701	0.709880	0.706132	0.708315	0.703521	0.704282	0.703203	0.703808
$^{87}Sr/^{86}Sr_{Blank}$	0.703544	0.709355	0.705689	0.707499	0.703357	0.703938	0.703159	0.703671
$^{87}Sr/^{86}Sr_i$	0.703479	0.709063	0.705488	0.707242	0.703309	0.703861	0.703064	0.703563
±2SE	0.000150	0.002420	0.001580	0.000804	0.000104	0.000191	0.000139	0.000094
$^{87}Rb/^{86}Sr_i$	0.075	0.337	0.232	0.297	0.055	0.089	0.109	0.124
Absolute trace element content (pg)								
Ti	20796	3361	5358	843	23173	7427	88241	24032
Rb	7.35	3.28	5.96	2.81	5.27	3.76	39.87	13.83
Sr	284.74	28.13	74.29	27.38	277.30	121.61	1060.80	321.97
Y	63.52	5.32	10.74	4.51	67.69	28.10	233.11	67.75
Zr	202.49	30.19	31.24	66.62	239.03	68.85	755.93	184.05
Nb	-	7.11	6.94	25.29	-	-	15.34	-
Ba	187.84	41.58	82.65	41.89	125.39	98.29	200.90	-
La	6.58	1.65	1.24	1.47	7.09	2.27	25.43	6.14
Ce	19.10	3.74	2.78	4.04	20.46	7.22	101.67	21.09
Pr	3.16	0.57	0.38	0.06	3.46	0.94	11.95	4.05
Nd	17.50	1.85	3.53	1.23	16.90	7.01	71.75	17.07
Sm	6.27	0.43	0.93	-	6.00	2.78	21.85	5.56
Eu	2.72	0.38	0.39	0.15	2.55	0.97	9.57	2.56
Gd	8.09	0.78	1.18	-	8.49	2.79	29.95	7.56
Dy	9.70	0.62	1.63	0.61	9.59	3.84	35.79	10.28
Er	6.33	0.47	0.99	0.54	6.97	3.17	23.61	7.41
Yb	8.19	0.51	1.31	0.97	8.64	3.82	27.08	9.05
PM normalized trace element ratios								
$(La/Sm)_N$	0.66	2.38	0.83	-	0.74	0.51	0.73	0.69
$(La/Y)_N$	0.69	2.06	0.76	2.17	0.70	0.54	0.72	0.60
$(La/Yb)_N$	0.55	2.21	0.64	1.04	0.56	0.40	0.64	0.46
$(Rb/Sr)_N$	0.86	3.87	2.66	3.40	0.63	1.02	1.25	1.42
$(Sr/Nd)_N$	1.02	0.95	1.32	1.39	1.03	1.09	0.93	1.18
$(Ba/Y)_N$	1.93	5.09	5.01	6.05	1.21	2.28	0.56	-
$(Zr/Y)_N$	1.31	2.32	1.19	6.04	1.45	1.00	1.33	1.11

Table 4.10: Sr isotope and trace element content of milled olivine-hosted MIs from the BIP collected by ICPMS and TIMS at *AHIGL* (Department of Earth Sciences, Durham University). The approximate size of each MI is given in μm. Zone indicate that an area with multiple (M) tiny MIs (<20 μm) were milled. Type denoted by *E* and *N* refer to the classification by Robillard et al. (1992), whereas *I* and *II* refer to the respective grouping observed described in section 4.6.4 (Figure 4.4). Subscribed i denotes initial age of 61 Ma. The trace element composition is listed as absolute concentration (pg). Also, listed is a selection of PM-normalized trace element ratios. Located in Appendix D9 are normalized trace element concentrations to 100 μm-sized MI. 'n' denotes the number of MIs analyzed, 'M' denotes that multiple MIs were sampled, 'Z' that a zone with several MIs were sampled. PM normalization is after McDonough & Sun (1995).

	M14-31	M14-21	M14-20	M14-6	M14-7	M14-8	M14-9	M14-10
Host rock ID	Pd12	Pd12	Pd12	Pd23	Pd23	Pd23	Pd23	Pd23
Size (μm)	Zone	Zone	Zone	40x80	40x80	100x80	100	50x70
n	M	M	M	1	1	1	1	1
Type	N (II)	N (II)	N(I)	E (I)	E (I)	E (II)	N (II)	E
Sr isotope composition								
$^{87}Sr/^{86}SrN_{orm}$	0.706659	0.705249	0.705932	0.703969	0.703813	0.706944	0.708491	-
$^{87}Sr/^{86}Sr_{Blank}$	0.705722	0.704756	0.703997	0.703794	0.703594	0.706742	0.707303	-
$^{87}Sr/^{86}Sr_i$	0.705618	0.704473	0.704063	0.703732	0.703485	0.706556	0.706608	-
±2SE	0.000492	0.000288	0.000640	0.000094	0.000094	0.004120	0.000924	-
$^{87}Rb/^{86}Sr_i$	0.120	0.326	-	0.071	0.125	0.215	0.802	-
Absolute trace element content (pg)								
Ti	2770	2772	1916	18811	19777	6460	4507	6713
Rb	1.34	8.50	-	6.04	8.70	10.66	5.01	5.10
Sr	32.37	75.37	17.49	246.95	200.84	143.50	18.08	60.76
Y	10.72	11.71	6.14	45.14	35.44	17.64	5.78	7.50
Zr	27.22	35.60	-	106.08	138.83	75.46	4.64	-
Nb	4.62	15.02	12.12	-	4.26	26.74	20.55	6.43
Ba	44.89	54.84	14.67	125.23	62.64	118.48	21.26	68.63
La	0.94	1.63	0.75	7.57	6.40	4.65	0.46	1.52
Ce	2.26	3.86	0.08	21.41	28.35	10.60	2.04	7.71
Pr	0.56	0.38	0.04	2.39	2.09	1.31	0.13	0.42
Nd	1.94	2.20	0.65	16.93	10.83	6.66	1.57	2.99
Sm	1.66	1.31	0.16	3.97	3.46	2.24	0.62	0.75
Eu	0.06	0.30	0.20	1.59	1.66	1.04	0.23	0.27
Gd	0.40	0.67	0.19	5.97	4.32	2.31	0.72	0.84
Dy	1.45	1.58	0.89	6.63	5.97	2.57	0.29	1.16
Er	1.14	1.16	0.64	4.58	4.05	1.78	0.54	0.85
Yb	2.07	2.06	1.35	5.14	4.16	1.89	1.17	1.17
PM normalized trace element ratios								
$(La/Sm)_N$	0.36	0.78	2.96	1.19	1.16	1.30	0.46	1.27
$(La/Y)_N$	0.58	0.92	0.81	1.11	1.20	1.75	0.52	1.35
$(La/Yb)_N$	0.31	0.54	0.38	1.00	1.05	1.68	0.26	0.89
$(Rb/Sr)_N$	1.37	3.74	0.00	0.81	1.44	2.46	9.19	2.78
$(Sr/Nd)_N$	1.05	2.15	1.68	0.92	1.16	1.35	0.72	1.28
$(Ba/Y)_N$	2.73	3.05	1.56	1.81	1.15	4.38	2.40	5.96
$(Zr/Y)_N$	1.04	1.25	0.00	0.96	1.60	1.75	0.33	-

Table 4.10: Continued

MI ID_{M14}	M14-11	M14-23	M14-22	M14-25	M14-24	M14-34	M14-32	M14-33
Host rock ID	Pd23	Pd26	Pb26	Pd26	Pd26	Pd26	Pd26	Pd26
Size (μm)	75	60	40	Zone	70	Zone	75	70
n	1	1	3	M	1	M	1	1
Type	E (II)	N (II)	N (II)	E (I)	E (II)	N (II)	N (II)	N (II)
Sr isotope composition								
$^{87}Sr/^{86}Sr_{Norm}$	0.705860	0.706436	0.707137	0.703470	0.705225	0.705851	0.705033	0.705444
$^{87}Sr/^{86}Sr_{Blank}$	0.704925	0.705239	0.705570	0.703418	0.704558	0.705525	0.704232	0.704272
$^{87}Sr/^{86}Sr_i$	0.704776	0.705138	0.705046	0.703395	0.704526	0.705397	0.704174	0.704242
±2SE	0.001030	0.001680	0.000922	0.000035	0.000380	0.001170	0.000382	0.000894
$^{87}Rb/^{86}Sr_i$	0.172	0.116	0.162	0.027	0.037	0.148	0.067	0.035
Absolute trace element content (pg)								
Ti	1135	2087	7535	65171	3519	12783	2302	1722
Rb	2.18	1.05	1.00	8.31	0.70	5.36	1.10	0.36
Sr	36.58	26.24	17.89	882.29	55.90	105.07	47.67	30.90
Y	4.69	6.45	6.33	171.92	8.59	23.10	6.78	2.09
Zr	22.93	41.41	2.02	612.11	14.31	149.90	-	-
Nb	15.34	-	30.28	53.61	19.43	10.56	10.84	12.79
Ba	44.99	56.19	45.90	331.22	38.29	56.80	19.56	19.30
La	1.15	1.27	0.37	33.88	2.30	4.57	-	0.02
Ce	7.96	13.12	1.09	80.50	5.06	6.00	8.55	1.18
Pr	0.39	0.20	0.38	10.21	0.55	1.06	4.32	-
Nd	1.96	2.06	1.34	58.89	2.97	4.52	11.36	0.35
Sm	0.71	1.13	0.35	17.08	1.77	1.88	1.37	0.94
Eu	0.29	0.24	0.17	6.96	0.40	0.55	0.37	0.07
Gd	0.38	0.66	0.36	23.05	1.13	1.38	0.81	0.13
Dy	0.57	0.87	0.90	26.68	1.51	3.12	1.14	0.26
Er	0.42	0.55	0.68	17.09	0.72	2.55	0.81	0.25
Yb	0.47	0.76	1.08	19.18	1.16	4.44	0.79	0.36
PM normalized trace element ratios								
$(La/Sm)_N$	1.02	0.70	0.66	1.24	0.81	1.52	-	0.01
$(La/Y)_N$	1.63	1.30	0.39	1.31	1.77	1.31	-	0.06
$(La/Yb)_N$	1.68	1.14	0.23	1.20	1.35	0.70	-	0.03
$(Rb/Sr)_N$	1.98	1.32	1.86	0.31	0.42	1.69	0.77	0.39
$(Sr/Nd)_N$	1.17	0.80	0.84	0.94	1.18	1.46	0.26	5.57
$(Ba/Y)_N$	6.25	5.68	4.73	1.26	2.90	1.60	1.88	6.02
$(Zr/Y)_N$	2.00	2.63	0.13	1.46	0.68	2.66	-	-

Table 4.10: Continued

MI ID_{M14}	M14-26	M14-35	M14-36	M14-29	M14-37	M14-38
Host rock ID	Pd66-1	Pd66-2	Pd66-2B	Pd66-3	Pd66-2	Pd66-3
Size (μm)	160	60	60	225	Zone	Zone
n	1	2	2	1	M	M
Type	E (I)	N (I)	N (II)	E (I)	E (I)	E (I)
Sr isotope composition						
$^{87}Sr/^{86}Sr_{Norm}$	0.703775	0.704806	0.704659	0.703906	0.703674	0.703700
$^{87}Sr/^{86}Sr_{Blank}$	0.703692	0.704283	0.704087	0.703842	0.703638	0.703645
$^{87}Sr/^{86}Sr_i$	0.703624	0.704193	0.704038	0.703761	0.703627	0.703637
±2SE	0.000057	0.000460	0.000334	0.000036	0.000039	0.000048
$^{87}Rb/^{86}Sr_i$	0.077	0.104	0.056	0.093	0.013	0.008
Absolute trace element content (pg)						
Ti	35906	3804	2381	49380	84176	41147
Rb	14.20	2.69	1.35	21.73	5.57	2.33
Sr	530.58	75.10	69.91	675.61	1242.86	806.57
Y	113.02	10.49	12.40	81.72	190.80	125.66
Zr	320.12	7.19	46.81	414.69	679.89	371.48
Nb	16.60	10.51	7.06	35.34	5.38	23.07
Ba	264.73	31.80	38.03	239.02	304.31	170.79
La	22.94	1.83	1.60	17.81	36.80	25.58
Ce	54.61	4.20	7.75	49.85	93.36	54.60
Pr	7.44	0.60	0.92	5.70	11.81	7.55
Nd	37.95	3.42	2.76	27.20	59.91	39.24
Sm	11.58	1.98	1.36	8.55	17.60	11.69
Eu	4.32	0.29	0.35	3.43	7.23	4.57
Gd	14.97	0.88	1.19	10.92	24.78	15.94
Dy	17.70	1.33	1.33	12.17	30.29	19.40
Er	10.83	1.09	1.15	7.62	17.97	10.67
Yb	12.10	1.25	1.64	8.21	19.18	11.66
***PM normalized* trace element ratios**						
$(La/Sm)_N$	1.24	0.58	0.74	1.31	1.31	1.37
$(La/Y)_N$	1.35	1.16	0.86	1.45	1.28	1.35
$(La/Yb)_N$	1.29	1.00	0.67	1.48	1.31	1.49
$(Rb/Sr)_N$	0.89	1.19	0.64	1.07	0.15	0.10
$(Sr/Nd)_N$	0.88	1.38	1.59	1.56	1.30	1.29
$(Ba/Y)_N$	1.53	1.98	2.00	1.91	1.04	0.89
$(Zr/Y)_N$	1.16	0.28	1.55	2.08	1.46	1.21

Table 4.10: *Continued*

The MIs show an enormous $^{87}Sr/^{86}Sr_i$ variation (0.70308-0.70906) that overlaps the narrower Sr isotope composition range of the host lavas, but clearly the MIs are more diverse and expand the range towards more radiogenic $^{87}Sr/^{86}Sr_i$ compositions - comparable to the relationship observed between the MIs and their host ankaramites of NW Iceland (*Chapter 3*, Figure 4.4). If the MIs are classified solely on the basis of their trace element characteristics, there is overlap between their Sr isotope compositions. *E-type* MIs have $^{87}Sr/^{86}Sr_i$ in the range 0.703406-0.709063, and *N-type* MIs vary from 0.703309-0.706608 (Figure 4.4a). However, the MI and the whole rock compositions show some systematic relations between the Sr isotope and trace-trace element ratios (Figure 4.4). There is a group of MIs, which together with the whole rock compositions display relative uniform $^{87}Sr/^{86}Sr_i$ ratios (0.703-0.704) over the range of $(La/Sm)_N$. Another group of MIs has a much more diverse range of $^{87}Sr/^{86}Sr_i$ ratios (0.704-0.709) over the range of $(La/Sm)_N$. Hereafter, these two groups of MIs are referred to as '*Group-I*' and '*Group-II*' MIs, respectively. The MIs of *Group-I* are further characterized by $(Rb/Sr)_N$ <1.5 and $(Ba/Y)_N$ both <1.9, whereas the $(Rb/Sr)_N$ and $(Ba/Y)_N$ ratios of *Group-II* MIs show more extreme variations (0.4-9.2, and 1.5-6.3 respectively, Figure 4.4). The MIs from the *N-type* lavas Pd6 and P12 are dominated by *N-type* melts, and MIs from *E-type* samples Pd23, Pd26, and Pd66 are predominately *E-type* melts (Figure 4.3a). Both *N-type* and *E-type* MIs are found among *Group-I* and *Group-II* MIs (Figure 4.4a). No obvious systematic variation is observed between the Fo-content of the host olivine and $^{87}Sr/^{86}Sr_i$, or the degree of enrichment of incompatible elements of their MIs (Figure 4.5). It is notable, that the majority of the *Group-II* MIs are hosted in olivine with $Fo_{>87}$.

4.7 Discussion & Implications

In general, major and trace element studies of the relationship between MIs and their host lavas have shown that MIs are more chemically diverse than their host lavas or other lavas in the suite. Such compositional differences have typically been ascribed to either source heterogeneity or variation in the melting conditions e.g. Sobolev & Shimizu (1993), Gurenko & Chaussidon (1995), Saal et al. (1998), Shimizu (1998), Jackson & Hart (2006). However, recently some compositional variation among MIs, especially those erupted in continental settings, have been suggested to be linked to crustal contamination (Kent et al., 2002b; Yaxley et al., 2004). At Baffin Island the focus of the discussion is whether or not crustal contamination has influenced the geochemistry of the BIP. This is important to constrain from the viewpoint of fully understanding the cause of the He isotope and lithophile element isotope variations seen in the BIP (Stuart et al., 2003; Ellam et al., 2004). First we examine the relationship between lavas, their olivine phenocrysts and the MIs within them, before going on to consider the possible causes of Sr isotope variation in the MIs and implications for BIP petrogenesis and the nature of MI sampling in magmas.

4.7.1 Relationship between lavas, olivine phenocrysts, and melt inclusions

The distribution of Mg^{2+} and Fe^{2+} between the olivine phenocrysts and their host melt can be used as a measure of the linkage between the two. At equilibrium the partition coefficient (K_d) of Fe^{2+} and Mg^{2+} between olivine and liquid equals 0.3 ±0.03 (Roeder & Emslie, 1970). Ideally glass compositions (or groundmass) should be used in these calculations and not the bulk rock composition, as the bulk rock composition may be compromised by the present of accumulated phenocryst phases. Still, useful information can be extracted using the relationship between the olivine and the whole rock composition. K_d values calculated for each olivine-host lava pair are >0.3. Only the olivine phenocrysts of sample Pd23 and Pd26 approach the field of equilibrium (Figure 4.6). This suggests that most of the olivine phenocrysts are too poor in Mg to have crystallized from melt compositions equal to their respective bulk host lavas. The more pronounced disequilibrium between the olivine phenocrysts and bulk rock compositions of Pd63, Pd12, and Pd66 suggest that the higher MgO content of these lavas (18.16-21.36 wt.% vs. 14.02-14.56 wt.% for Pd23 and Pd26) may be explained by accumulation of olivine, which likewise explains K_d values >0.3. The major element systematics and the strongly olivine porphyritic nature of the BIP confirm that the bulk lavas have fractionated and accumulated variable amounts of olivine (section 4.3.1). A simple estimate assuming a FeO content of the initial melt similar to the host lavas (10.6-10.8 wt.%) shows that our most primitive olivine of Fo_{90} composition is in equilibrium with melt of ~15 wt.% MgO, which is essentially equal to the bulk composition of Pd23 and Pd26. The most evolved olivine ($Fo_{84.3}$) is in equilibrium with a melt of ~10 wt.% MgO. However, the occurrence of rare olivine with Fo >90 (Francis, 1985; Kent et al., 2004; Yaxley et al., 2004) suggests that the parental melts were more primitive, as is typical in other picrites sequences (e.g. Thomspon & Gibson, 2000). The compositional changes due to olivine fractionation or accumulation are straightforward to model and have been quantified by Yaxley et al. (2004). The compositional range of the BIP analyzed here can be modelled by different degrees (up to 24 wt.%) of olivine fractionation of the parental BIP melt composition. None of the bulk lavas analyzed here seem to represent a likely primary melt composition of the BIP (Pd6 being the least fractionated composition). Instead these lavas correspond to more differentiated melt compositions carrying an olivine load that has been witness to progressive compositional changes due to olivine fractionation (Fo_{93-84}).

Yaxley et al. (2004) showed that the MIs extend the general olivine-controlled fractionation trends defined by host lavas towards lower MgO contents. Further evidence of a strong link between host lavas and MI compositions comes from the observed coherence between trace element systematics of the lavas and their MIs (Figure 4.2-4.4). Lava compositions plot within the field of MIs and show similar, but less extreme styles of trace element fractionation. A significant compositional overlap is observed between the MI spectrums of both *N-* and *E-type*

lavas (Figure 4.7). A close relationship is further suggested by the fact that the whole range of $^{87}Sr/^{86}Sr_i$ compositions can be regenerated by simply mixing the least radiogenic melt compositions with the most radiogenic composition (Figure 4.8). Hence, there are many supporting chemical characteristics for a strong petrogenetic link between the MIs, their olivine and lava hosts.

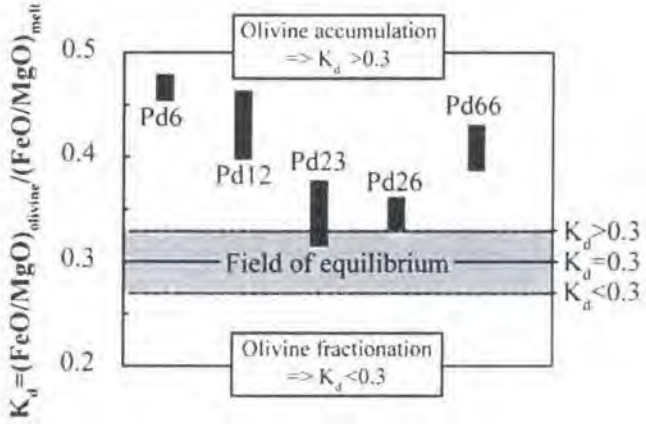

Figure 4.6: FeO and MgO relationship between BIP and their respective olivine phenocrysts. The graphic illustration shows the range of Fe-Mg distribution coefficient for each olivine-host lava pair. The olivine phenocrysts are expected to fall within the grey field if in equilibrium with their host lavas representing $K_d = 0.3 \pm 0.03$ (Roeder & Emslie, 1970). Olivine accumulation decreases the FeO/MgO of the melt (here the bulk lava) resulting in $K_d > 0.3$.

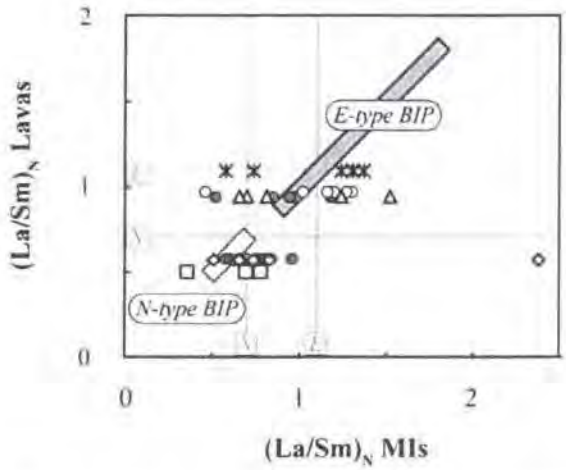

Figure 4.7: This plot show the relationship between the $(La/Sm)_N$ measured in the BIP MIs (x-axis) and their host lavas (y-axis). The $(La/Sm)_N$ range of the *N*- and *E-type* the BIP are shown in the white and grey rectangle. The legend for the individual MIs of this study and Yaxley et al. (2004) is found in Figure 4.3. The grey lines labelled *N* and *E* are the discriminatory boundary line between *N*- and *E-type* lavas by Robillard et al. (1992).

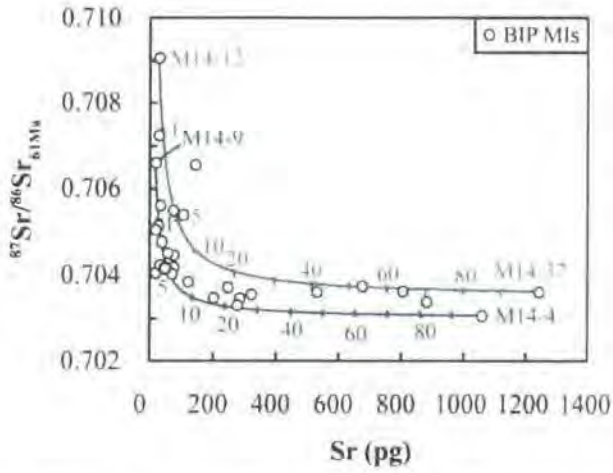

Figure 4.8: Mixing between MIs with highest and lowest $^{87}Sr/^{86}Sr_{61Ma}$ ratios can generate the total spectrum of the MIs of the BIP. Blue line shows mixing between M14-4 and M14-9, and green line mixing between M14-37 and M14-12. Numbers next to ticks on the mixing lines indicate percentages of respective M14-37 and M14-4 required to be mixed with M14-12 and M14-9 to reproduce compositions falling along the mixing lines.

4.7.2 Origin of chemical variations and Sr isotope heterogeneity within melt inclusions

The Sr isotope heterogeneity amongst the MIs of this study demonstrates that they pick up a much more detailed record of melt compositions present within a single magmatic system compared to the host lava suite (Figure 4.4). This is nicely demonstrated when comparing the $^{87}Sr/^{86}Sr_i$ isotope range of these MIs to the BIP, and also to the global range observed among MORB and OIB (Figure 4.9a). Interestingly, the MIs cover almost 3 times (~290%) the Sr isotope range of the global MORB, and ~120% of the OIB range. This is considerably more than the ~30% of the MORB range covered by the host lavas. The probability distribution curves clearly show the bimodal distribution of the BIP MIs versus the unimodal distributions e.g. among OIB from Hawaii and Iceland (Figure 4.9b). Previous studies of the Sr and Pb isotope composition of MIs from OIB have also revealed larger heterogeneities amongst the MIs compared to their respective host lavas (Saal et al., 1998; Kobayashi et al., 2004; Yurimoto et al., 2004; Saal et al., 2005; Jackson & Hart, 2006). This illustrates that MIs record geochemical details which appear hidden (or overwritten) in bulk analyses of the host lavas. Below, we explore the origin of the Sr isotope and trace element diversity among these MIs by looking at the compositional variations existing within the convecting mantle, and the changing '*environment*' (mantle, SCLM, crust, and seawater) to which the melts are subjected during ascent.

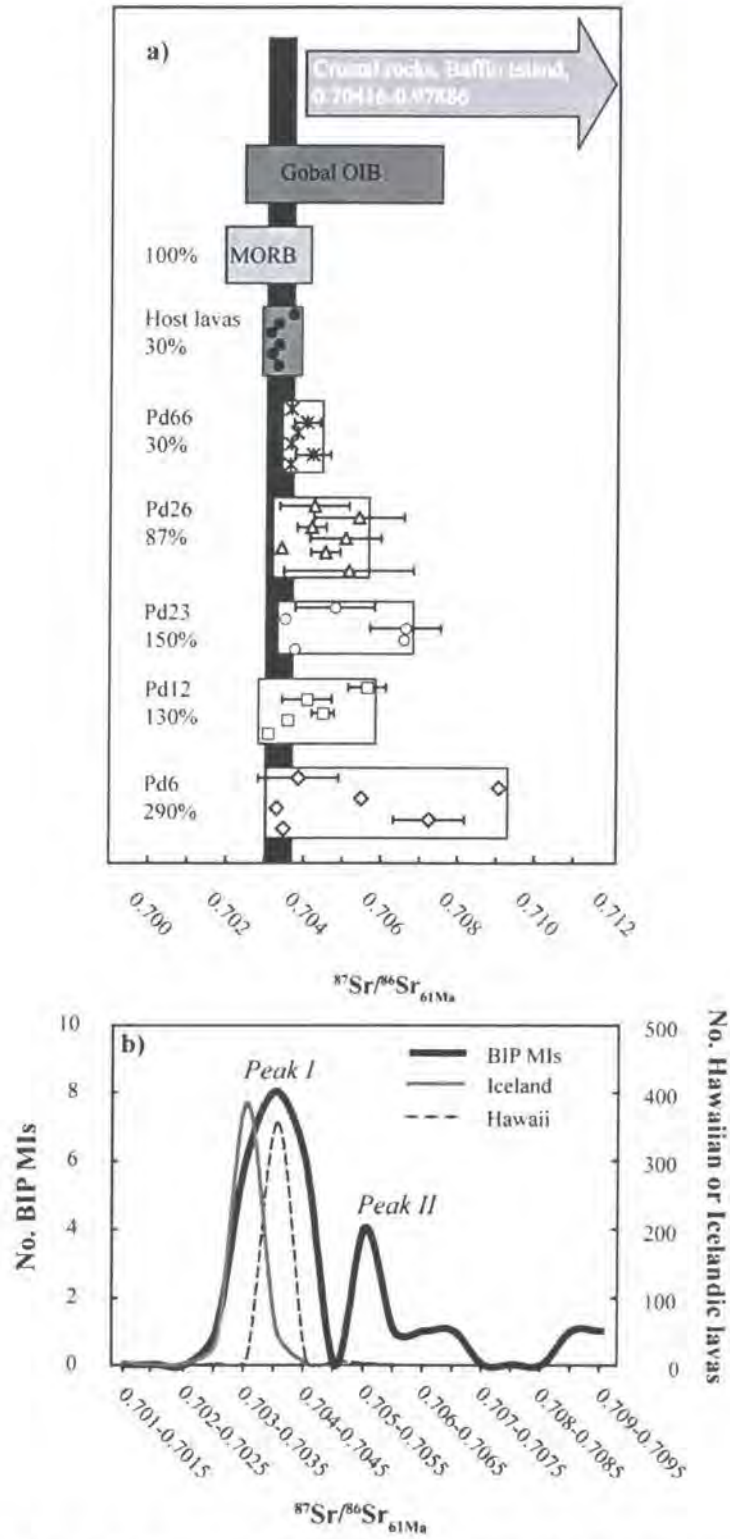

Figure 4.9: a) The $^{87}Sr/^{86}Sr$ range observed within the Baffin Island MIs and host lavas compared to the range of the North Atlantic MORB, Global OIB plus the crustal lithologies of Baffin Island. Vertical black bar shows the $^{87}Sr/^{86}Sr$ range host BIP. The percentages listed below sample ID (to the left of each box) indicate the size of the $^{87}Sr/^{86}Sr$ isotope variation for each '*population*' compared to the Sr isotope range observed for the global OIB (the 2SE error is not included in these calculation). b) Comparison between *bimodal distribution* of $^{87}Sr/^{86}Sr_{61Ma}$ ratios measured in the BIP MIs with the *unimodal distribution* observed e.g. in OIB lavas from Hawaii and Island. The Sr isotope compositions of the OIB lavas of Hawaii and Iceland are the present day values (O Ma). In reality the OIB lavas and the BIP MIs should be compared at the age. However, an age correction would not change the distribution of these lavas. Notice that the BIP MIs refer to the left y-axis and the OIB lavas of Hawaii and Iceland to the right y-axis.

4.7.2.1 Interaction with seawater

As oceanic crust forms it is exposed to chemical exchange with seawater e.g. Staudigel et al. (1995), and Hart et al. (1999). Seawater has a relative radiogenic $^{87}Sr/^{86}Sr$ composition (0.709) and elevated Sr (8100 ppb) and Rb (120 ppb) contents combined with a low concentration of Nd (0.003 ppb) and $^{143}Nd/^{144}Nd$ of 0.51245 (Drever, 1997). Interaction with seawater can strongly affect the $^{87}Sr/^{86}Sr_i$ of a lava, whereas the effect on the Nd budget is negligible (due to the low Nd concentration), hence $^{143}Nd/^{144}Nd$ composition should remain unaffected (except for rock/water ratios over $>10^5$, Figure 4.10b). The subaqueous eruption of the BIP means that these lavas have been exposed to seawater. Percolation of seawater through the BIP after their emplacement may result in more radiogenic Sr isotope compositions of the bulk rocks. Even so, it is unlikely that the MIs are affected, since the olivine crystallization and entrapment of MIs took place prior to extrusion and exposure to seawater. Hence, intact MIs should in general be protected by their host olivine from chemical exchanges with seawater. Simple two component mixing between seawater and respectively the BIP or the MIs show that such interaction is unable to explain the trend towards radiogenic $^{87}Sr/^{86}Sr_i$ and high Rb/Sr of the MIs, nor is the variation between $^{87}Sr/^{86}Sr_i$ and $^{143}Nd/^{144}Nd_i$ of the lavas consistent with seawater interaction (Figure 4.10b and 4.11a-b). Thus, we conclude that the variable Sr isotope compositions, high Rb/Sr of the MIs, and the correlation between $^{87}Sr/^{86}Sr_i$ and $^{143}Nd/^{144}Nd_i$ of the BIP is unlikely to reflect seawater interaction. This suggests, that the Sr isotope variation within the MIs existed prior to eruption thus reflecting mantle source variation, mantle melting and/or assimilation processes during ascent.

4.7.2.2 The convecting mantle

A compilation of the Sr-Nd isotope data of the BIP (*this Chapter*, Stuart et al. 2003, Kent et al. 2004) show that *N-type* lavas plot in the field of DM (represented by North Atlantic MORB), the *E-type* lavas overlap with HIMU or one of the intermediate components (FOZO, C, PHEM), while a few compositions plot towards more enriched mantle values (Figure 4.10a). In contrast to the host lavas, their MIs have Sr isotope compositions revealing much greater variation extending the field toward more extreme radiogenic $^{87}Sr/^{86}Sr$ compositions than those characteristic of melts derived from DM, HIMU, or any or the intermediate mantle components (Figure 4.10a). Thus, it is difficult to explain these radiogenic Sr compositions purely by melting of mantle peridotite (as traditionally thought for basaltic melts), and this implies the involvement of more radiogenic Sr component(s) in the genesis of the BIP e.g. a recycled component such as EMI or EMII. Recent models involving contributions from non-peridotite sources such as pyroxenite veins (streaks of recycled oceanic lithosphere) present within the convecting mantle have been used to explain the certain isotope systematics of OIB and MORB e.g. Allégre & Turcotte (1986), Hauri et al. (1996), Pearson & Nowell (2004). Below we

investigate whether postulated enriched components such as EMI and EMII, or the possible existence of pyroxenite veins within the mantle could produce the more Sr radiogenic signature of the BIP suite.

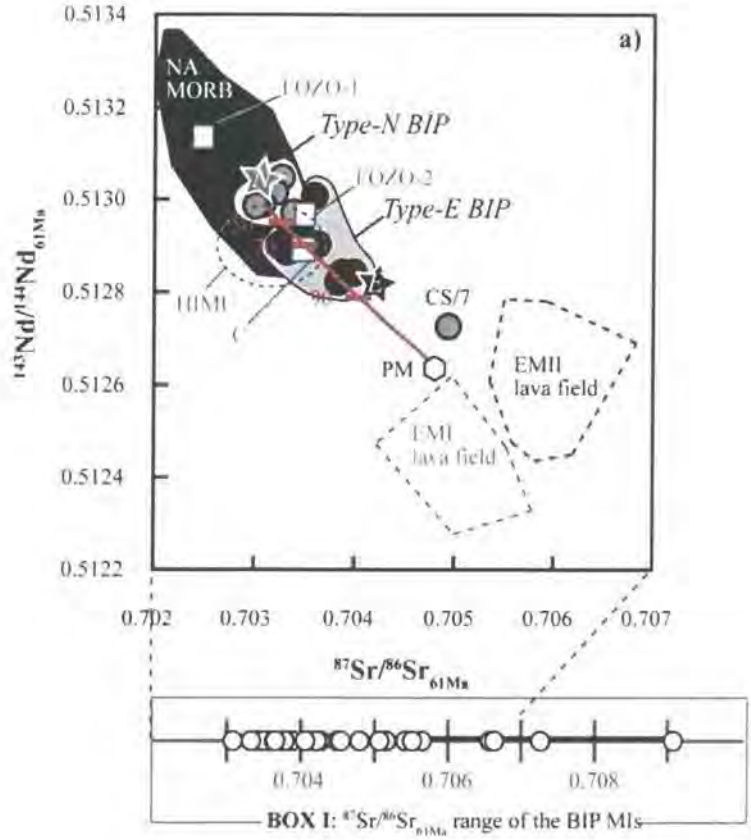

Figure 4.10: The relationship between the initial (61 Ma) Sr-Nd isotope of the MIs (this work) and BIP lavas (Stuart et al., 2003; Kent et al., 2004), and two-component mixing relationships in Sr-Nd space. a) The white and the grey field show respective the groupings of *N-type* (grey circles) and *E-type* (black circles) BIP. Only a single crustal contaminated *N-type* lava (CS/7) plot out side its field (Stuart et al., 2003). The grey star labelled *N* and the black star labelled *E* represent the *N-* and *E-endmember* compositions suggested by Stuart et al. (2003). PM denotes the composition of the primitive mantle (Hofmann, 1997). Shown are also the typical present day fields of the NA MORB, HIMU, EMI, and EMII lavas (Hofmann, 1997). Also, shown are the compositions of the intermediate mantle component known as FOZO-1 (Hart et al., 1992), FOZO-2 (Hauri et al., 1994), or C (Hanan & Graham, 1996). The red mixing line shows mixing between the *N-type* BIP (10013; Kent et al., 2004) and the PM, ticks marks with numbers gives the PM% of the mixture. b) Mixing trends generated between *N-type* BIP and seawater (Drever, 1997), SCLM (264093; Larsen et al., 2003), EMI (Pit89-8; Eisdle et al., 2002), EMII (Workman et al., 2004), and pyroxenite (GP81; Pearson et al., 1993). c) Mixing lines towards crustal components showing the range of expected composition to result from local crustal contamination using Nd isotope data from Thériault et al. (2001) compiled with the Sr isotope compositions obtained in this study. In all three plots ticks on mixing lines indicate in percentage the proportion of the most radiogenic Sr component. One exception are the numbers next to the mixing between seawater and BIP, these numbers give the seawater/rock ratio. The field marked by a grey broken lines show the view of a) in b) and c). For comparison in c) the fields of respective crustal contaminated and non crustal contaminated picrites of West Greenland (WGP) are included (Lightfoot et al., 1997). BOX I shows the range of $^{87}Sr/^{86}Sr_i$ of the BIP MIs, each MI is shown by an open circle. BOX II shows the maximum changes in Sr-Nd isotope ratios due to radioactive decay. Overall, the 61 Ma Sr-Nd isotope ratios (of PM, EMI, EMII, seawater, GP81, and the lave fields of NA-MORB, HIMU, EMI and EMII) lie within <0.07% and <0.06% of the present day (0 Ma) values used in the modelling. All other Sr and Nd isotope ratios used in the modelling are the initial ratios (61 Ma).

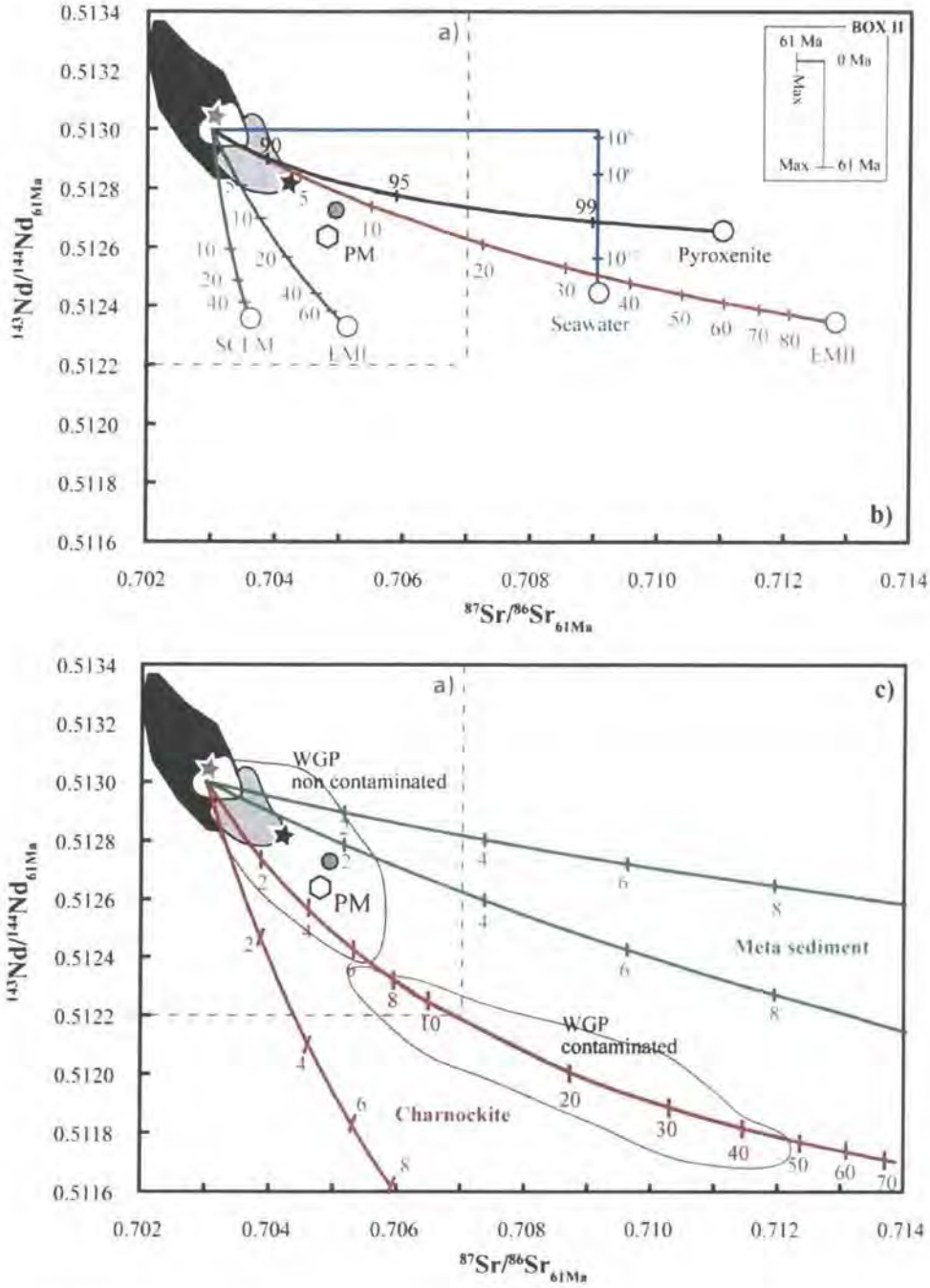

Figure 4.10: Continued

Workman et al. (2004) estimate the '*pure EMII*' component to have $^{87}Sr/^{86}Sr$ of 0.7128, $^{143}Nd/^{144}Nd$ of 0.51235, $(Rb/Sr)_N$ of 6.24, and extreme LREE/HREE e.g. $(La/Y)_N$ of 21.4. In comparison EMI has moderate $^{87}Sr/^{86}Sr$ (0.705-0.7055), similar $^{143}Nd/^{144}Nd$ of (0.5123-0.5125), combined with lower $(Rb/Sr)_N$ and possibly more extreme LREE/HREE (Weaver, 1991; Eisele et al., 2002). Lavas and olivine-hosted MIs flavoured by a EMI or EMII signature typically have intermediate to very radiogenic Sr isotopes, high Rb/Sr combined with LILE/HREE and LREE/HREE enrichment e.g. Weaver (1991), Eisele et al. (2002), Workman et al. (2004), Jackson & Hart (2006). If the radiogenic endmember of the BIP is EMI or EMII a maximum of

up to 5% and 20% respectively is required to reproduce the whole Sr isotope spectrum of the BIP (sample CS/7 excluded, Figure 4.10b). An even larger proportion of EMII component is required to mimic the $^{87}Sr/^{86}Sr_i$ of the most radiogenic MI composition (~40%), whereas the EMI fails to regenerate $^{87}Sr/^{86}Sr_i$ >0.7052 and thus cannot explain the most radiogenic MIs. Such a sizeable contribution from an EMII component should be reflected by enriched multi element patterns as for example observed for the EMII type MIs from Malumalu (Samoa) documented by Jackson & Hart (2006); however this is not compatible with the slightly enriched to depleted MIs and BIP compositions (Figure 4.2-4.3). The enriched characters of both EMI and EMII result in mixing trends predicting too high LREE/HREE at a given $^{87}Sr/^{86}Sr_i$ ratio (Figure 4.11a), and therefore both EMI and EMII are precluded as the possible radiogenic Sr endmembers of the BIP suite.

Pyroxenite veins display variable Sr isotope compositions from depleted compositions to $^{87}Sr/^{86}Sr$ ratios >0.711 e.g. Pearson et al. (1993), offering an alternative source of more radiogenic Sr. Other characteristics of pyroxenites are their very radiogenic Os isotope compositions, variable $\delta^{18}O$ values (4.9-9.4‰), and highly variable LREE/HREE depletion (Pearson & Nowell, 2004). Thus, it should be a straightforward matter to test if the elemental and isotope variability within the MIs could be caused by the existence of pyroxenite in the source region of BIP. A mixing trend calculated between a pyroxenite with radiogenic Sr (GP81, Pearson et al., 1993) and the most depleted BIP composition is shown in (Figure 4.10b, 4.11a-b). Given the low $(Rb/Sr)_N$ of the pyroxenite, unrealistic amounts (>90%) of pyroxenite are required to generate the Sr-Nd isotope variations of the host BIP and >99% of pyroxenite is needed to generate the more radiogenic Sr isotope compositions of the MIs. In addition, such a dominating contribution of pyroxenite-derived melts should be directly reflected by radiogenic Os isotope compositions, which contrasts with the unradiogenic $^{187}Os/^{188}Os_i$ nature of the BIP (0.1241-0.1303) documented by Kent et al. (2004). Furthermore, the low Rb/Sr and low LREE/HREE ratios of the pyroxenite makes this model fail to copy the overall systematic of trace elements observed within the MIs (e.g. La/Sm, La/Y, and variable Rb/Sr, Sr/Nd, Ba/Y values, Figure 4.11a-b). Hence, the existence of pyroxenite in the source region of BIP is inconsistent with the chemical properties of their MIs. The modelling further suggests that the component involved must posses a more radiogenic Sr isotope composition in addition to an elevated Rb/Sr ratio compared to typical pyroxenites.

4.7.2.3 Contamination by the subcontinental lithospheric mantle

The SCLM represents a reservoir separate from the convecting mantle, whose mineralogy and geochemistry is governed by ancient removal of basaltic melt, and the possible interaction of the residues with percolating melts or fluids (metasomatism). Evidence for interaction of picritic NAIP magmas with the SCLM has been found in the contemporaneous alkali picrites of West

Greenland (Larsen et al., 2003). Given their close proximity (both in time and space) such a scenario could also be true for the BIP. As a proxy of the SCLM in the Baffin Island region, an alkali basalt from West Greenland (264093) is used, which is thought to be derived from the SCLM (Larsen et al., 2003). Mixing with the SCLM component (Figure 4.10b and 4.11a-b) generates a trend toward moderate Rb/Sr and $^{87}Sr/^{86}Sr$, but the compositions generated are not as extreme as the most radiogenic MIs at high Rb/Sr (*Group-II*). Both *N-type* and *E-type* BIP plot above this mixing trend indicating that the SCLM composition affecting the West Greenland melts also has too low $^{87}Sr/^{86}Sr_i$ to be a suitable endmember of the BIP lava suite. More extreme $^{87}Sr/^{86}Sr$ ratios have been reported from SCLM lithologies (see Pearson et al., 2003 for review), but these extreme isotope compositions are characterised by very low Sr and Nd concentrations (Pearson & Nowell, 2002) and are not suitable magma sources for tholeiitic basalts. Lastly, the relatively depleted Nd isotope compositions of the BIP combined with the $^{187}Os/^{188}Os_i$ of around bulk Earth do not indicate involvement of SCLM in the genesis of the BIP (Kent et al., 2004). Hence, these findings support Kent et al. (2004) who found the Nd-Os systematics of the BIP are incompatible with contributions from the SCLM.

At this point, the simplest of explanations is that mantle source heterogeneities or melt contributions from several source components lead to a spectrum of heterogeneous liquids, which are sampled by the BIP MIs. The heterogeneities documented by olivine-hosted MIs sampling this melt spectrum, provided that MIs are kept isolated until the point of crystallisation, should match and map onto the heterogeneity in the host liquids. The fact that the BIP MIs are far more heterogeneous than the host lavas argues that additional variability is introduced after the parental melt spectrum has formed.

4.7.2.4 Contamination by continental crust

The compositional diversity of the Baffin Island MIs may result from interaction with the local continental crust during magma ascent. Compositionally, the continental crust makes up the other extreme end of the isotope spectrum, where the DM is its counterpart. Over time the crust has attained low $^{3}He/^{4}He$ (due to degassing and enrichment in U and Th), high $^{87}Sr/^{86}Sr$ (high Rb/Sr), low $^{143}Nd/^{144}Nd$ (low Sm/Nd), low $^{176}Hf/^{177}Hf$ (low Lu/Hf), high $^{187}Os/^{186}Os$ (high Re/Os). The relatively unradiogenic $^{87}Sr/^{86}Sr_i$ nature of the parental melts of BIP combined with their relatively flat multi-element patterns, strongly contrast with the radiogenic $^{87}Sr/^{86}Sr_{61Ma}$ and trace element enriched character of the crustal rocks of Baffin Island (Figure 4.2-4.4), and suggest that melts of these rocks provide a likely source of contamination. $^{143}Nd/^{144}Nd$ isotope compositions collected on crustal rocks from southern Baffin Island further show that these rocks have very low 0.510269-511668 (Thériault et al., 2001). Thus, assimilation of small amounts of crustal material should have a measurable compositional effect on the initial BIP

melts. In particular Sr-Nd isotope and $(Rb/Sr)_N$ systematics should be sensitive indicators of crustal assimilation.

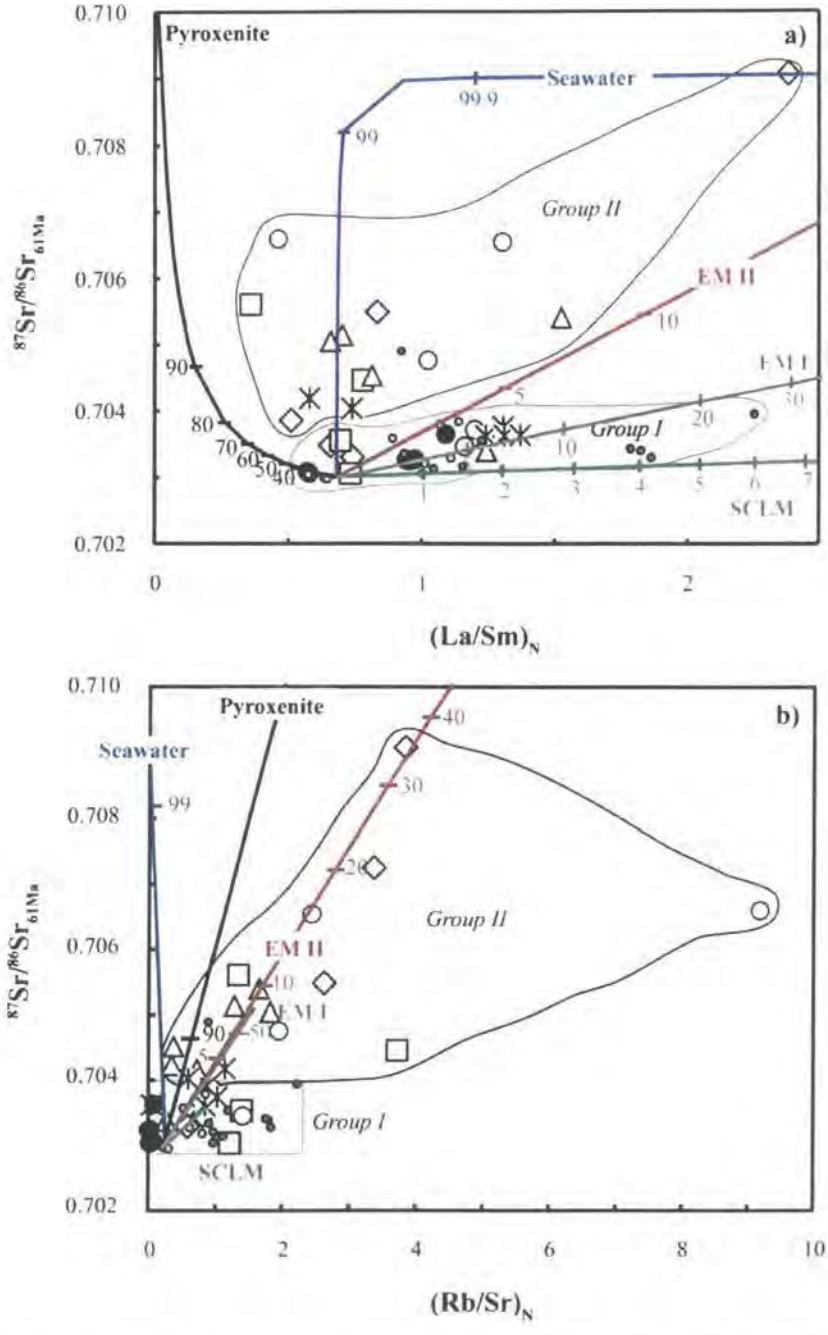

Figure 4.11: Continued a) and b) shown the mixing relationships with EMI, EMII, pyroxenite, SCLM plus seawater in respective $(La/Sm)_N$ vs. $^{87}Sr/^{86}Sr$ and $(Rb/Sr)_N$ vs. $^{87}Sr/^{86}Sr$ space. Modelling of contamination of the BIP melts by various crustal lithologies found at Baffin Island respectively in c) $(La/Sm)_N$ vs. $^{87}Sr/^{86}Sr$ and d) $(Rb/Sr)_N$ vs. $^{87}Sr/^{86}Sr$. Legend is as in Figure 4.3, and the source rock references are found in the caption of Figure 4.10. *Group-I* and *Group-II* are explained in section 4.6.4.

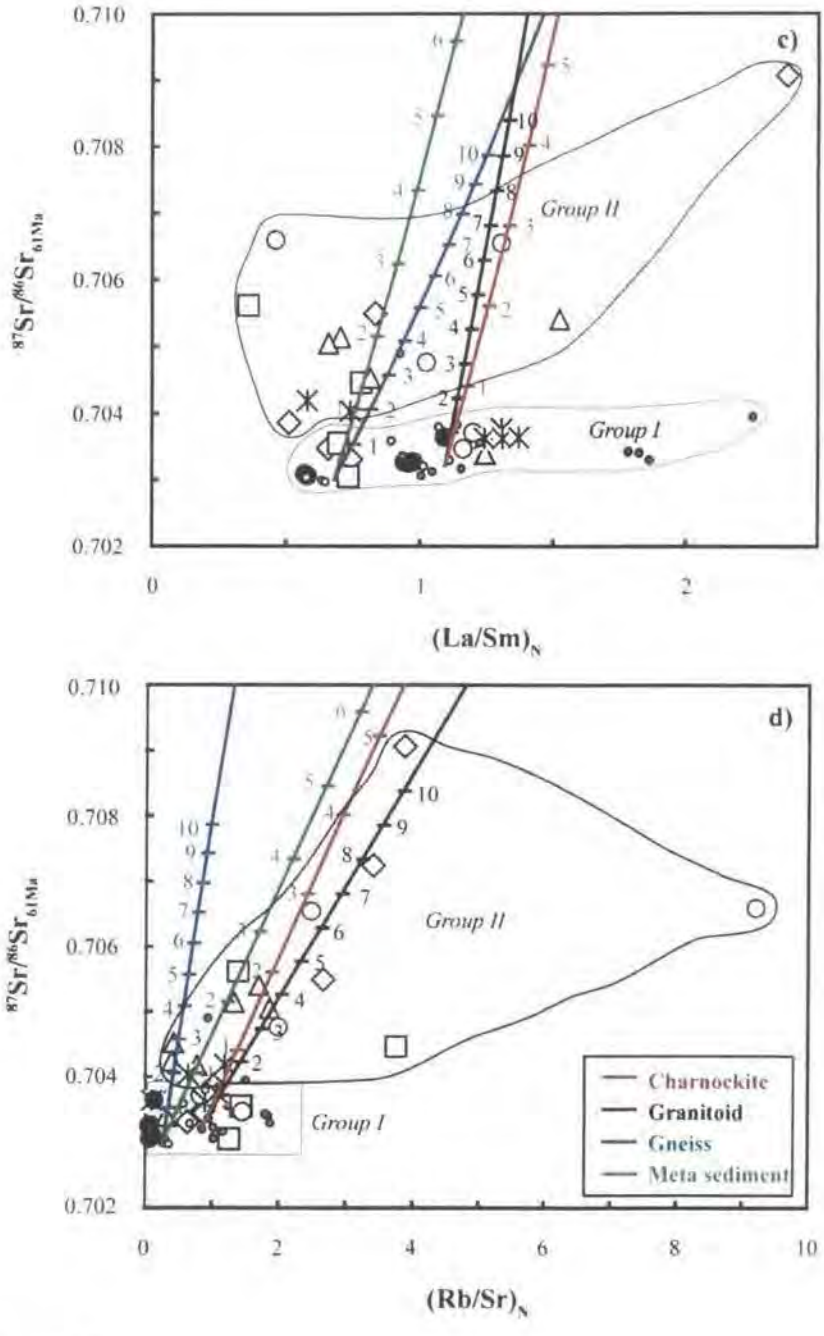

Figure 4.11: Continued

Mixing calculations between crustal components and the BIP compositions are presented in Figure 4.10c and 4.11c-d. The trend towards elevated $(Rb/Sr)_N$ and radiogenic $^{87}Sr/^{86}Sr_i$ displayed by *Group-II* MIs is consistent with a maxima of 5 to 10% crustal contamination by any of the crustal rocks analyzed, whereas the Sr-Nd systematics of the BIP (in particular sample CS/7) requires 2-4%. Also the variable Ba/Y ratios of the MIs can be related to contamination by various lithologies (Figure 4.4c and 4.4e). In particular, one of the charnockites (JD70-E256) seems very effective at generating a mixing trend matching the MIs with high $(Ba/Y)_N$ at lower $^{87}Sr/^{86}Sr_{61Ma}$ values. Likewise, high $(Ba/Y)_N$ combined with

intermediate $^{87}Sr/^{86}Sr_{61Ma}$ compositions are generated by assimilation of the gneisses and a metasediment (JD70-258-1), (Figure 4.4e). Contamination by any of the other crustal lithologies would generate compositions with lower $(Ba/Y)_N$ ratios at more extreme $^{87}Sr/^{86}Sr_{61Ma}$. The mixing models show that $(Sr/Nd)_N$ ratios are less affected by crustal contributions. Most of the crustal rocks have lower $(Sr/Nd)_N$ than the BIP and their MIs, and incorporation of partial melts of these lithologies will lower the $(Sr/Nd)_N$ ratios (Figure 4.3b and 4.3d). The only assimilants that can increase the $(Sr/Nd)_N$ are the granitoids (JD70-C280 and JD70-E418) with extreme, high $(Sr/Nd)_N$ (Figure 4.3). The effect on the LREE/HREE and LREE/MREE ratios from crustal input is a moderate increase (Figure 4.11c). The MIs with the highest $(La/Y)_N$ and $(La/Sm)_N$ are best modelled by contamination of crust with moderately radiogenic Sr combined with high LREE/HREE ratios e.g. charnockite (JD70-E256), metasediment (JD70-294-1, JD70-294-2, or JD70-303-2), or gneiss (JD70-214-1).

The lack of enrichment of whole rock lavas in K/Nb and $^{87}Sr/^{86}Sr$ was used by Kent et al. (2004) to argue against significant assimilation of crustal material by the BIP. Their argument is that the increase in $^{87}Sr/^{86}Sr$ is accompanied by too strong an increase in K/Nb, which is beyond what is observed for the BIP. However, the Sr isotope composition of their modelled crustal component is set at 0.710, which is very low compared to the $^{87}Sr/^{86}Sr_{61Ma}$ composition of the local crustal analyzed in this study (0.7148-0.9753; Table 4.8). If more radiogenic $^{87}Sr/^{86}Sr_{61Ma}$ values are used as proxies of crustal components smaller amounts of crust are needed to generate the observed enrichment in both K/Nb and $^{87}Sr/^{86}Sr$, and hence assimilation of crust can be compatible with the K/Nb systematics. Overall, Yaxley et al. (2004) showed, that the K/Nb ratios of the MIs are higher (85-742, average of 311) than the host lavas (166-207, average of 189, Kent et al., 2004). The higher K/Nb values of the MIs are thus consistent with crustal contamination. This has also been observed in whole rock suites of other NAIP magmas (Holm et al., 1993; Lightfoot et al., 1997). It is clear that the crustal signature is stronger in the MIs than in their host lavas, suggesting that there is a variable degree of assimilation throughout the channelling system of BIP.

Note, that the presented models are oversimplified by the fact that bulk mixing was used in the modelling whereas some crustal Sr could enter magmatic systems via incongruent melting cf. Knesel & Davidson (2002). One extreme example of selective melting of a particular mineral phase could be phlogopite, a mineral phase with high Rb/Sr, which is likely to introduce high Rb/Sr combined with radiogenic Sr isotope composition. Phlogopite has a very characteristic trace element composition, thus upon melting this would generate enrichment of Cs, Rb, Ba, K and Ti (Sun & McDonough, 1989). Such enrichment patterns are not observed among the BIP melts (Figure 4.2). Despite its simplicity, our modelling indicates that Sr-Nd isotope compositions, the Rb/Sr, Ba/Y and K/Nb ratios of MIs can be explained by addition of crustal

material, but it is difficult to be specific about the identity of the crustal rocks involved. Mixing calculations show that both host lavas and MIs, in particular those of *Group-II*, have assimilated crustal material, and that the local crust provides suitable sources of radiogenic Sr observed within the BIP MIs.

4.7.3 Source variation and melting systematics

The modelling above shows that the more extreme Sr isotope compositions and high Rb/Sr ratios of *group-II* MIs are likely to be generated by crustal assimilation (Figure 4.10-4.11). However, the crustal contributions are less efficient at explaining the differences in LREE/HREE between *N-* and *E-type* melts (Figure 4.11c). Variable fractionation of HREE over LREE may instead relate to variation in melting systematics, the chemistry of the source region(s), and possible mixing of melts derived from several sources. To evaluate the possibilities, we model the trace element variations generated by variable degrees of batch, factional, and critical melting of a fertile garnet peridotite in Figure 4.12. The chosen peridotite composition (KR4003, Walter, 1998) is suggested to be representative of the primitive upper mantle (McDonough & Sun, 1995).

While fractional and batch melting are unable to explain the overall trace element variation in the MI suite (Figure 4.12a-b), various permutations of batch melting are possible, but non-unique. A good match for the REE variations among the most enriched MIs can be obtained by 10% critical melting at 3 GPa of a PM source (α = 5%), whereas the more depleted compositions can be generated by 5-8% critical melting or 7-12% melting of a DM source with 2 or 5% melt retained respectively (Figure 4.12c-d). However, the linear relationships between the enriched (*E-type*) and depleted (*N-type*) compositions produced by critical melting models suggest that all compositions in between the '*end-compositions*' can mix to produce the spectrum of MI compositions.

4.7.3.1 Two component source

The result of the trace element modelling for the MI suite studied here agrees with previous studies of BIP, that have suggested mixing of melts derived from a heterogeneous mantle or from two discrete sources (Robillard et al., 1992; Stuart et al., 2003; Kent et al., 2004). Melting calculations show that it is difficult to distinguish the *N-type* from *E-type* melts based only on La/Sm systematics, since this characteristic not only reflects the sources, but also varies due to melting degree. Compiling the Sr-Nd data from Baffin Island including both MIs and lavas (Robillard et al., 1992; Stuart et al., 2003; Kent et al., 2004) shows that the depleted component has non-radiogenic $^{87}Sr/^{86}Sr_i \sim 0.7030$ at relatively radiogenic $^{143}Nd/^{144}Nd_i \sim 0.5130$, and the more enriched mantle component has a more radiogenic $^{87}Sr/^{86}Sr_i > 0.7032$ and a lower $^{143}Nd/^{144}Nd_i \sim 0.5129$-$0.5128$. However, none of the three binary melting models are able to

match the more extreme MI compositions with high $(Rb/Sr)_N$, $(Sr/Nd)_N$, $(Zr/Y)_N$, or $(Ba/Y)_N$ at a given $(La/Sm)_N$. Neither can they account for the more radiogenic $^{87}Sr/^{86}Sr_i$ compositions. As shown in the previous section, these more extreme compositions require variable degrees of crustal contamination. Thus, the full spectrum of MI compositions appears to be best explained by a combination of a two-component source region and the effects of crustal inputs. Hence, the compositional variation of *Group-I* MIs mainly reflect mixing between *N-type* and *E-type* melts, whereas *Group-II* MIs requires a crustal input superimposed on the process which produces *Group-I* MIs.

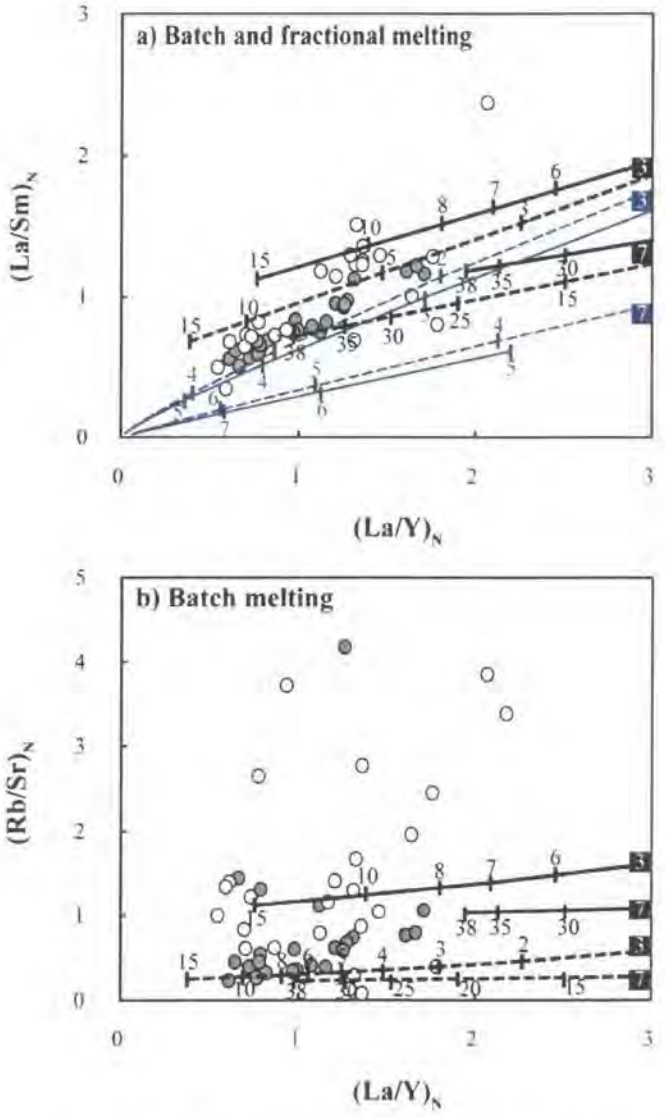

Figure 4.12: Melt trends generated in $(La/Y)_N$ vs. $(La/Sm)_N$, and $(La/Y)_N$ vs. $(Rb/Sr)_N$ space. a) and b) batch melting (black trends) and fractional melting (blue trends), c) and d) critical melting with respective α = 2% (green trends) or α = 5% (black trends). α gives the % melt retained within the source region. The source rock used is a fertile garnet peridotite (KR4003; Walter, 1998), phase assemblages and melt reactions at 3 and 7 GPa are from (Walter, 1998). The partition coefficients used are from Gurenko & Chaussidon, (1995) and McKenzie & O'Nions (1995). Broken lines indicate melt trends generated of a mantle with a depleted signature, and unbroken lines represents melts a PM (McDonough & Sun, 1995). For simplicity all of the MIs of this study is show by open circles, the MIs of Yaxley et al. (2004) are show by grey circles.

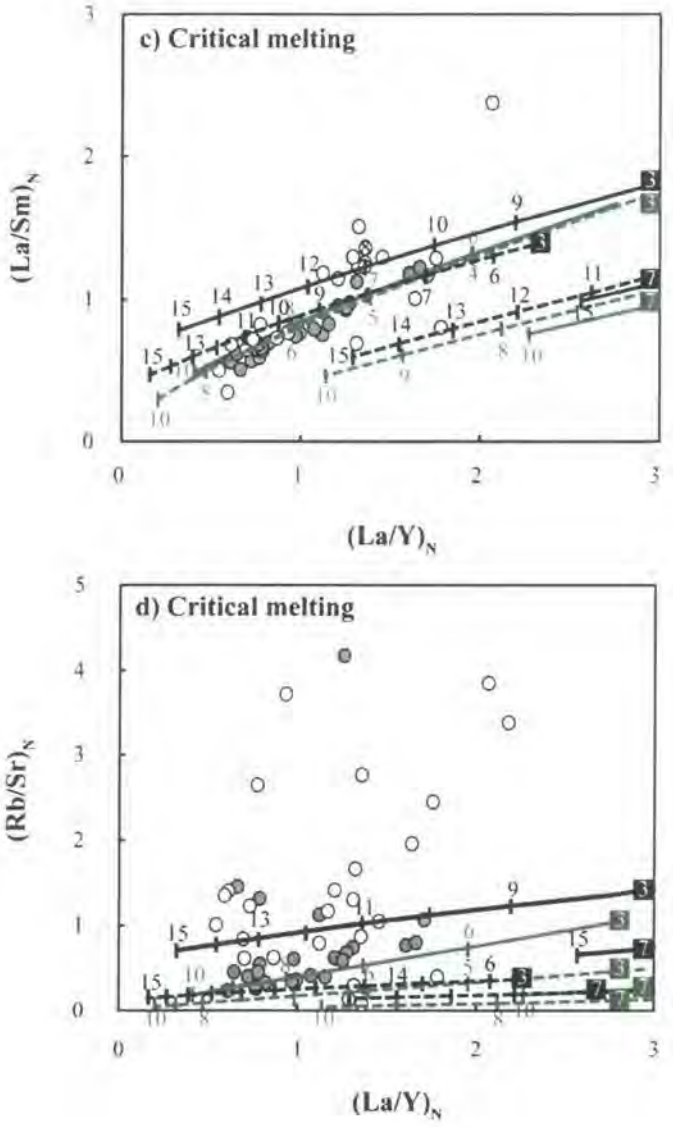

Figure 4.12: Continued

4.7.4 Possible implication for He isotope variations

Multiple He isotope studies on olivine separates from NAIP lavas show that an extreme, high ^{3}He signature is widespread, e.g. unradiogenic $^3He/^4He$ as high as 49.5 R/R_a are documented from BIP Stuart et al. (2003), Graham et al. (1998) report 30.6 R/R_a for the picrites of West Greenland, and preliminary studies by Starkey et al. (2007) report ~50 R/R_a for the picrites of West Greenland, 18.1 R/R_a for the alkaline lavas of East Greenland (Peate et al., 2003), 22.1 R/R_a for lava field of Skye (Stuart et al., 2000), and the ankaramites of Vestfirdir reach 37.7 R/R_a (Hilton et al., 1999; Breddam & Kurz, 2001) to 42.9 R/R_a (Breddam et al., in prep). The extreme unradiogenic He signature may be traced even further back than the NAIP volcanic activity (post 65 Ma), as $^3He/^4He$ determinations of olivine from 600 Ma kimberlites from West Greenland have 26.6 R/R_a (Tachibana et al., 2006).

The unique character of primary MIs and gas inclusions is that they preserve snapshots of the compositions present at the time of entrapment e.g. Nielsen et al. (1998). This study and that of Yaxley et al. (2004) document that the MIs in early-formed olivine phenocrysts of the BIP preserve a higher resolution picture of the compositional diversities of the earliest stages of this magma plumbing system than is evident from examination of the host lava suite. A strong genetic link is documented between the host BIP, their olivine crystals, and MIs (section 4.7.1). Distinct isotope, major and trace element characteristics describe the two melt types found within the BIP and are recognized in both host lavas and MIs (section 4.6). The He analyses of Stuart et al. (2003) show that the *N-type* olivines carry unradiogenic He signature $\leq$50 R/R_a, whereas *E-type* olivines hold more radiogenic $^3He/^4He$ ratios $\leq$38 R/R_a (Figure 4.13a). If the MIs affected by crustal contamination (*Group-II*) are excluded, we see that the *E-type* lavas dominantly host *E-type* MIs, and the *N-type* lavas dominantly contain *N-type* MIs (Figure 4.13b). We also know from experiments that the olivine-melt partition coefficient for He is <<0.01 (Hiyagon & Ozima, 1986; Marty & Lussiez, 1993; Brooker et al., 2003; Parman et al., 2005), which means that the He signature is preferentially recorded by melt or gas inclusions e.g. Roedder (1984), Kurz et al. (1996). Hence, we are confident that the He signatures held within olivine-hosted MIs also link directly to the major, trace, and isotope compositions of their MIs, and thus are characteristic of their mantle source. This assumption is also true if the He is partly contained within gas inclusions (hosted by olivine phenocrysts), since these segregated simultaneously and from the same melt as the MIs.

Except for the primitive He signature of the *N-type* lavas, the other isotope tracers such as Sr-Nd-Os and O plus trace elements strongly indicate a depleted upper mantle signature. The depleted nature is inconsistent with previous mantle models suggesting that excess ^3He is indicative of contributions from undegassed primordial mantle (e.g. Graham, 2002). This raises the question of whether the extreme $^3He/^4He$, coupled with low He concentrations could be a secondary feature. Dismissing the likelihood of the *N-type* lavas being derived from an undegassed primordial mantle source, Stuart et al. (2003) suggest that the unradiogenic $^3He/^4He$ ratio of the DM reservoir is due to '*He-recharging*', or due to mixing with He-rich unradiogenic melts derived from a primordial mantle component. Importantly, the mechanism that introduced the high ^3He did not seem to modify the other isotope and trace element characteristics of the depleted source. The preferred model proposes a '*He-recharged*' DM (HRDM) to be a hybrid mixture of small amounts (<10%) of unradiogenic He rich primordial mantle and radiogenic low He DM (Stuart et al., 2003; Ellam & Stuart 2004, section 3.6.3). This model requires the ^3He rich component to contain 50-100 times more He than the DM. The trace element and Sr isotope data for MIs from *N-type* lava presented here are consistent with such a model.

The *E-type* melts appear to represent an enriched mantle average (EMA) derived from small degree melting of enriched domains with high $^{87}Sr/^{86}Sr_i$, and low $^{143}Nd/^{144}Nd_i$, but MORB-like $^{3}He/^{4}He$ of 8 R/R_a (Stuart et al., 2003; Ellam & Stuart 2004). The MI data of this study is also consistent with this origin. Compiling the BIP whole rocks with the volcanics of NAIP, Ellam & Stuart (2004) propose that the whole proto-Iceland plume (PIP) trend (defined by the correlation in He-Sr and He-Nd isotope space) represents mixtures between HRDM, EMA, and DM (Figure 3.8). The authors further speculate that HRDM may represent an endmember of the global OIB-CFB trend.

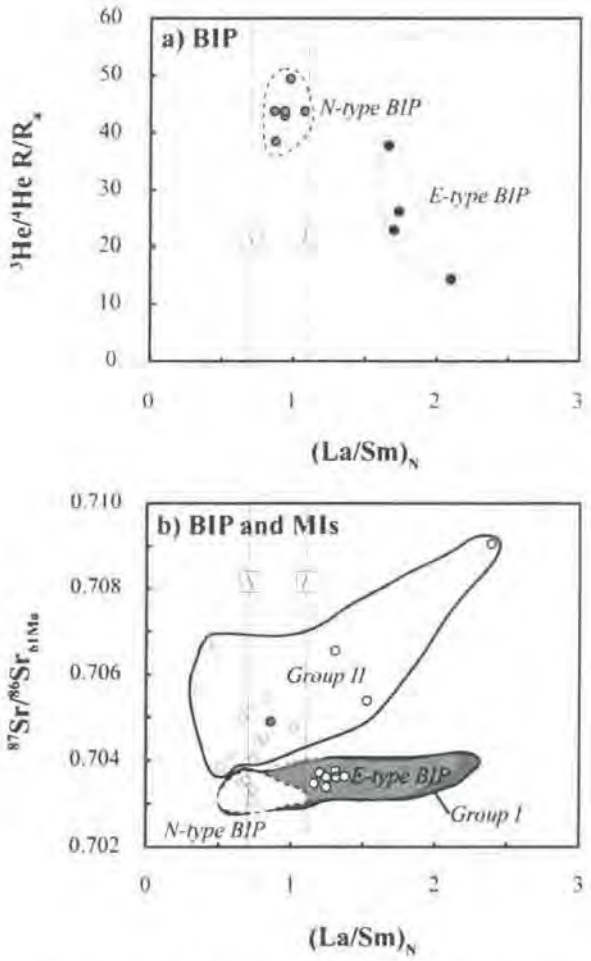

Figure 4.13: a) Correlation of $(La/Sm)_N$ and $^{3}He/^{4}He$ for the BIP with relationship to *N-type* and *E-type* lavas (Stuart et al., 2003). b) $(La/Sm)_N$ vs. $^{87}Sr/^{86}Sr$ plot show that *N-type* MIs (open grey circles) are found in *N-type* lavas, and *E-type* MIs in *E-type* lavas (open black circles). Non-contaminated compositions are described by *Group I*, and contaminated by *Group II* (Section 4.6.4). c) The overall variation between *N-type* and *E-type* lavas in $^{3}He/^{4}He$ and $^{87}Sr/^{86}Sr$ is explained by variation in the source and melting systematic. Displacement away from this main trend toward more radiogenic Sr isotope composition may be due to crustal contamination e.g. CS/7 (Stuart et al., 2003), whereas compositions plotting below this trend may have experienced degassing.

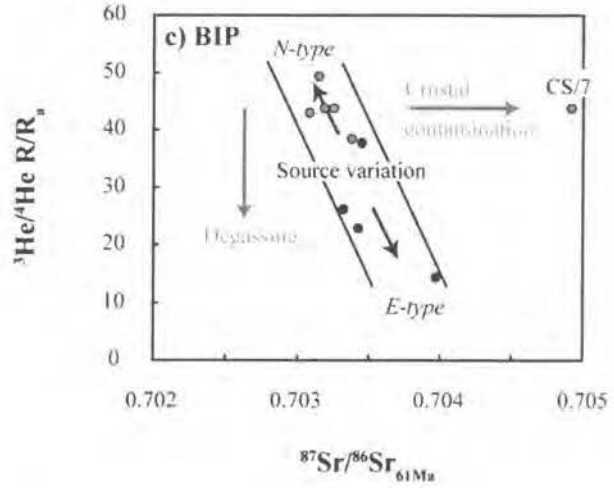

Figure 4.13: Continued

Recently, an alternative model was put forward by Parman et al. (2005) and Parman (2007), which explains how a DM component with high $^{3}He/^{4}He$ and low He concentration signature may be generated. Their experiments indicate that the olivine-melt partition coefficient of He is similar to other mantle minerals (clinopyroxene, orthopyroxene, and garnet), while Th and U strongly partition into clinopyroxene and garnet. In contrast to earlier assumptions, Parman et al. (2005) infer that He is more compatible than U and Th during non-modal mantle melting. Given that the initial reservoir was undegassed, it is therefore expected that upon melting the residues should posses high $^{3}He/^{4}He$ plus extremely low (Th+U)/He (Parman et al., 2005). A melt depleted source is clearly indicated by the trace element and radiogenic isotope systematic of the BIP whole rock and MIs. It seems beyond coincidence that the magmatic province with the most '*depleted*' He isotope signature in the context of the Parman et al. (2005) model should show among the most depleted Sr-Nd-Hf-Os isotope signatures of any intra-plate magmas. Once the effects of crustal contamination are removed, the MI data presented here provides matching, depleted isotope signatures for the He-rich undegassed melts, that dominated the He budget of the BIP magmas.

4.7.5 Generation of Sr isotope heterogeneities in magmatic systems and implications for He isotope analyses of olivine

The BIP MIs show a Sr isotope diversity that is well outside the range for global magmatism thought to originate from the convecting mantle and indicates that a significant proportion of the MIs trapped in the system have extensively interacted with the continental crust (section 4.7.2-4.7.3). A schematic model of a scenario in which such Sr isotope heterogeneities may be generated is presented in Figure 4.14. The initial melting and melt segregation takes place within the upper mantle e.g. for BIP scenario mixing of *N-* and *E-type* melts. As the melt collects it starts to ascend through newly established weaknesses formed due to extension in the overlying lithosphere. Contamination is likely to happen where melt is in contact with crust

along the walls of magma conduits (interaction zones), especially when passing through crustal lithologies with low melting temperatures (e.g. Morrison et al., 1985). Tiny melt parcels trapped near the interaction spot/zone between uprising melt and crust will reflect mixtures of the two components. Entrapment of such composite MIs happens along the periphery of the channelling system, and it is in this environment that we envisage that the MIs of *Group-II* were generated. The central portions of the magma body are less likely to come in contact with the wall rocks. Therefore, MIs formed within the main magma body are more likely to represent uncontaminated melt compositions, and are thus expected to dominantly reflect source characteristics (cf. *Group-I* MIs). Given the different cooling rates (increasing towards the boundaries) crystallization and entrapment of MIs should increase towards the margin of the magma conduits.

As the melt loaded with comagmatic olivine rises through the magma channelling system it may pick up olivine from various zones. Olivine might also be left behind on conduit walls, as the magma moves through the system. This means that the olivine phenocryst population of the resulting lava might not have crystallized from the same melts or from the host lava it was transported by (Danyushevsky et al., 2004). The result is a magma loaded with olivine representing a mixed olivine population that reflect various differentiation levels and degrees of contamination of the several comagmatic batches of rising melts. We would expect that this olivine cargo has variable Sr isotope MI compositions, which may not be fully in equilibrium with the bulk melt composition. The variable Sr isotope composition of the BIP MIs can thus reflect the Sr signatures of the source regions plus variable degrees of contamination by several crustal lithologies.

In this model, a gradual change from more radiogenic $^{87}Sr/^{86}Sr$ to low $^{87}Sr/^{86}Sr$ MI compositions is proposed to form away from the interaction zone, towards the centre of the magma conduit or chamber, as the melts become progressively less contaminated. In contrast to the Sr isotope signature of the olivine-hosted MIs, the dominant Sr isotope signal of the less contaminated carrier melt reflects the source region. This situation can lead to a bulk rock composition that is considerably less affected by crustal interaction than some of the melt parcels trapped as MIs in olivine cf. 2-3% crustal imput in the BIP versus 5-10% in the BIP MIs. If the He inventory of a given rock is dominated by gas-rich MIs then the He isotope signature of an olivine separate from a lava may be considerably more influenced by crustal contamination and degassing, than indicated by analysis of trace elements and radiogenic isotopes from the whole rock. Hence, the effects of crustal contamination on He isotope systematics may be underestimated. In this context it is surprising that the $^{3}He/^{4}He$ of olivines from most BIP are so unradiogenic. This may indicate that the basement had low U+Th, consistent with granulite-facies rocks, and the high metamorphic grade may have resulted in out-gassing of any radiogenic He. The BIP

suggest that $^{3}He/^{4}He$ and the initial Sr isotope signatures recorded by MIs can show a strong correlation in early-formed melts (Figure 4.13c). During ascent, this covariation may (partly) be destroyed in the lavas by contamination and degassing processes (Figure 4.13c). This might be why He is decoupled from other lithophile isotopes in many other studies.

4.7.5.1 General implications of isotope diversity among MIs

The extreme isotope diversity in the BIP MI dataset, with trends indicative of several different contaminants, supports the general model put forward by Danyushevsky et al. (2004), which proposes that anomalous MI compositions are entrapped near the margins of magma plumbing systems where partial dissolution of the wall rock takes place and where the cooling rates are fast. The somewhat large proportion of MIs that appear to be contaminated by continental crust (*1.5:1*) suggests that the probability of MI entrapment in the BIP system may be larger at the conduit margins than at then centre. In well-established systems, where the conduit margins are lined with a mixture of comagmatic crystals and melt (residues of previous rising magma batches), contamination is expected to be less extreme and might not lead to isotope anomalies (Danyushevsky et al., 2004). In this model we may expect to find MI suites that decrease in isotope diversity as the system matures.

Figure 4.14: Schematic illustrations of the Baffin Island setting, in which $^{87}Sr/^{86}Sr$ heterogeneities are generated. a) The conduit system for BIP. b) Enlargement of conduits at the transition between the SCLM and the continental crust (zone III from (a)). Legend below illustrations shows details of each Zone. Zone: I) Upper mantle melting and melt segregation. II) SCLM under extension (due to continental breakup). Zones of weakness develop as a result of the stress (both within the SCLM and the crust above), through which melt conduits form. III) Continued melt ascent through the conduits into the continental lithosphere crust, where ponding in magma chambers may occur, and crystallization of olivine takes place. IV) and V) represent two different crustal lithologies with distinctive radiogenic $^{87}Sr/^{86}Sr$ signatures. VI) Subaqueous eruption of the BIP. VII) and VIII) represent the periphery of conduits (reaction zones) where partial melting of the wall rock may take place as it is interacting with the hot rising melt. This potentially contaminates the rising melt resulting in melt compositions with strongly variable $^{87}Sr/^{86}Sr$ compositions (major and trace element compositions are also affected). Increased cooling facilitates crystallisation of olivine (shown by polygons) and thus the entrapment of MIs (smaller circles). The range of $^{87}Sr/^{86}Sr$ found within the MIs depends on the Sr isotope composition(s) of the contaminant(s), but also on the degree of contamination and contrast in Sr concentration between initial melt and contaminant. Black closed circles represent MIs captured near IV and grey MIs captured near V. IX) In contrast, the melts in the central parts of the magma system are less likely to interact with the local crust, and can therefore remain uncontaminated. MIs entrapped by olivine crystallizing in the central parts of the magma system will inherit the unradiogenic Sr isotope signature of the mantle source region. Uncontaminated MIs are colourless circles. X) The aggregated melts that erupt carry variable collections of olivine phenocrysts picked up from the different zones within the channelling system, some phenocryst may also be left behind. Phenocrysts formed from previous melt that passed through the system, may be incorporated (indicated by broken polygon shapes). Hence, the mixture of olivine phenocrysts provides a variable collection of MIs that sample local Sr isotope variations reflecting a combination of source characteristic and assimilation by crustal lithologies. It is speculated that a Sr isotope gradient can develop towards the edge of the conduits as a result of increasing degree of contamination, but also a gradient in the abundance of olivine phenocrysts plus MIs due to the increasing cooling rate and epitaxial nucleation towards the periphery.

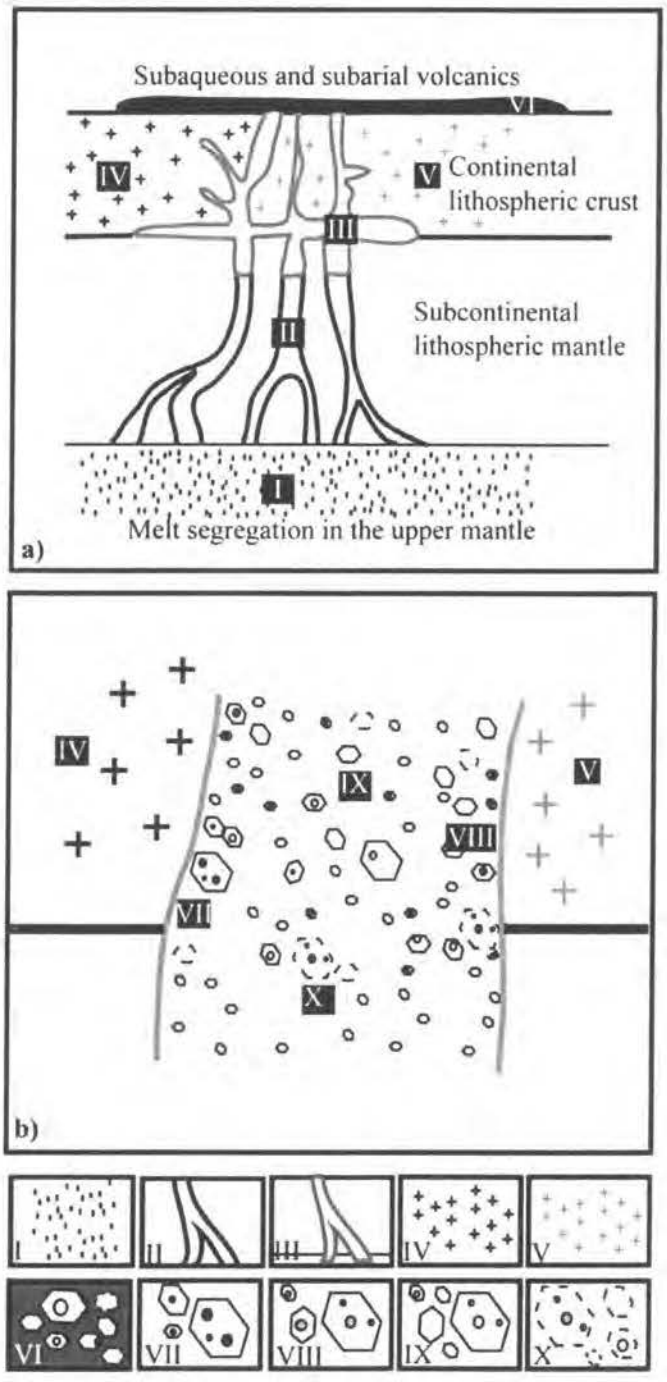

Figure 4.14: See figure caption on previous page.

Clearly, this study shows that the MIs of Baffin Island possess substantial $^{87}Sr/^{86}Sr_i$ variations plus major and trace element variations, strongly advocating the involvement of crustal assimilation *en route*. That these melts are affected by crustal contamination is consistent with the geological setting at Baffin Island, where the lavas erupted through ancient, isotopically diverse continental crust. These lavas represent the initial volcanism in the western part of the NAIP so they could have erupted through immature magma channelling systems. Such newly established systems ought to be more prone to assimilation of crustal material.

This Sr isotope study of individual MIs shows that crustal contamination can be expected to play a role in the genesis of lavas erupting through continental crust also in settings of continental rifting, thus contamination must be considered throughout the NAIP (e.g. Brooks & Nielsen, 1982; Thompson et al., 1984; Pedersen, 1985; Holm et al., 1993; Lightfoot et al. 1997; Kerr et al., 1999; Stuart et al., 2000). This study plus Yaxley et al. (2004) document that the BIP are significantly affected by crustal contamination, with MIs being suggested to have experienced up to 10% crust addition. Variability in major, trace, and Sr isotope composition of the MIs witness that the contamination took place from an early stage - namely during the crystallization of olivine, and not subsequent to olivine crystallization as suggested by Ellam & Stuart (2004). Also, Pb isotope studies of MIs from OIB of Polynesia have revealed large variabilities, which in addition to the involvement of different source components document assimilation of oceanic lithosphere during ascent (Saal et al., 1998; Saal et al., 2005). These findings underscore the difficulty of getting pristine magmas through both continental and oceanic crust without interaction. Preservation of primary melts calls for swift eruptions through well-established magma plumbing systems where the interaction with local wall-rock over time has become hindered by the formation of a mush zone. The heterogeneous nature of the $^{87}Sr/^{86}Sr_i$ isotope ratios combined with complex major and trace element compositions of olivine-hosted MIs of Baffin Island suggests that they, and to a lesser extent the host lavas, witnessed an overprint of crust that masks the source variations. We therefore urge that caution should be applied to the interpretation of isotope, major, and trace element compositional variations in these magmas as being exclusively of mantle origin.

4.8 Summary and conclusions

- Individual olivine-hosted MIs from the BIP reveal large $^{87}Sr/^{86}Sr_i$ isotope variability (0.70306-0.70906) compared to the modest range of their host lavas (0.70308-0.70366). These MIs are also shown to display larger variations in trace element compositions e.g. elevated $(Rb/Sr)_N$, $(Ba/Y)_N$, $(Sr/Nd)_N$. Two compositional groups are recognized based on the systematic relationship between $^{87}Sr/^{86}Sr_i$ and $(La/Sm)_N$, $(Rb/Sr)_N$, and $(Ba/Y)_N$. *Group-I* MIs have unradiogenic to moderate $^{87}Sr/^{86}Sr_i$ ratios over the range of $(La/Sm)_N$, while *Group-II* MIs more extreme $^{87}Sr/^{86}Sr_i$ ratios and display significantly higher $(Rb/Sr)_N$ and $(Ba/Y)_N$ ratios.

- Based on major, trace and Sr-Nd-Os isotope compositions of the lavas the BIP are shown to be mixtures between *N-type* and *E-type* melts derived from respectively a DM ($^{87}Sr/^{86}Sr_i$ <0.7032, $^{143}Nd/^{144}Nd_i$ >0.51299, and $^{187}Os/^{188}Os_i$ of 0.1220-0.1247) and a more enriched ($^{87}Sr/^{86}Sr_i$ of 0.7032-0.7039, $^{143}Nd/^{144}Nd_i$ <0.51296, and $^{187}Os/^{188}Os_i$ of 0.1261-0.1303) mantle source (e.g. Francis, 1985; Robillard et al., 1992; Kent et al.,

2004; Yaxley et al., 2004). These relatively subtle Sr isotope compositions of the two endmembers are consistent with the $^{87}Sr/^{86}Sr_i$ isotope range of *Group-I* MIs, but cannot account for the more radiogenic $^{87}Sr/^{86}Sr_i$ ratios of the *Group-II* MIs.

- Modelling shows that the large range of $^{87}Sr/^{86}Sr_i$ ratios among the *Group-II* MIs are impossible to generate by mixing melts purely derived from components found within the convecting mantle. The involvement of recycled lithosphere components (HIMU, EMI, EMII, and pyroxenite) and SCLM are likewise inconsistent with the data. Contamination by seawater during the subaqueous emplacement of the BIP provides a potential source of radiogenic Sr, but the low Rb/Sr of the seawater is inconsistent with *Group-II* MIs having both high $^{87}Sr/^{86}Sr_i$ and Rb/Sr. Instead, Sr isotope variability of the MIs is consistent with contamination by local crustal lithologies, and requires 0-10% crustal material. In contrast, the variation among the host lavas can be accounted for by assimilation of 2-4% crustal material. Our findings are thus in agreement with Yaxley et al. (2004), and provide clear evidence for a significant crustal overprint on the BIP olivine-hosted MI population.

- Variation of $^{87}Sr/^{86}Sr_i$ and $(La/Sm)_N$ cannot be modelled by input of a single parental melt plus melt contributions from crust. Such variations require melting of a two-component source region as suggested by the previous BIP studies. The best fit for the slightly enriched melt compositions were obtained by ~10% critical melting (leaving 5% melt in the source region) at 3 GPa of garnet peridotite source having a PM signature. The depleted melts were matched by 5-12% critical melting (leaving 2-5% melt in the source region) of depleted garnet peridotite, also at 3 GPa. The linear relationship between the *E-type* and *N-type* MIs show that these melts mixed, and it is also consistent with the *N-type* and *E-type* source components existing in close proximity of each other.

- Both depleted and enriched trace elemental and Sr isotope signatures are observed in MIs that are sampled during He isotope analyses. We infer from the link between MIs and whole rock geochemistry that the *N-type* MIs have the highest $^3He/^4He$. This link lends support to the notion of the unradiogenic He signature originating from ancient melt depletion of the mantle (Parman et al., 2005; Parman 2007). The deviation of the *E-type* melts from a recycled component implies that this component has a radiogenic He signature. The BIP suggest that $^3He/^4He$ and Sr isotope compositions of MIs can show strong correlation in early-formed melts, however this co-variation may partly be destroyed during ascent due to degassing and contamination/assimilation processes.

4.9 References

Allégre, C. J. & Turcotte, D. L. (1986): Implications of a two-component marble-cake mantle. Nature, 323: 123-127.

Breddam, K. & Kurz, M. (2001): Helium isotopic signatures of Icelandic alkaline lavas. American Geophysical Union, Fall Meeting 2001, abstract #V22B-1025.

Breddam, K., Stecher, O., Harlou, R., Peate, D. W., & Kurz, M.D. (in prep): Miocene high-$^{3}He/^{4}He$ ankaramites in NW-Iceland: Trace element constraints on the common component in mantle plumes.

Brooker, R. A., Du, Z., Blundy, J. D., Kelly, S. P., Allan, N. L., Wood, B. J., Chamorro, E. M., Wartho, J. -A., & Purton, J. A. (2003): The 'zero charge' partitioning behavior of nogle gases during mantle melting. Nature, 423: 738-741.

Brooks, C. K. & Nielsen, T. F. D. (1982): The E Greenland continental margin: a transition between oceanic and continental magmatism. Journal of the Geological Society, 139: 265-275.

Charlier, B. L. A., Ginibre, C., Morgan, D., Nowell, G. M., Pearson, G. D., Ottley, C. J., & Davidson, J. P. (2006): Methods for the microsampling and analysis of strontium isotopes at the crystal scale for petrological and geochronological studies of igneous rocks. Chemical Geology: 114-133.

Clarke, D. B. (1970): Tertiary basalt s of Baffin Bay: possible primary magma from the mantle. Contribution to Mineral and Petrology, 25: 203-223.

Clarke, D. B. & Upton, B. G. J. (1971): Tertiary basalts of Baffin island:field relationships and tectonic setting. Canadian Journal of Earth Science, 8: 248-258.

Danyushevsky, L. V., Leslie, A. G., Carwford, A. J., & Durance, A. (2004): Melt inclusions in primitive olivine phenocrysts: the role of localized reaction processes in the origin of anomalous compositions. Journal of Petrology, 45(12): 2531-2553.

Drever, J. I. (1997): The Geochemistry of Natural Waters: Surface and Groundwater Environments (3rd Edition), Prentice Hall, 436 pages.

Eisele, J., Sharma, M. Galer, J. G., Blicher-Toft, J. Devey, C. W., & Hofmann, A. W. (2002): The role of sediment recycling in EM-1 inferred from Os, Pb, Hf, Nd, Sr isotope and trace element systematics of the Pitcairn hotspot. Earth and Planetary Science Letters, 196: 197-212.

Ellam, R. M. & Stuart, F. M. (2004): Coherent He-Nd-Sr isotope trends in hight 3He/4He basalts: implications for a common reservoir, mantle heterogeneity and convection. Earth and Planetary Science Letters, 228: 511-523.

Farley, K. A., Natland, J. H.; & Craig, H. (1992): Binary mixing of enriched and udegassed (primitive?) mantle components (He, Sr, Nd, Pb) in Samoan lavas. Earth and Planetary Science Letters, 111: 183-199.

Farley, K. A. & Neroda, E. (1998): Noble gases in the Earth's Mantle. Annual Review of Earth and Planetary Sciences, 26: 189-218.

Francis, D. (1985): The Baffin Bay lavas and the value of picrites ans analougues of primary magmas. Contributions to Mineralalogy and Petrology, 89: 144-154.

Graham, D. W. (2002): Nobel gas isotope geochemistry of mid-ocean island basalts: Characterization of mantle source reservoirs. Reviews of Mineralogy & Geochemistry, 47.

Graham, D. W., Larsen, L. M., Hanan, B. B., Storey, M., Pedersen, A. K., & Lupton, J. E. (1998): Helium isotope composition of the early Iceland mantle plume inferred from the Tertiary picrites of West Greenland. Earth and Planetary Science Letters, 160: 241-255.

Gurenko, A. A. & Chaussidon, M. (1995): Enriched and depleted primitive melts included in olivine from Icelandic tholeiites: origin by continuous melting of a single mantle column. Geochimica et Cosmochimica Acta, 59(14): 2905-2917.

Hanan, B. B. & Graham, D. W. (1996): Lead and helium isotope evidence from oceanic basalts for a common deep source of mantle plumes. Science, 272: 991-995.

Harlou, R., Pearson, D. G., Davidson, J. P., Kamenetsky, V. S., & Yaxley, G. M. (2006): Source variability and crustal contamination of the Baffin Island picrites – coupled Sr isotope and trace element study of individual melt inclusions. Geochimica et Cosmochimica Acta, Supplement 1, 70(18): A231.

Harlou, R., Pearson, D. G., Nowell, G. M., Davidson, J. P., & Kent, A.J.R. (2005): Sr isotope studies of melt inclusions by TIMS. Geochimica et Cosmochimica Acta, Supplement 1, 69(10): A380.

Hart, S. R., Blusztajn, J., Dick, H. J. B., Meyer, P. S. and Muehlenbachs, K. (1999): The fingerprint of seawater circulation in a 500-meter section of ocean crust gabbros. Gechimica er Cosmochimica Acta, 63: 4059-4080.

Hart, S. R., Hauri, E. H., Oschmann, L. H., & Whitehead, J. A. (1992): Mantle plumes and entrainment: Isotopic evidence. Science, 256: 517-520.

Hauri, E. H., Lassister, J. C., & DePaolo, D. J. (1996): Osmium isotope systematics of drilled lavas from Mauna Loa, Hawaii. Journal of Geophysical Research, 101(B5): 11793-11806.

Hauri, E. H., Whitehead, J. A., & Hart, S. R. (1994): Fluid dynamic and geochemical aspects of entrainment in mantle plumes. Journal of Geophysical Research, 99(B12): 24275-24300.

Hilton, D. R., Gronvold, K., Macpherson, C. G., & Castillo, P. R. (1999): Extreme $^{3}He/^{4}He$ ratios in northwest Iceland: constraining the common component in mantle plumes. Earth and Planetary Science Letters, 173: 53-60.

Hiyagon, H. & Ozima, M. (1986): Partition of noble-gases between olivine and basalt melt. Gechimica er Cosmochimica Acta, 50: 2045-2057.

Hofmann, A. W. (1997): Mantle geochemistry: the message from oceanic volcanism. Nature, 385: 219-229.

Holm, P. M., Gill, R. C. O., Pedersen, A. K., Larsen, J. G., Hald, N., Nielsen, T. F. D., & Thirlwall, M. F. (1993): The Tertiary picrites of West Greenland: Contributions from 'Icelandic' and other sources. Earth and Planetary Science Letters, 115: 227-244.

Jackson, G. D. (1998): Geology, Oka Bay-padloping Island area, District of Franklin, Northwest Territories, Geological Survey of Canada, Open File 3532, scale1.250000.

Jackson, M. G. & Hart, S. R. (2006): Strontium isotopes in melt inclusions from Samoa balsatls: Implications fro heterogeneity in the Samoan Plume. Earth and Planetary Science Letters, 245: 260-277.

Kent, A. J. R., Baker, J. A., & Wiedenbeck, M. (2002a): Contamination and melt aggregation proceses in continental flood basalts: constraints from melt inclusions in Oligocene basalts from Yemen. Earth and Planetary Science Letters, 202: 577-594.

Kent, A. J. R., Norman, M. D., Hutcheon, I. D., & Stolper, E. M. (1999): Assimilation of seawater-derived components in an oceanic volcano: evidence from glasses and glass inclusions from Loihi seamount, Hawaii. Chemical Geology, 156: 299-319.

Kent, A. J. R., Peate, D. W., Newman, S., Stolper, E. M., & Pearce, J. A. (2002b): Chlorine in submarine glasses from the Lau Basin: seawater contamination and constraints on the composition of slab-derived fluids. Earth and Planetary Science Letters, 202: 361-377.

Kent, A. J. R., Stolper, E. M., Francis, D., Woodhead, J., Frei, R., & Eiler, J. (2004): Mantle heterogeneity during the formation of the North Atlantic Igneous Province: Constrains from trace element and Sr-Nd-Os-O isotope systematics of Baffin Island picrites. Geochemistry Geophysics Geosystems, 5(11): 10.2039/2004GC000743.

Kerr, A. C., Kent, R. W., Thomson, B. A., Seedhouse, J. K., & Donaldson, C. H. (1999): Geochemical evolution of the Tertiary Mull volcano, Western Scotland. Journal of Petrology, 40: 873-908.

Knesel, K. M. & Davidson, J. P. (2002): Insights into collisional magmatism from isotopic fingerprints of melting reactions. Science, 296: 2206-2208.

Kobayashi, K., Tanaka, R., Moriguti, T., Shimizy, K., & Nakamura, E. (2004): Lithium, boron, and lead isotope systematics of glass inclusions in olivines from Hawaiian lavas: evidence for recycled components in the Hawaiian plume. Chemical Geology, 212: 143-161.

Kurz, M. D., Kenna, T. C., Lassister, J. C., & DePaolo, D. J. (1996): Helium isotopic evolution of Mauna Kea Volcano: First results from the 1-km drill core. Journal of Geophysical Research, 101(B5): 11781-11792.

Larsen, L. M., Pedersen, A. K., Sundvoll, B., & Frei, R. (2003): Alkali Picrites formed by melting of old metaomatized lithospheric mantle: Manitdlat Member, Vaigat Formation, Palaeocene of West Greenland. Jounal of Petrology, 44(1): 3-38.

Lightfoot, P. C., Hawkesworth, C. J., Olshefsky, K., Green, T., Doherty, W., & Keays, R. R. (1997): Geochemistry of Tertiary tholeiites and picrites from Qeqertarssuaq (Disko Island) and nuussuaq, West Greenland with implications for the mineral potential of comagmatic intrusions. Contribution to Mineral and Petrology, 128: 139-163.

Marty, B. & Lussiez, P. (1993): Constraints on rare-gass partition-coefficients from analysis of olivine glass from a picritic midocean ridge basalt. Chemical Geology, 106: 1-7.

McDonough, W. F. & Sun, S. -s. (1995): The composition of the Earth. Chemical Geology, 120: 223-253.

McKenzie, D. & O'Nions, K. (1995): The Source Regions of Ocean Island Basalts. Journal of Petrology, 36: 133-159.

Morrison, M. A., Thomas, R. N., & Dickin, A.P. (1985): Geochemical evidence for complex magmatic plumbing during development of a continental volcanic center. Geology, 13: 581-584.

Nielsen, R. L., Michael, P. J., & Sours-Page, R. (1998): Chemical and physical indicators of compromised melt inclusions. Geochimica et Cosmochimica Acta, 62(5): 831-839.

Norman, M. D., Garcia, M. O., Kamenetsky, V. S., & Nielsen, R. L. (2002): Olivine-hosted melt inclusions in Hawaiian picrites: equilibration melting, and plume source characteristics. Chemical Geology, 183: 143-168.

Nowell, G. M., Pearson, D.G., Ottley, C.J., Schwieters, J., & Dowall, D. (2003): Long-term performance characteristics of a plasma ionisation multi-collector mass spectrometer (PIMMS): The ThermoFinnigan Neptune. Plasma Source Mass Spectrometry, applications and emerging technologies: 307-320.

Ottley, C. J., Pearson, D. G., & Irvine, G. J. (2003): A routine method for the dissolution of geological samples for the analysis of REE and trace elements via ICP-MS. Plasma Source Mass Spectrometry, applications and emerging technologies: 221-239.

Parman, S. W., Kurz, M. D., Hart, S. R., & Grove, T. L. (2005): Helium solubility in olvine and implicatios for high $^{3}He/^{4}He$ in ocean island basalts. Nature, 437: 1140-1143.

Parman, S. W. (2007): Helium isotopic evidence for episodic mantle melting and crustal growth. Nature 446, 900.902.

Pearson, D. G., Davies, G. R., & Nixon, P. H. (1993): Geochemical constraints on the petrogenesis of diamond facies pyroxenites from the Beni Bousera Peridotite Massif, North Morocco. Jounal of Petrology, 34(1): 125-172.

Pearson, D. G. & Nowell, G. M. (2002): The continental lithospheric mantle: characteristics and signigicance as a mantle reservoir. Philosophical transactions of the Royal Society Mathematical, Physical and Engineering Sciiences, 360(150).

Pearson, D. G., Canil, D., & Shirey, S. B. (2003): Mantle Samples Included in Volcanic Rocks: Xenoliths and Diamonds, Treatise on Geochemistry, Volume 2. Editor: Carlson, R. W. Executive Editors: Holland, H. D. & Turekian, K. K. pp. 568. ISBN 0-08-043751-6. Elsevier, p.171-275.

Pearson, D. G. & Nowell, G. M. (2004): Re-Os and Lu-Hf isotope constraints on the origin and age of pyroxenites from the Beni Bousera Peridotiet Massif: Implicatoins fro mixed peridotite-pyroxenite mantle sources. Journal of Petrology, 45: 439-455.

Peate, D. W., Baker, J. A., Blichert-Toft, J., Hilton, D. R., Storey, M., Kent, A. J. R., Brooks, C. K., Hansen, H., Pedersen, A. K., & Duncan, R. A. (2003): The Prinsen af Wales Bjerge Formation lavas, East Greenland. The transition from tholeiitic to alkalic magmatism during Palaeogene continental break-up. Journal of Petrology, 44 (2): 279-304.

Pedersen, A. K. (1985): Reaction between picrite magma and continentla crust: early Tertiary silicic basalts and magnesian adesites from Disko, west Greenland. Bullitin Grønlands Geologiske Undersøgelser, 124: 1-126.

Pedersen, A. K., Larsen, L. M., Rissager, P., & Dueholm, K. S. (2002): Rates of volcanic deposition, facies changes and movements in a dynamic basin: the Nuussuaq Basin, West Greenland, around the C27n-C26r transition, in The North Atlantic Igneous Province: Stratigraphy, Tectonic, Volcanic and Magmatic Processes, edited by D. W. Jolley and B. R. Bell. Geological Society Special Publication, 197: 157-181.

Robillard, I., Francis, D., & Ludden, J. N. (1992): The relation ship between E- and N-type magmas in the Baffin Bay Lavas. Contribution to Mineral and Petrology, 112: 230-241.

Roedder, E. (1984): Fluid inclusions. Mineralogical Society of America, Washington, DC: 644pp.

Roeder, P. L. & Emslie, R. F. (1970): Olivine-liquid equilibrium. Contribution to Mineral and Petrology, 29: 275-289.

Saal, A. E., Hart, S. R., Shimizu, N., Hauri, E. H., & Layne, G. D. (1998): Pb isotopic variability in melt inclusions from oceanic island basalts, Polynesia. Science, 282: 1481-1484.

Saal, A. E., Hart, S. R., Shimizu, N., Hauri, E. H., Layne, G. D., & Eiler, J. M. (2005): Pb isotopic variability in melt inclusions from the EMI-EMII-HIMU mantle end-members and the role of the oceanic lithosphere. Earth and Planetary Science Letters, 240: 605-620.

Saunders, A. D., Fitton, J. G., Keer, A. C., Norry, M. J.; & Kent, R.W. (1997): The North Atlantic Igneous Province In: J.J. Mahoney, M. F. Coffin (Eds), Large Igenous Provinces: Continental, Oceanic and Planetary Flood volcanism, Geophysical Monograph, 100: 45-93.

Shimizu, N. (1998): The geochemistry of olivine-hosted melt inclusions in a FAMOUS basalt ALV519-4-1. Physics of the Earth and Planetary Interiors, 107: 183-201.

Sobolev, A. V. & Shimizu, N. (1993): Ultra-depleted primary melt included in an olivine from the Mid-Atlantic Ridge. Nature, 363: 151-154.

Starkey, N, A., Stuart, F. M., Ellam, R. M. Fitton, J. G. & Larsen, L. M. (2007): High $^{3}He/^{4}He$ depleted mantle? Insights from high $^{3}He/^{4}He$ in West Greenland. VMSG winter meeting 2007, abstract 3.5, 16-17.

Staudigel, H., Davies, G. R., Hart, S. R., Marchant. K. M., & Smidt, B. M. (1995): Large scale isotopic Sr, Nd and O isotopic anatomy of altered oceanic crust: DSDP/ODP sites 417/418. Earth and Planetary Science Letters, 130: 169-185.

Storey, M., Duncan, R. A., Pedersen, A. K., Larsen, L. M., & Larsen, H. C. (1998): $^{40}Ar/^{39}Ar$ geochronology of the West Greenland Tertiary volcanic province. Earth and Planetary Science Letters, 160(3-4): 569-586.

Stuart, F. M., Ellam, R. M., Harrop, P. J., Fitton, J. G., & Bell, B. R. (2000): Constraints on mantle plumes from the helium isotopic composition of basalts from the British tertiary igneous Province. Earth and Planetary Science Letters, 177: 273-285.

Stuart, F. M., Lass-Evans, S., Fitton, J.G., & Ellam, R. M. (2003): High $^{3}He/^{4}He$ ratios in picritic basalts from Baffin Island and the role of a mixed reservoir in mantle plumes. Nature, 424(3): 57-59.

Sun, S. -s. & McDonough, W. F. (1989): Chemical and isotopic systematics of oceanic basalts: implications for mantle composition and processes. Geological Society Special Publication, No. 42: 313-345.

Tachibana, Y., Kaneoka, I., Gaffney, A., & Upton, B. (2006): Ocean-island basalt-like source of kimberlite magmas from West Greenland revealed by high $^{3}He/^{4}He$ ratios. Geology, 34(4): 273-276.

Thériault, R. J., St-Onge, M. R., & Scott, D. J. (2001): Nd isotopic and geochemical signature of the Paleoproterozoic Trans-Hudson Orogen, southern Baffin Island, Canada: implications for the evolution of eastern Laurentia. Precambrian Research, 108: 113-138.

Thompson, R. N. & Gibson, S. A. (2000): Transient high temperatures in mantle plume heads inferred from magnesian olivines in phanerozoic picrites. Nature, 407: 502-506.

Thompson, R. N., Morrison, M. A., Hendry, G. L., Parry, S. J., Simpson, P. R., Hutchison, R., & O'Hara, M. J. (1984): An Assessment of the Relative Roles of Crust and Mantle in Magma Genesis: An Elemental Approach. Philosophical Transactions of the Royal Society of London. Series A, Mathematical and Physical Sciences, Vol. 310, No. 1514: 549-590.

Walter, M. J. (1998): Melting of Garnet Peridotite and the Origin of Komatiite and Depleted Lithosphere. Jounal of Petrology, 39(1): 29-60.

Weaver, B. L. (1991): The origin of ocean island basalt end-member compositions: trace element and isotopic constraints. Earth and Planetary Science Letters, 104: 381-397.

Weis, D., Kieffer, B., Maerschalk, C., Pretorius, W., & Barling, J. (2005): High-precision Pb-Sr-Nd-HF isotopic characterization of USGS BHVO-1 and BHVO-2 reference materials. Geochemistry Geophysics Geosystems, 6(2).

White, R. & McKenzie, D. (1989): Magmatism at Rift Zones: The generation of volcanic continental margins and flood basalts. Journal of Geophysical Research, 94(No. B6): 7685-7729.

White, R. S. & McKenzie, D. (1995): Mantle plumes and flood basalts. Jounal of geophysical Research, 100: 17543-17585.

Workman, R. K., Hart, S. R., Jackson, M., Regelous, M., Farley, K. A., Blusztajn, J., Kurz, M., & Staudigel, H. (2004): Recycled metasomatized lithosphere as the origin of the enriched mantle II (EM2) end-members: Evidence for the Samoan volcanic Chain. Geochemistry Geophysics Geosystems, 5(4).

Yaxley, G. M., Kamenetsky, V. S., Kamenetsky, M., Norman, M. D., & Francis, D. (2004): Origins of compositional heterogeneity in olivine-hosted melt inclusions from the Baffin Island picrites. Contribution to Mineral and Petrology, 148: 426-442.

Yurimoto, H., Kogiso, T., Abe, K., Barsczus, H. C., Utsunomiya, A., & Maruyama, S. (2004): Lead isotopic compositions in olivine-hosted melt inclusions from HIMU basalts and possible link to sulfide components. Physics of the Earth and Planetary Interiors, 146: 231-242.

SUMMARY & CONCLUSIONS

The melt inclusion studies presented in ***Chapter 1*** and Yaxley et al (2004) describe the major and trace element composition of individual MIs from the Vestfirdir ankaramites and the Baffin Island picrites. Both studies reveal MIs showing substantial compositional variations, which may partly be explained by the involvement of multiple mantle sources, or a heterogeneous mantle source combined with variation in melting systematics. However, it is difficult to resolve the full picture of the mantle sources ± crustal components involved in the genesis of these lavas on the basis of major and trace element data. In order to further constrain, the origin of the chemical diversity among the MIs of these rocks it is necessary to obtain isotopic ratios on single MIs to examine the true variation of coupled elemental and isotopic systematics in the melts that aggregate to form the host lava suite.

The need for isotope information on individual MIs was recognized and pursued by the pioneering work of Saal et al. (1998), who introduced a technique to obtain Pb isotope ratios on individual MIs by SIMS. Since that work, several MI Pb isotope studies have followed. These show that MIs also record larger Pb isotope variability than their host lavas (e.g. Kobayashi et al., 2004; Yurimoto et al., 2004; Saal et al., 2005). However, due to large uncertainties associated with *in situ* Pb isotope analysis and the limitation of obtaining only $^{207}Pb/^{206}Pb$ and $^{208}Pb/^{206}Pb$ ratios, it has proven problematic to distinguish fully between the different end-member components involved e.g. EMII, MORB, FOZO, and PM. In this respect the Rb-Sr isotope system has an advantage over the Pb isotope system, as the different mantle end-members have distinctive $^{87}Sr/^{86}Sr$ ratios. Also, Sr isotope ratios are an excellent tracer of crustal involvement. Therefore, this Ph.D. thesis has revolved around: I) the development of a technique to obtain precise and accurate Sr isotope and trace element data of individual MIs (*Chapter 2*), II) the examination of the potential for Sr isotope studies on MIs to reveal new information on the origin of CFB and OIB magmas (*Chapter 3 and 4*).

Chapter 2 introduces a technique that facilitates precise and accurate Sr isotope and trace element analysis of individual MIs at sub-ng levels, which was developed as part of this Ph.D. at the *AHIGL* (Department of Earth Sciences, Durham University). The technique was developed in line with the micro-sampling and Sr analytical work carried out by Charlier et al. (2006), see also the summary paper on '*Microsampling and isotopic analysis of igneous rocks:*

Implications for the study of magmatic systems' by Davidson et al. (2007). This technique combines: I) off-line sampling of individual MIs using a New Wave MicroMill, II) micro chemical processing, which includes sample dissolution, aliquoting, and sub-ng Sr column chemistry, III) low level trace element determination by double focusing magnetic sector field ICPMS (Finnigan ELEMENT2), and IV) Sr isotope determination by TIMS (Thermo-Finnigan Triton). The combination of TIMS and ICPMS analyses allow age corrections to be applied to the measured $^{87}Sr/^{86}Sr$ ratios using the Sr and Rb concentrations.

During the course of this work 91 sub-ng NBS 987 standards were analyzed for which an $^{87}Sr/^{86}Sr$ average of 0.710261 ±0.000042 (58 ppm, 2SD) was obtained. Substantial work was carried out to monitor the magnitude of, and isotopic composition of the total procedural blank (TPB). This was done to evaluate the effect of the TPB on the measured isotope composition of sub-ng samples, and to allow accurate blank corrections to be applied to the data. The TPB relevant to the data presented in this Ph.D. thesis had a Sr content of 4.86 ±0.26 pg (2SD) and a Rb of 1.32 ±0.69 pg (2SD). The $^{87}Sr/^{86}Sr$ ratio was established to be 0.712932 ±0.000234 (2SE). The study shows that for Sr samples down to ~1 ng the shift in Sr isotope composition due to the TPB is minimal, mainly within the typical 2SE error of an analysis. The TPB affects the Sr isotope composition of samples sizes <500 pg more significantly. The accuracy of the data collected on samples <500 pg Sr is improved by the application of a blank correction. The Sr isotope determinations of samples containing 500-250 pg and 50-25 pg Sr can be done to an accuracy within 150 and 400 ppm, respectively. This is more than adequate to resolve the very large (~6500 to 8550 ppm) isotopic variations recorded within the MI suites studied here.

The result is a novel technique which permits individual MIs as small as 50 μm, containing as little as 200 ppm Sr, to be analysed for their trace element and Sr isotope composition. The overall uncertainty propagates to a typical uncertainty of 100-1000 ppm when correcting measured $^{87}Sr/^{86}Sr$ to the initial ratios, and the overall Rb/Sr uncertainty is estimated to be <25%. This sensitivity makes the method presented here much more adaptable to a larger variety of MI suites in depleted rocks compared with the LA-MC-ICPMS technique. It also provides the option of studying very small MIs by digestion of whole olivine crystals. In general, this technique has a wide range of application where precise and accurate Sr isotope and trace element information is needed on sub-ng Sr samples. The method has been applied to two suites of MIs from OIB (*Chapter 3*, Harlou et al., 2005) and CFB (*Chapter 4*, Harlou et al., 2006), within this thesis, and to a set of inclusions in diamonds (Pearson et al. in prep).

Chapter 3 presents the first $^{87}Sr/^{86}Sr$ isotope determination of individual olivine hosted MIs from three ankaramites from Vestfirdir in NW Iceland. This data is presented together with Sr isotope measurements obtained on olivine phenocrysts hosting multiple MIs (both single grains and grain aggregates). The range of $^{87}Sr/^{86}Sr$ in single MIs (0.70315-0.70625) and the olivine

grains rich in MIs (0.70350-0.70768) is considerably more variable than both the host lavas (0.70342-0.70368) and the entire Icelandic lava field (0.7028-0.7038). The Sr isotope compositions measured on the Vestfirdir MIs are the most radiogenic Sr isotope ratios ever reported from Iceland. In fact, the Sr isotope variation seen among the Vestfirdir MIs cover >75% of the Sr isotope range displayed by the global OIB. In contrast, the host lava suite only covers 5%. The Sr isotope heterogeneity revealed by the MIs suggests that MIs, in contrast to their host lava suite, provide a more detailed record of the chemical diversity and processes taking place during the earliest stages within the magmatic system.

Two trends are recognized among the MIs when Sr isotope composition is plotted against trace element ratios e.g. $(Rb/Sr)_N$, $(La/Sm)_N$, and $(Ti/Zr)_N$. *Trend I* MIs are characterized by relatively unradiogenic and homogenous $^{87}Sr/^{86}Sr$ ($\leq$0.704) over the range of $(La/Sm)_N$ and $(Ti/Zr)_N$, but $(Rb/Sr)_N < 1.5$. The MIs of *Trend II* display positive correlations between $^{87}Sr/^{86}Sr$ and $(Rb/Sr)_N$ and $(La/Sm)_N$, but an inverse correlation with $(Ti/Zr)_N$. The MIs of *Trend II* have significant more radiogenic Sr isotope ratios (0.704-0.708) combined with higher $(Rb/Sr)_N$ (0.5-4.2) than the MIs of *Trend I*. There is no evidence to suggest that secondary alteration processes or severe crustal assimilation has affected the Sr isotope ratios or the geochemistry of the Vestfirdir lavas and their associated MI suite. Thus, it is concluded that the Sr isotope range displayed by the MIs is linked to geochemical variations within the mantle domains sampled by the Icelandic mantle plume. The model developed from these data proposes mixing of melts derived from a depleted mantle and a recycled oceanic lithospheric mantle containing both a pyroxenite and a sediment component. This diversity of source components seems to be required to generate the trace element and Sr isotope variability of the MIs and Sr-Nd-Hf-Os-Pb isotope systematics of the host ankaramites. The genetic model predicts that the MIs of *Trend I* are dominantly derived from the depleted mantle component. The MIs of *Trend II* require up to 15% input of the recycled mantle component, whereas the variation among the host ankaramites demands <3%.

The proposed model for explaining the MI geochemistry has important implications for the unradiogenic $^3He/^4He$ signature of the Vestfirdir ankaramites. The He analysed in noble gas studies is derived from volatile rich MIs hosted within olivine and so the MI elemental and Sr isotope geochemistry relates directly to the He isotope signatures. Because the MIs and host lava suite are dominated by a DM component and inputs from recycled components are relatively minor, the He isotope signature could be dominated by the depleted component. Recycled mantle components are likely to be extensively processed and thereby degassed. They are also likely to have appreciably high U contents compared with depleted components. As such they are unlikely to possess a high $^3He/^4He$ signature. On this basis, the high $^3He/^4He$ signature present in the Vestfirdir MIs is most likely linked to the DM component. A link between high $^3He/^4He$ and a DM component contradicts the general assumption that

unradiogenic He signatures are indicative of contribution from the primordial mantle. However, this linkage gains support from recent experimental studies by Parman et al. (2005), which suggests that He may be more compatible than U-Th during mantle melting. The DM source is envisaged to have obtained its high $^{3}He/^{4}He$ and depleted Sr-Nd-Hf-Os signatures through previous melt extraction events. This scenario leads to an alternative model to that proposed by Ellam & Stuart (2004). The model presented here shows that the relationship between He and Sr-Nd isotope compositions can be generated by binary mixing between high $^{3}He/^{4}He$ DM component and low $^{3}He/^{4}He$ enriched recycled mantle component (REM). This model nicely explains the relationship between the unradiogenic He isotope signature found in the Vestfirdir ankaramites, and the variable Sr signature documented by the MIs. It also provides a relatively straightforward explanation for a high $^{3}He/^{4}He$, DM endmember within many of the global high $^{3}He/^{4}He$ lavas. It implicates a high $^{3}He/^{4}He$ depleted reservoir with a low He concentration, which also provides an explanation of the lower gas contents of many OIB, in contrast to MORB.

In a global perspective, the composition of the recycled endmember most likely varies from one province to the other, as diverse material has been subducted through time. The Vestfirdir ankaramites may require a less extreme REM component than the more enriched high $^{3}He/^{4}He$ OIB lavas of e.g. Samoa and Heard Island. The linkage of the extreme, high $^{3}He/^{4}He$ signature to a DM component as observed for the Vestfirdir ankaramites, Central Iceland lavas (Macpherson et al., 2005) and as suggested for the Baffin Island picrites (Stuart et al., 2003; Ellam & Stuart; 2004, *Chapter 4*) may be a widespread phenomenon within the NAIP - if not globally.

Chapter 4 reveals that the olivine hosted MIs retrieved from the Baffin Island picrites display a large variability in $^{87}Sr/^{86}Sr$ ratios (0.70306-0.70906). This contrasts the narrow range of the host lavas (0.70308-0.70366), and exceeds the Sr isotope diversity of the North Atlantic MORB. Based on previous isotope, major, and trace element studies of the BIP, these laves have been shown to be mixtures of an '*N-type*' or depleted (DM-like) source ($^{87}Sr/^{86}Sr$ <0.7032, $^{143}Nd/^{144}Nd$ >0.51299, and $^{187}Os/^{188}Os$ of 0.1220-0.1247) and an '*E-type*', EM-like source ($^{87}Sr/^{86}Sr$ of 0.7032-0.7039, $^{143}Nd/^{144}Nd$ <0.51296, and $^{187}Os/^{188}Os$ of 0.1261-0.1303) respectively (Francis, 1985; Robillard et al., 1992; Stuart et al., 2003; Ellam & Stuart 2004; Kent et al., 2004; Yaxley et al., 2004). This classification also applies to the MIs. The BIP MI study presented here finds two groupings that have distinct trace element and Sr isotope geochemistry. The trends for these two groups (*Group I* and *Group II*) on plots of $^{87}Sr/^{86}Sr$ versus $(La/Sm)_N$ and $(Rb/Sr)_N$ are distinct from the trends defined by the previous classification into *N-type* and *E-type* melts. The MIs of *Group I* have unradiogenic to moderate $^{87}Sr/^{86}Sr$ ratios (<0.704) over the range of $(La/Sm)_N$ combined with $(Rb/Sr)_N$ <2. The MIs of *Group II* have

significantly more radiogenic $^{87}Sr/^{86}Sr$ (0.704-0.709) over a similar range of $(La/Sm)_N$ ratios, but also higher $(Rb/Sr)_N$. The relatively subtle Sr isotope variation of the *N-type* and *E-type* mantle endmember cannot account for the more radiogenic $^{87}Sr/^{86}Sr$ ratios of *Group II*, however may explain the Sr isotope variation of *Group I*.

Modelling shows that it is impossible to regenerate the Sr isotope variations of *Group II* MIs by mixing of melts purely derived from components found within the convecting mantle. Neither can the combination of radiogenic $^{87}Sr/^{86}Sr$ and higher $(Rb/Sr)_N$ ratios of the MIs of *Group II* be produced by seawater contamination. Instead, the models show that the systematic between $^{87}Sr/^{86}Sr$ and $(Rb/Sr)_N$ of *Group II* is consistent with contamination by the local Archean to Paleoproterozoic continental crust. The model predicts that the MIs of *Group II* have assimilated 0-10% crustal material, whereas the variation among the host BIP lava suite requires contributions of up to 4%. The large input of crust material to the early-formed MIs, is supported by modelling of trace elements alone, performed by Yaxely et al (2004).

In detail, the relationship between $^{87}Sr/^{86}Sr$ and $(La/Sm)_N$ cannot be explained by crustal contamination of a single parental melt, but requires melt contributions from two source regions, in agreement with previous BIP studies (Francis, 1985; Robillard et al., 1992; Stuart et al., 2003; Ellam & Stuart 2004; Kent et al., 2004; Yaxley et al., 2004). A best match for the *E-type* melts is obtained by 10% critical melting (α of 5%) at 3 GPa of a garnet peridotite source with a PM signature. The *N-type* melts are matched by 5-12% critical melting (α: 2-5%) at 3 GPa of a garnet peridotite with a DM signature. The fact, that MIs sample both *N-type* and *E-type* melts within a single lava, suggests that their source components exist in close proximity to each other.

If the host lavas most strongly affected by crustal contamination are excluded, it can be seen that the olivine phenocrysts of *N-type* lavas contain the highest $^{3}He/^{4}He$ (49.5 R/R_a) of the BIP collection of Stuart et al. (2003). Furthermore, if the crustally contaminated *Group II* MIs are excluded in a plot of $^{87}Sr/^{86}Sr$ versus $(La/Sm)_N$ it is clear that *E-type* and *N-type* MIs mainly are found in *E-type* and *N-type* BIP, respectively. Given that the He inventory is dominated by melt and gas inclusions in olivine, this strongly suggests that the unradiogenic He signature of the BIP is carried by the *N-type* MIs. Except from the unradiogenic He signature of the *N-type* lavas, the other isotope tracers such as Sr-Nd-Os and trace elements strongly indicate a depleted upper mantle signature. These observations are again inconsistent with a high $^{3}He/^{4}He$ primordial mantle component. Stuart et al. (2003) and Ellam & Stuart (2004) have proposed that the correlation between He and Sr-Nd isotope ratios of the BIP results from mixing between a *He-recharged* DM (or a mix of primordial and DM derived melts) and an average enriched mantle component. However, the data set presented in this thesis suggests that the unradiogenic

He signature is an integrated part of the DM source of the BIP. Hence, following the ideas of Parman et al. (2005), it is proposed that the DM source obtained its high $^{3}He/^{4}He$ signature through melt extraction events in the past. Lava compositions deflected from the trend shown by the He and Sr-Nd isotope systematics of the BIP may be explained by crustal contamination or degassing.

The generations of Sr isotope heterogeneities in a magmatic plumbing system, such as that documented by the BIP MIs, are envisaged to form in two stages. First, mixing of the *N-type* and *E-type* melts happens in the upper mantle as the melts start to segregate from the source region and ascend. Secondly, the uprising melts come into contact with continental crustal lithologies along the walls of the magma plumbing system that contain highly radiogenic Sr in the case of the BIP. Small melt droplets entrapped by growing phenocryst phases along the interaction zone between the uprising melt and the crust may reflect mixtures of the uprising melt and partial melts of the wall rock, whereas MIs entrapped within the central parts of the magma body are more likely to remain uncontaminated. In this way, a magma can be generated which transports phenocrysts formed during different stages and at different locations within the plumbing system. MIs hosted by early-formed olivine phenocrysts sample this complex environment and reflect the chemical heterogeneities within it.

Summary: In general, this study shows that Sr isotope and trace element measurements on individual MIs provide a higher resolution picture of the pre-aggregated melt compositions and the different mantle and crustal components involved in the magma genesis, which otherwise were obscured within the whole rock data. The elemental and isotope variability documented by the olivine-hosted MIs contrast with the more subtle variations of the host lava suites and raises the question of whether the $^{3}He/^{4}He$ ratios measured in MIs in olivine phenocrysts should be related to chemistry of MIs rather than the bulk lava chemistry. This study has provided strong evidence that the extreme, high $^{3}He/^{4}He$ signatures observed in NAIP magmas is derived from a depleted component in their source and hence such He isotopic signatures should no longer be regarded as canonical evidence for '*primitive*', lower mantle sources. However, a full understanding of the message delivered by the unradiogenic He signature of the these high $^{3}He/^{4}He$ lavas awaits further analytical developments that would make it possible to obtain He isotopic measurements on individual MIs in addition to major, trace element, and lithophile isotope compositions.

"... as science is always in a state of flux, and as earth scientists are busy in working out new results all the time, it is a sign of the times that this collection is necessarily incomplete."

(Jacoby & Gudmundsson, 2007)

References

Davidson, J. P., Morgan, D. J., Charlier, B. L. A., Harlou, R. & Hora, J. M. (2007): Microsampling and isotopic analysis of igneous rocks: Implications for the study of magmatic systems. Annual Review of Earth and Planetary Sciences, 35: 273-311.

Ellam, R. M. & Stuart, F. M. (2004): Coherent He-Nd-Sr isotope trends in high $^{3}He/^{4}He$ basalts: implications for a common reservoir, mantle heterogeneity and convection. Earth and Planetary Science Letters, 228: 511-523.

Francis, D. (1985): The Baffin Bay lavas and the value of picrites as analogues of primary magmas. Contributions to Mineralalogy and Petrology, 89: 144-154.

Jacoby, W. & Gudmundsson, M. T. (2007): Hotspot Iceland: An introduction. Journal of Geodynamics 43 (2), 1-5.

Kent, A. J. R., Stolper, E. M., Francis, D., Woodhead, J., Frei, R., & Eiler, J. (2004): Mantle heterogeneity during the formation of the North Atlantic Igneous Province: Constrains from trace element and Sr-Nd-Os-O isotope systematics of Baffin Island picrites. Geochemistry Geophysics Geosystems, 5(11): 10.2039/2004GC000743.

Kobayashi, K., Tanaka, R., Moriguti, T., Shimizy, K., & Nakamura, E. (2004): Lithium, boron, and lead isotope systematics of glass inclusions in olivines from Hawaiian lavas: evidence for recycled components in the Hawaiian plume. Chemical Geology, 212: 143-161.

Parman, S. W., Kurz, M. D., Hart, S. R., & Grove, T. L. (2005): Helium solubility in olvine and implications for high $^{3}He/^{4}He$ in ocean island basalts. Nature, 437: 1140-1143.

Robillard, I., Francis, D., & Ludden, J. N. (1992): The relation ship between E- and N-type magmas in the Baffin Bay Lavas. Contribution to Mineral and Petrology, 112: 230-241.

Saal, A. E., Hart, S. R., Shimizu, N., Hauri, E. H., & Layne, G. D. (1998): Pb isotopic variability in melt inclusions from oceanic island basalts, Polynesia. Science, 282: 1481-1484.

Saal, A. E., Hart, S. R., Shimizu, N., Hauri, E. H., Layne, G. D., & Eiler, J. M. (2005): Pb isotopic variability in melt inclusions from the EMI-EMII-HIMU mantle end-members and the role of the oceanic lithosphere. Earth and Planetary Science Letters, 240: 605-620.

Stuart, F. M., Lass-Evans, S., Fitton, J.G., & Ellam, R.M. (2003): High $^{3}He/^{4}He$ ratios in picritic basalts from Baffin Island and the role of a mixed reservoir in mantle plumes. Nature, 424(3): 57-59.

Yaxley, G. M., Kamenetsky, V. S., Kamenetsky, M., Norman, M. D., & Francis, D. (2004): Origins of compositional heterogeneity in olivine-hosted melt inclusions from the Baffin Island picrites. Contribution to Mineral and Petrology, 148: 426-442.

Yurimoto, H., Kogiso, T., Abe, K., Barsczus, H. C., Utsunomiya, A., & Maruyama, S. (2004): Lead isotopic compositions in olivine-hosted melt inclusions from HIMU basalts and possible link to sulfide components. Physics of the Earth and Planetary Interiors, 146: 231-242.

ACKNOWLEDGMENTS

I like to take this opportunity to express my gratitude to my supervisors D.G. Pearson, J.P. Davidson and A.J.R. Kent, and the scientific staff, post. doctors, and students at Durham University, DLC, Copenhagen University, and Oregon State University, - and to family and friends who have been a great support throughout the duration of my Ph.D.

I'm grateful to **D.G. Pearson** - for excellent supervision, you scientific vision, expertise, guidance and ideas! Thanks for spending lots of time in the lab and in the office with me trying to figure out the next '*MI attack*' ... for reading through my thesis and being very thoroughly! For being super supportive, caring and for standing by me throughout the duration of my Ph.D. For the fieldtrips, conference trips, pints - and thanks to both you and Sam for fantastic dinners and parties! I only have one complaint ... you still cannot say my name!

J.P. Davidson - I'm grateful for your supervision, scientific expertise and micro Sr inputs - and for keep telling me that it is possible! Thanks for reading through my thesis and for your comments, which I greatly appreciated. I thanked you for being extremely supportive, caring, and for standing by me throughout the duration of this Ph.D. - and for the good company on field and conference trips, and during lunch.

A.J.R. Kent - thank you for introducing me to the study of melt inclusions and all its complications! For working with me at DLC and giving me the opportunity to go back to Oregon State University. I'm grateful for your supervision, guidance, and advice! Also, D. Wildenschild is thanked for introducing me to K. Cullingan, and for giving me the opportunity to go to Argonne National Lab. Tusind tak til jer alle - Adam, Dorthe, Mads og Sisse - for hyggeligt selvskab og ikke mindst de mange middage og kaffe pauser!

G.M. Nowell - I'm grateful for your support, advice and for sharing your laboratory and analytical expertise and experiences with me. Also, for giving me a '*home away from home*' – and thank you for lots of fun – working, talking, cooking, kiting, climbing, sledging etc ... those High Pittington days I do miss!

C. Ottley - I'm grateful for your guidance and for sharing your expertise with the low abundance trace element analysis, and for introducing me to the safety rules! Also, thank you very much for helping me with my bike.

The textures and isotopic microanalysis group - Thanks to B. Charlier, D.J. Morgen, C. Ginibre for introducing me to the micro-milling and micro Sr procedures. Also thanks to L. Font for good company and collaboration.

C. Macpherson and T. Elliott - for being examiners. Thank you for taking the time to reading through my thesis and being very thoroughly, and for the constructive discussions and your point of view on my work!

N. Wittig - alias Dr. Wittig a truly valuable friend and colleague! Thanks for sharing the office at DLC/Durham and your coffee and chocolates with me! For the many good dinners, late evening discussions over wine, and the DEET rewarding chart – for your support and re-bouncing skills!

M. Webb – thanks for being a good friend and a fantastic office mate. Thanks for sharing the office with me, for lots of fun times and dinners ... and for being the bubbly spice of the lab!

H. C. Larsen, S. Bernstein and the Danish Lithosphere Centre - are thanked for the inspiring and fantastic working environment in Copenhagen - and for your support both during my masters and during my Ph.D. study! Thank you for giving me the opportunity for being part of the DLC team and for doing fieldwork in East Greenland! Også tak for de mange gode løbeture og kaffe ad libitum!

B. Wenzell - thank you for offering you expertise and guidance during my numerous days/nights working on the electron microprobe in the ØV10 basement at the University of Copenhagen. Thanks for the good company og ikke mindst go' kaffe!

S. Bernstein (GEUS) and **C. K. Brooks** (University of Copenhagen) - my supervisors during my masters at University of Copenhagen. I'm grateful for your recommendations! Thanks for your support through the years and for showing your interest in my work.

K. Breddam (Danish Lithosphere Centre) - thank you for providing me with the sample material from Vestfirdir, and introduction to the geology of the *Vestfirdir* ankaramites.

V.S. Kamenetsky (CODES, University of Tasmania) and **G.M. Yaxley** (Reasearch School of Earth Sciences, the Australian National University) are also thanked for providing med with grain mounts with olivine hosting melt inclusions from the *Baffin Island picrites*. Thank you very much for you scientific advice and for showing interest in my work!

B. Kærsgaard (Geological Survey of Canada) thank you for sending me the geological map of *Baffin Island* and for getting G. Jackson involved in the *Baffin Island* study.

G. Jackson (Geological Survey of Canada) thank you for provided me with a valuable sample collection of crustal rocks from *Baffin Island.*

D. Peate (Danish Lithosphere Centre) thanks for providing me with samples from *Prinsen of Wales Bjerge* and for showing interest in my work.

K. Cullingan - for being a great friend, for good company and for our expedition to Starbucks, Portland, San Francisco, Argonne National Laboratory, Ribe, Copenhagen etc. For being supportive and understanding - and for who you are!

Finally, I would like to thank **my family and friends** for always standing by me, and for being extremely patient and tolerant - especially over the last couple of years! **Søren** for being there for me no matter what, for your unquestionable support, understanding, pertinence, and love! Thanks for reading through my thesis hope you enjoyed it - keep in mind melt inclusions are as interesting to geologist as superchargers are to mechanical engineers!